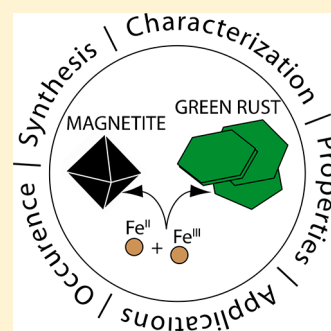


Magnetite and Green Rust: Synthesis, Properties, and Environmental Applications of Mixed-Valent Iron Minerals

M. Usman,^{*,†,‡,§} J. M. Byrne,[§] A. Chaudhary,^{†,||} S. Orsetti,[†] K. Hanna,^{⊥,§} C. Ruby,[@] A. Kappler,^{§,||} and S. B. Haderlein^{†,§}[†]Environmental Mineralogy, Center for Applied Geosciences, University of Tübingen, 72074 Tübingen, Germany[‡]Institute of Soil and Environmental Sciences, University of Agriculture, Faisalabad 38040, Pakistan[§]Geomicrobiology, Center for Applied Geosciences, University of Tübingen, 72074 Tübingen, Germany^{||}Department of Environmental Science and Engineering, Government College University Faisalabad 38000, Pakistan[⊥]Univ Rennes, École Nationale Supérieure de Chimie de Rennes, CNRS, ISCR – UMR6226, F-35000 Rennes, France[@]Laboratoire de Chimie Physique et Microbiologie pour l'Environnement, UMR 7564 CNRS-Université de Lorraine, 54600 Villers-Lès-Nancy, France

ABSTRACT: Mixed-valent iron [Fe(II)-Fe(III)] minerals such as magnetite and green rust have received a significant amount of attention over recent decades, especially in the environmental sciences. These mineral phases are intrinsic and essential parts of biogeochemical cycling of metals and organic carbon and play an important role regarding the mobility, toxicity, and redox transformation of organic and inorganic pollutants. The formation pathways, mineral properties, and applications of magnetite and green rust are currently active areas of research in geochemistry, environmental mineralogy, geomicrobiology, material sciences, environmental engineering, and environmental remediation. These aspects ultimately dictate the reactivity of magnetite and green rust in the environment, which has important consequences for the application of these mineral phases, for example in remediation strategies. In this review we discuss the properties, occurrence, formation by biotic as well as abiotic pathways, characterization techniques, and environmental applications of magnetite and green rust in the environment. The aim is to present a detailed overview of the key aspects related to these mineral phases which can be used as an important resource for researchers working in a diverse range of fields dealing with mixed-valent iron minerals.



CONTENTS

1. Introduction	B		
2. Properties of Mixed-Valent Iron Minerals	C		
2.1. Structural Properties	C		
Magnetite	C		
Green Rust: Chemical Composition of the Interlayer and Structural Models	C		
2.2. Fe(II):Fe(III) Ratio	D		
2.3. Redox Potential	E		
2.4. Magnetic Properties	F		
2.5. Thermodynamic Properties	G		
3. Occurrence of Mixed-Valent Iron Minerals in the Environment	H		
3.1. Natural Environments	H		
3.2. Corrosion Products in Engineered Systems	I		
4. Synthesis of Mixed-Valent Iron Minerals	I		
4.1. Abiotic Synthesis of Mixed-Valent Iron Minerals	I		
4.1.1. Co-Precipitation of Dissolved Fe(II) and Fe(III) Species	I		
4.1.2. Partial Oxidation of Hydroxylated Dissolved Fe(II) and [Fe(II) _{aq} , Fe(OH) ₂] Mixture	J		
4.1.3. Chemical or Electrochemical Oxidation of Zero-Valent Iron	K		
4.1.4. Interaction of Fe(II) with Fe(III) (Oxyhydr)oxides	K		
4.2. Synthesis of Mixed-Valent Iron Minerals by Microbial Activity	N		
4.2.1. Synthesis by Bacterial Fe(III) Reduction	N		
4.2.2. Synthesis of Mixed-Valent Iron Minerals by Bacterial Fe(II) Oxidation	O		
4.2.3. Magnetotactic Bacteria	Q		
5. Identification and Quantification Techniques	R		
5.1. X-ray Diffraction	R		
5.2. Mössbauer Spectroscopy	T		
Hyperfine Parameters	T		
Determination of Oxidation State	T		
Mineral Identification	T		
5.3. Vibrational Spectroscopy	V		
5.4. Synchrotron X-ray Absorption	V		
5.5. Transmission Electron Microscopy and Scanning Electron Microscopy	Y		

Received: April 27, 2017

5.6. Magnetic Measurements	Y
6. Application of Mixed-Valent Iron Minerals for Environmental Remediation	AA
6.1. Sorption of Contaminants	AA
6.1.1. Inorganic Compounds	AA
6.1.2. Organic Compounds	AC
6.2. Reductive Transformation of Inorganic and Organic Contaminants	AD
6.3. Use of Mixed-Valent Iron Minerals to Promote Advanced Oxidation Processes	AJ
7. Conclusions and Outlook	AL
Author Information	AM
Corresponding Author	AM
ORCID	AM
Notes	AM
Biographies	AM
Acknowledgments	AN
References	AN

1. INTRODUCTION

Iron (Fe) is the fourth most abundant element in the earth crust with an average mass concentration of 5.6% and is the second most abundant metal after aluminum.¹ Fe exists in almost all aquatic and terrestrial environments. Fe is commonly found to form together with O, and/or OH either oxides, hydroxides, or oxide-hydroxides which are collectively referred to as “iron oxides” in this review article. There are 16 known iron oxides (Table 1) having different crystal structure, chemical composition, and Fe valence state.² Iron oxides are categorized into three different groups based on Fe oxidation state including: (i) ferric oxides bearing only trivalent Fe(III), including ferrihydrite, goethite, hematite, lepidocrocite etc., (ii) very rare ferrous oxides containing exclusively divalent Fe(II), with only examples of Fe(II)O and Fe(II)(OH)₂, and (iii) mixed-valent iron oxides containing both Fe(III) and Fe(II) in their structure which include magnetite and green rust (GR). Iron predominantly exists as Fe(III) oxides, especially near the surface of Earth’s crust due to the presence of oxygen. However, under appropriate redox conditions in aquatic or terrestrial environments, Fe(III) oxides can serve as electron acceptors for microbial respiration or react with Fe(II) or other reductants to form mixed-valent Fe minerals such as magnetite and GR which are the focus of this review. Magnetite [Fe(II)Fe(III)₂O₄], a black ferromagnetic mineral, is a member of the spinel group of minerals while GRs are layered double hydroxides.³ GRs appear in intense bluish green colors. Structurally, GRs contain both Fe(II) and Fe(III) cations in brucite-like layers along with intercalated anions. Most common types of GRs are hydroxysulfate GR [GR(SO₄²⁻)], hydroxycarbonate GR [GR(CO₃²⁻)], and hydroxychloride GR [GR(Cl⁻)] according to the type of intercalated anions [i.e., sulfate (SO₄²⁻), carbonate (CO₃²⁻), or chloride (Cl⁻), respectively]. A detailed description of structural properties of both magnetite and GR is presented in the section 2 of this review.

Mixed-valent Fe minerals are among the most reactive iron compounds due to their role in biogeochemical cycling of trace elements, their ability to affect the mobility, redox transformation, and toxicity of various organic and inorganic pollutants, and their use in various environmental remediation strategies. A large amount of research concerning mixed-valent iron oxides has been carried out in recent decades, but despite

the immense amount of collected research data, no comprehensive review of this topic has been published. Our review article is intended to compile the research data related to all aspects of mixed-valent Fe minerals (magnetite and GR), including their characteristics, presence, formation, and role in the environment.

Only narrow aspects of this wide research field were reviewed so far. For example, a very recent review article by Su⁴ describes the environmental applications of engineered magnetite nanoparticles and its hybrid composites. Munoz et al.,⁵ in 2015, reviewed various methods to form magnetite-based catalysts followed by their efficiency to improve Fenton oxidation for treatment of industrial wastewater. In 2013, Tang et al.⁶ presented a comprehensive review of various factors to be considered for sustainable environmental application of magnetic nanomaterials like magnetite, maghemite, and zero-valent iron (Fe⁰). Another review article in 2012 discussed the catalytic role of various iron oxides to improve Fenton oxidation.⁷ In 2008, Trolard et al.⁸ reviewed the iron cycle with a special focus on the GR and consequences of its reactivity on geochemical cycles of Fe and other elements. The monography by Cornell and Schwertmann² (first published in 1996 and revised in 2003) is by far the most comprehensive document on iron oxides that compiles all related aspects in one volume. In 2001, Hansen³ reviewed the environmental chemistry of GRs with focus on their formation, stability, and environmental applications. In addition to these reviews, mixed-valent iron oxides were also discussed as a part of review articles along with other reactive minerals.^{9–13} It should be noted that biomedical applications of magnetite are not within the scope of this review and thus are disregarded as well as modified forms of these minerals or pure end member minerals such as Fe(III) oxides (e.g., goethite) with adsorbed Fe(II).

Here, we compile the research data from numerous publications working on different aspects related to magnetite and GR in the environment. As a first part of this review, the properties of these mixed-valent Fe minerals are discussed. Depending on the nature of the initial precursor, routes of synthesis can be tailored to tune the properties of the final product. This connection to the structural properties, magnetic measurements, redox potential, and stoichiometry [i.e., the relative proportions of Fe(II) and Fe(III)] is critically illustrated in the properties section. Next the occurrence of these mixed-valent Fe minerals is discussed both in near surface natural settings and engineered systems (as the corrosion of manmade materials) in the environment. Note that reactions and formation of these minerals in deep geological settings at high temperature or pressure are outside the scope of this work. Common methods of synthesizing mixed-valent Fe minerals are outlined, including abiotic [coprecipitation, Fe(II) oxidation, Fe⁰ oxidation, and transformation of Fe(III) oxides] and biotic techniques [bacterial Fe(II) oxidation or Fe(III) reduction]. The synthesis section highlights various mechanisms involved in the formation of mixed-valent Fe minerals. The characterization section describes various techniques which are frequently used to identify the mineralogy or morphology of the target minerals. The environmental applications section reviews the use and efficiency of mixed-valent Fe minerals to remediate pollutant contamination via sorption, reductive transformation, and advanced oxidation processes. This review article intends to provide an authoritative reference for the numerous researchers working on various aspects of mixed-valent Fe minerals in near surface environments.

Table 1. Overview of Iron Oxides^a

oxide-hydroxides and hydroxides	oxides
goethite α -FeOOH	hematite α -Fe ₂ O ₃
lepidocrocite γ -FeOOH	magnetite Fe ₃ O ₄ [Fe(II)Fe(III) ₂ O ₄]
akaganéite β -FeOOH	maghemite γ -Fe ₂ O ₃
schwertmannite Fe ₁₆ O ₁₆ (OH) _y (SO ₄) _z ·nH ₂ O	β -Fe ₂ O ₃
δ -FeOOH	ϵ -Fe ₂ O ₃
feroxyhyte δ' -FeOOH	wüstite FeO
high pressure FeOOH	
ferrihydrate Fe ₃ HO ₈ ·4H ₂ O	
bernalite Fe(OH) ₃	
Fe(OH) ₂	
green rusts Fe(III) _z Fe(II) _y (OH) _{3x+2y-z} (A ⁻) _z ; A ⁻ = Cl ⁻ ; 1/2 SO ₄ ²⁻	

^aReproduced with permission from ref 2. Copyright 2003 Wiley-VCH.

2. PROPERTIES OF MIXED-VALENT IRON MINERALS

2.1. Structural Properties

Magnetite. Magnetite is a member of the spinel class of minerals (named after spinel; MgAl₂O₄) that contain mixed anions and cations. The general formula for spinels is AB₂O₄ where A and B designate divalent and trivalent metallic cations, respectively. A spinel structure contains all divalent cations on tetrahedral sites, while all trivalent cations are in octahedral coordination. However, in an “inverse” spinel structure, octahedral sites are shared by divalent and trivalent cations. Magnetite is an inverse spinel, and its structural formula can be written as Fe(III)_{tet}[Fe(II) Fe(III)]_{oct}O₄²⁻. Structurally, it contains two iron sublattices (Figure 1) including a tetrahedral coordination (Fe_{tet}) occupied by Fe(III) and an octahedral coordination (Fe_{oct}) bearing Fe(II) and Fe(III).¹⁴ Alternating planes of Fe_{tet} and Fe_{oct} are stacked along [111] in magnetite structure (Figure 1). Magnetite exhibits the highest electrical conductivity (1 – 10 Ω⁻¹ m⁻¹) among iron oxides,² which is attributed to the rapid migration of mobile charges by electron hopping on Fe occupied sites¹⁴ or by hopping of mobile Fe(II) between unoccupied lattice sites.¹⁵

It is interesting to point out that many studies have evidenced that iron dissolution in magnetite preferentially occurs at Fe_{oct} in mildly acidic medium (pH 2–2.5).^{16–18} Only

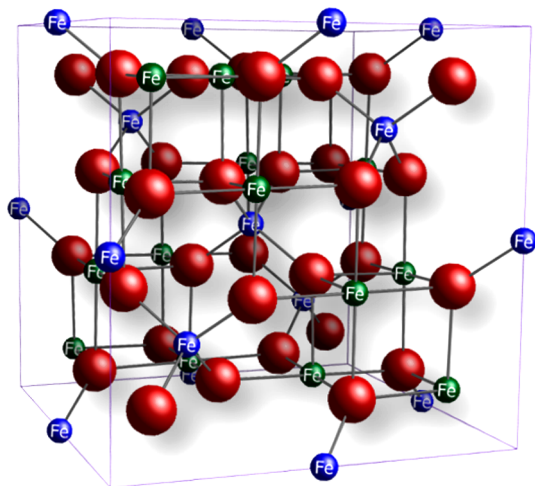


Figure 1. Ball and stick model of the unit cell of magnetite. Octahedral Fe ions are in green, tetrahedral Fe ions are in blue, oxygen ions are in red. Created using CrystalMaker for Windows version 2.2.

octahedral Fe was preferentially exchanged when magnetite is reacted with aqueous Fe(II).^{16–18} However, Gorski et al.¹⁵ did not indicate any preferential exchange of octahedral or tetrahedral sites when ⁵⁶Fe(II) was reacted with magnetite at circumneutral pH. In this regard, they proposed two mechanisms (Fe atom diffusion and bulk electron conduction) that might be responsible for atom exchange of aqueous Fe(II) and magnetite.¹⁵

Green Rust: Chemical Composition of the Interlayer and Structural Models. The general structural formula of GRs can be written as [Fe(II)_{1-x}Fe(III)_x(OH)₂]^{x+}. [(x/n)Aⁿ⁻, mH₂O]^{x-}, where Aⁿ⁻ denotes intercalated anions and *x* represents the molar fraction of trivalent cation that usually ranges from 0.25–0.33. Structurally, GR consist of brucite-like layers containing both divalent and trivalent cations that are interlayered by anions and structural water. Owing to this type of layered structure, GRs are placed in layered double hydroxides class of minerals, also known as anionic clays. Detailed description of iron-based layered double hydroxides has been provided by Ruby et al.¹⁹ Metal hydroxide sheets have a positive charge which is correlated to the partial replacement of divalent by trivalent metal cations. There are a variety of anions which are intercalated in the GR structure including (i) simple monovalent anions (e.g., Br⁻, Cl⁻, F⁻), (ii) divalent oxoanions (e.g., CO₃²⁻ and SO₄²⁻), (iii) organic anions of varying sizes (e.g., HCOO⁻, C₂O₄²⁻, and CH₃(CH₂)₁₀COO⁻), and surfactants. The chemical formula, space group, cell parameters, and interlayer distance of GR(SO₄²⁻), GR(CO₃²⁻), and GR(Cl⁻) are summarized in Table 2. GR intercalating other anions such as selenite,²⁰ formate,²¹ C₉–C₁₄ linear alkyl carboxylates,²² and oxalate²³ can be obtained by oxidation of [Fe(OH)₂ and Fe(II)] mixtures (section 4.1.2).

The structure and composition of GRs is dependent on the nature of intercalated anions. For instance, Bernal et al.²⁷ divided the GR family into two groups based on their X-ray diffraction (XRD) data: GR-I with a rhombohedral unit cell and GR-II with a hexagonal unit cell. Planar or spherical anions (e.g., CO₃²⁻, Br⁻, and Cl⁻) lead to GR-I consisting of three repeat units (Figure 2a) and three-dimensional anions (e.g., SO₄²⁻ and SeO₄²⁻) are indicative of GR-II that are composed of 2 repeat units (Figure 2b).^{24,26,28,29} These types represent quite different interplanar distances of the stacking sequence along the *c* axis (*d*₀ = 7.6–8 Å and 10.9 Å for GR-I and GR-II, respectively). The hydroxide sheets in GR-II are separated by interlayers composed of two adjacent planes of anions and water molecules, as compared to the one plane in GR-I.²⁴ In an elementary stratum of GR-II, stacking sequence is described as

Table 2. Crystallographic Data of Three Types of Green Rust (GR)^a

type of green rust	GR(SO ₄ ²⁻)	GR(CO ₃ ²⁻)	GR(Cl ⁻)
chemical formula	Fe(II) ₄ Fe(III) ₂ (OH) ₁₂ SO ₄ ·8H ₂ O	Fe(II) ₄ Fe(III) ₂ (OH) ₁₂ CO ₃ ·3H ₂ O	Fe(II) ₃ Fe(III)(OH) ₈ Cl·~1.5H ₂ O
space group	<i>P</i> $\bar{3}$ <i>m</i> 1	<i>R</i> $\bar{3}$ <i>m</i>	<i>R</i> $\bar{3}$ <i>m</i>
<i>a</i> (Å)	5.5524 ²⁴	3.1759 ²⁵	3.19 ²⁶
<i>c</i> (Å)	11.011 ²⁴	22.7123 ²⁵	23.85 ²⁶
<i>d</i> ₀ (Å)	11.011	7.57	7.95

^aThe values of *a* and *c* are the cell parameters and *d*₀ corresponds to the interlayer distance.

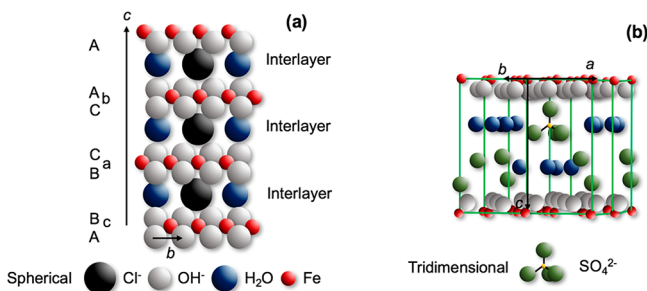


Figure 2. General view of the crystal structure of green rusts: (a) GR-I (Cl⁻) and (b) GR-II (SO₄²⁻). Image (a) is adapted with permission from ref 26. Copyright 1998 Elsevier. Image (b) is adapted with permission from ref 24. Copyright 2003 Elsevier Masson SAS.

AcBij..., where *A* and *B* denote planes of OH⁻ ions, *c* represents that of Fe cations and *i* and *j* denote interlayers planes. In this stratum, molecules of *i* and *j* planes are located close to the positions of *A* and *B* [(~*A*) and (~*B*)], respectively, yielding a hexagonal close-packed stacking of oxygen atoms *AcB*(~*A*)-(~*B*)... On the other hand, *AcB*(~*B*)..., is the sequence in an elementary stratum of GR-I where water molecules in interlayers are located vertically above OH⁻ ions of adjacent hydroxide layers.^{24,26}

The successive strata are also arranged differently in crystal structure of both GRs that is due to location of intercalated water molecules.²⁴ Simon et al.²⁴ proposed that the *AcB*(~*B*)...sequence in GR-I induces a three-layer repeat *AcB*(~*B*)*BaC*(~*C*)*CbA*(~*A*)...leading to a rhombohedral structure. In GR-II, only one single-layer repeat is induced by *AcB*(~*A*)-(~*B*)...sequence yielding a primitive hexagonal cell. However, Christiansen et al.³⁰ proposed a different structural model with Na inside structure based on their data for GR-II (GR-SO₄) (contrary to the model by Simon²⁴ et al. without Na). Structural model by Christiansen et al.³⁰ proposed different orientation of SO₄²⁻ anions and inclusion of Na atoms in the interlayer. They pointed out that SO₄²⁻ tetrahedra bases were nearest to the hydroxide layers; their apexes point into the interlayer space, and they are surrounded by three water molecules. However, Simon et al.²⁴ oriented the SO₄²⁻ so the apical oxygen was nearest to the hydroxide layer to achieve best refinement results. It should be noted that the solid was prepared in the presence of Na in both cases. Christiansen et al.³⁰ proposed its chemical formula as NaFe(II)₆Fe(III)₃(SO₄)₂(OH)₁₈·12H₂O that led to a Fe:SO₄²⁻ ratio of 9:2 = 4.5 due to an excess of Na inside the structure. However, this ratio was found very close to 6:1 (without Na) in another laboratory measurement³¹ as proposed in the previous formula of Fe(II)₄Fe(III)₂(OH)₁₂SO₄·H₂O by Simon et al.²⁴ Some quantity of Na (<3 at. %) is often found associated to GR as observed by transmission electron microscopy coupled with an energy dispersive X-ray system (TEM-EDX),³² but there is no clear evidence that the Na atoms are located in the interlayer.

On the basis of this disagreement in literature, further research should be conducted to identify a definitive structural model. It should be noted that if alkaline metal cations are part of the GR interlayer, then many chemical compositions reported in the literature should be reconsidered.

Génin et al.³³ described GR-I with stacking sequence of *AcBiBaCjCbAkA...*, where *A*–*C*, *a*–*c*, and *i*–*k* denote OH⁻ planes, metal cation layers, and intercalated layers, respectively.^{24,34}

2.2. Fe(II):Fe(III) Ratio

Mixed-valent Fe minerals can have a range of oxidation states dependent upon the amount of structural Fe(II) which can be discussed quantitatively as their stoichiometry ($x = \text{Fe(II)}/\text{Fe(III)}$).³⁵ Magnetite containing ideal Fe(II) contents ($x = 0.5$) is known as stoichiometric magnetite (assuming Fe(II)Fe(III)₂O₄ formula). In stoichiometric magnetite, Fe(III) occupies both tetrahedral and octahedral sites equally, while Fe(II) is only located in the octahedral sites. However, stoichiometric GRs ($\sim 3 \leq x \leq 2$) contain at least two times more Fe(II) than stoichiometric magnetite. Oxidation of mixed-valent Fe minerals causes a decrease in Fe(II)/Fe(III) ratio ($x < 0.50$ and $x < 2$ for magnetite and GR, respectively) which is denoted as a partially oxidized or nonstoichiometric phase. Stoichiometry is also defined in the literature as $R = (\text{Fe(III)})/(\text{Fe(II)} + \text{Fe(III)})$ and its value is 0.67 and 0.25–0.33 for stoichiometric magnetite and GR.³⁶ The structure of nonstoichiometric magnetite is often expressed as Fe_{3- δ} O₄, where δ represents the departure from stoichiometry. Its (δ) value can range from zero (stoichiometric magnetite) to 1/3 (completely oxidized). Complete oxidation of magnetite ($x = 0$) yields maghemite. This formula can be written as Fe(III)_{tet}[Fe(II)_{1-3 δ} Fe(III)_{1 + 2 δ}]_{oct}O₄, where \square are vacancies formed in the crystal structure to account for charge balance.³⁵ For magnetite, the following equation can be used to easily convert the stoichiometry to and from the different notations:³⁵

$$x = \frac{\text{Fe(II)}}{\text{Fe(III)}} = \frac{1 - 3\delta}{2 + 2\delta} \quad (1)$$

Stoichiometry is mainly dictated by the synthesis method, source, experimental conditions, and aging time, etc.^{36,37} For example, Zegeye et al.³⁶ reported that the stoichiometry was different when magnetite was formed from lepidocrocite by bioreduction ($\delta \sim 0$) or by abiotic Fe(II)-induced mineralogical transformation ($\delta \sim 0.05$). In case of biogenic magnetite, the value of δ was very low (0.025) after one day of incubation but a full stoichiometric magnetite ($\delta \sim 0$) was obtained after one month of incubation.³⁶ The stoichiometry of the final mineral phase was also found to be dependent on the nature of the initial ferric oxides when magnetite was formed by abiotic transformations of ferrihydrite ($\delta \sim 0.04$), lepidocrocite ($\delta \sim 0.05$), and goethite ($\delta \sim 0.08$).³⁷

The stoichiometry of mixed-valent Fe minerals dramatically influences their reactivity and structural properties including crystalline structure,³⁸ reduction potential,^{39,40} sorption capacity,⁴¹ and catalytic ability in advanced oxidation processes.^{42–45} Stoichiometric phases ($\delta = 0$) or the ones containing higher Fe(II) contents are considered as the most reactive phases in this regard while nonstoichiometric phases have lost their reactive nature.^{39,43,44} A detailed description of the effect of stoichiometry of mixed-valent Fe minerals on their reactivity is presented in section 6. Exposing nonstoichiometric magnetite to a Fe(II) source can restore its stoichiometry ($x = 0.5$ or $\delta = 0$) through oxidation of adsorbed Fe(II), accompanied by reduction of the octahedral Fe(III) in the underlying magnetite to octahedral Fe(II).⁴⁰ The extent of aqueous Fe(II) uptake depends on the stoichiometry of magnetite. Gorski and Scherer⁴⁰ showed that Fe(II) uptake by the least stoichiometric magnetite ($x = 0.28$) was four times higher than by the most stoichiometric phase ($x = 0.48$). However, uptake of Fe(II) was limited by formation of stoichiometric magnetite.⁴⁰

Owing to the strong influence of stoichiometry, an accurate and precise measurement of stoichiometry is crucial in characterization of mixed-valent Fe minerals. There are various methods which are commonly used to measure their stoichiometry including (i) complete acidic dissolution,^{17,40,42,44} (ii) ⁵⁷Fe Mössbauer spectroscopy,^{36,37,46} (iii) powder XRD,^{46,47} and (iv) X-ray magnetic circular dichroism (XMCD).⁴⁸ Acidic dissolution is a simple way to measure stoichiometry, but care should be taken to avoid oxidation of Fe(II) in air. This method has limited application in natural and mixed phases containing redox-active compounds or functional groups that are attached to the particle surface.³⁵ For such samples, spectroscopic techniques are preferred because samples can be characterized without any additional pretreatment (such as washing). To measure stoichiometry, Mössbauer spectroscopy (section 5.2 for details) relies on the hyperfine parameters extracted from mineral spectra [relative area of Fe(II) and Fe(III) doublets] by appropriate fitting models.^{2,36} Powder XRD is based on the unit-cell length of magnetite which becomes smaller upon oxidation due to the lower size of Fe(III) as compared to the Fe(II) and formation of vacancies.³⁵ XMCD provides precise information of the relative site occupancies in spinels,^{49,50} which can be used to determine the stoichiometry of magnetite, especially at the surface of the mineral.⁴⁸ A detailed description of the XMCD technique is provided in section 5.4. It should be noted that many reported stoichiometry measurements of mixed-valent Fe minerals have relied mostly on singular techniques without validation by secondary analyses.^{36,37,44,51} Gorski et al.³⁵ indicated an excellent agreement between stoichiometry of magnetite measured by acidic dissolution and Mössbauer spectroscopy. A significant linear correlation was also reported between the unit-cell length of magnetite measured by powder XRD and magnetite stoichiometry measured by acidic dissolution or Mössbauer spectroscopy.³⁵

2.3. Redox Potential

In aqueous environments, the reactivity of a Fe mineral is strongly dependent upon its ability to undergo reduction (gain electrons) and oxidation (lose electrons) in redox reactions. As electrons do not freely exist in aqueous solution each reduction must be coupled to an oxidation and vice versa.⁵² The tendency of a mineral to gain or lose electrons is commonly referred to as

the redox potential (E) which is reported in volts (V) or millivolts (mV). The more positive the redox potential is, the stronger the oxidizing power of the mineral is, while by contrast the lower (more negative) the redox potential is, the strongest the reducing power of the mineral is. Redox potentials depend strongly upon several factors, including pH, temperature, and concentration of reactants. For example the self-induced redox potential reported for magnetite reduction to aqueous Fe(II) by White et al.⁵³ is seen to vary from +0.38 V at pH 3 to +0.27 V at pH 7. The presence of dissolved Fe(II) is a particularly important factor, since Fe minerals become significantly more reducing even in the presence of small Fe(II) concentrations. Due to the semiconducting properties of Fe minerals, there are several processes that might take place upon sorption of Fe(II) to the solid, including electron transfer, conduction, dissolution, atom exchange, and formation of secondary minerals. Gorski and Scherer presented a revised conceptual framework where the Fe(II) becomes oxidized upon sorption to Fe(III) minerals and different possible fates for the lost electron are presented.⁵⁴ The exact mechanism of this process is still under discussion. Furthermore, the redox potentials of solid oxides varies with crystal phase and grain size.⁵⁵

While there is extensive research into redox potential measurements of minerals, an in-depth understanding of mineral redox processes is still difficult to achieve. There are two main classic techniques to determine the redox potential of minerals: noninvasive electrochemical methods (e.g., redox electrodes) and dissolving the mineral to quantify the ratio of oxidized and reduced species and using these to calculate a theoretical Nernstian potential. Metallic redox electrodes commonly used to estimate redox potentials (such as Pt ring) usually do not provide reliable measurements in the case of minerals due to a number of factors such as sorption of mineral to the electrode, lack of redox equilibria between the analyte and the electrode, and absence of active species in solution, among others.⁵⁶ On the other hand, dissolving the sample and quantifying the activity of redox active species is a time-consuming and experimentally troublesome method, where anoxic conditions are required for satisfactory results.

Nevertheless, in order to determine redox potentials of minerals, many studies have developed indirect measurements such as through reactions between the Fe minerals and probe compounds (e.g., nitrobenzene and quinones).^{56,57} Alternatively, mediated electrochemical techniques make use of dissolved redox active compounds, which facilitate electron transport between mineral and electrode.⁵⁸ Consequently, through various theoretical and measurement-based techniques,^{58,59} the standard redox potentials of a number of different Fe(III) minerals have been determined for their reduction to Fe(II) (Table 3).

The redox behavior of the mixed-valent mineral magnetite, however, remains relatively poorly understood. This is in part due to the complication that more than one redox-active species [e.g., Fe(II) and Fe(III)] at different potentials are present in magnetite at the same time, which can lead to “mixed potentials” which simultaneously contribute to the net measured potential.⁶⁰ Similar observations have been reported for iron-bearing clays at different Fe(II) to Fe(III) ratio, where a distribution of redox potentials was modeled.⁶¹ Therefore, a wide range of redox potentials for magnetite at neutral pH have been quoted in the literature, including +0.27 V,⁵³ −0.314 V,⁵⁵ and −0.38 V⁶² when measured against the standard hydrogen electrode (SHE). The reason for this discrepancy in redox

Table 3. Standard Redox Potentials (E^0) of Iron Minerals (vs SHE)^a

	ferrhydrite	lepidocrocite	goethite	hematite
reaction	$\text{Fe}(\text{OH})_3 + \text{e}^- + 3\text{H}^+ = \text{Fe}^{2+} + 3\text{H}_2\text{O}$	$\gamma\text{-FeOOH} + \text{e}^- + 3\text{H}^+ = \text{Fe}^{2+} + 2\text{H}_2\text{O}$	$\alpha\text{-FeOOH} + \text{e}^- + 3\text{H}^+ = \text{Fe}^{2+} + 2\text{H}_2\text{O}$	$0.5\alpha\text{-Fe}_2\text{O}_3 + \text{e}^- + 3\text{H}^+ = \text{Fe}^{2+} + 1.5\text{H}_2\text{O}$
theoretical ⁵⁹	1.06 V	0.86 V	0.71 V	0.73 V
chemical reduction ⁵⁹	0.939–1.031 V	0.892–0.938 V	0.720–0.790 V	0.764–0.828 V
mediated potentiometry ⁵⁸	–	–	0.768 V	0.769 V

^a“Theoretical” refers to values calculated from free standard enthalpies of formation; ⁵⁹“chemical reduction” refers to experimental quantification of ferrous iron after reduction of minerals with H_2 ; ⁵⁹“mediated potentiometry” refers to values obtained by measuring redox potential of mineral suspensions using a Pt redox electrode in the presence of a soluble electron transfer mediator. ⁵⁸ $\text{Fe}(\text{OH})_3$ is a generic form of a more complex structure of ferrhydrite which is still under debate.

potentials for magnetite has been suggested to be due to variations in the Fe(II)/Fe(III) ratio of the samples under investigation.³⁹ Gorski et al.³⁹ measured the redox potential in terms of the open circuit potential (E_{OCP}) of a wide range of magnetite’s with different stoichiometry. The study found that stoichiometric magnetite [Fe(II)/Fe(III) = 0.5] had the lowest redox potential, while the fully oxidized end member maghemite [Fe(II)/Fe(III) = 0] had the highest redox potential (Figure 3). This linear relation between redox

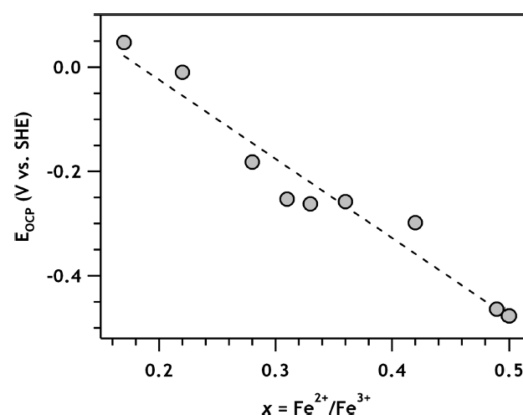


Figure 3. Open circuit potentials (E_{OCP}) of magnetite as a function of stoichiometry [Fe(II)/Fe(III) ratio]. Reproduced from ref 39. Copyright 2010 American Chemical Society.

potential and stoichiometry also has important implications in the ability for magnetite to be used as a remediation agent for different environmental pollutants.^{40,63}

2.4. Magnetic Properties

This section will focus primarily on the magnetic properties of magnetite (also known as Lodestone) which is thought to be the oldest magnetic material known to man and has been described as the most important magnetic mineral on Earth. In the environment, iron deposits can be naturally magnetized though lightning strikes; however, it is also derived from a number of different sources, including the breakdown of igneous rocks (e.g., basalt), from volcanic eruptions, Fe(III)-reducing, Fe(II)-oxidizing, and magnetotactic bacteria (see section 4.2), as well as through anthropogenic pollution.⁶⁴ The magnetic properties of these types of magnetite are hugely diverse, making it challenging to specify any one particular type being more environmentally relevant than the other. For instance, titanium-substituted magnetite (ilvospinel) typically forms via magmatic processes as oppose to microbiological pathways or during sedimentation. Nevertheless, it is often reported as the most common magnetic mineral and is the main source of rock magnetism on Earth;⁶⁵ however, its inclusion in this review is restricted.

To most effectively understand the reasons why magnetite is magnetic, it is important to consider the general crystal structure of the mineral. Magnetite has an inverse spinel crystal structure with a cubic unit cell ($a = 8.396 \text{ \AA}$) in which 32 oxygen ions are arranged in an approximately close packed array (Figure 1). Iron ions fill some of the spaces between the oxygen ions. Specifically, eight Fe(II) and eight Fe(III) ions are arranged in octahedral (B) coordination surrounded by six oxygen ions, and eight Fe(III) ions are arranged in tetrahedral (A) coordination surrounded by four oxygen ions. This means that the ratio of Fe(III) to Fe(II) is 2:1 which maintains charge

neutrality in combination with the O^{2-} ions. Each Fe(II) and Fe(III) ion has a magnetic moment of 4 and 5 μ_B , respectively. Magnetic exchange interactions exist between neighboring Fe ions in which the A site ions are arranged in antiparallel orientation to the B site ions. This results in the magnetic spin orientations of all A site ions being arranged in parallel and opposite directions to magnetic spin orientations of all B site ions. Since Fe(III) ions occupy A and B sites equally, there is no net magnetization from these ions because their spin states cancel each other out. This gives rise to a net magnetization due to the Fe(II) ions in the B site which for bulk magnetite is reported as 92 $Am^2 kg^{-1}$.⁶⁶ As a result of this distribution of magnetic ions within the mineral, any changes to the Fe(II)/Fe(III) ratio can have a significant effect on the bulk magnetic properties of the magnetite. For example, maghemite ($Fe(III)_{Tet}[Fe(III)_{5/3}\square_{1/3}]_{Oct}O_4$) is the fully oxidized form of magnetite, containing no Fe(II), and is known to have a lower bulk saturation magnetization (M_s) of $\sim 75 Am^2 kg^{-1}$ at room temperature. Other factors which also influence the magnetic properties of the mineral include the particle size⁶⁷ and the inclusion of transition metals such as cobalt, zinc, and titanium.^{68,69} For zinc, Zn(II) ions replace Fe(III) in tetrahedral lattice sites which suppresses part of the antiparallel magnetic moment. This means that the magnetic moment of the octahedral lattice becomes larger relative to the tetrahedral moment and the Zn-doped magnetite becomes more magnetic. In the case of cobalt, Co(II) replaces octahedral Fe(II) which should in principle make the mineral less magnetic; however, due to the magnetic moment of the Co(II) ion, this decrease is relatively minor. Instead, the presence of Co(II) increases the coercivity of the Co-doped magnetite, which makes it harder to switch the magnetization direction of the mineral. Such a property is advantageous for biomedical applications such as cancer therapy or targeted drug delivery.⁷⁰ In titanomagnetite, Ti(IV) are situated in the B sites which means that in order to maintain overall charge neutrality, some of the Fe(III) ions must be replaced to Fe(II). Ülvospinel (Fe_2TiO_4) consists of Fe(II) ions on the A site, and an equal amount of Fe(II) and Ti(IV) on the B site. Since Ti(IV) has no magnetic moment, the net magnetization of ülvospinel is consequently much lower than that of magnetite (Table 4).

Table 4. Magnetic Properties of Some Typical Environmental Minerals^{77a}

mineral	formula	T_c (°C)	M_s ($Am^2 kg^{-1}$)
iron	Fe	770	218
magnetite	Fe_3O_4	575–585	90–922
ülvospinel	Fe_2TiO_4	–153	0
jacobsite	$MnFe_2O_4$	~ 300	77
trevorite	$NiFe_2O_4$	585	51
greigite	Fe_3S_4	~ 333	~ 25

^a T_c , Curie temperature and M_s , saturation magnetization.

Several of the magnetic properties of magnetite depend upon temperature with one of the most characteristic features of magnetite referred to as the Curie temperature (T_c). T_c corresponds to the temperature above which magnetite is no longer magnetic and acts as a paramagnet. Essentially, above this temperature there is sufficient thermal energy for the magnetic ions within the mineral to become randomly orientated to each other, resulting in zero net magnetization. T_c can be determined through the measurement of magnetic

susceptibility over a range of temperatures and is generally observed to take place at ~ 580 °C. For a sample of pure stoichiometric magnetite, when the temperature is decreased again, the susceptibility curve will follow the heating curve. When these curves do not match, this could indicate the presence of nonstoichiometry or the presence of impurities in the mineral.⁶⁵

A second important characteristic temperature-dependent feature of magnetite is called the Verwey transition (T_v). The transition is often characterized by a significant step in the magnetization of magnetite at ~ 120 K and is a result of magnetite undergoing a transition from cubic crystal symmetry to a lower symmetry (likely monoclinic) structure.⁷¹ T_v is known to be sensitive to the presence of additional elements [e.g., Ti(IV)⁷² and Al(III)]⁷³ as well as the Fe(II)/Fe(III) ratio,⁷⁴ while its dependence upon size is less clear, especially in the superparamagnetic regime,⁷⁵ and for many synthetic magnetite does not appear to be present at all.⁷⁶ This transition is also observable to some extent using Mössbauer spectroscopy and is thought to correspond to the point at which electron hopping between Fe(II) and Fe(III) sites within the A site no longer takes place. Within Mössbauer, this is characterized by the requirement to add an additional sextet during fitting.

Ultimately, it is possible to identify the presence of different mixed-valent minerals, in particular magnetite and minerals from the spinel group, within environmental samples through the use of magnetic characterization methods.

2.5. Thermodynamic Properties

The standard Gibbs energy of formation (ΔG_f°) of the synthetic GR minerals were most often determined by redox potential measurements performed during oxidation of $[Fe(OH)_2, Fe(II)_{aq}]$ mixtures by dissolved O_2 in contact with ambient air (detailed in section 4.1.2). As discussed in a recent reevaluation of thermodynamic data concerning GR ($C_2O_4^{2-}$),²³ the position of the redox potential plateau is used for the determination of the value of ΔG_f° (GR). These authors indicated that the equilibrium potential of the $Fe(OH)_2/GR$ couple should be determined under anoxic conditions and should be calculated by using the same initial value of the Gibbs energy of $Fe(OH)_2$ [i.e., ($\Delta G_f^\circ(Fe(OH)_2) = -490 \pm 1 kJ mol^{-1}$)].²⁹ The values of ΔG_f° of both GR intercalating different anions and stoichiometric magnetite⁷⁸ are given in Table 5. The ΔG_f° value of anhydrous GR(SO_4^{2-}) is

Table 5. Gibbs Standard Energy of Formation (ΔG_f°) of the Dehydrated (Anhydrous) Forms of Green Rust and Magnetite

mineral type	ΔG_f° ($kJ mol^{-1}$)	ref
$Fe(II)_4Fe(III)_2(OH)_{12}SO_4$	-3790 ± 10	29
$Fe(II)_4Fe(III)_2(OH)_{12}SO_4$	-3819.44 ± 6.44	79
$Fe(II)Fe(III)_2(OH)_{12}CO_3$	-3590 ± 10	23
$Fe(II)_6Fe(III)_2(OH)_{16}C_2O_4$	-4712 ± 9	23
$Fe(II)_3Fe(III)(OH)_8Cl$	-2146 ± 5	23
Fe_3O_4	-1012.57	78

very reliable since it was determined independently by Ayala-Luis et al.⁷⁹ and Refait et al.²⁹ by using a completely different experimental approach {i.e., slow acid titration of $GR(SO_4^{2-})$ and oxidation of $[Fe(OH)_2, Fe(II)_{aq}]$ mixtures}. GR is thermodynamically metastable in comparison with magnetite. Indeed, Refait et al.⁸⁰ showed that if $GR(SO_4^{2-})$ and magnetite are considered in a Eh-pH Pourbaix diagram, the large stability



Figure 4. Soil containing fougèrite with bluish-green color. From Trolard et al.⁸⁶ (2007, Figure no. 1). Reproduced with kind permission from The Clay Minerals Society, publisher of *Clays and Clay Minerals*.

domain of magnetite will always overlap the stability domain of GR(SO_4^{2-}). For kinetic reasons, GR can form much more rapidly than magnetite, in particular in Fe(II)-rich aqueous medium as observed in coprecipitation experiments⁸¹ and during transformation of ferric minerals.⁵¹ However, in strongly alkaline solution ($\text{pH} > 10$) or acidic solution ($\text{pH} < 5$), GRs rapidly transform either into $[\text{Fe}_3\text{O}_4$ and $\text{Fe}(\text{OH})_2]$ or $[\text{FeOOH}$ and $\text{Fe}(\text{II})_{\text{aq}}]$ mixtures, respectively.

3. OCCURRENCE OF MIXED-VALENT IRON MINERALS IN THE ENVIRONMENT

Mixed-valent Fe minerals are commonly present under very diverse environmental and geochemical conditions or as the products of the corrosion of manmade materials. The occurrence of these mineral phases is discussed below.

3.1. Natural Environments

The occurrence of Fe(II)/(III) hydroxides, termed “green rusts”, was mentioned for the first time in a Ph.D. dissertation by Keller in 1948 (cited by McGill et al.⁸² and Bearcock et al.⁸³). The mineralogist Reginald Taylor was the first to propose that the bluish-green color in hydromorphic gleysol (Figure 4) could be associated to the presence of GR.⁸⁴ For the first time in 1997, Trolard et al.⁸⁵ identified GR in hydromorphic soil sampled from the forest of Fougères (Brittany, France) by using Mössbauer and Raman spectroscopies. In recognition of its original sampling location, this GR sample has been named fougèrite, which was approved by the International Mineralogical Association in 2004.^{86,87} Feder et al.⁸⁷ used a miniaturized Mössbauer spectrometer (MIMOS) for an in situ study of gleysol. Formation of fougèrite was observed by coprecipitation of Fe(II), Fe(III), and Mg(II) when soil is oversaturated with water and dissolved O_2 enters the system. The authors linked GR formation to the interconversion of lepidocrocite and fougèrite due to seasonal fluctuations and soil medium characteristics (dissolved O_2 , higher organic matter supply, alternating oxic/anoxic conditions). Feder et al.⁸⁷ also observed that Fe(II)/Fe(III) of fougèrite increases with depth as x [i.e., the Fe(II)/Fe(III) ratio] was 0.5 in upper soil horizon displaying oximorphic characteristics but increased to 2 in the deepest horizons showing reductomorphic properties.

Owing to its high reactivity and poor stability, the occurrence of GR has rarely been reported in natural settings. More recently, the occurrence of GRs have also been reported in five other natural environments: (i) within ochreous sediments from an abandoned coal mine drainage system where the GR layer was formed below (4 mm) the surface (South Wales, UK),⁸³ (ii) in groundwater sampled below the water table from an artesian well in a chalk aquifer and from deep granite fractures in an underground tunnel (Denmark),⁸⁸ (iii) in the iron(II)-rich stratified (oxic/anoxic) lake Matano (Indonesia),⁸⁹ in CO_2 -rich soils on a mofette field (Czech Republic),⁹⁰ and in metal-polluted uranium mine drainage crossing the transition zone between anoxic subsurface and the oxic surface (Thuringia, Germany).⁹¹ Similarly, putative identifications of GR-like phases were reported in buried 700,000 year old lacustrine deposits (Ohio, USA),⁹² in iron-rich sediment cores from a water reservoir (California, USA),⁹³ and in redox-morphic soil downhill from a perennial spring (Iowa, USA).⁹⁴ GRs in soil and water can form under circumneutral to alkaline conditions in anoxic or reduced environments by different abiotic or biotic processes which are described in detail in section 4. Keeping in view the order of preference for interlayer ions to replace each other ($\text{CO}_3^{2-} > \text{SO}_4^{2-} > \text{Cl}^-$),⁹⁵ Christiansen et al.⁸⁸ proposed that the formation of GR- (CO_3^{2-}) would be favored in freshwaters having abundant CO_3^{2-} . However, SO_4^{2-} dominates in replacement order when $\text{SO}_4^{2-}/\text{CO}_3^{2-}$ is high and therefore will favor the formation of GR(SO_4^{2-}) in saline water because of higher SO_4^{2-} contents.^{88,96}

In contrast to GR, magnetite has widespread occurrence in natural environments due to higher stability and has been identified in multiple locations such as in river bed sediments (USA),⁹⁷ in well-drained soils (UK, USA),^{98,99} in semiarid wetland soils (Israel),¹⁰⁰ in gleysol (Germany),¹⁰¹ in Chinese loess and paleosols,¹⁰² in tholeiitic basalt (Brazil),¹⁰³ in Proterozoic zoned carbonatites (India),¹⁰⁴ in sand fraction of deeply weathered oxisol in savanna ecosystem (Brazil),¹⁰⁵ in alluvial soils near Fe–Pb mining site (Bulgaria),¹⁰⁶ in tropical lateritic soil profiles from southern India,¹⁰⁷ in sediments of three different Asian rivers draining into the South China Sea,¹⁰⁸ and in Fe-rich hydrocarbon contaminated soils and sediments from a former oil field (Germany)¹⁰⁹ and hydro-

carbon-contaminated sediments form a former military air base¹¹⁰ and in soils of a mofette field⁹⁰ (Czech Republic). Recently, magnetite has been suggested to have also precipitated in early Archean ocean environments.¹¹¹

Magnetite usually exists in the sand and silt fractions of soil rather than the clay fraction and is generally considered to have been inherited by weathering of the parent rock.^{105,112} Both biotic¹⁰¹ and abiotic⁹⁸ pathways were proposed to be relevant for magnetite formation in soils (for details, see section 4). However, a pedogenic origin for magnetite has been invoked by studies such as Viana et al.,¹⁰⁵ where magnetite and hematite were identified in an oxisol which has been developed from magnetite-free parent materials. Previously, Auerswald et al.¹⁰⁰ suggested formation of pedogenic magnetite by fire under reducing conditions in soil. Oldfield and Crowther¹¹³ proposed distinctive magnetic measurements to differentiate the magnetite formed by weathering and pedogenic magnetite formed by burning. Geiss et al.¹¹⁴ proposed anhysteretic remanent magnetization ratios and coercivity distributions to estimate pedogenic magnetite and this estimation was suggested as a tool to reconstruct past climate during paleosol formation.

Owing to the widespread occurrence and stability in natural environments, reactivity of natural magnetite has been explored for environmental remediation via sorption,^{115–118} reduction,¹¹⁹ and chemical oxidation (for details, see section 6).¹²⁰

3.2. Corrosion Products in Engineered Systems

Magnetite and GR have been observed as corrosion products of elemental iron in many engineered systems. In 1969, Stampfl¹²¹ discovered GR(CO₃²⁻) as corrosion product in municipal water pipes. McGill et al.⁸² reported the formation of GR, magnetite, and γ -FeOOH by corrosion of cast iron. Boucherit et al.¹²² used Raman spectroscopy for the first time to identify GR in the pitting corrosion films. Génin et al.⁹⁶ reported the coexistence of GR(SO₄²⁻), magnetite, and sulfate-reducing bacteria at steel piles corroded in a harbor area. Abdelmoula et al.¹²³ identified a layer of GR(CO₃²⁻) on the surface of metallic iron corroded in NaHCO₃ solution (0.1 M). Only GR(CO₃²⁻) was noted even when samples were corroded at higher Cl⁻/HCO₃⁻ of 40. However, corrosion of mild steel in bicarbonate solution (0.1 M NaHCO₃) in the presence of Cl⁻ (0.15 M) and SO₄²⁻ (0.1 M) generated GR(Cl⁻) and GR(SO₄²⁻), respectively.¹²⁴ When both Cl⁻ (0.15 M) and SO₄²⁻ (0.1 M) were present along with bicarbonate, pitting corrosion product was a mixture of GR(Cl⁻) and GR(SO₄²⁻) as revealed from in situ investigations by Raman spectroscopy.¹²⁴ However, the presence of Cl⁻ ions was necessary to induce pitting in phosphate buffer (0.1 M) as no pitting was observed by SO₄²⁻ alone (i.e., without Cl⁻). Marine corrosion of steel immersed above the mudline for more than two decades resulted in rust layers which contained GR(SO₄²⁻) (outer strata), Fe(III) (oxyhydr)oxides (intermediate strata), and magnetite (inner strata).¹²⁵ Pineau et al.¹²⁶ identified GR(SO₄²⁻) during marine corrosion of steel at three French harbors and associated its formation with the presence of SO₄²⁻-reducing bacteria.

Neff et al.¹²⁷ identified magnetite as the dominant corrosion product in iron archeological artifacts buried in soil for centuries. Colombari et al.¹²⁸ identified the corrosion products for steel sheets either from automobiles in circulation for years or from sheets corroded in the laboratory. GR was only observed in the latter case; however, magnetite was present along with other iron oxides in both cases.

GR has also been observed as a corrosion product in Fe⁰ permeable reactive barriers.¹²⁹ The mineralogy of the corrosion products was correlated to the chemical composition of the water, type of water contaminants, amount of dissolved O₂ and presence of sulfate-reducing bacteria.^{129,130}

4. SYNTHESIS OF MIXED-VALENT IRON MINERALS

This section describes various routes through which mixed-valent Fe minerals can be synthesized including abiotic and biotic pathways. A brief sketch of these pathways is provided in the Figure 5 which are detailed in the following subsections.

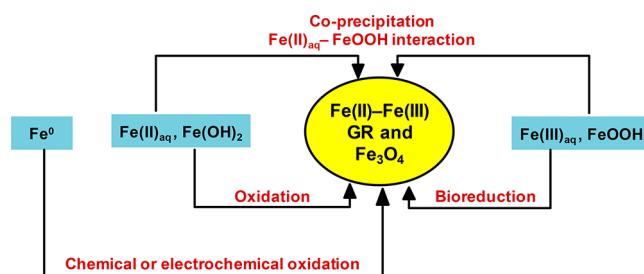


Figure 5. Overview of different pathways for the formation of magnetite (Fe₃O₄) and green rust (GR).

4.1. Abiotic Synthesis of Mixed-Valent Iron Minerals

4.1.1. Co-Precipitation of Dissolved Fe(II) and Fe(III) Species. Among various techniques to synthesize mixed-valent Fe minerals, coprecipitation is widely recognized as a convenient method due to ease, simplicity, and lack of any toxic intermediates.^{17,31,81,131} This method involves the mixing of a base with an aqueous mixture containing dissolved species of Fe(II) and Fe(III) at room temperature. Experiments are conducted under an inert atmosphere to prevent the inclusion of oxygen that is known to rapidly oxidize Fe(II) at circumneutral pH.¹³²

Formation of mixed-valent Fe minerals depends on Fe(II)/Fe(III) ratio, concentration of total Fe, pH, ionic strength, and the identity of present anions such as chloride, carbonate, or sulfate (in the case of GR).^{17,133} The coprecipitation route used to synthesize mixed-valent Fe minerals can be explained by a mass-balance diagram (Figure 6) which was created to interpret

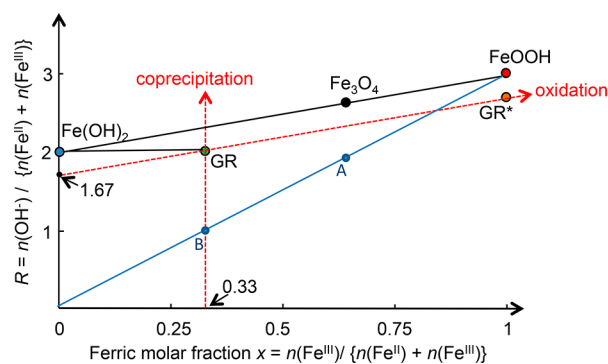


Figure 6. Mass-balance diagram representing the synthesis of magnetite (Fe₃O₄) and green rust via coprecipitation and oxidation. GR correspond to green rust and GR* to the fully oxidized form of GR (i.e., Mössbauerite). Point A corresponds to the mixture [2/3 FeOOH, 1/3 Fe(II)] and point B is mixture [1/3 FeOOH, 2/3 Fe(II)]. Adapted with permission from ref 31. Copyright 2006 Elsevier Masson SAS.

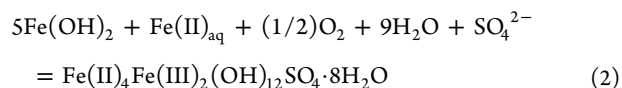
pH titration curves obtained during the coprecipitation of Fe(II) and Fe(III) soluble species in sulfate solutions.⁸¹ In this diagram (Figure 6), the ordinate $R = n(\text{OH}^-)/[n(\text{Fe(II)}) + n(\text{Fe(III)})]$ denotes the number of OH^- species per mole of Fe that are consumed during the formation of a given mixed-valent iron mineral. The abscissa $x = n(\text{Fe(III)})/[n(\text{Fe(II)}) + n(\text{Fe(III)})]$ denotes the molar fraction of trivalent cations. This mass-balance diagram allows visualization of the identity and relative extents of the Fe phase that may form depending upon the ferric molar fraction x of the initial reactants³¹ and the quantity of base added (i.e., the value of R). The formation of a biphasic system (A, B) is expected when the experimental point $P(x, R)$ is situated on a segment joining both P_A and P_B , where P_A and P_B correspond to the position of the compounds A and B in the mass balance diagram, respectively. The formation of a mixture of 3 phases [A, B, C] is expected if the experimental point $P(x, R)$ is located inside the triangle (P_A, P_B, P_C). The relative proportions of iron present in each phase can easily be determined by using the lever rules well-known for equilibrium binary and ternary phase diagrams.³¹ By using the values of $P(x, R)$ of the equivalent points of various titration curves combined to quantitative measurements performed with Mössbauer spectroscopy, it was demonstrated that $\text{GR}(\text{SO}_4^{2-})$ exists with a unique ferric molar fraction of $x = 1/3$ (i.e., $\text{Fe(II)}:\text{Fe(III)} = 2:1$). For x values higher and lower than $1/3$ of the formation of $[\text{GR}(\text{SO}_4^{2-}), \text{Fe}_3\text{O}_4]$ and $[\text{GR}(\text{SO}_4^{2-}), \text{Fe}(\text{OH})_2]$ mixtures was observed. On the contrary to $\text{GR}(\text{SO}_4^{2-})$, $\text{GR}(\text{CO}_3^{2-})$ was synthesized by coprecipitation with variable ferrous to ferric molar ratios ranging from $x \sim 1/4$ [$\text{Fe(II)}:\text{Fe(III)} \sim 3:1$] to $x = 1/3$.³² Formation of GR occurred in two steps: (i) the precipitation of a disordered solid compound and (ii) an interfacial reaction between clusters of hydroxylated ferrous species and the surface of the disordered solid compound leading to the formation of the GR crystals. $\text{GR}(\text{SO}_4^{2-})$ and $\text{GR}(\text{CO}_3^{2-})$ suspensions were shown to be unstable in strong alkaline condition ($\text{pH} > 10$) and both transform abiotically into $[\text{Fe}_3\text{O}_4, \text{Fe}(\text{OH})_2]$ and $[\text{Fe}_3\text{O}_4, \text{FeCO}_3]$ mixtures, respectively.

The formation of magnetite by coprecipitation of dissolved Fe(II) and Fe(III) species was studied in detail for a stoichiometric ferrous to ferric molar ratios, $x = 0.67$ [i.e. $\text{Fe(II)}:\text{Fe(III)} = 1:2$].¹³⁴ The experiments were performed at 25 °C by maintaining a constant pH with various types of bases (NaOH, NH_3 , and $\text{N}(\text{CH}_3)_4\text{OH}$). The size of the magnetite spheroidal crystals were kept in the range of ~ 1.5 – 12.5 nm by controlling the pH and the ionic strength of the solution. Interestingly, a critical pH, named pH^* and situated in a narrow range from 10.3 to 10.7 that depended on the value of the ionic strength, was identified. For pH values higher than pH^* , the secondary particle growth by Ostwald ripening did not occur anymore, and thermodynamically stable nanocrystals of magnetite were obtained due to a lowering of the interfacial tension γ induced by the adsorption of chemical species such as HO^- or cations of the electrolyte. For this reason, a strong decrease of crystal size was observed in the medium containing the smallest cations (e.g. Na^+ as compared to $[\text{N}(\text{CH}_3)_4]^+$), these species being the best screening ions.

4.1.2. Partial Oxidation of Hydroxylated Dissolved Fe(II) and $[\text{Fe(II)}_{\text{aq}}, \text{Fe}(\text{OH})_2]$ Mixture. *Formation of Green Rust.* The kinetics of oxidation of dissolved Fe(II) species by dissolved O_2 was studied by several authors^{135–137} with the general goal to obtain a better understanding of the behavior of Fe in natural aquatic environments. In their early work,¹³⁵

Stumm and Lee demonstrated that the kinetics of oxidation of dissolved Fe(II) species by air- O_2 at low concentration of Fe(II) ($\sim 10^{-5}$ M) was strongly dependent on the pH. The oxidation kinetics were accelerated by a factor of ~ 100 when the pH was increased by one unit in a narrow pH range situated between 7 and 8. In this range of pH, it was shown before¹³⁸ that fully hydroxylated dissolved Fe(II) species (i.e., $[\text{Fe}(\text{OH})_2]_{\text{aq}}^0$) are predominant as compared to other species such as $[\text{Fe}(\text{OH})]_{\text{aq}}^+$ and $\text{Fe(II)}_{\text{aq}}$, these being more stable at acidic pH. Interestingly, Stumm and Lee¹³⁵ note also that the oxidation of Fe(II) species may occur “in a stepwise fashion over the mixed iron(II)-iron(III) hydroxide” as suggested by Feitknecht and Keller.¹³⁹ This observation was confirmed later by Bernal et al.²⁷ who showed that GR compounds may incorporate various types of anions (Cl^- , Br^- , F^- , and SO_4^{2-}) when formed by aeration of ferrous salts solution and partially precipitated by NaOH. GR intercalating other anions such as selenite,²⁰ methanoate,²¹ C_9 – C_{14} linear alkyl carboxylates,²² and oxalate²³ were also obtained by oxidation of $[\text{Fe}(\text{OH})_2, \text{Fe(II)}]$ mixtures.

Other studies have also focused in depth on aeration of $[\text{Fe}(\text{OH})_2, \text{Fe(II)}]$ mixtures^{140,141} with Génin et al.¹⁴² able to determine that an accurate $\text{OH}^-:\text{Fe(II)}$ ratio of 5:3 (or 1.67) was necessary to fully transform the initial $[\text{Fe}(\text{OH})_2, \text{Fe(II)}]$ mixture into a single phase of $\text{GR}(\text{SO}_4)$. As later explained by Ruby et al.,¹⁴³ the oxidation reaction is represented by a line of slope 1 in the mass balance diagram (Figure 6) and corresponds to a chemical reaction that is independent of the pH. In the case of $\text{GR}(\text{SO}_4)$, this reaction can be written as the following:



The reaction was monitored by recording both the pH and redox potential E_h of the suspension and equilibrium condition leading to the observation of well-defined pH and E_h plateaus. By using this methodology, the Gibbs standard energy of formation ΔG_f° of $\text{GR}(\text{SO}_4^{2-})$, $\text{GR}(\text{CO}_3^{2-})$, and $\text{GR}(\text{Cl}^-)$ was determined (Table 5).

Formation of Magnetite. Ferrous hydroxide was easily transformed into magnetite during its oxidation by air at low temperature situated in a range between 25 and 65 °C.^{144–146} Similarly to the reaction leading to GR, the $\text{OH}^-:\text{Fe(II)}$ ratio used for the precipitation of the ferrous soluble species was shown to have a strong influence on the nature of the final products. For instance, an $\text{OH}^-:\text{Fe(II)}$ ratio lower than 2 can lead to the formation of ferric (oxyhydr)oxides such as goethite ($\alpha\text{-FeOOH}$) or lepidocrocite ($\gamma\text{-FeOOH}$) with GR as an intermediate compound. Both Olowe et al.¹⁴⁵ and Domingo et al.¹⁴⁶ demonstrated that pure magnetite is most frequently obtained for an initial $\text{OH}^-:\text{Fe(II)}$ ratio of 2, corresponding to the stoichiometric ratio leading to the formation of $\text{Fe}(\text{OH})_2$. In the presence of an excess of base ($\text{OH}^-:\text{Fe(II)} > 2$), either ($\text{Fe}_3\text{O}_4, \alpha\text{-FeOOH}$) mixture or single phase of $\alpha\text{-FeOOH}$ were observed. In order to better control the shape and the size of the magnetite crystals, other oxidants, most frequently nitrate (NO_3^-),^{147–149} were chosen to oxidize ferrous hydroxide. As proposed in the pioneering work of Sugimoto and Matijević,¹⁴⁷ these experiments need to be performed at a temperature of ~ 90 °C. Vereda et al.¹⁴⁹ showed recently that the presence of an excess of OH^- species in the initial solution promotes the formation of nanometric magnetite crystals (30–100 nm),

while micrometric crystals (0.4–1.1 μm) with increasing surface roughness were obtained in the presence of an excess of Fe(II) species.

4.1.3. Chemical or Electrochemical Oxidation of Zero-Valent Iron. *Electro-Generation of Green Rust.* Electro-generated GR was often synthesized by controlling the redox potential of the zero-valent anode (potentiostatic mode), while on the contrary, electro-generation experiments leading to magnetite were performed at an imposed current density (galvanostatic mode). Legrand et al.¹⁵⁰ studied in a systematic way the nature of the oxidation products formed on Fe⁰ in carbonated solutions. Voltammograms exhibited active domains with anodic peaks situated in a redox potential range situated in between ~ -0.55 V/SHE and ~ -0.45 V/SHE. For such values of redox potential imposed at the zero-valent anode, the chronoamperometric measurements exhibited a decrease of the current density showing that the Fe⁰ surface was rapidly covered by solid oxidation products. Depending on the concentration of carbonate species varying in a range situated in between 5×10^{-2} M and 1 M, the pH and the temperature ($25^\circ\text{C} < T < 90^\circ\text{C}$), 3 types of oxidation products [i.e., siderite (FeCO₃), GR(CO₃²⁻), and an amorphous ferric oxyhydroxide] were observed. The formation of GR(CO₃²⁻) as a single phase was observed in the whole temperature range at the lowest carbonate concentration for a pH range situated in between 8.4 and 9.8. For higher carbonate concentration, an imposed pH higher than 9 was necessary to avoid the formation of siderite. Refait et al.¹⁵¹ performed similar experiments (applied potential of ~ -0.6 V/SHE) in an aqueous medium containing a mixture of Cl⁻, SO₄²⁻, and CO₃²⁻ anions in a relative molar proportion of 50:3:0.3, respectively. Such an aqueous medium was used to mimic the condition found in seawater. It led to the formation of GR(SO₄²⁻) with some traces of GR(CO₃²⁻). As expected from the general trends observed for other layered double hydroxides, monovalent ions such as Cl⁻ were not preferentially intercalated into GR. Another study of Antony et al.¹⁵² performed on a gold anode was devoted to determining the Fe(II):Fe(III) ratio of electro-generated GR. It was shown that for both GR(SO₄²⁻) and GR(CO₃²⁻), this ratio was always very close to 2:1 in agreement with the values determined for GR synthesized by coprecipitation or by air oxidation of Fe(OH)₂.^{24,149} The lower Fe(II):Fe(III) value of 1:1 observed previously¹⁵³ was later attributed to the formation of an oxidized form of GR, a Fe(II)-Fe(III) oxyhydroxycarbonate named recently Mössbauerite,¹⁵⁴ that can be easily synthesized by oxidizing GR in situ without dissolution-reprecipitation.^{143,152}

Electro-Generation of Magnetite. The formation of magnetite on the surface of Fe⁰ electrodes has been the subject of several studies.^{155–157} The control of the imposed electro-oxidation current density, the type of anions present in the electrolyte, and the distance between the anode and the cathode were shown to be crucial for obtaining both magnetite as a single phase and a relatively narrow crystals size distribution. The presence of complexing agents (e.g., thiosulfates¹⁵⁵ and amine surfactants¹⁵⁶) were used to obtain nanoparticles of magnetite in a size range situated in between ~ 20 and ~ 45 nm. In a more recent study,¹⁵⁷ it was demonstrated that nanoparticles of magnetite can also be easily synthesized in surfactant-free electrolyte. The size of the crystals generally increased with increasing current density or by decreasing the distance between the anode and the cathode. The formation of a ferric precursor (γ -FeOOH) that formed

before magnetite was identified by X-ray diffraction¹⁵⁵ and later confirmed by Cabrera et al.¹⁵⁶ by analyzing the electrolyte suspension by UV spectroscopy. The role of the OH⁻ species generated by the reduction of water at the cathode or by adjusting the pH of the electrolyte with an alkaline solution was investigated more recently. It was suggested that the diffusion of OH⁻ species from the cathode to the anode governed the formation of the ferric precursor and finally magnetite. Indeed, the ferric precursor was proposed to be formed by the oxidation of ferrous hydroxide by dissolved O₂ at the surface of the Fe⁰ anode. The reaction was kinetically governed by both the rate of dissolution of Fe⁰ species into Fe(II)_{aq} species from the anode and by the diffusion of OH⁻ species produced on the cathode. The formation of magnetite was proposed to be due to “coprecipitation” between Fe(OH)₂ and the ferric precursor FeOOH at the surface of the Fe⁰ anode.¹⁵⁷

Controlled Chemical Oxidation of Zero-Valent Iron. The oxidation of Fe⁰ at the open circuit potential (i.e., without any applied current or potential) may also lead to the formation of magnetite or GR as single phases. Abdelmoula et al.¹²³ demonstrated that an α -iron(0) disk immersed in an aerated 0.1 M NaHCO₃ solution at a pH of 8.3 is covered after 5 days of reaction by a thick green film that was characterized to be GR(CO₃²⁻) by conversion electron Mössbauer spectroscopy (CEMS) performed at 78 K. The reaction of Fe⁰ powder in contact with a flow of deaerated water solution containing carbonate and calcium ions was studied in column experiments by Jeon et al.¹⁵⁸ Raman spectroscopy revealed that magnetite was formed at the surface of iron with Fe(OH)₂ forming as an initial precursor. Huang and Zhang¹³⁰ studied the role of dissolved Fe(II) species during the oxidation of Fe⁰ by dissolved oxygen and NO₃⁻. It was shown that the oxidation of Fe⁰ by dissolved oxygen was strongly enhanced by the presence of dissolved Fe(II)_{aq}, leading to the formation of a bilayer structure consisting of an inner layer of magnetite and an outer layer of γ -FeOOH. The study of the kinetics of formation of the corrosion products indicated that γ -FeOOH was formed initially at the Fe⁰ surface and was progressively replaced by Fe₃O₄ concomitantly to the decrease of DO observed during the oxidation reaction. The formation of magnetite was suggested to occur at the Fe⁰/ γ -FeOOH layer by the autoreduction of γ -FeOOH by Fe⁰. After 24 h of reaction, γ -FeOOH disappeared completely and magnetite as a single phase was observed on the Fe⁰ surface.

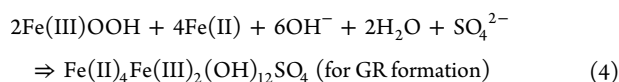
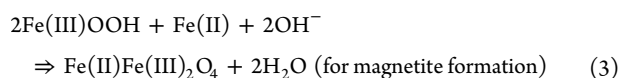
4.1.4. Interaction of Fe(II) with Fe(III) (Oxyhydr)oxides.

Interaction of ferric (oxyhydr)oxides with aqueous Fe(II) can transform them into other ferric and/or mixed-valent phases. The synthesis procedure involves introduction of dissolved Fe(II) species into a suspension of ferric (oxyhydr)oxides at neutral pH. At this pH, the hydroxylation rate of the Fe(II) species is sufficient, which is required to initiate the transformation process. However, to form mixed Fe(II)–Fe(III) oxides, a specific Fe(II)/Fe(III) ratio (2 for GR and 0.5 for magnetite), and hydroxylation ratio ($R = \text{OH}^-/\text{Fe}$) (1 for GR and 2/3 for magnetite) is required (reactions 3 and 4). The values of R can be easily visualized on the Fe(II)–Fe(III) mass balance diagram by the segment joining points A and B to points Fe₃O₄ and GR, respectively (Figure 6).

The extent of such mineralogical transformations is controlled by various factors, including the nature of the initial ferric mineral, Fe(II)/Fe(III) ratio, reaction pH, OH⁻/Fe ratio and ligands. For example, at low Fe(II) levels, ferrihydrite was transformed either into lepidocrocite,^{159,160} goe-

thite,^{47,159,161,162} or hematite.¹⁶³ At high Fe(II) concentrations, mixed-valent Fe minerals such as magnetite^{17,37,47,160,164–169} or GR^{51,81,170,171} were formed from different ferric (oxyhydr)-oxides. For example, Ishikawa et al.¹⁶⁵ investigated the transformation of various ferric oxides [Fe(II)/Fe(III) ratio of 0.5] under changing OH⁻/Fe ratios (0–4). They reported that transformation of ferric oxides into magnetite was highest at OH⁻/Fe = 2 and was on the order of akaganéite > lepidocrocite > goethite. Similarly, Hansel et al.^{172,173} reported that at low Fe(II) concentration (<1.0 mmol Fe(II)/g ferrihydrite), ferrihydrite was transformed into lepidocrocite and goethite while magnetite formation was favored at elevated Fe(II) concentration (>1.0 mmol Fe(II)/g ferrihydrite). In another study by Pedersen et al.¹⁶⁰ at pH of 6.5, ferrihydrite was completely transformed into other stable phases like lepidocrocite at low Fe(II) contents [Fe(II)/Fe(III) = 0.4] or goethite at higher Fe(II) concentration [Fe(II)/Fe(III) = 1]. At high Fe(II) levels, lepidocrocite was transformed into magnetite, while it remained untransformed at low Fe(II) levels. Goethite or hematite were not transformed either at lower [Fe(II)/Fe(III) = 0.4] or at higher Fe(II) concentration [Fe(II)/Fe(III) = 1] which was attributed to their strong stability and crystallinity.¹⁶⁰

When experimental conditions were fully controlled to form stoichiometric magnetite³⁷ or GR⁵¹ through the following reactions, significant amount of goethite was transformed into mixed Fe(II)–Fe(III) oxides.



However, the kinetics of magnetite formation was much slower than that observed for GR under similar experimental conditions (Figure 7). The extent of ferrihydrite transformation into magnetite and GR was 91 and 100%, respectively. In contrast, only 4% of goethite was transformed into magnetite, while the extent of goethite transformation was higher (62%) when GR was formed.⁵¹ This difference in formation kinetics could be correlated to structural differences between both GR

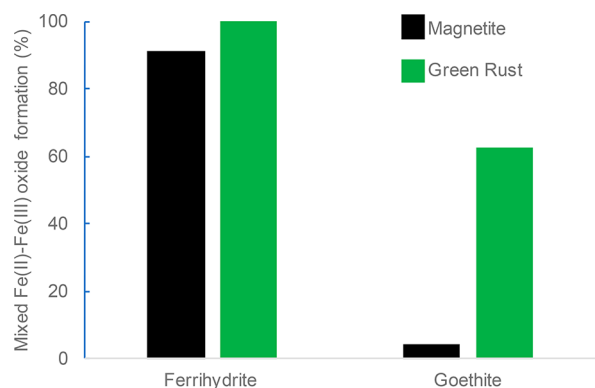


Figure 7. Transformation extent of ferrihydrite and goethite into mixed-valent iron minerals (magnetite and green rust) measured by Mössbauer Spectroscopy. Ferrihydrite and goethite were reacted with stoichiometric amounts of soluble Fe(II) and NaOH to form magnetite and green rust according to the reactions 3 and 4. Figure prepared by using the data reported in Table 2 of ref 51.

and magnetite. GR is an “open” and hydrated phase which might develop much more rapidly in aqueous solution. Conversely, magnetite is a very dense and compact iron oxide, and its formation requires full deprotonation of the initial Fe(II) and Fe(III) species. Therefore, it is considered that the formation of GR is favored when dissolved Fe(II) species interact with ferric (oxyhydr)oxides in anoxic environments.⁵¹

The exact mechanism of these transformations is not yet well understood. However, as summarized in the literature,^{2,169} the Fe(II)-induced mineralogical transformations of ferric (oxyhydr)oxides can be represented as (i) topotactic transformation (also called solid-state conversion or structural rearrangement) or as (ii) reconstructive/recrystallization (dissolution/precipitation). Each of these processes are supported by sometimes contradictory evidence. Topotactic conversions involve the transformation of ferric oxides without dissolution, and magnetite formed through this pathway retains the particle size and morphology of initial phase (Figure 8).^{37,47,51,160,174} Formation of GR via topotactic transformation of ferrihydrite following Fe(II) sorption has also been proposed.¹⁶⁷ Topotactic transformations are initiated by surface adsorption of Fe(II) and interfacial transfer of electrons.^{17,47,175}

On the contrary, in the reconstructive process, a complete breakdown of initial iron phases proceed via their dissolution followed by the precipitation of new secondary phases. Interfacial electron transfer between iron (oxyhydr)oxides and adsorbed Fe(II) initiates the reductive dissolution and then reprecipitation of the adsorbed Fe(II) on oxides particle surfaces.⁴⁷ However, both transformation pathways involve the adsorption of Fe(II) onto ferric (oxyhydr)oxides followed by electron transfer from the sorbed Fe(II) to structural Fe(III) in ferric minerals.¹⁷⁶ Williams and Scherer¹⁷⁷ provided spectroscopic demonstration of reduction of structural Fe(III) in the presence of adsorbed Fe(II) and electron transfer therein. They exposed ferrihydrite (made from ⁵⁷Fe) and exposed it to aqueous Fe(II) (made from ⁵⁶Fe) considering that Mössbauer spectroscopy will detect the structural ⁵⁷Fe(III) but not the adsorbed ⁵⁶Fe(II). Obtained Mössbauer results clearly indicated appearance of the ⁵⁷Fe(II) line, which provides evidence for reduction of structural ⁵⁷Fe(III) in ferrihydrite and electron transfer between adsorbed Fe(II) and the underlying Fe(III) oxide. Similarly, enriched Fe isotope experiments have shown compelling evidence for the exchange of aqueous Fe(II) with structural Fe(III) in ferrihydrite, goethite, and hematite.^{176,178,179}

Transformation of Fe(III) (oxyhydr)oxides is mainly initiated by adsorption of Fe(II) to singly coordinated sites forming inner-sphere surface complexes. The key role of Fe(II) sorption has also been highlighted when the formation of magnetite was inhibited due to the inclusion of organic matter¹⁸⁰ or phosphate¹⁶⁸ in transformation experiments. Microbial transformation of ferrihydrite to magnetite was inhibited when instead of Fe(II), humic substances were adsorbed onto the surface sites of ferrihydrite.¹⁸⁰ Similarly, phosphate forms very strong inner sphere complexes with the iron (oxyhydr)oxide surface, and therefore its presence decreased the adsorption of Fe(II) and thus consequently hindered interfacial electron transfer and the solid-state reaction.^{168,181–184} Loosely bound ligands such as salicylate anion did not significantly affect the magnetite formation,¹⁶⁸ which is perhaps explained by the fact that the affinity of phosphate to the surface of iron (oxyhydr)oxide was much stronger than salicylate (i.e., intrinsic constant of surface

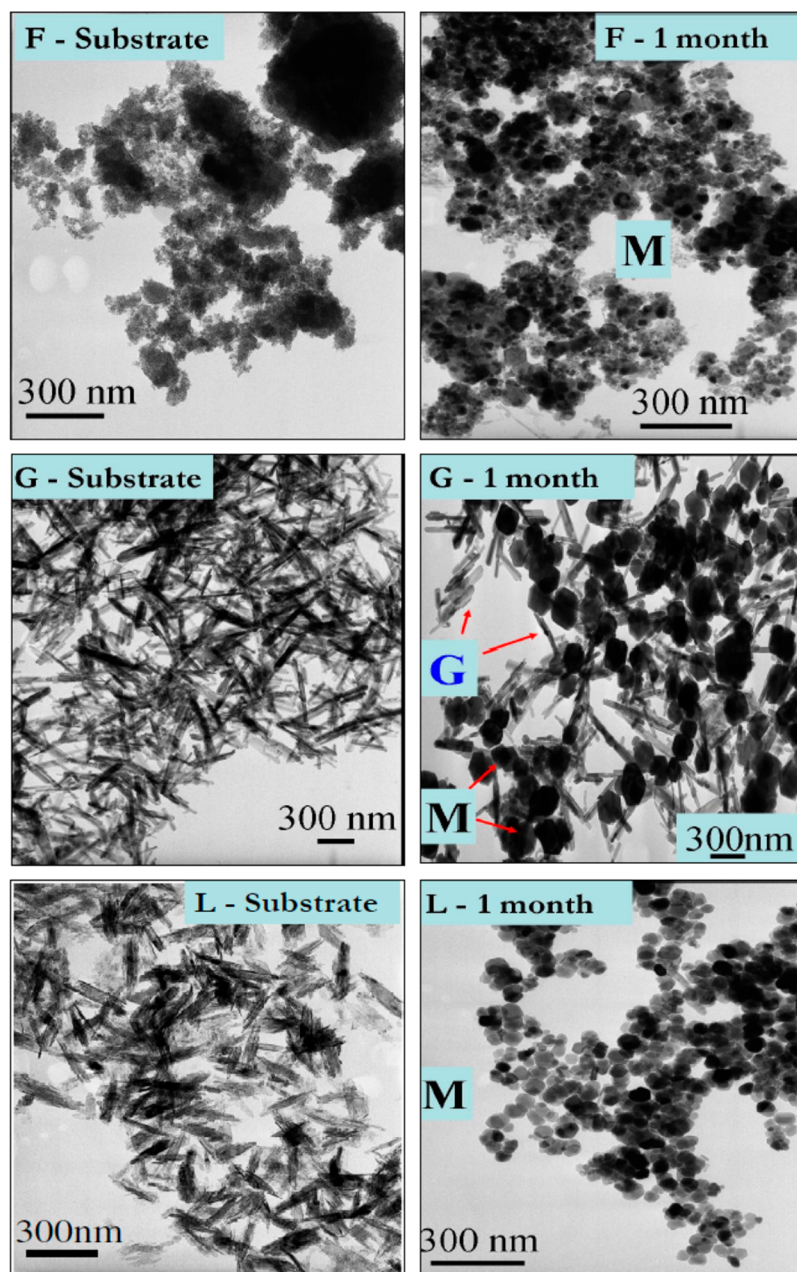


Figure 8. Bright field transmission electron microscopy images showing initial ferric (oxyhydr)oxides (ferrihydrite-F, lepidocrocite-L, and goethite-G) and their transformation products after their reaction with suitable amounts of Fe(II) and OH⁻ to form stoichiometric magnetite (M). Transformation product of G indicates the presence of M and untransformed G. Reproduced with permission from ref 37. Copyright 2012 Elsevier.

complexation of phosphate lies at $\log K_{\text{int}} = 30$, while that of salicylate is around $\log K_{\text{int}} = 8$.^{185,186}

Mössbauer spectroscopy has been used to experimentally monitor the result of mineralogical transformation from interfacial electron transfer reactions between ferric (oxyhydr)oxide and adsorbed Fe(II).^{177,187} Transfer of electrons between sorbed Fe(II) and ferric crystal can be affected by microscopic sorption mechanism (i.e., inner- or outer-sphere complexation).^{177,187} However, Yang et al. argued against relying completely on surface sorption in transformation and pointed out the importance of semiconductor properties of ferric (oxyhydr)oxides to determine their reaction via an electron transfer mechanism.¹⁶⁹ As the inner-sphere complexes are most likely to form on surfaces with singly coordinated surface groups, adsorption of Fe(II) on these sites should be the key

step for interfacial electron transfer and ultimately the mineralogical transformations via both processes.^{187,188} Therefore, the transformation extent of different kinds of goethite was found directly correlated to their site density of the singly coordinated surface groups.¹⁶⁸ Moreover, variation in crystal faces of ferric minerals also influences their transformation extent by affecting the nature of surface complexes (bidentate or tridentate) between Fe(II) and the ferric mineral. Higher transformation extents can be obtained when specific crystal faces are present, which promote the development of inner-sphere complexes and ultimately interfacial electron transfer. The adsorption behavior of divalent cations may probably be dominated by the crystal faces terminating the chains (021/001 like faces), and formation of bidentate or tridentate complex is favored due to the presence of the face 021 or 121.^{188–190}

Indeed, 021 crystal faces are highly reactive and usually denote the main growth direction of crystallites.¹⁸⁹ Owing to the much lower surface area of 021 faces as compared to that of the 100 and 110 faces, 021 faces are characterized by higher growth velocity and relatively higher affinity surface sites to sorb cations.^{188,189,191} In addition to the 021 face, the 110 face was likely implied in the adsorption of the Fe(II), especially at a high Fe(II) level.¹⁹² Owing to these differences, goethite with higher proportions of 021 or 121 faces was more likely to transform into magnetite than goethite which had a lesser amount of these crystal faces.¹⁶⁸

It should be noted that studies on surface-mediated transformation of iron (oxyhydr)oxides have been conducted primarily in model systems devoid of natural organic matter. In natural systems, however, mineral surfaces are inevitably in contact with organic matter and iron (oxyhydr)oxides that rarely exist as pure phases. The existence of organic matter-iron oxides coprecipitates is therefore expected in soils, sediments, and subsurface aquifers. The presence of associated organic matter (adsorbed or coprecipitated) is likely to influence heterogeneous electron transfer processes and formation of reactive Fe(II) surface sites. For example, it was demonstrated that the presence of coprecipitated organic matter caused a linear decrease in ferrihydrite transformation with increasing C/Fe amount because the presence of organic matter improves the stability of ferric minerals.¹⁹³ Coprecipitated organic matter also inhibited the growth of ferric minerals as coprecipitated ferrihydrite has smaller particle size and greater structural disorder than organic-free ferrihydrite.¹⁹⁴ Coprecipitation of organic matter could lead to higher organic matter content in Fe minerals as compared to simple adsorption of OM due to the fact that coprecipitated OM is more strongly bound to the mineral and more difficult to desorb from the mineral surface.¹⁹⁵ Such minerals also have lower surface area than pure ones as mineral surface sites are blocked by organic matter with lower specific surface area.^{194–196} Similar is also true for biogenic minerals¹⁹⁷ (see section 4.2).

In subsurface environments, iron (oxyhydr)oxides generally do not occur as homogeneous assemblages. Frequently iron (oxyhydr)oxides can exist as coatings on less reactive or less soluble soil particles such as quartz sand or clay.¹⁹⁸ In addition, the iron can be found in assemblages of different iron (oxyhydr)oxides coatings which form the interface between mineral grains and groundwater.¹⁹⁸ Therefore, mineralogical transformations of ferric (oxyhydr)oxide coatings have been investigated in many studies devoted to form mixed-valent Fe minerals.^{168,199,200} The extent of mineralogical transformations can vary depending upon the nature of support. For example, coating of ferrihydrite onto quartz sand (10% w/w) did not influence its subsequent transformation extent to magnetite.²⁰⁰ Similar trends were observed for goethite coated onto sand.¹⁶⁸ However, the use of clay (kaolinite) as a support for goethite resulted in a decreased transformation extent into magnetite under similar experimental conditions.¹⁶⁸ As Si may inhibit the direct adsorption of aqueous Fe(II) onto Fe(III) minerals, it is possible silicate release from Si-bearing minerals may hinder the solid-state transformation of coating phases.²⁰¹ The sorption of silicate resulted in an approximate 10-fold decrease in the rate of the Fe(II)-catalyzed process.²⁰¹ Thus, the presence of inorganic or organic ligands might act to retard the transformation of ferric minerals.

4.2. Synthesis of Mixed-Valent Iron Minerals by Microbial Activity

The ubiquity of iron in the environment, in particular on early Earth when the atmosphere was anoxic and Fe was more available in its reduced and mobile form,²⁰² has led to the evolution of microorganisms with enzymatic pathways used to access different oxidation states of Fe as either an electron donor for Fe(II) oxidation or as an electron acceptor for Fe(III) reduction. Microbial Fe mineralization mechanisms are key components in the global iron cycle and link different biogeochemical cycles, including the iron, carbon, and nitrogen cycles.²⁰³

Through microbial iron redox transformations, a variety of different Fe minerals are formed, several of which contain both Fe(II) and Fe(III) and thus can be considered to be mixed-valent (e.g., magnetite or GR). Some of these minerals are persistent in the environment for billions of years [i.e., in banded iron formations (BIFs)]^{204,205} and, as such, represent important biomarkers for the understanding of how life emerged on Earth. Others, such as GR, are very reactive and have a much shorter lifetime before they convert into more stable mineral phases.³³

Here we detail the different pathways through which microbial processes induce the formation of such mixed-valent Fe minerals including through microbial Fe(III) reduction and Fe(II) oxidation. This will be complemented by a summary of magnetite biomineralization by magnetotactic bacteria (i.e., microorganisms that synthesize magnetite not as part of their catabolism but rather for navigation purposes using the magnetic properties of this mineral).

4.2.1. Synthesis by Bacterial Fe(III) Reduction. *Physiology and Diversity of Fe(III)-Reducing Bacteria.* Microbial Fe(III) reduction occurs in almost all natural environments, including sediments and soils and involves the oxidation of organic matter (e.g., acetate or lactate) or hydrogen which act as electron donors coupled to the reduction of Fe(III) which acts as the terminal electron acceptor. Most of our knowledge on this process stems from studies with microorganisms belonging to the groups of *Geobacter* sp. and *Shewanella* sp. (*Geobacter metallireducens* strain GS-15, *Geobacter sulfurreducens*, *Shewanella oneidensis* MR-1, *Shewanella putrefaciens* strain 200 and strain ATCC 8071), and from *Desulfuromonas acetoxidans*.^{206–211} These heterotrophic Fe(III)-respiring bacteria are able to use various electron donors including a broad range of organic compounds as well as H₂ at neutral pH.^{208,212–215} The organic compounds used as electron donor include simple fatty acids such as acetate and lactate but also more complex organic molecules such as aromatic compounds. Some of the Fe(III)-reducing microorganisms are unable to degrade their organic electron donor completely, usually accumulating acetate.²¹⁴ In recent years, some evidence for coupling the microbial reduction of ferric iron to the oxidation of ammonium has been found.^{216–218} Similarly, lab and field experiments have suggested the coupling of anaerobic methane oxidation to ferric iron reduction.^{219–221} However, no pure cultures of microorganisms have been isolated yet that are able to catalyze and grow by these two processes.

Fe(III)-reducing microorganisms can reduce Fe(III) that is in solution or present as poorly soluble ferric iron minerals. At neutral pH in the absence of organic ligands, Fe(III) is poorly soluble and precipitates as Fe(III) mineral. However, in the presence of citrate, nitritotriacetate, or other ligands (including humic substances), Fe(III) can form soluble complexes and can

serve as terminal electron acceptor in anaerobic respiration for Fe(III)-reducers.²²² Examples of Fe(III) minerals that can be reduced are poorly crystalline (oxyhydr)oxides such as ferrihydrite, lepidocrocite, schwertmannite, and goethite but also more crystalline representatives such as hematite.^{223–226} Mixed-valent Fe(II)/Fe(III) minerals such as magnetite and Fe(III) present in clay minerals can also be microbially reduced.^{227–231}

Due to the poor solubility of Fe(III) (oxyhydr)oxides, electrons have to be transferred from the microbial cells to the Fe(III) mineral either via direct cell contact (involving transfer of the electrons from the cell interior to cell surface c-type cytochromes) or via different mechanisms for extracellular electron transfer (Figure 9).²³² Although the currently

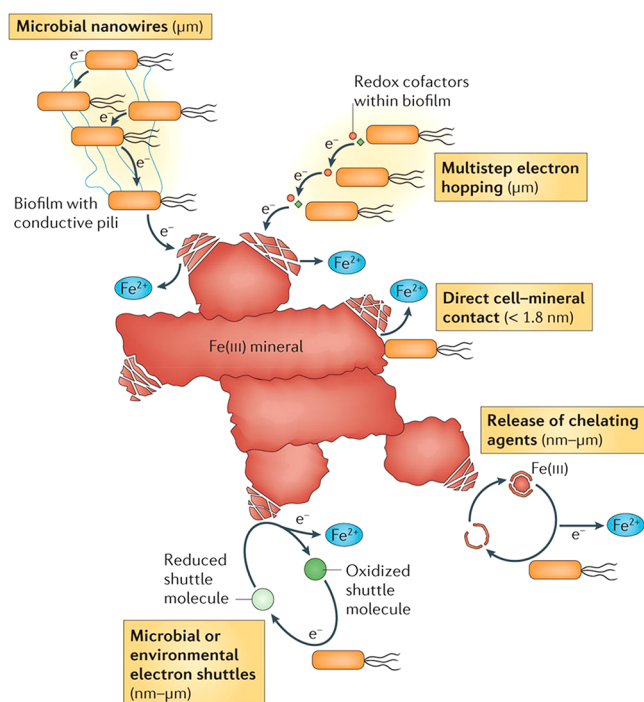


Figure 9. Possible electron transfer pathways during Fe(III) reduction. Direct contact between the Fe(III) minerals and the bacterial cell facilitates Fe(III) reduction over short distances. Bacteria secrete chelating agents or exploit microbial or environmental redox-active electron shuttles (such as flavins or dissolved and solid-state humic substances, respectively) to facilitate electron transfer over short (nm) and long (μm) distances. Electrically conductive pili and multistep electron hopping via redox cofactors that are present in biofilms have been implicated in long-distance extracellular electron transfer. Reproduced with permission from ref 232. Copyright 2014 Nature Publishing Group.

described electron transport pathways in different Fe(III)-reducing microorganisms including *Shewanella* and *Geobacter* sp. contain similar components, they are considerably different, suggesting that electron transport for Fe(III) reduction can occur via many different biochemical pathways, including electron shuttling via dissolved or solid-phase electron shuttles, Fe(III) solubilization, or the use of conductive cell-appendages, so-called microbial nanowires (summarized recently by Melton et al. and Shi et al.).^{232,233}

Formation of Mixed-Valent Iron Minerals during Microbial Fe(III) Reduction. Following microbial Fe(III) mineral reduction, Fe(II) is released into solution and either remains

dissolved, precipitates as a Fe(II) mineral phase, or can further react with remaining Fe(III) precipitates. Commonly, it is seen that ferrihydrite can undergo microbial Fe(III) reduction leading to the formation of goethite, magnetite, or siderite with the exact nature of the minerals dependent upon a number of different physical and geochemical parameters such as Fe(III) reduction and Fe(II) formation rates, pH, temperature, cell density, or Fe(III) concentration.^{172,173,180,234,235} Piepenbrock et al.¹⁸⁰ showed that a certain Fe(II)/Fe_{tot} ratio is required during Fe(III) reduction to trigger the formation of magnetite, and the presence of organic matter such as humic substances can also inhibit the formation of the mixed-valent mineral. Such humic substances have been shown to be able to shuttle electrons to and from both biogenic and chemically synthesized magnetites.²³⁶ Furthermore, the identity of the mineral phases produced by the Fe(III)-reducing strain *Shewanella oneidensis* MR-1 has been shown to be dependent upon other physico-geochemical factors including geometric orientation of the bottles that the bacteria and minerals are incubated in, with magnetite formation favored when the ferrihydrite pellet was most dense.²³⁵ In the environment, microbial magnetite has been shown to form at hydrocarbon-contaminated field sites and was even used by its magnetic signal to locate the hotspot of microbial activity.²³⁷ In the deep ocean, iron reduction by *Shewanella piezotolerans* WP3, which was isolated from the Pacific Ocean at a water depth of ~ 1914 m, has also been shown to produce magnetite via reduction of hydrous ferric oxide at rates much faster than many other known iron(III)-reducing bacteria.²³⁸ *Shewanella putrefaciens* has been shown to be able to reduce magnetite to GR.²³⁹ This study shows agreement with the fact that GR(CO₃²⁻) formation can occur via Fe(III) reduction by *Shewanella putrefaciens* when lepidocrocite is the starting Fe(III) phase.^{240,241}

The physical and chemical characteristics of mixed-valent minerals produced by bacteria are highly dependent upon their formation conditions. This includes the effect of cell density on particle size. By increasing the cell concentration, the reduction of the ferrihydrite starting material proceeds faster and small magnetite nanoparticles ($d \sim 12$ nm) are produced. When low cell numbers are present, however, the reduction takes place more slowly, leading to the formation of larger grains of magnetite ($d \sim 40$ – 50 nm).²³⁴ It was also shown by Zhang et al.²⁴² that larger grained magnetite ($d > 30$ nm) is produced by thermophilic Fe(III)-reducing bacteria in contrast to the often superparamagnetic magnetite produced by other Fe(III)-reducing strains.

4.2.2. Synthesis of Mixed-Valent Iron Minerals by Bacterial Fe(II) Oxidation. Fe(II)-oxidizing bacteria are capable of drawing energy and/or electrons for growth by oxidizing ferrous iron to ferric iron.²⁴³ At low O₂ concentrations and neutral pH, a habitat is called microoxic and molecular oxygen can serve as terminal electron acceptor for Fe(II) oxidation. The microorganisms catalyzing this process use the Fe(II) as electron and energy source and are called microaerophilic Fe(II)-oxidizers.²⁴⁴ As soon as O₂ is consumed and the geochemical conditions become anoxic, Fe(II)-oxidizing microorganisms need to use other terminal electron acceptors. Photoautotrophic Fe(II)-oxidizers can use light as an energy source and transfer the electrons from Fe(II) to carbon dioxide for biomass synthesis. In contrast, nitrate-reducing Fe(II)-oxidizers use Fe(II) as an electron and energy source to reduce nitrate as terminal electron acceptor producing different

N-species as intermediates and metabolic products. For the described microbially catalyzed Fe(II) oxidation processes, until now no general biogeochemical mechanisms are known [i.e., the proteins involved in Fe(II) oxidation and their genetic information is mostly unclear]. Limited information on Fe(II) oxidation enzymatics and genetics is available only for individual strains.^{245,246}

Although microaerophilic Fe(II)-oxidizing bacteria such as *Gallionella* sp., *Leptothrix* sp., or the known marine strains (*Mariiprofundus* sp.) can produce unique cell-mineral structures of organic templates associated with Fe(III) minerals (twisted stalks and elongated sheaths), the identity of the biomineral produced is relatively simple. So far mainly poorly crystalline Fe(III) (oxyhydr)oxides including ferrihydrite, goethite, and lepidocrocite have been described.^{247,248} No strong and convincing evidence for mixed-valent Fe minerals such as magnetite or GR has so far been published, although in a few rare cases greenish minerals have been seen by eye and some magnetite particles have been found in deep sea samples that contained microaerophilic Fe(II)-oxidizers.^{249,250} However, one can imagine that microbial reduction of the poorly crystalline Fe(III) (oxyhydr)oxide biominerals could potentially lead to the formation of magnetite or GR, although the presence of organic biomolecules is certainly expected to slow down or even prevent the formation of magnetite.^{194,196,251,252}

Anaerobic nitrate-reducing Fe(II)-oxidizing bacteria have been detected in soils, freshwater, and marine habitats.^{253–257} Microbial Fe(II) oxidation coupled to nitrate reduction produces Fe(III) minerals and dinitrogen or intermediates of the denitrification reaction, including NO_2^- , NO , and N_2O .^{258,259} Interestingly, almost all described nitrate-reducing Fe(II)-oxidizers are mixotrophic, meaning that they require an organic cosubstrate to allow for continuous cultivation and Fe(II) oxidation.^{253,255,259–263} In the last two decades, a large number of mixotrophic nitrate-reducing Fe(II)-oxidizers has been described; however, examples of autotrophic ones are rare. The enrichment culture KS described by Straub et al.²⁵⁶ is the first described culture that can oxidize Fe(II) autotrophically and can be maintained under chemolithoautotrophic conditions continuously. Since then a few more strains capable of autotrophic nitrate-reducing Fe(II) oxidation have been described in different studies.^{264–271} However, the capability for continuous Fe(II) oxidation and growth under autotrophic conditions over several generations has not been demonstrated for all of these cultures.

When nitrate-reducing Fe(II) oxidation occurs at neutral pH, the produced Fe(III) is poorly soluble and precipitates rapidly as a Fe(III) mineral. Interestingly, cells in all described mixotrophic strains heavily encrust in Fe(III) minerals,^{263,272,273} while the autotrophic culture KS does not form any cell encrustation under autotrophic conditions.²⁷⁴ From these observations, it was concluded that in the autotrophic nitrate-reducing Fe(II)-oxidizing cultures the Fe(II) is oxidized enzymatically and directly coupled to nitrate reduction, while under mixotrophic conditions the nitrate is reduced coupled to oxidation of the organic cosubstrate thus producing reactive nitrite (NO_2^-) that oxidizes the Fe(II) abiotically.^{262,263,275}

These two biotic and abiotic Fe(II) oxidation mechanisms also have consequences for the identity of the minerals formed during nitrate-reducing Fe(II) oxidation: while for the autotrophic culture KS the poorly crystalline Fe(III) mineral ferrihydrite has been observed,²⁷⁴ for the mixotrophic strains (and for some of the ones where it is currently unclear whether

they are autotrophic or mixotrophic), more crystalline minerals (such as goethite) and even mixed-valent Fe(III) minerals such as magnetite and GR have been observed: Kappler et al.²⁵⁴ described the formation of goethite for *Acidovorax* sp. strain BoFeN1 and later Pantke et al.²⁷⁶ showed that this goethite formation goes via a green-rust intermediate (Figure 10). This

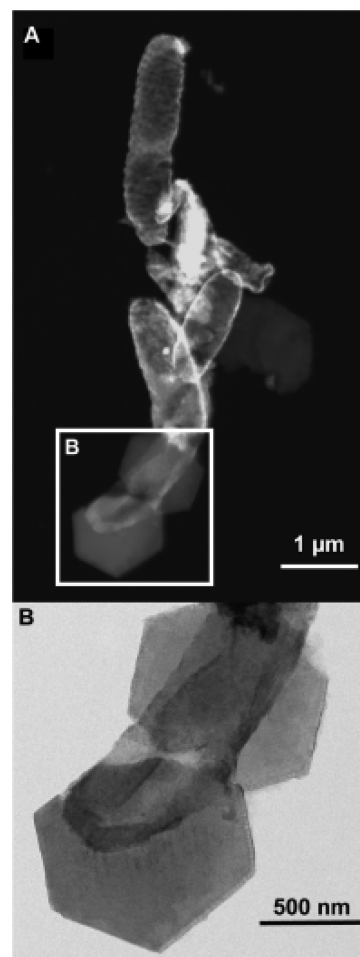


Figure 10. (A) Scanning transmission electron microscopy (STEM) image of BoFeN1 culture suspension after 2 days measured in the high angular annular dark field mode (HAADF). (B) Magnified transmission electron microscopy image of BoFeN1 cell with hexagonal carbonate GR flakes measured in brightfield mode. Reproduced from ref 276. Copyright 2012 American Chemical Society.

has been confirmed by Etique et al. for *Klebsiella mobilis*²⁷⁷ and by Miot et al. for *Acidovorax* sp. strain BoFeN1²⁷⁸ who furthermore demonstrated that the GR can also turn into magnetite. GR formation has also been observed recently by the heterotrophic coculture strains in the autotrophic nitrate-reducing enrichment culture KS.²⁷⁴ Magnetite formation by nitrate-reducing Fe(II)-oxidizers was first suggested by Chaudhuri et al.²⁷⁹ Furthermore, it has been demonstrated that magnetite formation can even be initiated under conditions under which magnetite does not usually form, simply by the addition of magnetite crystals.²⁸⁰ These magnetite nucleation sites function as seeds for more magnetite formation by lowering the activation energy for magnetite precipitation. One can easily imagine that this plays an important role in the environment where Fe(III)-reducing or even magnetotactic

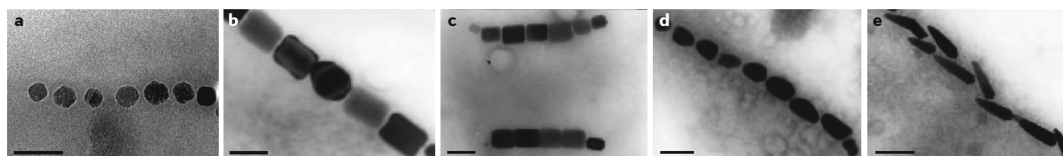


Figure 11. Different morphologies of magnetite produced by MTB's. Reproduced with permission from ref 296. Copyright 2016 Nature Publishing Group.

bacteria are responsible for providing such magnetite nucleation sites.

Although biogenic magnetites (or other mixed-valent Fe(II)-Fe(III)-phases) produced by Fe(II)-oxidizing bacteria have not been systematically studied in environmental samples, in part because they are hard to distinguish from the abiotic counterparts, it can be expected that their properties are distinctly different from abiotic ones. First, the association with organic matter (similar to the association with other geochemical species such as silicates) has the potential to stabilize and preserve them to a larger extent than expected.²⁸¹ Second, compared to synthetic minerals, the mixed-valent phases produced by Fe(III)-reducing and magnetotactic bacteria have been shown to have a higher Fe(II) content than abiotic Fe(II)/Fe(III) minerals.^{282,283}

In addition to microaerophilic and nitrate-reducing microorganisms, phototrophic Fe(II)-oxidizing bacteria also oxidize Fe(II) to Fe(III) with the potential for the formation of mixed-valent Fe(II)-Fe(III) minerals including GR and magnetite. For most of these so-called phototrophs, including representatives of the purple nonsulfur, the purple sulfur, and the green-sulfur bacteria, the precipitation of poorly crystalline ferric (oxyhydr)oxides (including ferrihydrite and goethite) has been described in both freshwater and marine media conditions.^{284,285} For one of the freshwater strains, *Rhodospseudomonas palustris* TIE-1, and also for one of the marine strains, *Rhodovulum iodolum*, formation of small amounts of magnetite have been observed.^{286,287}

Evidence for GR formation by phototrophic microorganisms in the environment might come from studies of Archean ocean model environments, such as Lake Matano in Indonesia. In this lake, an anoxic water layer with Fe(II) in the photic zone and the abundance of phototrophic Fe(II)-oxidizing bacteria has been described and GRs have been identified as minerals formed potentially by the activity of the Fe(II)-oxidizers but maybe also by Fe(III)-reducers using the Fe(III) minerals produced by the Fe(II)-oxidizers.^{89,288,289}

4.2.3. Magnetotactic Bacteria. While the formation of magnetite outside of the cellular membrane by Fe(III)-reducing and Fe(II)-oxidizing bacteria can be considered to be a biologically induced mechanism, magnetotactic bacteria (MTB) are able to produce magnetite, greigite, or both^{290,291} internally via biologically controlled mechanisms. These bacteria produce chains of magnetite or greigite within individual membranes (denoted magnetosomes), which are small vesicles containing grains of magnetic mineral. When placed under the influence of a magnetic field, the bacteria propel themselves along the field lines at speeds of 100 $\mu\text{m/s}$ using flagella⁶⁵ and are thus considered to use the magnetosomes for a form of navigation along the Earth's magnetic field (magnetotaxis). While these organisms were first identified in the 1960's, it was not until they were later rediscovered by Blakemore (1975)²⁹² in a marine sediment that MTB started to gain widespread attention. Since then it has been shown that MTB are

ubiquitous and can grow in almost any aquatic environment, with strains identified in freshwater ponds, river sediments, soils, marine waters, and marine sediment.²⁹³ Most MTB exist at the oxic-anoxic interface (i.e., microoxic environments) where oxygen concentrations are much lower than that of the atmosphere.²⁹⁴ In most cases, oxygen is the terminal electron acceptor used during respiration of the bacteria, and small concentrations of O_2 are required for magnetite formation. *Magnetospirillum magnetotacticum* MS-1 is able to use NO_3^- as an electron acceptor for respiration; however, it has been observed that at least 1% O_2 is required for the formation of magnetosomes to occur.²⁹⁵

In terms of understanding the mechanisms of formation of magnetosomes, two of the most frequently studied strains include *Magnetospirillum magneticum* AMB-1 (AMB) and *Magnetospirillum gryphiswaldense* MSR-1 (MSR)²⁹⁶ due to their ability to be cultivated in reasonable quantities. Over 30 genes have been identified within MTB that regulate the uptake of iron, deposition, and controlled precipitation of mineral within the magnetosome membrane.²⁹⁷ It appears that while the formation of magnetosome membranes occurs even when magnetite does not form, magnetite cannot be produced in mutant strains which do not possess the membrane.^{298–300} This suggests that the magnetosome acts as a specialized nanoreactor in which optimum redox and pH environments (pH > 7, low redox potential) can be strictly regulated in order to promote magnetite formation. This formation is thought to take place either through the coprecipitation of Fe(II) and Fe(III) or via the secondary transformation of a precursor mineral such as ferrihydrite.²⁹⁰ In total, the Fe contained within all of these magnetosomes accounts for >4% of the cell's mass (dry cell weight) and for more than 99.5% of the iron content of the bacteria.^{301,302}

Magnetites formed within MTB are notable for their high chemical purity,³⁰³ though it has been shown that additional metal cations (e.g., Cu, Mn, and Co) can be incorporated into the mineral.^{304–306} Depending upon the strain, the size of the magnetosomes can vary between 10 and 120 nm and almost all with very narrow size distributions.^{296,307} A number of different shapes have been observed including cuboctahedral, elongated prismatic, tooth-shaped, and bullet-shaped (Figure 11).^{296,308} Currently, however, the genetic factors which affect the size and shape of the magnetosomes are not well-understood. Many of these particles are single domain at room temperature³⁰⁹ which helps to ensure they retain a remanent magnetization and the magnetic moment is dictated by the number and size of the magnetosomes. Since the magnetic dipole is effectively fixed within the cell, when the magnetic field changes direction, so do the bacteria.

It is generally regarded that the use of magnetosomes within MTB is in order to provide an internal compass for navigation. More specifically, MTB orient themselves via magnetotaxis along the Earth's magnetic field. This reduces a three-dimensional coordinate-based movement to a one-dimensional

problem (i.e., if the bacteria know the position of north, south, east, and west then they are able to consider movement in the vertical water column, likely along chemically stratified inclines to search for redox gradients). This is further supported by the fact that both north-seeking and south-seeking MTB have been found living in the Northern and Southern hemispheres, respectively.²⁹⁴ However if such a mechanism is so beneficial for MTB, why do other bacteria not also form magnetic particles for navigation? Also, many of these bacteria are able to survive without forming magnetite within their magnetosomes which might suggest that the magnetite is also able to provide other uses. For instance, other potential advantages of producing magnetosomes which have so far been suggested include the following: (i) for detoxification of metal ions or reactive oxygen species which can form during oxygen respiration and can react with magnetite;^{310,311} (ii) as a store for Fe in a compact, nonhydrated, inert, and nontoxic form, although to date no evidence has been able to suggest such a mechanism;³¹² (iii) for electron storage in which, depending upon the geochemical conditions, the magnetite (or greigite) could be used as either an electron donor or an electron acceptor.^{313,314} While this theory has so far not been proven, recent evidence has shown that Fe(III)-reducing and Fe(II)-oxidizing bacteria can use magnetite in such a capacity (termed biogeobattery).^{48,315} Furthermore, it is known that environmental conditions can influence the interior of the magnetosome membrane directly, thus what happens outside of the cell can affect the contents of the magnetosome.^{299,316}

From an environmental perspective, the magnetite formed by MTB has been frequently suggested as a potential biomarker (microfossil) which can be used to reconstruct geochemical conditions from ancient Earth. The idea is that when the bacteria die the biological component degrades and the magnetite is incorporated into the sediment and eventually sedimentary rocks, forming a significant contribution to their magnetic properties.^{317–319} Magnetotactic bacteria have even been suggested to be the source of chains of magnetite found within the Martian meteorite ALH84001³²⁰ although this study was heavily debated and much doubt surrounds the claims.³²¹ Potential problems for using the magnetic properties as biosignatures includes the fact that they are almost indistinguishable from abiotic magnetite or magnetite produced by Fe(II)-oxidizing and Fe(III)-reducing bacteria.^{286,322,323} Furthermore, diagenetic or metamorphic processes might result in changes to the magnetic properties of the mineral inclusions. It has recently been suggested that a combination of physical, mineralogical, and chemical characterization could be used to identify magnetite with trace element incorporations. Specifically, Amor et al.³⁰⁴ looked for the incorporation of 34 trace elements into magnetosomes formed by *Magnetospirillum* AMB-1 and identified the fact that biogenic magnetite incorporates 100 times less trace elements than synthetic magnetite. Alternatively, mass-dependent and -independent fractionation of Fe isotopes within magnetosomes might also be used as a potential proxy to investigate their ability to serve as biomarkers.³²⁴

5. IDENTIFICATION AND QUANTIFICATION TECHNIQUES

This section is devoted to illustrate various methods and techniques that are frequently used to identify the mineralogy or morphology of mixed-valent Fe minerals. We have focused on XRD, Mössbauer spectroscopy, and vibrational spectroscopy,

including Raman and infrared (IR), synchrotron methods such as extended X-ray absorption fine structure (EXAFS), X-ray absorption near edge spectroscopy (XANES), scanning transmission X-ray microscopy (STXM), XMCD, magnetic measurements, as well as imaging techniques including transmission electron microscopy (TEM) or scanning electron microscopy (SEM). Combined, these powerful techniques can provide accurate quantitative determination of particle size, mineralogy, morphology, and stoichiometry.

5.1. X-ray Diffraction

This technique is commonly considered to be one of the most effective and rapid methods of mineral identification as diffraction data is able to provide information on mineral composition, crystallinity, and unit cell parameters.² The XRD diffraction patterns of magnetite and GRs have been well-studied with corresponding reflections are shown in Figure 12.

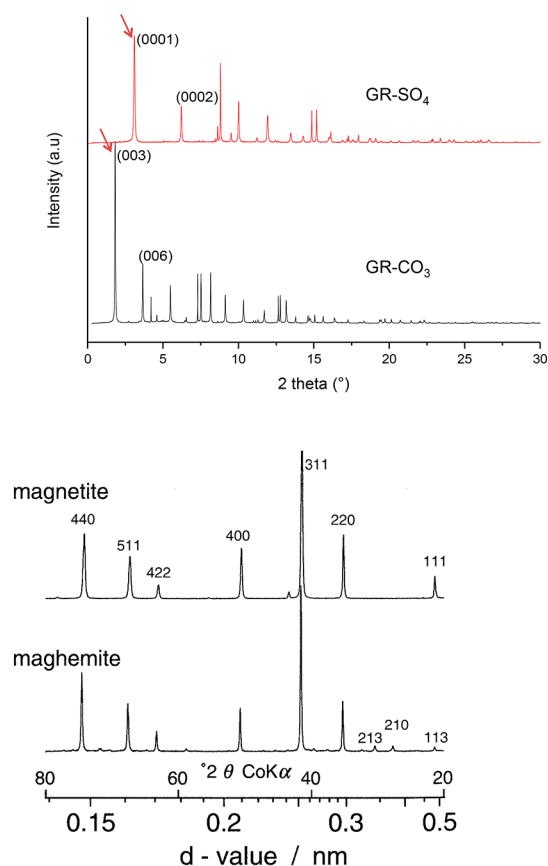


Figure 12. X-ray diffractograms of green rusts namely $\text{GR}(\text{SO}_4^{2-})$ and $\text{GR}(\text{CO}_3^{2-})$, magnetite, and maghemite. Diffractograms of $\text{GR}(\text{SO}_4^{2-})$ and $\text{GR}(\text{CO}_3^{2-})$ are reproduced with permission from ref 19. Copyright 2010 Elsevier. Diffractograms of magnetite and maghemite are reproduced with permission from ref 2. Copyright 2003 Wiley-VCH.

The diffractogram of magnetite is typically characterized by several well-defined reflections (Table 6), the most intense of which occurs at 0.253 Å (311). Magnetite has a cubic crystal structure with d -spacing of 8.397 Å. One complication which can arise when identifying magnetite through XRD is due to the similarity of its diffractogram to that of maghemite. Both iron oxides have almost identical lattice parameters and spinel structure (Figure 12), and consequently, their respective reflections heavily overlap.^{2,325–328} Minor differences in the

Table 6. X-ray Powder Diffraction Data for Magnetite and Both Kinds of Green Rusts (GR-I and GR-II)

magnetite ³³³			GR-I ²⁷			GR-II ²⁷		
d Å	i	hkl	d Å	i	hkl	d Å	i	hkl
4.85200	8	111	8.02	vs	003	10.92	vs	001
2.96700	30	220	4.01	v	006	5.48	s	002
2.53200	100	311	2.701	m	102	3.65	s	003
2.42430	8	222			104			
2.09930	20	400	2.408	m	105	2.747	m	004
1.71460	10	422			107			100
1.61580	30	511	2.037	w	108	2.660	ms	101
1.48450	40	440	1.598	mw	101	2.459	ms	102
1.41920	2	531			110			
1.32770	4	620	1.567	mw	113	2.195	ms	005
1.28070	10	533						103
1.26590	4	622	1.487	w	116	1.938	ms	104
1.21190	2	444						
1.12210	4	642				1.712	w	105
1.09300	12	731						
1.04960	6	800				1.587	w	110
0.98960	2	660				1.570	w	111
0.96950	6	751						
0.96320	4	662				1.525	w	112
0.93880	4	840						
0.89520	2	664						
0.88020	6	931						
0.85690	8	844						
0.82330	4	1020						
0.81170	6	951						
0.80800	4	1022						

diffraction of maghemite exist in the form of additional reflections at 0.373 Å (210) and 0.340 Å (213). These reflections can possibly be used to distinguish magnetite from maghemite, but in reality, their intensities are too weak (~5%) for the positive identification of the maghemite phase. Moreover, even if these reflections are successfully observed, it does not necessarily guarantee the sample to be single-phase maghemite since it could be a mixture of both magnetite and maghemite mineral phases.³²⁸ Thus, distinction of both phases is difficult by using XRD. Recent studies have, however, (very few in number) showed the possibility of quantitative determination of both phases in their mixture by using X-ray diffraction data. For example, Kim et al.³²⁵ proposed the use of high-angle diffraction peaks as (511) and (440) to quantify magnetite and maghemite in their mixture by constructing a calibration curve using the pure phases. Mikhaylova et al.³²⁷ used a Rietveld XRD method to quantify both phases in magnetite-maghemite mixture and the obtained data matched that of Mössbauer spectroscopy. Furthermore, Pearce et al.³²⁹ were able to show a relationship between mineral stoichiometry and *d*-spacing using the following relationship:

$$R = 0.89598 / \left(\frac{0.1989}{(\alpha - 8.3344)} - 1 \right)^{1/1.1988} \quad (5)$$

Where $R = \text{Fe(II)}/\text{Fe(III)}$ and α is the cell parameter (*d*-spacing) in angstroms. Using such a relationship could provide information about whether the mineral is fully reduced (i.e., magnetite), fully oxidized (i.e., maghemite), or somewhere in between (i.e., mixture of phases or partially oxidized magnetite).

In the case of GRs, samples need to be carefully prepared to protect samples against oxidation during XRD analysis, for example through preparation and analysis under anoxic conditions and/or by coating samples with glycerol during analysis.^{42,330–332} The XRD diffractograms of GR are typically characterized by reflections at low 2-theta values (Figure 12) with *d*-spacing of 7–10 Å (Figure 13). Different GRs can easily

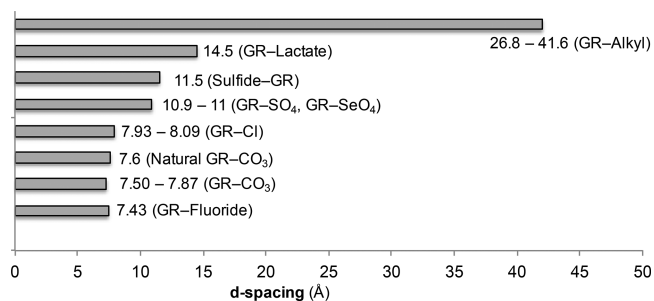


Figure 13. Variation of *d*-spacings in XRD parameters of different GRs depending upon their type and nature of intercalated molecules. This figure is based on the data compiled in previous studies^{22,26,88,334,335} and refs cited therein.

be distinguished by the position of intense reflections in XRD diffractograms and corresponding parameters (Table 6). For example, the position of the most intense (003) reflection of GR(CO₃²⁻) (*d*-spacing = 7.57 Å) is located at a much lower angle than corresponding reflection (0001) of GR(SO₄²⁻) (*d*-spacing = 10.96 Å) simply because of different *d*-spacing (Figure 13).¹⁹

For GRs, quantification of the d -spacing value is perhaps the most important information to extract from XRD diffractograms in order to determine the nature and size of the intercalated molecules. The d -spacing's obtained from GR diffractograms typically increase through the incorporation of large organic anions in GR structure. For example, XRD data revealed very high d -spacing (42 Å) when GR was synthesized by incorporating bulky alkyl anions.²² A range of d -spacings corresponding to different GRs is provided in Figure 13 to illustrate the impact of the incorporated anions on the d -spacing values.

5.2. Mössbauer Spectroscopy

Since its discovery in 1958,³³⁶ Mössbauer spectroscopy has established itself as an important technique for determining the mineral composition, oxidation state, and even crystallinity of Fe minerals. The technique has increasingly been applied to different areas of geoscience, especially with regard to biogeochemistry, nanomaterials, and Mars.^{337,338}

The Mössbauer effect is based upon the resonant absorption of γ -radiation by atomic nuclei. In the case of ^{57}Fe Mössbauer spectroscopy, a radioactive ^{57}Co source (often embedded in a Rubidium matrix) decays to ^{57}Fe , resulting in the emission of γ -rays of 14.4 keV which are then absorbed by an absorber nucleus (i.e., the sample). The simplest Mössbauer spectrum can be described as having a Lorentzian line shape with half width at half-maximum (HWHM) of 0.097 mm/s. The HWHM is limited by Heisenberg's uncertainty principle, although instrumental broadening will often lead to a slightly larger value. To change the energy range over which the γ -radiation is absorbed by a sample, the source is moved back and forth to take advantage of the Doppler effect. Consequently, Mössbauer spectra are routinely shown with x axis units in mm/s, which refers to the velocity of the moving source.

Hyperfine Parameters. The formation of hyperfine interactions (parameters) are key characteristics of the Mössbauer effect. These parameters are related to the local coordination environment of the atoms in a sample and can be used to determine both the mineralogy and redox state of a sample. The main parameters that are routinely considered include the isomer shift (δ), quadrupole splitting (ΔE_Q), quadrupole shift (ϵ), and the magnetic hyperfine splitting (B_{hf}) (Figure 14).

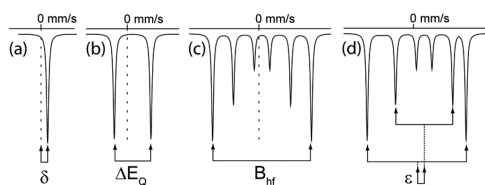


Figure 14. Mössbauer parameters: (a) isomer shift δ , (b) quadrupole splitting ΔE_Q , (c) magnetic hyperfine field B_{hf} and (d) quadrupole shift ϵ .

The isomer shift (δ) is an observable shift in the center of the absorption lines of a Mössbauer spectrum from the center of the absorption spectrum of reference material, commonly α -Fe(0) that is defined as 0 mm/s. It arises due to the s -orbital electron cloud of an absorber atom interacting with its nucleus and can be used to provide information on the electron density at the nucleus and chemical changes in the atom or lattice. The s -electron density depends upon the bonding environment of an atom, which means that different compounds or minerals

have different δ . Since Fe(III) and Fe(II) ions have different numbers of d -electrons (5 and 6, respectively), the nucleus is shielded from s -electrons to different extents meaning that, in general, Fe(II) ions thus have larger values for δ than Fe(III) ions, although this is not necessarily the case for all minerals (see example of pyrite).

The quadrupole splitting (ΔE_Q) emerges in the case of asymmetric (i.e., nonspherical) absorber nuclei which includes almost all Fe minerals. The interaction presents itself as two clearly resolved symmetrical absorption lines (denoted a doublet) the distance between which is highly dependent upon oxidation state. In general, high spin Fe(III) atoms show much lower ΔE_Q than high spin Fe(II) atoms which means that ΔE_Q can often be readily used for the determination of oxidation state in environmental samples without any additional treatment. Conversely, however, low spin Fe(II) atoms (e.g., in pyrite and other iron sulfur minerals) tend to have very low ΔE_Q meaning that caution should be taken when assigning the oxidation state to different doublets.

The magnetic hyperfine field (B_{hf}) is a measure of the magnetic field at an atom which emerges either due to intrinsic magnetization or through the application of an external magnetic field. The B_{hf} is a very convenient parameter for mineral identification with many minerals showing distinct values. In essence, the hyperfine field manifests as a six-line spectrum (sextet) with is symmetrical about the isomer shift with B_{hf} defined as the distance between the outermost peaks. In powdered samples, the relative intensities of peaks 1 to 6 are 3:2:1:1:2:3, respectively. A parameter which is related to the quadrupole splitting and is only observable in the case of a magnetic hyperfine field is the quadrupole shift (ϵ). This occurs when the peaks of the sextet are not equidistant, with peaks 1 and 6 moving in the opposite velocity direction to peaks 2, 3, 4, and 5 (Figure 14). ϵ is related to ΔE_Q by the expression $\epsilon = \Delta E_Q/2$; however, it is often very small in comparison to B_{hf} . Combined with other parameters, however, it is able to provide valuable information for mineral identification (e.g., for goethite or hematite).

Determination of Oxidation State. The ability to distinguish between oxidation states, most notably Fe(II) and Fe(III), and their local atomic coordination is one of the most powerful aspects of ^{57}Fe Mössbauer spectroscopy. This applies in particular to soils and sediments. In general, the redox state of Fe affects the δ and ΔE_Q values of the paramagnetic part of each sample. A δ value of < 0.8 mm/s combined with a $\Delta E_Q < 1$ mm/s is characteristic for Fe(III). In contrast, high spin Fe(II) shows δ values > 1.05 mm/s and $\Delta E_Q > 1.3$ mm/s.³³⁹ It is important, however, to note that certain ferrous phases, in particular low spin octahedral Fe(II) exhibit low δ and ΔE_Q . Such phases include pyrite (FeS_2) which contains Fe(II) covalently bonded to sulfur atoms and has an ΔE_Q of 0.61 mm/s.³⁴⁰ Another point to consider is that in cases where samples are magnetically ordered, ΔE_Q is often smeared out by the hyperfine field; however, the isomer shift remains a valid indicator of oxidation state.

Mineral Identification. Through the comparison of hyperfine parameters against established databases, it is possible to use ^{57}Fe Mössbauer spectroscopy for mineral identification. This is particularly useful when other mineralogical techniques cannot provide such information, for example when using XRD on samples which are dominated by non-Fe containing mineral phases. Furthermore, Mössbauer spectroscopy is particularly useful for measuring short-range ordered minerals (poorly

Table 7. Mössbauer Parameters for Mixed-Valent Fe Minerals Magnetite and Green Rust (GR)^a

mineral	T (K)	oxidation state	δ (mm/s)	ΔE_Q mm/s	B_{hf} (T)	R.A. (%)	ref
magnetite	140	Fe(III) _{Td}	0.38	0.00	50.2	35.9	35
		Fe(II)Fe(III) _{Oh}	0.72	-0.04	47.4	64.1	
GR(SO ₄ ²⁻)	78	Fe(II)	1.27	2.88		66	343
		Fe(II)	0.47	0.44		34	
GR(CO ₃ ²⁻)	78	Fe(II)	1.27	2.93		51	343
		Fe(II)	1.28	2.64		15	
		Fe(III)	0.47	0.42		34	
GR(Cl ⁻)	78	Fe(II)	1.26	2.80		36	343
		Fe(II)	1.27	2.55		37	
		Fe(III)	0.47	0.44		27	

^a δ , isomer shift; ΔE_Q , quadrupole splitting ($\Delta E_Q = 2\epsilon$), where ϵ is quadrupole shift; B_{hf} , hyperfine field; R.A., relative abundance. The reference corresponding to each set of mineral parameters is also included.

Table 8. Raman Mode Frequencies and IR Bands of Magnetite

magnetite	raman shift (cm ⁻¹)						ref
	670	550					122, 349
		560					
	676	550	470	418	319	298	354
	665	540					355
	662.7	533.6			301.6		344
	670	540			308	193	356
	706	570	490		336	226	357
	665	540			311		358
	669	540		410	300		359
	668	538			306	193	352
	666	541			311		360
magnetite	IR bands (cm ⁻¹)						ref
	560						349, 356
	560				350		350
	572 with a shoulder around 700 (nanosized)						361
	570 (nanosized)						362
	570				400		148

crystalline phases), or samples which are X-ray amorphous, though this often applies to Fe(III) (oxyhydr)oxides rather than to mixed-valent Fe minerals. Some examples of Mössbauer spectroscopy being used for mixed-valent minerals include magnetite, GR, greigite, and phyllosilicates which will be briefly discussed here.

Table 7 includes the key Mössbauer mineral parameters of magnetite and GR. The Mössbauer spectrum for magnetite is characterized by two overlapping sextets corresponding to the tetrahedral lattice (tet) which is comprised of only Fe(III) [i.e., Fe(III)_{tet}] and the octahedral lattice (oct) which is comprised of both Fe(II) and Fe(III) [i.e., Fe(II)Fe(III)_{oct}]. Full details of the crystallographic structure of magnetite are provided in section 2.1. The presence of just one sextet for both octahedral ions is attributed to the existence of electron hopping between the Fe(II) and Fe(III) within the octahedral lattice,³⁴¹ although this hopping becomes less prevalent at low temperatures. The spectrum at 140 K for stoichiometric magnetite has an Fe(II)Fe(III)_{oct} sextet with $\delta \sim 0.72$ mm/s, $\epsilon \sim -0.02$ mm/s, and B_{hf} of 47.4 T combined with a Fe_{tet} sextet with $\delta \sim 0.38$ mm/s, $\epsilon \sim 0.00$ mm/s, and B_{hf} of 50.2 T.³⁵ As the measurement temperature decreases below the Verwey transition (~ 121 K), the Fe(II)Fe(III)_{oct} splits into two sextets, resulting in the low temperature spectrum having at least three distinct sextets.³⁴² It is possible to calculate the Fe(II)/Fe(III) ratio from a magnetite spectrum based on the relative areas of

the Fe(II)Fe(III)_{oct} and Fe(III)_{tet} sextets³⁵ according to the formula $\text{Fe(II)/Fe(III)} = [0.5 \times \text{Fe(II)Fe(III)}_{\text{oct}}] / [0.5 \times \text{Fe(II)Fe(III)}_{\text{oct}} + \text{Fe(III)}_{\text{tet}}]$. However, the calculation is most effectively applied when the sample is fully magnetically ordered and above T_v , thus ideally a spectrum obtained at 140 K is considered to be the most effective for determining Fe(II)/Fe(III).³⁵ The incorporation of additional transition elements into the magnetite crystal lattice can also be probed using Mössbauer spectroscopy, which is directly relevant to processes which can occur in the environment. Such incorporations of Zn or Co can lead to changes in δ , ϵ , and B_{hf} .^{68,69}

The presence of both Fe(II) and Fe(III) in GR lends to its suitability for Mössbauer spectroscopy as both sites are observable as distinct doublets. Several studies have even tried to distinguish the different anion groups within different GRs, which has been summarized by Génin et al.³⁴³ Sulfate GR(SO₄²⁻) comprises of Fe(II) and Fe(III) doublets with Fe(II)/Fe(III) of 1.9. Carbonate GR(CO₃²⁻) requires a third Fe(II) doublet and also has Fe(II)/Fe(III) of 1.9. Chloride GR(Cl⁻) comprises of three doublets, though with a Fe(II)/Fe(III) of 2.7. These values of Fe(II)/Fe(III) depend upon level of oxidation and should be noted that many of the parameters of GR are often indistinguishable from Fe-bearing clays.⁹⁴

5.3. Vibrational Spectroscopy

Raman and infrared spectroscopies are commonly used to qualitatively identify the iron phases on corrosion products.^{344–348} Normally, the vibrational characteristics of a solid are affected by crystallinity, particle size, and temperature. To accurately quantify the iron oxides and hydroxides, the use of vibrational spectroscopy is, however, not common.^{344–348}

Raman spectroscopy is generally the vibrational spectroscopy of choice to characterize oxide powders and films as distinct Raman signatures are displayed by various iron oxide polymorphs, and it is possible to take benefit of so-called phonon confinement for better assessment of the sample crystallinity.^{344,349–352} Several Raman bands are identified for magnetite where the most representative band is found at about 667 cm^{-1} .^{352,353} An overview of Raman mode frequencies at room temperature reported in different studies^{122,349,354–360} is shown in Table 8. Generally, the Fe–O bond of bulk magnetite is characterized by the two distinct absorption bands at 570 and 375. For nanosized magnetite, the two bands at 632 and 585 arise due to a split of the band at 570 and a shift to higher wavenumbers, and the band at 440 results when the 375 band is shifted to a higher wavenumber. There is some confusion over the assignments of the phonons for magnetite, particularly the Raman-active phonons. When interpreting Raman data, De Faria et al.³⁴⁴ highlighted the importance of considering laser power to interpret the Raman data. Magnetite can be converted to hematite and maghemite by moderate laser power or heating, and therefore, some of the earlier Raman data evidenced the attribution of phonons of maghemite or hematite impurity to the parent magnetite phase. Findings of De Faria³⁴⁴ were confirmed when laser-induced thermal effects on magnetite were studied by Shebanova and Lazor.³⁵² Figure 15 shows the Raman spectrum of natural sample of GR (called fougérite), extracted in the forest of Fougères (Brittany-France). This spectrum displays the same characteristic bands at 518 and 427 cm^{-1} as the synthetic $\text{GR}(\text{CO}_3^{2-})$ or $\text{GR}(\text{Cl}^-)$.⁸⁵

Although IR is less frequently used, some works reported two IR bands for magnetite located between 360 and 800 cm^{-1} (e.g., bands at 360 cm^{-1} and 565 cm^{-1}) and/or a band at 570 cm^{-1} .^{345,346} Oxidation of magnetite to maghemite leads to the change in the IR spectra where the number of bands significantly increases signaling a transition to a structure of lower symmetry.¹⁴⁸

For GR, the Raman or IR analysis focused mainly on the interlayer anions,^{334,363–370} which are generally used to distinguish the formation of $\text{GR}(\text{SO}_4^{2-})$ and $\text{GR}(\text{CO}_3^{2-})$.

Zegeye et al.^{36,371} pointed out that a typical IR spectrum of $\text{GR}(\text{SO}_4^{2-})$ contains bands due to brucite-like sheets at 515, 780, 880, and 1550 cm^{-1} and bands arising from intercalated SO_4^{2-} at around $620/660$ and $1105/1138\text{ cm}^{-1}$. Two bands, at 1100 and 1145 cm^{-1} , were recorded by Peulon et al.³⁷² for GR-II when deposited electrochemically on inert gold substrate and were assigned to the split $\nu_3\text{SO}_4$ mode. In a GR-I structure, a very intense peak at 1351 cm^{-1} was recorded with a shoulder at 1395 cm^{-1} assigned to the intercalated CO_3^{2-} .³⁶³

5.4. Synchrotron X-ray Absorption

In recent decades, synchrotron-based analytical methods have become extensively used within the geosciences for the analysis of environmentally relevant elements in natural soils and sediments. Synchrotron radiation lends itself toward this field due to its element specificity combined with spatial resolution

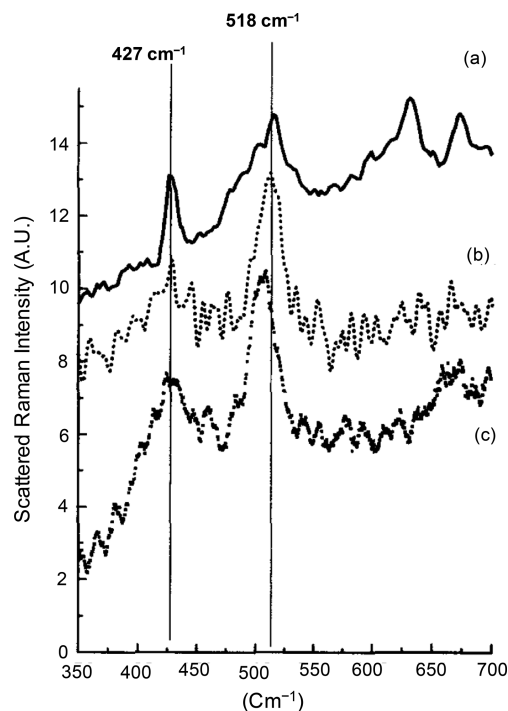


Figure 15. Microprobe Raman spectra of different green rusts (GRs): (a) natural GR, (b) synthetic $\text{GR}(\text{CO}_3^{2-})$, and (c) correspond to synthetic $\text{GR}(\text{Cl}^-)$. Reproduced with permission from ref 85. Copyright 1997 Elsevier.

for analyzing either bulk or nanoscale materials. Synchrotron radiation is produced when electrons are accelerated in circular paths at speeds close to the speed of light, resulting in the release of X-rays (photons) which are then used for probing a sample. In the most basic setup, a sample is irradiated with monochromatic X-rays at a specific energy. As the energy increases, atoms of a specific element absorb the X-rays at an absorption edge. A wide range of techniques making use of this principle are available, including XANES, EXAFS, XMCD, and STXM which are discussed below. For more detailed information, Templeton and Knowles³⁷³ provide an excellent overview of the use of synchrotron-based methods for microbes, minerals, and metals.

The XANES is a general term which is often used when describing absorption edge spectra collected at the *K*-edge. The XANES spectrum is generated when photons are absorbed by an element of interest at its respective absorption edge (for Fe the *K*-edge $\sim 7112\text{ eV}$) causing a core electron to be excited into an unoccupied orbital or ejected from the atom. Information about the oxidation state of Fe mineral phases at the *K*-edge can be obtained by probing the pre-edge features which are obtained in typical XANES spectra (Figure 16a). The energy of an absorption edge shifts to higher values as the oxidation state increases so Fe(II) mineral phases have a lower absorption energy than Fe(III) mineral phases. The method to obtain the element oxidation state from XANES requires the normalization of the absorption pre-edge feature, which is located ~ 15 – 20 eV before the main *K*-edge (see inset Figure 16a). From the normalized pre-edge spectrum, the centroid (for more details see Wilke et al.³⁷⁴) is compared against the integrated pre-edge intensity to reveal both oxidation state and coordination environment (Figure 16b). The separation between the pre-edge centroids of Fe(II) and Fe(III) is

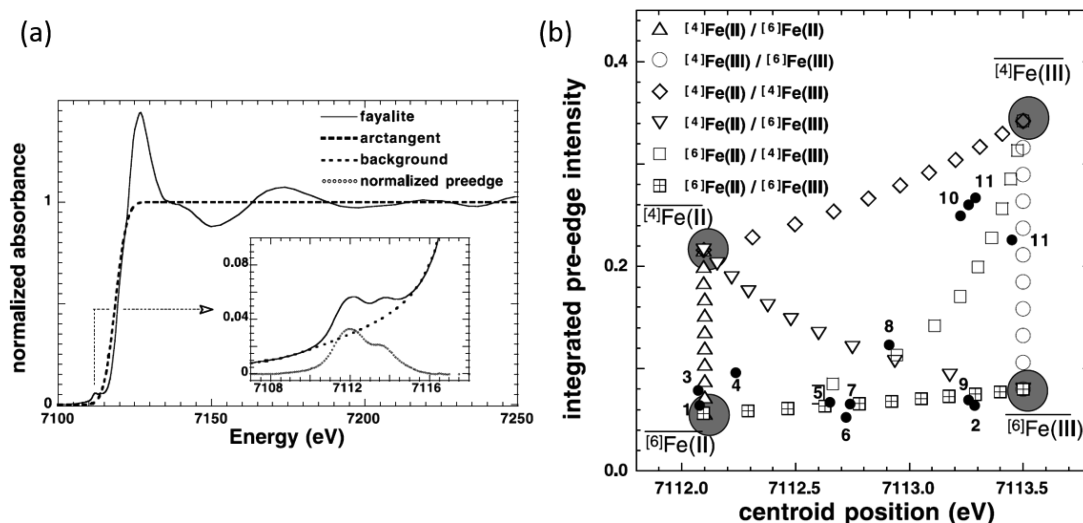


Figure 16. (a) The Fe K-edge absorption spectrum. The inset figure shows the pre-edge feature, which when normalized can be used to calculate the centroid position and integrated pre-edge intensity. (b) Comparison between pre-edge intensity and centroid position (eV) for different oxidation and coordination states of Fe in various Fe minerals. Black circles are 1, humite; 2, rhodonite no. 1; 3, rhodonite no. 2; 4, dumortierite; 5, potassian kaersutite; 6, kaersutite; 7, vesuvianite no. 1; 8, vesuvianite no. 2; 9, franklinite; 10, magnetite no. 1 and no. 2; 11, labradorite; and 12, maghemite. Both (a) and (b) are reproduced with permission from ref 374. Copyright 2001 Mineralogical Society of America.

reported to be 1.4 ± 0.1 eV.^{374,375} Using this approach ThomasArrigo et al. were able to observe small traces of Fe(II) in association with Fe(III) minerals in iron-rich organic floc material isolated from a wetland in Switzerland.³⁷⁶

The EXAFS is also often collected in addition to XANES. EXAFS spectra provide information about the local coordination environment of atoms in a mineral. The EXAFS spectra are characterized by spectral oscillations which are generated when a photoelectron is backscattered by surrounding atoms. The wave patterns of these backscattered electrons interfere with the wave patterns of the outgoing electrons resulting in fine structural differences at energies just above the absorption edge. EXAFS is used to provide information about coordination number, nearest, and next-to-nearest neighbor atom positions and their interatomic distances. Pantke et al. used EXAFS to find that GR is produced as an intermediate phase during the oxidation of Fe(II) to goethite by the nitrate-reducing bacteria *Acidovorax* sp. BoFeN1.²⁷⁶

The XMCD is a form of X-ray absorption spectra (XAS) which utilizes soft X-rays (typically at energies below 10 keV) to investigate the oxidation and coordination state of magnetic minerals. The ferrimagnetic properties of magnetite arise due to the antiparallel alignment of Fe cations within the crystal lattice sites. Specifically, this includes Fe(II) and Fe(III) in octahedral coordination (oct) and Fe(III) in the tetrahedral coordination (tet). XAS collected under the application of oppositely polarized magnetic fields (-0.6 T and $+0.6$ T parallel and antiparallel to the direction of the beam, respectively) will yield small differences (provided that the X-rays are circularly polarized either left or right). Subtraction of one of these spectra from the other results in the origin of the XMCD. Careful analysis of XMCD spectra can be used to reveal changes in magnetization, valence state (i.e., number of *d* electrons), site location, and provide information about magnetic cations with different oxidation states at different lattice sites.³⁷⁷ For instance fitting of the Fe $L_{2,3}$ edge XMCD to atomic multiplet calculations^{378,379} can be used to determine the cation distribution of Fe(II) and Fe(III) in oct and tet sites. Each peak corresponds to a different lattice site with the first

negative peak corresponding to Fe(II) in octahedral environment, the middle positive peak corresponding to Fe(III) in tetrahedral coordination, and the third (negative) peak corresponding to Fe(III) in octahedral coordination. In the case of titanomagnetite, the XMCD spectra contains an additional positive peak which occurs at the low-energy side of the Fe L_3 edge corresponding to Fe(II) in tetrahedral coordination.³⁸⁰ XMCD can thus provide unambiguous determination of the relative site occupancies in spinels,^{49,50} which can be used to obtain information about the Fe(II)/Fe(III) ratio of magnetite, especially at the surface of the mineral.⁴⁸ XMCD has been utilized for the investigation of biogenic magnetite formed through the reduction of ferrihydrite by Fe(III)-reducing bacteria.²⁸² Using the technique, it is also possible to determine how different metals are incorporated into the mineral structure, including arsenic,³⁸¹ chromium,^{382–385} cobalt,^{69,386,387} manganese, nickel, technetium³⁸³ and palladium³⁸⁸ zinc, which have all been investigated. Furthermore, greigite has also been probed using XMCD,^{389–391} which furthermore demonstrates the versatility of the technique for magnetic mixed-valent minerals.

The STXM combines chemical speciation with microscopy at resolutions down to 12 nm.³⁹² It is advantageous over more conventional electron microscopies (e.g., scanning and transmission electron microscopies) because it is able to provide information on the distribution, oxidation state, and coordination environment of different elements. STXM uses soft X-rays and can measure dry samples, hydrated polymers, or biological material, which means it is highly suited to measuring environmentally relevant samples. The basic setup of a STXM beamline enables monochromated X-rays to pass through a zone plate which focuses the X-ray beam onto a single spot (i.e., pixel). Each single pixel then contains a distinct absorption spectra (or XANES) which can be analyzed. von der Heyden et al.³⁹² used STXM on trace amounts of Fe minerals which were extracted from the euphotic zone in the Southern ocean. In this study, XANES were collected at the Fe L_3 absorption edge (~ 710 eV). The energy difference (ΔE) and intensity ratios of the two primary peaks in the L_3 edge,

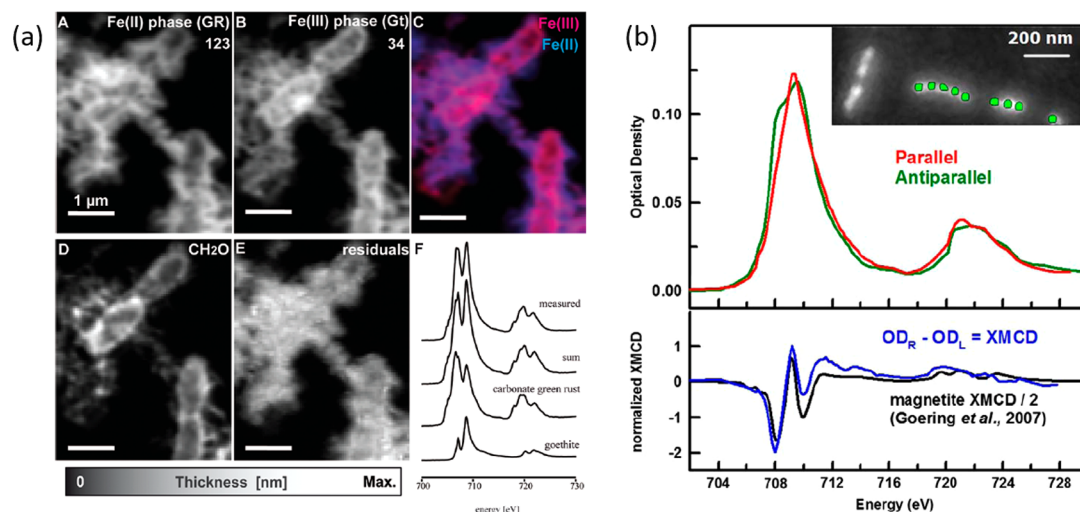


Figure 17. (a) The formation of mixed-valent green rust as an intermediate phase before goethite formation during microbial Fe(II) oxidation was shown using STXM. Reproduced from ref 276. Copyright 2012 American Chemical Society. (b) STXM can be combined with XMCD to provide the cation distribution of Fe(II) and Fe(III) in individual magnetosomes formed within magnetotactic bacteria. Reproduced with permission from ref 283. Copyright 2010 Elsevier.

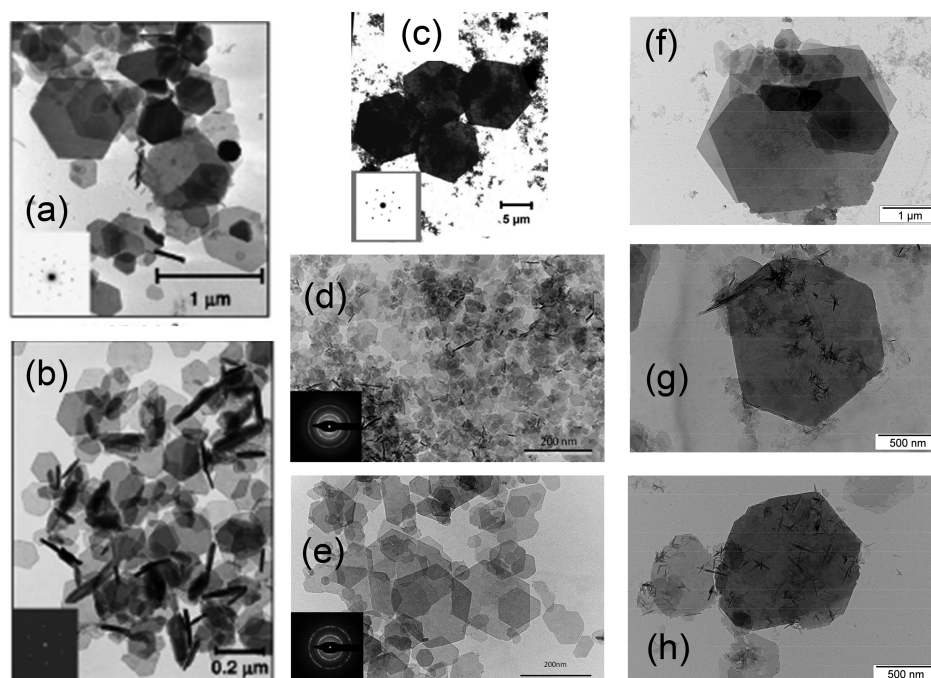


Figure 18. TEM images of different green rusts formed by different procedures. (a) $\text{GR}(\text{SO}_4^{2-})$ and (b) $\text{GR}(\text{CO}_3^{2-})$ were formed by coprecipitation.³¹ Reproduced with permission from ref 31. Copyright 2006 Elsevier Masson SAS. (c) $\text{GR}(\text{CO}_3^{2-})$ formed by bioreduction of lepidocrocite.³⁹⁴ Reproduced from ref 394. Copyright 2002 American Chemical Society. (d and e) correspond to $\text{GR}(\text{CO}_3^{2-})$ formed by coprecipitation but samples are aged for 0 and 24 h, respectively.³⁹⁵ Reproduced with permission from ref 395. Copyright 2012 Elsevier. (f, g, and h) correspond to the $\text{GR}(\text{SO}_4^{2-})$ formed by abiotic mineralogical transformations of ferrihydrite, goethite, and hematite, respectively, where traces of goethite and hematite are still visible in (g and h, respectively).⁵¹ Reproduced with permission from ref 51. Copyright 2012 Elsevier.

corresponding to Fe(II) (lower energy) and Fe(III) (higher energy), were compared to obtain information on the oxidation state, coordination number, and mineral identity of individual grains of Fe minerals at resolutions of ~ 12 nm.³⁹² Other studies using STXM have been able to observe the formation of GR by the nitrate-reducing Fe(II)-oxidizing bacterium *Acidovorax* sp. BoFeN1 (Figure 17a).²⁷⁶ Aqueous Fe(II) was oxidized, leading to the formation of the GR as an intermediate phase which then in turn underwent transformation to goethite. It has also been shown that STXM can be combined with XMCD to determine

the cation distribution of Fe(II) and Fe(III) within individual magnetosomes grown inside magnetotactic bacteria (Figure 17b).²⁸³ The study confirmed that the magnetic moment of the individual magnetosomes were aligned in the same direction and was also able to show that magnetosomes were slightly enriched in Fe(II) (i.e., they were reduced). The cation distribution within magnetite produced via dissimilatory Fe(III) reduction by *Shewanella oneidensis* have also been analyzed using this combination of STXM and XMCD.³⁹³

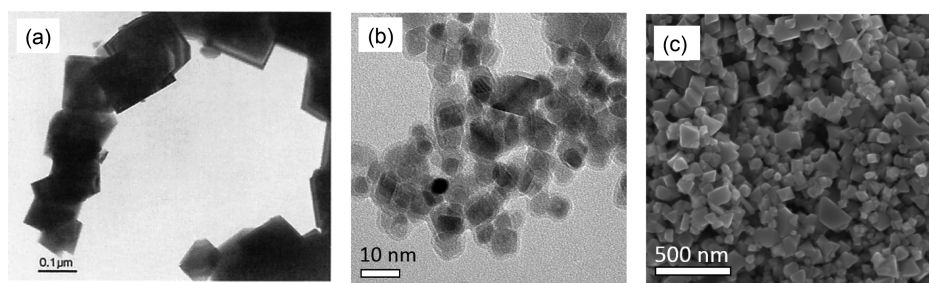


Figure 19. TEM images of magnetites synthesized by different procedures. (a) Magnetite synthesized by Schwertmann and Cornell³⁹⁷ from FeSO_4 solution. Reproduced with permission from ref 397. Copyright 2000 John Wiley and Sons. (b) Nanomagnetite synthesized by Byrne et al.⁴⁸ from FeSO_4 solution by modifying method of Schwertmann and Cornell,³⁹⁷ and (c) micromagnetite synthesized by Byrne et al.⁴⁸ from FeCl_2 and FeCl_3 solution. Both (b) and (c) images are reproduced with permission from ref 48. Copyright 2016 Nature Publishing Group. TEM images of magnetite formed by abiotic transformation of ferrihydrite, lepidocrocite, and goethite can be seen in Figure 8.

5.5. Transmission Electron Microscopy and Scanning Electron Microscopy

The morphology of mixed-valent iron oxides is routinely examined by TEM and SEM.² These imaging techniques provide insights into the micron and nanoscale structure of these minerals. TEM usually provides 2D image while SEM can provide more information on topology (i.e., pseudo 3D).² Shape of GR particles varies from hexagonal to rhombohedral (Figure 18), while magnetite can have commonly cubic, octahedral, or hexagonal crystal structure (Figure 8 and Figure 19).^{31,37,51} GRs typically have thin, platelike hexagonal crystals (Figure 18); however, crystals of $\text{GR}(\text{SO}_4^{2-})$ have been observed to be much larger³¹ and flatter³² than $\text{GR}(\text{CO}_3^{2-})$.

It should be noted that the morphology of magnetite or GR can vary significantly with the method of formation and other reaction conditions. Hexagonal platelets are the typical crystal habit of GR; however, slight variations in GR morphology varied according to the method of synthesis as evident from TEM images of GRs formed by various methods (Figure 18). Owing to the strong diffraction behavior of these plates, derived structural data is often comparable to that obtained through XRD. Similarly, magnetite occurs most commonly as octahedral crystals,² but varying methods of synthesis can yield different crystal habits (Figure 19). For example, magnetite crystals obtained by slow oxidation of a FeCl_2 solution at room temperature were round-shaped³⁹⁶ as compared to the octahedral particles which were formed by oxidation of a FeSO_4 (0.5 M) solution with KNO_3 in KOH (1.43 M) at 90 °C.^{2,397} Recently, Byrne et al.⁴⁸ modified the later synthesis method where a FeSO_4 solution (absence of Fe(III)) was ensured by storing it with Fe^0 for one month prior to oxidation) was oxidized in alkaline solution of KNO_3 at 90 °C under strict N_2 atmosphere. Obtained product was micromagnetite ($d \sim 100\text{--}200$ nm) with rounded particles along with some squared ones. However, nanosized magnetite particles ($d \sim 12$ nm) with similar shape (rounded with squared) were obtained by Byrne et al.⁴⁸ when anoxic solution of 1 M FeCl_2 and 2 M FeCl_3 in 0.3 M HCl was added dropwise into 25% NH_4OH solution. Usman et al.³⁷ reported that magnetite formed by abiotic mineralogical transformations of ferrihydrite, lepidocrocite, and goethite, have different morphologies, particle size, and surface area (Figure 8). They reported that magnetite formed ferrihydrite was characterized by smaller particles with nonuniform shape and size (<50 nm). However, when magnetite was formed from lepidocrocite or goethite, the shape of its particles varied between hexagonal to octahedral (Figure 8). Moreover, size of magnetite particles was

70–80 nm and 200–300 nm when formed from lepidocrocite and goethite, respectively.³⁷

5.6. Magnetic Measurements

The ubiquity of magnetic minerals in almost all natural environments means that magnetic-based measurements provide a powerful tool for investigating past and present changes to the Earth's geology, ocean currents, windblown deposits, pollution, and climate. For example, the use of magnetic methods on soils taken from the Chinese Loess Plateau has enabled changes to the extent of ice age glaciers to be determined throughout time by probing the type of magnetic material deposited during warm and moist conditions compared to cold and dry conditions.³⁹⁸ Furthermore, magnetic measurements are also being used to measure the effects of anthropogenic pollution in plant matter as well as to human health.^{64,399}

Magnetism is dependent upon the movement of electrons around an atom which generates a magnetic dipole (or magnetic moment). The magnetic behavior of Fe minerals, particularly mixed-valent magnetite and greigite mean that a number of different magnetic based measurements can be used to obtain information about their relative abundance, grain size, chemical composition, and stoichiometry. Here we present a very brief overview of some of the parameters typically investigated using magnetic measurement techniques as well as a short introduction to some of the instruments with which such measurements can be performed.

The most commonly occurring magnetic minerals are Fe minerals, but within most of these minerals the magnetic moments of the Fe atoms do not interact with each other and are randomly orientated due to thermal energy. Consequently, the magnetic moments cancel each other out, resulting in paramagnetism (e.g., ferrihydrite). In ferromagnetic materials, the magnetic moments of each atom are coupled together and are aligned parallel to one another leading to strong magnetic behavior. In some minerals, coupled layers of Fe atoms form in which the net magnetic moment of these layers are in antiparallel orientation to each other, thereby canceling each other out and resulting in no overall magnetization (antiferromagnetism), though in some cases these moments are slightly misaligned and result in canted antiferromagnetism (e.g., hematite). Magnetite is a ferrimagnetic mineral in which Fe(II) and Fe(III) ions exist in octahedral coordination with magnetic moments antiparallel to Fe(III) in tetrahedral coordination leading to a cancellation of the Fe(III) moments and an overall net magnetic moment due to only Fe(II) atoms.

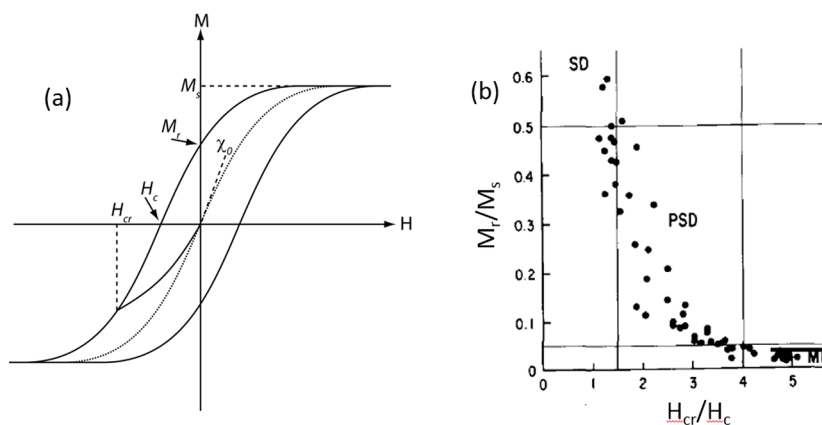


Figure 20. (a) A hysteresis loop shows how the magnetization (M) of a sample changes with applied field (H). From the loop, it is possible to determine saturation magnetization (M_s), remanent magnetization (M_r), coercivity (H_c), coercivity of remanence (H_{cr}), and susceptibility. (b) Data from a hysteresis loop can be inserted into a Day plot to show the approximate grain size of magnetite in a sample. Reproduced with permission from ref 400. Copyright 1977 Elsevier B.V.

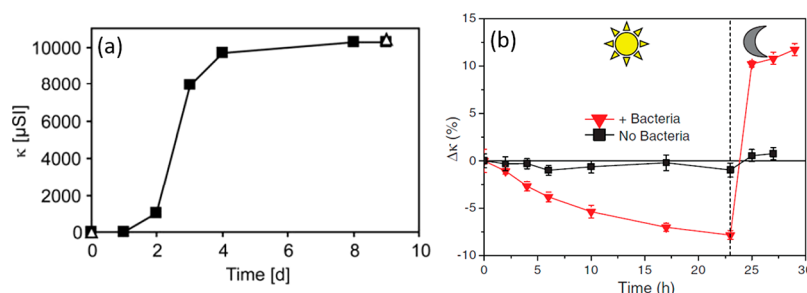


Figure 21. (a) Changes to volume-dependent magnetic susceptibility (κ) during microbial reduction of ferrihydrite to magnetite.⁴⁰³ Reproduced from ref 403. Copyright 2010 American Chemical Society. (b) Relative changes to κ during the incubation of magnetite with Fe(II)-oxidizing and Fe(III)-reducing bacteria. Decreases in κ correspond to oxidation while increases in κ correspond to reduction.³¹⁵ Reproduced with permission from ref 315. Copyright 2015 The American Association for the Advancement of Science.

Superparamagnetism describes materials which are small enough so that at room temperature they show no residual magnetic behavior, however, when cooled through their blocking temperature (T_b) show very strong magnetic characteristics (e.g., nanomagnetite).

Several different techniques are used for measuring magnetic properties including several temperature dependent tools. A hysteresis loop (Figure 20) contains information about the magnetization M of a mineral when it is subject to an applied magnetic field H . The point at which all magnetic moments within the mineral are aligned and there is no increase in M is called the saturation magnetization (M_s). If a sample retains magnetic ordering at room temperature, this is called the remanent magnetization (M_r). The field required to ensure a sample has no magnetization is called the coercivity (H_c). A superparamagnetic material is one which has no coercivity (i.e., $H_c = 0$). The applied field required to remove remanence once the magnetic field is removed is called the coercivity of remanence (H_{cr}). Finally the susceptibility (χ) describes the initially linear increase in magnetization in a low field.

Hysteresis loops can also be used to approximately determine the grain size of a mineral under investigation by following the definitions of superparamagnetic (SP), pseudo single domain (SD), and multidomain regimes (MD) as outlined previously.⁴⁰⁰ SP describes magnetite with particle size $d < 30$ nm, $M_r/M_s \ll 0.01$, and $H_{cr}/H_c > 10$. PSD magnetite falls within the range of $30 < d < 100$ nm and has $0.1 < M_r/M_s < 0.5$ and $2 < H_{cr}/H_c < 4$ combined with $10 \text{ mT} < H_c < 15 \text{ mT}$. Finally MD

magnetite has $d > 100$ nm, $M_r/M_s < 0.1$, $H_{cr}/H_c > 4$, and $H_c < 10 \text{ mT}$.⁴⁰¹ Such a method is particularly useful in environmental samples where it is not possible to isolate individual magnetic grains to determine their particle size by microscopy. This approach, however, can be affected by mixtures of particles with different size distributions. Several types of instruments can be used to obtain a hysteresis loop, including alternating gradient force magnetometer (AGFM), vibrating sample magnetometer (VSM), or superconducting quantum interference device (SQUID) magnetometer. These different techniques are often coupled with cryostats or furnaces to obtain temperature-dependent measurements.

Other techniques frequently used within geosciences focus on the determination of magnetic susceptibility (χ), often in the form of volume-dependent magnetic susceptibility (κ). This technique applies a low AC magnetic field (e.g., 300 A/m with frequency of 875 Hz) onto a sample which is held within a pick-up coil. For example Porsch et al.²³¹ used volume-dependent magnetic susceptibility to track Fe(III) mineral reduction by the Fe(III)-reducing bacteria *Shewanella oneidensis* MR-1. Over time it was shown that κ increased as the mineral sample transformed from paramagnetic ferrihydrite to ferrimagnetic magnetite (Figure 21a). A small decrease in κ after the magnetite formation was ascribed to be due to either siderite formation or the increase in magnetite grain size. This is because κ is related to grain size with superparamagnetic particles exhibiting higher susceptibility than single domain magnetite.⁴⁰² Using κ has also been used to determine regions

of high magnetic content in hydrocarbon contaminated soils, which was suggested to be due to microbial activity.^{109,237} Furthermore, κ was recently used to observe redox changes (i.e., oxidation or reduction) in magnetite induced by Fe(II)-oxidizing or Fe(III)-reducing bacteria under the influence of different geochemical conditions (Figure 21b). Thus, using such techniques offer noninvasive, rapid, and inexpensive approaches to quantifying relative changes to the magnetic content of a sample which can often include cores and complex model environments.

6. APPLICATION OF MIXED-VALENT IRON MINERALS FOR ENVIRONMENTAL REMEDIATION

This section illustrates the role of mixed-valent Fe minerals in biogeochemical cycling of trace elements, their ability to affect the mobility, redox transformation, and toxicity of various organic and inorganic pollutants, and their use in various remediation strategies for contaminated water and soils. Mineral properties such as surface area, particle size, and stoichiometry have a dramatic impact on their efficiency in such applications and that will also be highlighted. Due to the presence of structural Fe(II), mixed-valent Fe minerals are considered as highly reactive to catalyze chemical oxidation (Fenton-like, persulfate, and photocatalytic) of organic pollutants at circumneutral pH and that is discussed as a last part of this section.

6.1. Sorption of Contaminants

Mixed-valent Fe minerals play a significant role in the sorption of organic and inorganic compounds in the environment and thus influence the transport and mobility of contaminants in natural and engineered systems. For instance, magnetite commonly occurs in natural and engineered settings,⁹⁹ and due to its reactive and high surface area, it plays a significant role in the sorption of environmental pollutants (Table 9). Magnetite is used in analytical chemistry to separate a wide variety of substances, such as dissolved metal species, organic, and biological materials.⁴⁰⁴ From an engineering point of view, the magnetic properties of magnetite and its thermodynamic stability make it very suitable for its use as a sorbent in environmental remediation processes. Indeed, the use of magnetite in wastewater treatment, in situ groundwater remediation, and for recovery of valuable metals from mine waters has several advantages over conventional techniques. Owing to its ferromagnetic character (further details in section 2.4), it can be used to treat the contaminated water supply where it can be kept in place using a magnetic trap or can be separated by using a magnet with low field strength. Magnetic separation offers quick recovery and reuse of magnetite for further remediation.⁴⁰⁵ The removal of particles from solution with the use of magnetic fields is therefore likely to be more efficient, selective, and much faster than filtration or centrifugation.⁴⁰⁵

The GRs have been widely reported to transform several inorganic and organic contaminants through redox processes (see section 6.2); however, this has led to a distinct lack of information of the sorption ability of GR which is rarely investigated independently of the redox reaction. Indeed, as the binding of substrate to oxide surfaces is a prerequisite to induce heterogeneous reduction reactions, both of these processes are often considered together in published reports, particularly in the case of redox-active elements. Despite this lack of understanding of sorption behavior, GRs are anion-exchangers

and clearly represent potential sorbents in anoxic environments. Due to the amphoteric surface hydroxyl groups, GR can also sorb anions (organic and inorganic) and cationic metals. Similarly to hydroxalite, GR may also sorb acidic compounds, which typically exist in anionic form at neutral pH. This adsorption may proceed through (i) anion exchange or (ii) ligand exchange or surface complexation reaction on external sites.^{406–408}

To best describe the sorption properties of mixed-valent Fe minerals, this section has been subdivided into (i) sorption of inorganic compounds including oxyanions, heavy metals, and radionuclides and (ii) sorption of organic compounds, including naturally occurring ligands and emerging contaminants. Salient sorption studies in environmental and engineering contexts using GR and unsubstituted pure magnetite are summarized in Table 9.

6.1.1. Inorganic Compounds. Recently, there has been a growing interest in the use of magnetite in the removal of metals and oxyanions from water, with the aim of developing new cost-effective, nontoxic, and magnetic filtration/sorption remediation strategies.^{409–413} Magnetite nanoparticles have shown to be very efficient for the removal of arsenic (As) and chromium (Cr) from water, as the adsorption capacity generally increases with decreasing particle size.^{414,415} Magnetite showed high affinity for both arsenite-As(III) and arsenate-As(V)⁴¹⁶ in comparison to conventional techniques (ion exchange, coagulation, adsorption onto activated alumina) which require preoxidation of As(III) to As(V) in order to enhance sorption efficiency.⁴¹⁷ Variations in pH, temperature, and ionic strength can also affect the speciation and adsorption of oxyanions to magnetite.⁴¹⁸ The adsorption of As(III) as well as As(V) onto magnetite (point of zero charge ~ 7) was found to be pH-dependent.^{116,411} Arsenic sorption decreased with increasing ionic strength, probably due to compression in diffused double layer, increase in particle aggregation and decrease in the available surface area for arsenic adsorption. High adsorption of arsenic was observed at high temperatures, which may be due to an increase in the kinetic activity or increase in the mass transfer rate from solution to surface.⁴¹⁵

From a microscopic perspective, Jönsson and Sherman⁴¹⁹ pointed out that As(V) sorbs to magnetite and $\text{GR}(\text{CO}_3^{2-})$ by forming inner-sphere surface complexes resulting from corner sharing between AsO_4 groups and FeO_6 octahedra. GR and magnetite strongly sorb As(V) with sorption capacities greater than $100 \mu\text{mol As g}^{-1}$ around pH 7, with no indication of abiotic reduction of adsorbed As(V) by structural Fe(II). For the very first time, Wang et al.⁴²⁰ showed the predominant formation of tridentate As(III)O_3 complexes occupying the vacant tetrahedral sites on (111) surfaces of magnetite. The EXAFS spectra by Liu et al.⁴¹⁶ suggested the existence of bidentate binuclear corner-sharing complexes for As(V) and tridentate hexanuclear corner-sharing complexes for As(III) on magnetite surfaces. However when sorption of arsenic was studied onto $\text{GR}(\text{Cl}^-)$, As(V) sorbs more efficiently than As(III).⁴²¹ Both arsenic species formed inner sphere complexes at surface coverages of 0.27 and $2.70 \mu\text{mol m}^{-2}$. With EXAFS derived data for As(V), they proposed the presence of monodentate mononuclear corner-sharing complexes and binuclear bidentate double-corner complexes. However, they suggested the predominant binding of As(III) pyramids to the edges of $\text{GR}(\text{Cl}^-)$ layers by corner sharing with FeO_6 octahedra.⁴²¹ Other inorganic ligands such as silicate and

Table 9. Summary of Quantitative Findings of Sorption of Different Compounds to Magnetite or GR^a

sorbent type	target pollutant and its initial concentration	experimental conditions	extent/rate of adsorption	ref
magnetite (natural) < 180 μm; 18.3 m ² g ⁻¹	Cs (I): 2 × 10 ⁻⁵ mol L ⁻¹ ; Ba (II): 5 × 10 ⁻⁵ mol L ⁻¹ ; Eu (III): 2 × 10 ⁻⁴ mol L ⁻¹	pH 3–11, magnetite 2 g L ⁻¹ , ionic strength (I) = 10 ⁻² and 10 ⁻¹	90% for Ba (II) at I = 10 ⁻² and pH > 11, 100% for Eu (III) at pH > 7 and I = 10 ⁻¹ , <50% of sorption for Cs(I) which was independent of pH	428
magnetite (natural) 33.3 μm; 1.8 m ² g ⁻¹	Yb(III): 2.10 ⁻⁵ mol L ⁻¹ ; Ni(II): 2.10 ⁻⁵ mol L ⁻¹ ; Cs(I): 4.10 ⁻⁵ mol L ⁻¹	pH 3–11, NaNO ₃ = 0.1 mol L ⁻¹ for Yb(III) and Ni(II), 0.01 mol L ⁻¹ for Cs(I); magnetite = 12 g L ⁻¹ for Yb(III) and Cs(I), 8 g L ⁻¹ for Ni(II)	100% for Yb(III) and Ni(II) (pH 7) and negligible for Cs(I) (<10%),	117, 118
magnetite (commercial) 0.1 μm; 2 m ² g ⁻¹	Cs, Sr, and Co 1000 ppm each	pH 6–9 (for Cs and Sr) and 5–8 (for Co), magnetite 10 g L ⁻¹ , NaNO ₃ = 0.01 N	q _{max} (μmol m ⁻²) = 0.70 (Cs, pH 6), 3.92 (Sr, pH 7), and 3.88 (Co, pH 8)	429
magnetite (lab synthesized) 50–200 nm; 8.5 m ² g ⁻¹	U(VI), 4.4 × 10 ⁻⁷ mol L ⁻¹	pH 6, I = 0.1 mol L ⁻¹ solid/liquid ratio 2 g L ⁻¹	90% after 1 day	412
magnetite (lab synthesized), 90 m ² g ⁻¹	As(III) and As(V), 100 μM As(III)	pH 9, magnetite 0.5 g L ⁻¹ , 0.01 M NaClO ₄	maximum sorption density 140 μmol g ⁻¹ after 24 h for As(III)	411
magnetite (natural) < 5 μm; 0.89 m ² g ⁻¹	Se(IV) and Se(VI), 3 × 10 ⁻⁶ to 5 × 10 ⁻⁴ dm ³ mol ⁻¹	pH 4, 5 g L ⁻¹ magnetite, reaction time 30 h	K _L (dm ³ mol ⁻¹) = 3 × 10 ⁵ and 1.19 × 10 ⁶ for Se(VI) and Se(IV), respectively, with maximum sorption (mol m ⁻²) of 3.5 × 10 ⁻⁶ and 3.13 × 10 ⁻⁶	410
magnetite (commercial) < 5 μm; 1.58 m ² g ⁻¹	U(VI), 10 ⁻⁴ mol L ⁻¹	1 g of magnetite, acidic pH, 0.1 mol L ⁻¹ NaClO ₄	existence of both U(IV) and U(VI) during uranium sorption, which was correlated to the reduction of U(VI) to U(IV) by magnetite	430
three kinds of magnetite: M1: lab-synthesized 11.72 nm, 98.8 m ² g ⁻¹ ; M2: commercial 20 nm; 60 m ² g ⁻¹ ; M3: commercial 300 nm; 3.7 m ² g ⁻¹	As(III) and As(V), 0–250 μmol L ⁻¹	pH 4.8, 6.1 and 8; magnetite = 0.1 g L ⁻¹ for M1 and M2 and 2.5 g L ⁻¹ for M3 0.01 M NaNO ₃	q _{max} (μmol g ⁻¹) for As(III) = 20 (M3), 388 (M2) and 1532 (M1) after 24 h	414, 415
magnetite (lab synthesized) 40 nm; 31 m ² g ⁻¹	phosphate, 0–1600 mg L ⁻¹	pH 3, magnetite 1 g L ⁻¹ , 24 h	maximum adsorbed amount is 5.2 mg g ⁻¹ at equilibrium P concentration above 300 mg L ⁻¹	439
magnetite (commercial) 1.6 m ² g ⁻¹	H ₄ SiO ₄ , 1.85 × 10 ⁻⁴ mol L ⁻¹	pH 7, magnetite 4 g L ⁻¹ , I = 10 ⁻² M (NaNO ₃)	magnetite sorbed almost 40% of silicates after one week (equilibrium reached)	438
magnetite (natural) 0.1 nm; 0.89 m ² g ⁻¹	As(III) and As(V), 2 × 10 ⁻⁵ M	pH 6.5, magnetite 5 g L ⁻¹ , 0.1 mol L ⁻¹ NaCl	sorption rate constant k (m ² mol ⁻¹ h ⁻¹) was 0.82 and 0.47 for As(III) and As(V), respectively; K _L (dm ³ mol ⁻¹) = 2.50 × 10 ⁴ for As(III) and 1.4 × 10 ⁵ for As(V)	116
magnetite (commercial) 20 nm; 60 m ² g ⁻¹	As(III) and As(V), 100 μg L ⁻¹	pH 8, magnetite 0.5 g L ⁻¹	>90% removal of both species within 2 h; values of k _{SA} (L min ⁻¹ m ⁻²) were 0.0055 and 0.0064 for As(V) and As(III), respectively	418
magnetite (lab synthesized) 12 nm; 74 m ² g ⁻¹	radionuclides ¹³⁷ Cs (4 × 10 ⁻¹⁰ M), ⁹⁰ Sr (4 × 10 ⁻¹⁰ M), ¹⁵⁴ Eu (2 × 10 ⁻⁹ M), ¹⁴⁷ Pu (7.5 × 10 ⁻⁸ M)	pH 7, magnetite 2 g L ⁻¹ , I = 0.01 M (NaClO ₄)	sorption extent was 30% (Cs), 60% (Sr), 100% (Eu and Ce)	427
magnetite (commercial) 1.59 m ² g ⁻¹	Th(IV) 1.1 × 10 ⁻⁶ M	pH 3, magnetite 10 g L ⁻¹ , I = 0.01 M (NaClO ₄), T = 298 K	maximum sorption (almost 100%) after 14 days	431
magnetite (commercial) 720 nm; 1.68 m ² g ⁻¹	sulfate 1.5 × 10 ⁻⁵ M	pH 4, magnetite 10 g L ⁻¹ , I = 0.001 M (KCl), T = 25 °C	a constant concentration of sorbed sulfate (0.35 at nm ⁻²) was attained quickly (within 24 h)	441
GR(Cl ⁻) (lab synthesized) 49 m ² g ⁻¹	As(III) and As(V), 1.67 mM	pH 7.2, T = 25 °C, GR 12.5 g L ⁻¹ , I = 0.1 M (NaCl), anoxic conditions	sorption extent was almost 100% for both species after 24 h	421
magnetite (lab synthesized) 50–100 nm	U(VI), 30 mg L ⁻¹	pH 7, magnetite 1 g L ⁻¹ , I = 0.01 mol L ⁻¹ (NaClO ₄)	quick sorption (5.5 mg g ⁻¹) attained after 4–6 h	435
magnetite (commercial) 23–50 nm; 52.5 m ² g ⁻¹	U(VI), 0.5 mg L ⁻¹	pH 8.5, magnetite 0.25 g L ⁻¹	approximately 20% removal of uranium after 48 h	434
magnetite (natural)	U(VI), 0.1 mM	pH 5 and 10; 1 mM NaNO ₃ ; anaerobic conditions	sorption loadings (μmol m ⁻²) were 22.34 (pH 5) and 25.23 (pH 10) after 12 h of exposure	436, 437
three kinds of magnetite (lab synthesized), (1) 8 nm; 190 m ² g ⁻¹ ; (2) 12 nm; 110 m ² g ⁻¹ ; (3) 35 nm; 46 m ² g ⁻¹	Ni(II), 41.87 mg L ⁻¹ ; Cu(II), 47.44 mg L ⁻¹ ; Cd(II), 45.87 mg L ⁻¹ ; and Cr(VI), 43.61 mg L ⁻¹	pH 4, T = 20 °C, magnetite 25 g L ⁻¹ was used to treat wastewater containing all the target metals	MI showed the highest sorption efficiency (mg L ⁻¹): 0.86, 0.13, 0.89, and 1.62 for Ni(II), Cu(II), Cd(II), and Cr(VI), respectively	461
magnetite (lab synthesized) 8 nm; 95.5 m ² g ⁻¹	Pb(II), Cu(II), Zn(II), and Mn(II), 150 mg L ⁻¹	pH 5.5, T = 298 K, magnetite, 4 g L ⁻¹	the maximum adsorption capacities ranged between 0.14 to 0.18 mmol g ⁻¹ for these metals	423
magnetite (natural) 20–40 nm; 11.9 m ² g ⁻¹	As(III), 5 mg L ⁻¹	pH 7.9, magnetite, 8 g L ⁻¹ (mechanically activated)	maximum sorption efficiency of 96% was obtained after 6 h	462
two kinds of magnetite (lab synthesized by different methods), (1) 25 nm; (2) 27 nm	Cr(III) and Cr(VI), 100 ppb	pH 4, magnetite, 2.5 g L ⁻¹	more than 90% was observed for both species after 1 h	463

Table 9. continued

sorbent type	target pollutant and its initial concentration	experimental conditions	extent/rate of adsorption	ref
magnetite (lab synthesized), 2 and 7 nm 125 m ² g ⁻¹	Cr(VI), 100 mg L ⁻¹	pH 5.5, magnetite, 2 g L ⁻¹	88% of pollutant was removed after 1 h (equilibrium)	424
magnetite (lab synthesized), 34 nm; 39 m ² g ⁻¹	As(III) and As(V), 0.75 mM	pH 5, T = 25 °C, I = 0.01 M (NaNO ₃), magnetite, 1 g L ⁻¹	adsorption rate was 7.7 and 6.7 mmol g ⁻¹ h ⁻¹ for As(V) and As(III), respectively; k ₂ (g mmol ⁻¹ h ⁻¹) = 192 for As(V) and 179 for As(III)	416
magnetite (lab synthesized), 15 nm	Ce(IV), 50 mg L ⁻¹	pH 3.8, T = 25 °C, magnetite, 250 mg L ⁻¹	maximum sorption capacity was 160 mg g ⁻¹ (equilibrium reached in 60 min)	432
magnetite (commercial) < 50 nm, 40 m ² g ⁻¹	oxytetracycline, 2 mM	pH 5.55, T = 35 °C, magnetite, 20 g L ⁻¹ , I = 0.01 M (KCl)	>90% was sorbed within 25 min, pseudo-first-order rate coefficient = 8 × 10 ⁻⁵ s ⁻¹	444
magnetite (lab synthesized), 10 nm, 127 m ² g ⁻¹	chlorotetracycline, 5 mg L ⁻¹	pH 6.5, T = 298 K, magnetite, 0.05 g L ⁻¹ , I = 10 mM (NaCl)	maximum adsorption capacity was 476 mg g ⁻¹ with K _L value of 23 051 L mg ⁻¹	445
magnetite (commercial), 4 μm, 2.4 m ² g ⁻¹	pentachlorophenol, 50 mg L ⁻¹	pH 7, T = 20 °C, magnetite 2 g L ⁻²	langmuir maximum sorbed amount = 0.023 mmol m ⁻² and K _L = 10.5 L mmol ⁻¹	460
GR(CT) (lab synthesized), 19.1 m ² g ⁻¹	benzoic acid, phthalic acid, and mellitic acid, 0.1–5 mM	pH 8, GR, 10 g L ⁻¹ , I = 50 mM (NaCl)	q _{max-langmuir} (mmol g ⁻¹) = 4.18 × 10 ⁻³ for benzoic acid, 2.7 × 10 ⁻² for phthalic acid, and 2.56 × 10 ⁻¹ for mellitic acid; K (L mmol ⁻¹) = 0.58 for benzoic acid, 21 for phthalic acid, and 218 for mellitic acid	447
magnetite (lab synthesized), 95.3 m ² g ⁻¹	gallic acid and humic acid 10 mmol L ⁻¹	pH 6.5, room temperature, magnetite 1–20 g L ⁻¹ , I = 0.01 M NaCl	highest sorption was observed in case of humic acid (0.9 mmol g ⁻¹) vs < 0.4 mmol g ⁻¹ for gallic acid	452, 453
three kinds of magnetite: (1) lab-synthesized 30 nm, 103 m ² g ⁻¹ ; (2) lab synthesized 60 nm, 25 m ² g ⁻¹ ; (3) commercial, 1.5 μm, 1.7 m ² g ⁻¹	nalidixic acid 200 μM	pH 6.5, T = 20 °C, magnetite, 0.5 g L ⁻¹ , I = 10 ⁻² M (NaCl)	maximum sorbed amount (μmol g ⁻¹) was in the following order: M1 (172 μmol g ⁻¹) > M2 (74 μmol g ⁻¹) > M3 (16 μmol g ⁻¹) with K _d (g μmol ⁻¹ min ⁻¹) values of 1.85 × 10 ⁻⁴ (M1), 1.26 × 10 ⁻³ (M2), and 2.22 × 10 ⁻² (M3)	446

^aThe source of magnetite (natural or synthetic) is indicated, while all GR samples were lab-synthesized. Studies are arranged according to their order of appearance for inorganic and organic compounds.

phosphate have also been shown to sorb to the external faces of GR.^{408,422}

Studies have shown the ability for magnetite nanoparticles to sorb heavy metals such as Pb(II), Cu(II), Zn(II), and Mn(II).^{423,424} The adsorption capacity of magnetite nanoparticles toward metal ions was found dependent on the electronegativity of these ions. Moreover, the adsorption capacity of heavy metals strongly varied according to the pH and temperature of solution. The adsorption mechanism seems to be mainly an electrostatic attraction between metal ions and the magnetite affected by the hydrated ionic radius of the metal cations. Modification of magnetite particles by coating with humic acid or chitosan has also been reported for enhancing removal of cationic metals such as Cd(II), Cu(II), Hg(II), Pb(II), and Ni (II) from water.^{425,426}

Numerous studies have focused on using magnetite to target the migration and fate of persistent radionuclides in the environment, especially in the context of nuclear waste disposal.^{427–432} This is of particular interest because it is thought that magnetite formation may occur during the anoxic corrosion of steel containers used to store nuclear waste. Environmental factors strongly affect the sorption of elements onto magnetite. For instance, Catalette et al.⁴²⁸ reported that magnetite has a high retention capacity for Ba(II) and Eu(III), while Cs(I) is sorbed on magnetite only if magnetite contains some impurities such as silica. The sorption of ¹³⁷Cs and ⁹⁰Sr increases with pH, with higher sorption for ⁹⁰Sr than that for ¹³⁷Cs at any pH.⁴²⁷ Both of these radionuclides were sorbed primarily by electrostatic interaction between the positively charged cation and the negatively charged magnetite surfaces (pH ≥ PZC). Magnetite showed strong sorption of the tetravalent radionuclide, ¹⁴¹Ce(IV), at all pH values, with the sorption being nearly independent of ionic strength, advocating the participation of inner sphere type of coordination between the metal ion and the surface sites or surface precipitation.⁴²⁷ In Martínez et al.,⁴¹⁰ the variation of the sorption of selenium (Se) on magnetite with pH has been described as two inner-sphere complexes for Se(IV) and an outer-sphere complex for Se(VI). Magnetite nanoparticles have been also used to remove U(VI) from contaminated waters.^{433,434} Das et al.⁴³⁵ showed that high adsorption of U was observed at neutral pH, whereas reduced species U(IV) on the magnetite surface was detected by X-ray photoelectron spectroscopy (XPS). Adsorption and reduction of U(VI) and subsequent growth of UO₂ nanoprecipitates have also been reported using XANES and atomic force microscopy (AFM).^{436,437}

Adsorption of naturally occurring inorganic ligands such as carbonate, sulfate, silicate, and phosphate have been largely studied at both macroscopic and molecular levels and are known to be strong competitors of oxyanions (e.g., As or Cr) for sorption on magnetite surfaces.^{438–443} XPS, Mössbauer, and IR spectroscopies have provided evidence that Fe(III) in octahedral sites is involved in phosphate adsorption with formation of protonated binuclear species,⁴³⁹ while outer-sphere complexation was rather suggested for ligands such as sulfate and carbonates.

6.1.2. Organic Compounds. In contrast to inorganic compounds, only few studies are available on the mechanism and extent of sorption of organic contaminants (classical or emerging) on magnetite or GR. Generally, binding of organic compounds proceed through hydrogen bonding, van der Waals interactions, and surface complexation reactions with magnetite surfaces or external sites of GR,^{330,444–447} interlayer anion

Table 10. Reactive Elements towards GR and the Type of Reactions^a

elements	type of interaction with green rust			
	adsorption	redox transformation	octahedral incorporation	interlayer incorporation
As, Mo, P, W, Si	✓			
Cr, Hg, Np, Sb, U	✓	✓		
Se	✓	✓		✓
Ag, Au, Cu, Tc		✓		
Fe, O		✓	✓	
C, N		✓		✓
Al, Co, H, Mg, Ni, Zn			✓	
Na, K, Rb, Cs, S, F, Cl, Br, I				✓

^aIt is based on the data compiled by Latta et al.⁴⁷³.

exchange only in the case of GR,^{330,447} and hydrophobic interactions to engineered systems such as organic-amended magnetite and surfactant-interlayered GRs.^{4,448–451}

Adsorption of citric acid, gallic acid, poly(acrylic acid), poly(acrylic-co-maleic acid), and humic acid onto magnetite nanoparticles have been investigated at neutral pH commonly prevailing in natural waters.⁴⁵² The adsorption of organic matter such as humic acid on magnetite particles is further considered in the context of colloidal stabilization, as it prevents particle aggregation in a wide range of pH and enhances salt tolerance.⁴⁵³ The adsorption of bacterial cells to magnetite has been investigated with the aim to develop water purification methods⁴⁵⁴ or for the removal of lindane (γ -HCH) from water by microbial cells immobilized on magnetite.⁴⁵⁵ Magnetite has been efficiently used to remove tetracyclines (antibiotics) from aqueous media.^{444,445} Kinetics and extent of sorption of nalidixic acid (quinolone antibiotic) on magnetite have been recently investigated by Usman et al.⁴⁴⁶ While the effect of ionic strength was of less significance, the adsorption was found to be strongly affected by particle size and surface properties of magnetite.⁴⁴⁶ Very recently, magnetite stoichiometry has been shown to strongly influence the capacity of magnetite to bind organic and inorganic compounds (e.g., quinolone antibiotics, natural organic matter, and dissolved silicates).⁴⁵⁶ Binding of tested ligands was enhanced with an increase in stoichiometry of magnetite by Fe(II) recharge.

Kone et al.³³⁰ reported that pentachlorophenol can bind to the external surface of GR although no reductive transformation was observed. Pentachlorophenol cannot penetrate the GR interlayer and displace anion from the interlayer. At neutral pH, pentachlorophenolate adsorption proceeds probably through electrostatic attraction between the anionic sorbate and the positively charged centers in the hydroxide sheets of GR. Liang and Butler⁴⁴⁷ studied the sorption of various carboxylic acids onto GR(Cl⁻) and reported that carboxylic ligands sorb on the internal as well as external surface sites of the GR. It was suggested that carbon tetrachloride transforms only on external surface sites of GR, since this compound does not enter GR interlayers.^{447,457}

Due to the hydrophilic surface of magnetite, it is unable to efficiently uptake organic compounds, and so consequently, chemical modifications to make the magnetite surface more suitable for retention of hydrophobic compounds have recently been attracting attention.⁴ For instance, the formation of mixed hemimicelles from adsorption of cation surfactants, cetyltrimethylammonium bromide (CTAB) and cetylpyridinium chloride (CPC), on magnetic nanoparticles, can enhance sorption of organic compounds by strong hydrophobic and electrostatic interactions.⁴⁴⁸ Alternatively, nontoxic ligands may also appear

as an environmentally friendly approach to remove organic pollutants. For instance, 6-deoxy-6-ethylenediamino- β -cyclodextrin grafted thiodiglycolic acid modified magnetic nanoparticles were used to effectively remove pharmaceutically active compounds and endocrine disrupting compounds such as naproxen and carbamazepine and bisphenol A.⁴⁴⁹ Activated carbon combined with magnetite or magnetite-immobilized chitin has also been investigated in order to produce magnetic adsorbents of volatile organic compounds and chlorinated compounds.^{458,459}

In general, magnetite and GR likely play a considerable role in the sorption and immobilization of inorganic and organic compounds in the environment. Table 9 summarizes the studies which have determined the adsorption parameters for magnetite or GR.

6.2. Reductive Transformation of Inorganic and Organic Contaminants

Abiotic reductive transformation processes play a crucial role in the fate, mobility, and toxicity of redox sensitive contaminants in natural and engineered systems. Such reactions often lead to less toxic, more bioavailable, and easy-to-degrade species than the parent pollutant. The prominent role of Fe(II) in reductive transformation of pollutants is evident from the large number of laboratory and field studies. Generally, structural Fe(II) or Fe(II) complexes with oxygen ligands are more reactive than aqueous Fe(II).^{464–466} Therefore, mixed-valent Fe minerals have been widely used to transform numerous inorganic^{436,467–471} and organic contaminants^{39,40,170,452,464} through redox processes. In general, reduction of contaminants by mixed-valent Fe minerals follow first-order law in contaminant concentration.⁴⁶⁶

Very recently, Latta et al.⁴⁷³ presented a comprehensive survey of literature which highlighted that GR is involved in cycling of 35 elements (Table 10). These elements can interact with GR through four major pathways (Table 10): (i) adsorption onto the external surface of GR, (ii) interlayer incorporation of anions and monovalent cations, (iii) incorporation of divalent and trivalent metals into the octahedral sheets, and (iv) redox transformations.⁴⁷³ A compilation of studies reporting the use of GR or magnetite for reduction of various pollutants is provided in Table 11.

Due to its high content of structural Fe(II), most of the reduction studies focused on the reactivity of GR. There are, however, other factors that contribute to the high reactivity of GR, such as the bonding environment of Fe(II). Magnetite contains strong ionic bonds between Fe(II) and O, whereas in GR layers, OH⁻ and Fe(II) are bound by weaker ionic bonds. Sharing of electrons with O by hydrogen weakens this bond

Table 11. Summary of Studies Using Mixed-Valent Fe Minerals for Redox Transformation of Pollutants in Contaminated Matrices^a

type of mixed-valent Fe mineral	target pollutant and its initial concentration	experimental conditions	extent/rate of pollutant degradation	mineral stability/Fe leaching	ref
magnetite as reductant					
magnetite (commercial) 44 m ² g ⁻¹ + 0.27 mmol g ⁻¹ Fe(II)	hexahydro-1,3,5-trinitro-1,3,5-triazine (RDX) 50 μM	magnetite 44 m ² L ⁻¹ , pH 7 (HEPES)	100% after 3 days pseudo-first-order kinetics initially, $k_{\text{obs}} = 1.0 \times 10^{-1} \text{ h}^{-1}$	ND	472
magnetite (lab synthesized), 57.2 m ² g ⁻¹ Fe(II):Fe(III) = 206:516	chlorinated ethylenes (PCE) and Cr(VI) (51.5 mM)	magnetite = 0.1 w/w pH 7, no buffer 10 mM NaHCO ₃	reductive capacity for Cr(VI) 3–16 times higher than for PCE	ND	481
two magnetites (lab synthesized), (a) 9 nm, 63.5 m ² g ⁻¹ (b) 80 nm, 14.5 m ² g ⁻¹	CCl ₄ , 114 μM	magnetite, 5 g L ⁻¹ , pH 7.8 (HEPES) 0.1 M NaCl	first-order kinetics; $k_{\text{obs}} = 0.29 \text{ h}^{-1}$ (a) $3 \times 10^{-3} \text{ h}^{-1}$	ND	493
magnetite (lab synthesized), 18 m ² g ⁻¹	CCl ₄ , 20 μM	magnetite, 25 g L ⁻¹ , pH 6–10, 0.1 M NaCl	pseudo-first-order $k_{\text{obs}} = 7 \times 10^{-6} - 1.1 \times 10^{-4} \text{ L m}^{-2} \text{ h}^{-1}$	ND	494
magnetite (lab synthesized) 20 nm, 54–72 m ² g ⁻¹ , Fe(II):Fe(III), 0.28–0.48	nitrobenzene, 40 μM	magnetite, 1 g L ⁻¹ , pH 7.2 (MOPS)	first-order ($x = 0.48$) $k_{\text{obs}} = 0.20 \text{ min}^{-1}$, no significant reaction for $x = 0.28$	ND	39,40
magnetite (commercial), 1.54 m ² g ⁻¹ Fe(II)/Fe(III) = 0.47 + Fe(II)	nitrate (NO ₃ ⁻) and nitrite (NO ₂ ⁻), 0.5 mM	magnetite, 10 g L ⁻¹ , pH 5.5–7.5	NO ₃ ⁻ , $k_{\text{obs}} = (1.2-0.6) \times 10^{-3} \text{ h}^{-1}$ (pH 5.5–7.5); Fe(II), $k_{\text{obs}} = (3.2-1.3) \times 10^{-3} \text{ h}^{-1}$ (pH 5.5–7.5); NO ₂ ⁻ , $k_{\text{obs}} = 1.4 \times 10^{-4} \text{ h}^{-1}$ (pH 5.5)	ND	476
magnetite (lab synthesized), 26.1 m ² g ⁻¹	Cr(VI), 1 mM	magnetite 1:100 w/w pH 1, 7, and > 13	100% Cr(VI) oxidation in < 50 h (pH 1) and 400 h (pH 7); only 20% oxidation after 800 h at pH > 13	goethite	492
magnetite (lab synthesized) [+ Fe(II) 86 mg L ⁻¹]	Cr(VI), 80 mg L ⁻¹	magnetite, 6.5 g L ⁻¹ , pH 7.2	80% Cr(VI) oxidation in 1 h [magnetite + Fe(II)], 60% Cr(VI) oxidation in 1 h (magnetite only)	ND	483
seven different magnetites, 5 samples (natural), 39–52 nm, 1.4–7.6 m ² g ⁻¹ ; 2 samples (commercial) 20 nm (39.3 m ² g ⁻¹) and 41 nm (7.3 m ² g ⁻¹); Fe(0)	Cr(VI), 50 mg L ⁻¹	magnetite, 6 g L ⁻¹ , pH 4, 6 and 8; NaCl, 10 mM	>85% Cr(VI) oxidation pH 4 commercial magnetite 20 nm (25 days); no extensive reduction for other magnetite samples; Fe(0), general increase in reduction rates	ND	119
Magnetite (lab synthesized), different stoichiometries and origins (a) $x = 0$ (magnetite), (b) $x = 0.33$, (c) $x = 0.43$ (biogenic magnetite), (d) $x = 0.50$; Fe(II) for $x < 0.50$ green rust (GR) as reductant GR(SO ₄ ²⁻) (lab synthesized)	U(VI), 500 μM	magnetite, 5 g L ⁻¹ , pH 7.2 (MOPS) or NaHCO ₃	complete U(VI) reduction for $x > 0.42$, no significant U(VI) reduction for $x < 0.42$ after one week	magnetite	63
	NO ₃ ⁻ , 14.28 mM	pH between 7–8.5, $T = 25 \text{ }^\circ\text{C}$, 1 mmol of GR, Fe(II) in GR ($t = 0$) = 6.63	pseudo-first-order rate constant $k_{\text{obs}} = 1.161 \times 10^{-5} \text{ s}^{-1}$	GR oxidized to magnetite	468, 487
(a) GR(Cl ⁻) (lab synthesized), Fe(II):Fe(III) = 3:1, (b) GR(Cl ⁻) modified to GR(SO ₄ ²⁻) with similar Fe(II):Fe(III) ratio	NO ₃ ⁻ , 14.28 mM	pH 8.2, $T = 25 \text{ }^\circ\text{C}$, 2.5 mM GR	$k_{\text{obs}} (\text{s}^{-1}) = 30.8 \pm 10.4 \times 10^{-5}$ for GR(Cl ⁻) and 4.7×10^{-5} for GR(Cl ⁻ →SO ₄)	GR transformed to magnetite	133
GR(CO ₃ ²⁻) (lab synthesized), Fe(II):Fe(III) = 2:1	NO ₃ ⁻ , 3.2 mM	pH 10.5, $T = 25 \text{ }^\circ\text{C}$, initial Fe(II) concentration by GR = 167 mM	nitrate removal efficiency was 91%	magnetite as the main oxidation product	488
GR(CO ₃ ²⁻) (lab synthesized), 47 m ² g ⁻¹ , Fe(II):Fe(III) = 5:1 (initial solutions)	Cr(VI), 192 μM	pH 7, 0.25 g L ⁻¹ GR	k_{obs} is $3.3 \times 10^{-3} \text{ s}^{-1}$	ND	466
(a) GR(SO ₄ ²⁻) (lab synthesized), Fe(II):Fe(III) = 2, (b) GR(Cl ⁻) (lab synthesized), Fe(II):Fe(III) = 2.3	Cr(VI); Fe(II)/Cr(VI) = 6	pH 8, Fe(II)/Cr(VI) = 6	complete reduction of Cr(VI) to Cr(III) in < 2.5 h	Cr(III)–Fe(III) oxyhydroxide, similar to the “2 line ferrihydrite” was obtained in both cases	477
three types of GR (lab synthesized), (a) GR(Cl ⁻) 19.0 m ² g ⁻¹ , Fe(II):Fe(III) = 3:1:1, (b) GR(SO ₄ ²⁻), 3.6 m ² g ⁻¹ , Fe(II):Fe(III) = 1.9:1, (c) GR(CO ₃ ²⁻), 30.1 m ² g ⁻¹ , Fe(II):Fe(III) = 2:1	Cr(VI), 192 μM	pH 7, 0.5 g L ⁻¹ GR	k_{obs} is $3.66 \times 10^{-2} \text{ s}^{-1}$ for GR(Cl ⁻), $2.39 \times 10^{-2} \text{ s}^{-1}$ for GR(CO ₃ ²⁻), and $1.81 \times 10^{-2} \text{ s}^{-1}$ for GR(SO ₄ ²⁻)	magnetite and lepidocrocite were observed as oxidation products in all	480
GR(CO ₃ ²⁻) (lab synthesized), Fe(II)/Fe(III) = 2	Cr(VI), 111 μM	pH 9.3, 25 °C, 1000 μmol of Fe in GR (CO ₃ ²⁻)	complete removal of Cr(VI) within 20 min	chromium containing ferric oxyhydroxycarbonate as oxidation product	491

Table 11. continued

type of mixed-valent Fe mineral	target pollutant and its initial concentration	experimental conditions	extent/rate of pollutant degradation	mineral stability/Fe leaching	ref
GR(SO ₄ ²⁻) (lab synthesized)	Cr(VI), Cr(VI)/Fe(II) 5 to 110%	Cr(VI)/Fe(II) 5 to 110%	complete removal of Cr(VI) in 5 min for Cr(VI)/Fe(II) < 100%	Cr-substituted goethite	475
GR(SO ₄ ²⁻) (lab synthesized), 86.3 m ² g ⁻¹ , Fe(II):Fe(III) = 464:212	chlorinated ethylenes: 0.19 mM tetrachloroethylene (PCE), 0.25 mM trichloroethylene (TCE), 0.41 mM cis-dichloroethylene (cis-DCE), and 0.40 mM vinyl chloride (VC)	pH 7, GR 7 g L ⁻¹	rate constants <i>k'</i> for reductive dechlorination were 1.59 day ⁻¹ for PCE, 0.90 day ⁻¹ for TCE, 0.59 day ⁻¹ for cis-DCE, and 0.94 day ⁻¹ for VC	oxidation product was magnetite and/or maghemite	482
GR(SO ₄ ²⁻) (lab synthesized), 86.3 m ² g ⁻¹ , Fe(II):Fe(III) = 464:212	PCE (10 equiv mol ⁻¹ of ethane) and Cr(IV) (51.5 mM)	pH 7, solid/liquid ratio = 0.007 for GR	reductive capacity for Cr(IV) was ~1400 μeq g ⁻¹ and for PCE was ~90 μeq g ⁻¹	ND	481
GR(SO ₄ ²⁻) (lab synthesized), Fe(II):Fe(III) = 2:1	CCl ₄ , 20.7–264 mM	pH 8, 25 °C, 4–8 mM Fe(III) from GR	first-order rate constant ranged <i>k</i> _{obs} ranged from 0.47 × 10 ⁻⁵ s ⁻¹ to 2.18 × 10 ⁻⁵ s ⁻¹	GR was oxidized to magnetite	457
three GRs (lab synthesized), (a) GR(SO ₄ ²⁻), (b) GR(CO ₃ ²⁻), (c) GR(Cl ⁻)	U(VI), 400 μM	pH 8, GR 5 g L ⁻¹	<i>k</i> _{obs} was 8.3 × 10 ⁻⁴ s ⁻¹ , 7.3 × 10 ⁻⁴ s ⁻¹ , and 5.4 × 10 ⁻⁴ s ⁻¹ for GR(CO ₃ ²⁻), GR(SO ₄ ²⁻), and GR(Cl ⁻), respectively	ND	473
two GRs (lab synthesized), (a) GR(SO ₄ ²⁻), (b) GR(CO ₃ ²⁻)	[TcO ₄] ⁻ , 0.076 mM	pH 7–8, GR 15 g L ⁻¹	complete reduction	GR was oxidized to goethite	471
GR(SO ₄ ²⁻) (lab synthesized)	Se(VI), 1.13 mM (pH 3.8), 44 μM (pH 6.8 and 9.3)	pH 3.8, 6.8 and 9.3	no Se(VI) reduction at pH < 4 (no GR, all Fe(II) dissolved), Se(VI) reduction faster when it was present during GR formation (first-order rate)	magnetite, lepidocrocite	479
two GRs (lab synthesized): (a) GR(SO ₄ ²⁻), 20 m ² g ⁻¹ , Fe(II):Fe(III) = 2:1, (b) GR(CO ₃ ²⁻), 36 m ² g ⁻¹ , Fe(II):Fe(III) = 2:1	hexahydro-1,3,5-trinitro-1,3,5-triazine (RDX) 100 μM	pH 7, GR, 2 g L ⁻¹ in 0.1 M KBr	>90 of RDX removed by both GRs in 60 min	no transformation or surface passivation occurred after reaction	170
GR(SO ₄ ²⁻) (lab synthesized)	Ag ^I , Au ^{III} , Cu ^{II} , and Hg ^{II} (400 μM)	GR, 5 g L ⁻¹	concentrations of Ag, Au, Cu, and Hg were decreased to 890 nM, 360 nM, 1.2 μM, and 1.7 μM, respectively	magnetite	470

“Stoichiometry of magnetite or GR is missing from literature where it was not reported. All experiments were performed in batch reactors. Studies are arranged according to their order of appearance, first for magnetite and then for GR.

and thus GR is easy to oxidize.⁴⁷⁴ Moreover, the cubic structure of magnetite is closely packed with similar appearance in every direction. Therefore, the amount of available surface Fe(II) is lower compared to GR which has a looser structure and platy crystals with a high fraction of structural Fe(II) available for reduction. Higher interlayer thickness also facilitate the exchange of even relatively large compounds.^{468,475} Hence, magnetite is known for its stability during reduction (apart from small passivation layer)⁴⁷⁶ while GR quickly transforms into other products such as ferrihydrite,⁴⁷⁷ goethite,^{330,475} magnetite,^{133,330,457,475,478,479} or mixtures of lepidocrocite and magnetite.⁴⁸⁰ Similar oxidation products (magnetite and lepidocrocite) were formed from three types of GR with decreasing yields of magnetite as oxidation product followed the order $\text{GR}(\text{CO}_3^{2-}) > \text{GR}(\text{SO}_4^{2-}) > \text{GR}(\text{Cl}^-)$.⁴⁸⁰

Reduction rates of Fe(II)-bearing minerals increase with their Fe(II) content. For example, Lee and Batchelor⁴⁸¹ showed that the reduction rate for chlorinated ethylenes and Cr(VI) was highest for $\text{GR}(\text{SO}_4^{2-})$ [Fe(II):Fe(III) = 464:212] followed by magnetite [Fe(II):Fe(III) = 206:516], pyrite [Fe(II):Fe(III) = 94.8:120], biotite [Fe(II):Fe(III) = 114:3.1], montmorillonite [Fe(II):Fe(III) = 1.2:6.3], and vermiculite [Fe(II):Fe(III) = 14.2:42.5]. Similar results were found for magnetite with different Fe(II):Fe(III) stoichiometries. Gorski and Scherer⁴⁰ demonstrated that Fe(II) contents of magnetite strongly influences the rate of nitrobenzene reduction. Partially oxidized or substoichiometric magnetite ($x < 0.5$) slowly reduced nitrobenzene (first-order rate coefficient, $k_{\text{obs}} = 5.36 \times 10^{-6} \text{ min}^{-1}$), while reduction by stoichiometric magnetite ($x = 0.50$) was much more rapid ($k_{\text{obs}} = 0.20 \text{ min}^{-1}$). Gorski et al.³⁹ also observed increased rates of nitrobenzene reduction with increasing Fe(II) stoichiometry in magnetite from $x = 0.31$ to $x = 0.50$. Half-lives of nitrobenzene were 1.2 min, 3.5 min, 74 min, 3.8 days, and 90 days with magnetite $x = 0.50, 0.48, 0.42, 0.36,$ and 0.31 , respectively.³⁹ Similarly, Latta et al.⁶³ found that the extent of U(VI) reduction was highly dependent upon magnetite stoichiometry. They reported that stoichiometric ($x = 0.5$) or partially oxidized magnetite ($x = 0.42$ and 0.48) completely reduced the U(VI) while very little to no reduction was observed with more oxidized magnetite with $x < 0.33$ after one week. However, a rapid rate of reduction was re-established by oxidized magnetite when it was reacted with aqueous Fe(II) to form stoichiometric magnetite upon Fe(II) uptake.^{39,40,63} Reaction of nonstoichiometric magnetite with aqueous Fe(II) can recharge its Fe(II) contents and increase its reactivity, thus aqueous Fe(II) content and magnetite stoichiometry should always be reported in comparative reactivity studies.⁴⁰ Rates of nitrobenzene reduction by initially stoichiometric magnetite were comparable to nonstoichiometric magnetite recharged with Fe(II) underscoring the significance of structural Fe(II) contents.⁴⁰ Therefore, recharge of structural Fe(II) in magnetite was proposed to stimulate reduction of contaminants like chlorinated ethylenes,⁴⁸² Cr(VI),⁴⁸³ U(VI),⁶³ NO_3^- ,⁴⁷⁶ and nitroaromatic compounds^{39,40,472} in various studies. Note that, Fe(II) bound to magnetite resulted in significant reduction of nitroaromatic compounds while negligible transformation occurred by aqueous Fe(II) or magnetite alone.^{472,484} Thermodynamic calculations indicate that aqueous Fe(II) is capable of reducing some organic pollutants in the absence of Fe minerals, for example nitroaromatic compounds.⁵⁸ However, numerous experimental evidence has shown that the reaction is exceedingly slow in the absence of Fe minerals and that the amount of oxide-associated Fe(II) controls the reaction

rate.^{485,486} Whether the mineral acts as a heterogeneous catalyst by forming surface complexes or by enhancing the electron transfer steps has not been elucidated until now.

The limiting step in the electron transfer process from magnetite to contaminants has not been conclusively identified yet. Recent studies³⁹ propose conceptual models that combine mass and electron transfer processes. Experimental evidence is still not decisive toward whether Fe(II) diffusion through magnetite structure or charge transfer is the rate-limiting step.

Regarding GR, reduction of inorganic compounds such as nitrogen and chromium species were among the first reactions studied.^{466,477,478,487} Both NO_3^- and NO_2^- can be reduced by GR^{478,487} or magnetite,⁴⁷⁶ though the reaction of NO_3^- was slower compared to NO_2^- .^{478,487} While $\text{GR}(\text{SO}_4^{2-})$ and $\text{GR}(\text{CO}_3^{2-})$ (Fe(II):Fe(III) ratio of 2:1) had the same reduction rate for nitrate,^{478,487} $\text{GR}(\text{Cl}^-)$ with a Fe(II):Fe(III) ratio of 3:1 exhibited a five times higher reduction rate.¹³³

When the interlayer Cl^- was exchanged by SO_4^{2-} to obtain $\text{GR}(\text{SO}_4^{2-})$ with similar Fe(II):Fe(III) ratio (3:1), reduction of NO_3^- by the resulting $\text{GR}(\text{SO}_4^{2-})$ was six times slower as compared to the original $\text{GR}(\text{Cl}^-)$.¹³³ These studies^{133,478,487} applied NO_3^- from a sodium salt (NaNO_3) and interpreted the results in terms of reactions taking place at the external mineral surface. However, reactivity studies of $\text{GR}(\text{SO}_4^{2-})$ with nitrate in the presence of different counter-cations [i.e., NaNO_3 and $\text{Ba}(\text{NO}_3)_2$ at similar initial NO_3^- concentration (14 mM)], the rate of reaction increased by 40 times in the presence of Ba^{2+} .⁴⁶⁸ This difference was attributed to the forced exchange of SO_4^{2-} by NO_3^- in the GR interlayer due to the formation of BaSO_4 precipitates, which is not the case for NaNO_3 .⁴⁶⁸ Recently, Etique et al.⁴⁸⁸ investigated the reduction of NO_3^- by $\text{GR}(\text{SO}_4^{2-})$ in the presence of phosphate anions. They showed that increasing phosphate concentration significantly impaired the NO_3^- reduction probably due to the adsorption of phosphate on lateral surface sites of GR crystal that restrains the interaction of NO_3^- with Fe(II) species. Phosphate surface complexes preferentially form at the lateral sites due to the presence of mono- and dicoordinated OH^- surface groups of [1010] faces, which is known to stabilize GR.³² The presence of phosphate or bacterial cells (which can also stabilize GR⁴⁸⁹) also affected the reduction of methyl red and Hg(II).⁴⁹⁰ However, the effects of stabilizing agents were dependent on the nature of the target pollutant as reduction of methyl red was more affected than Hg(II). Moreover, different types of GRs [chemically synthesized $\text{GR}(\text{CO}_3^{2-})$ vs $\text{GR}(\text{SO}_4^{2-})$ vs biogenic $\text{GR}(\text{CO}_3^{2-})$] showed similar reactivity toward these pollutants when rate constants were normalized to the concentration of structural Fe(II) of the GRs.⁴⁹⁰

The reduction of Cr(VI) by GR has been studied at different experimental conditions to analyze effects of pH, surface area of mineral, and initial metal concentration. For example, at low Cr(VI) concentrations, the rate of metal reduction by $\text{GR}(\text{CO}_3^{2-})$ was proportional to the surface area of GR,^{466,491} whereas reduction rates became more complex at higher Cr(VI) concentration. At higher GR concentrations in terms of specific surface area ($8.3 \text{ m}^2 \text{ L}^{-1}$ and $16.7 \text{ m}^2 \text{ L}^{-1}$), first-order kinetics was observed while zero-order kinetics was obtained at low surface area concentration of GR ($4.2 \text{ m}^2 \text{ L}^{-1}$).⁴⁶⁶ These findings can be rationalized by surface site saturation by Cr(VI) or surface passivation by oxidized precipitates that physically cover the otherwise available Fe(II) on the surface of GR. Electron transfer within the GR lattice [Fe(II) to Fe(III)] and in the interlayer region have been proposed.^{480,491} Surface

Table 12. Summary of Studies Using Mixed-Valent Iron Minerals to Promote Chemical Oxidation in Contaminated Matrices^a

oxidant	catalyst type	target pollutant and its initial concentration	medium	experimental conditions	extent/rate of pollutant degradation	mineral stability/Fe leaching	ref
H ₂ O ₂	magnetite (commercial), 0.675 m ² g ⁻¹ , screened through 0.6 mm sieve.	pentachlorophenol, 250 mg L ⁻¹	spiked sand/batch	pH 3, magnetite, 10 wt %, H ₂ O ₂ , 7 wt %	complete pollutant degradation and mineralization after 24 h, highest degradation rate constant was in first 8 h (5 × 10 ⁻⁴ mol m ⁻² h ⁻¹)	ND	515, 518
H ₂ O ₂	magnetite (commercial), screened through 0.3 mm sieve	petroleum hydrocarbons, 1000 mg kg ⁻¹	spiked sand/batch	pH 3, magnetite, 5 wt %, H ₂ O ₂ , 15 wt %	50% hydrocarbon removal after 8 days	ND	556
H ₂ O ₂	magnetite (commercial), 2 m ² g ⁻¹	2,4,6-trinitrotoluene (2 g kg ⁻¹ when spiked onto soil or 0.11 mM in aqueous phase)	aqueous medium or soil slurry system/batch	pH 3, H ₂ O ₂ , 80 mM, magnetite, 1.76 g L ⁻¹	reaction rate constants $k_{\text{surf}} = 1.47 \cdot 10^{-3}$ L min ⁻¹ m ⁻²	Fe leaching was 14 mg L ⁻¹	511
H ₂ O ₂	magnetite (lab synthesized), 2.9 μm; 8.6 m ² g ⁻¹	methyl red, 50 μm	aqueous medium/batch	pH 7, T = 20 °C, H ₂ O ₂ /Fe molar ratio of 20	decolorization rate constant $k_s = 2 \times 10^{-4}$ L min ⁻¹ m ⁻²	Fe leaching ≤ 1 mg L ⁻¹	525
H ₂ O ₂	GR(Cl ⁻) (lab synthesized), 20 m ² g ⁻¹ , magnetite (lab synthesized), 2 m ² g ⁻¹	2,4,6-trinitrotoluene, 0.11 mM	aqueous medium/batch	pH 7, H ₂ O ₂ , 3% w/v, mineral content, 2 g L ⁻¹	highest degradation (60%) was obtained with GR, pseudo-first-order rate constant's (k) values for pollutant degradation were 5.1 × 10 ⁻³ min ⁻¹ (GR) > 2.03 × 10 ⁻⁴ min ⁻¹ (magnetite)	ND	512
H ₂ O ₂	GR(Cl ⁻) (lab synthesized), 21 m ² g ⁻¹ , magnetite (commercial), 2 m ² g ⁻¹	phenol, 0.53 mmol L ⁻¹	aqueous medium/batch	pH 7, GR or magnetite = 5 g L ⁻¹ , H ₂ O ₂ , 155 mM	100% phenol degradation after one minute in the presence of GR while reaction kinetics was much slower with magnetite (<10% after 1 h)	GR was transformed into a mixture of ferrihydrite and lepidocrocite after reaction, ND for magnetite	522
H ₂ O ₂	magnetite (lab synthesized) SSA: 2~90 m ² g ⁻¹	PAH (phenanthrene), 200 mg kg ⁻¹	spiked sand/batch	pH buffered (2.8) and unbuffered, magnetite, 10 wt%, 3 mL of 30% H ₂ O ₂	40% removal in unbuffered and 88% in buffered system after 16 days	ND	509
H ₂ O ₂	GR(SO ₄ ²⁻) (lab synthesized), 74 m ² g ⁻¹	methyl red, 0.011 mmol	aqueous medium/batch	pH 7, H ₂ O ₂ , 9.79 mmol	complete decolorization was obtained within one hour	GR was transformed into poorly crystallized goethite	523
H ₂ O ₂	magnetite (Commercial), 4 μm; 2.4 m ² g ⁻¹	pentachlorophenol, 50 mg L ⁻¹	aqueous medium/batch	pH 7, magnetite, 2 g L ⁻¹ , H ₂ O ₂ , 0.8 M	90% dechlorination after 30 h, total dechlorination after 4 days and complete mineralization after 7 days	Fe leaching (<0.05 mM), good structural stability	460, 503
H ₂ O ₂	nanomagnetite (lab synthesized), 10 nm	phenol/aniline, 1 mM	aqueous medium/batch	pH 6~7, magnetite, 5 g L ⁻¹ , H ₂ O ₂ , 1.2 M	100% removal of both pollutants after 6 h	80% removal of pollutant after eight times of recycle	529
H ₂ O ₂	two kinds of magnetite (commercial), M1: < 50 nm, 40 m ² g ⁻¹ , M2: < 5 μm, 2.4 m ² g ⁻¹	rhodamine B, 5 mg L ⁻¹	aqueous medium/batch	pH 7, T = 20 °C, magnetite, 2 g L ⁻¹ , H ₂ O ₂ /Fe molar ratio = 100	higher decolorization kinetic constant, k_{app} (min ⁻¹) for M2 (0.011) than M1 (0.003)	low iron leaching, good structural and catalytic stabilities	43
H ₂ O ₂	three types of GR (lab synthesized), (1) GR (CO ₃ ²⁻), 39 m ² g ⁻¹ , (2) GR(SO ₄ ²⁻), 74 m ² g ⁻¹ , (3) GR(Cl ⁻), 25 m ² g ⁻¹ and magnetite, 11 m ² g ⁻¹	phenol, 1 mM	aqueous medium/batch	pH 7.1, T = 20 °C, 1 g L ⁻¹ of GR or magnetite; H ₂ O ₂ , 30 mM	degradation pseudo-first-order rate constants (k_{app}) values: 13 × 10 ⁻⁴ , 3.3 × 10 ⁻⁴ , 3.5 × 10 ⁻⁴ , and 0.4 × 10 ⁻⁴ L m ⁻² s ⁻¹ for GR (Cl ⁻), GR(SO ₄ ²⁻), GR(CO ₃ ²⁻), and magnetite, respectively	GRs were transformed into ferrihydrite or poorly crystallized goethite; ND for magnetite	42
H ₂ O ₂ generated through O ₂	nanomagnetite (commercial) 30 nm; 48 m ² g ⁻¹	4,6-dinitro- <i>o</i> -cresol, 11.4 mg L ⁻¹	aqueous medium/batch	pH 2.8, magnetite, 1 g L ⁻¹ , Na ₂ SO ₄ , 0.08 M, 0.025 A of current and 40 mL/min of O ₂ flow	total removal after 60 min, and pseudo-second-order degradation rate constant 1.79 × 10 ⁻² μg ⁻¹ mL min ⁻¹	ND	557
H ₂ O ₂	nanomagnetite (commercial), 30 nm; 48 m ² g ⁻¹	<i>p</i> -nitrophenol, 45 mg L ⁻¹	aqueous medium/batch	pH 7.0, magnetite, 1.5 g L ⁻¹ , 620 mM H ₂ O ₂	>90% of <i>p</i> -NP was degraded after 10 h	ND	520
H ₂ O ₂ + ultrasonics	nanomagnetite (lab synthesized), 10~20 nm; 55.7 m ² g ⁻¹	bisphenol A, 20 mg L ⁻¹	aqueous medium/batch	pH 3, 7, and 9, T = 35 °C, magnetite, 585 mg L ⁻¹ , H ₂ O ₂ , 160 mmol L ⁻¹ , under ultrasonics	>95% of BPA was removed at three pH values	25~30% decline in efficiency in second cycle which remained steady for 5 cycles	531
H ₂ O ₂	three kinds of pure nanomagnetite, (M1) commercial 46 m ² g ⁻¹ , (M2) NaBH ₄ pretreated M1 to improve Fe(II), (M3) lab-synthesized 95 m ²	phenol, 25 mg L ⁻¹	aqueous medium/batch	pH 7.0, magnetite, 3 g L ⁻¹ , H ₂ O ₂ , 5 g L ⁻¹	42~65% phenol removal in 24 h	20% loss of efficiency in third cycle while negligible decrease in second cycle	45

Table 12. continued

oxidant	catalyst type	target pollutant and its initial concentration	medium	experimental conditions	extent/rate of pollutant degradation	mineral stability/Fe leaching	ref
	g^{-1} , (M3) $95 \text{ m}^2 \text{ g}^{-1}$ particle size for all; 20–30 nm						
H_2O_2 or $\text{Na}_2\text{S}_2\text{O}_8$	magnetite (lab synthesized), 30 nm; $103 \text{ m}^2 \text{ g}^{-1}$	petroleum hydrocarbons 4 g kg^{-1} of crude and weathered oil	spiked sand/batch or saturated column	pH 6.7, $T = 20\text{--}25 \text{ }^\circ\text{C}$, magnetite, 10% w/w, oxidant:Fe molar ratio = 10:1 (H_2O_2) and 1:1 ($\text{Na}_2\text{S}_2\text{O}_8$)	80–90% of hydrocarbon removal by both oxidants after one week	ND	200, 517
H_2O_2 or $\text{Na}_2\text{S}_2\text{O}_8$	magnetite (lab synthesized), 30 nm; $103 \text{ m}^2 \text{ g}^{-1}$	PAHs 200–300 $\mu\text{g g}^{-1}$ (spiked sand) 1200–1300 $\mu\text{g g}^{-1}$ (aged soil)	spiked sand, real soil/batch or saturated column	pH 7–8, $T = 20\text{--}25 \text{ }^\circ\text{C}$, magnetite, 10% w/w, oxidant:Fe molar ratio = 20:1 (H_2O_2) and 2:1 ($\text{Na}_2\text{S}_2\text{O}_8$)	80–90% of PAH degradation in spiked sand while 50–60% of degradation in real soils (1 week)	ND	507, 508, 517
H_2O_2 or $\text{Na}_2\text{S}_2\text{O}_8$	magnetite (commercial), 150 nm; $8 \text{ m}^2 \text{ g}^{-1}$	ibuprofen, 0.1 mM	aqueous medium/batch	pH 6.6, magnetite, 1 g L^{-1} , oxidant dose, 10 mM	pollutant removal up to 60% (H_2O_2) and 73% ($\text{Na}_2\text{S}_2\text{O}_8$) after 48 h	ND	516
UV irradiation + H_2O_2 Or + $\text{Na}_2\text{S}_2\text{O}_8$	four magnetites, (M1) 30–50 nm; $75 \text{ m}^2 \text{ g}^{-1}$, (M2) lab-synthesized, 60–80 nm; $26 \text{ m}^2 \text{ g}^{-1}$, (M3) 1–2 μm , $1.7 \text{ m}^2 \text{ g}^{-1}$, (M4) 100–300 nm, $8.5 \text{ m}^2 \text{ g}^{-1}$	phenol, 0.1 mM	aqueous medium/batch	pH 3, magnetite, 0.2 g L^{-1} , 1 mM H_2O_2 or 0.5 mM $\text{Na}_2\text{S}_2\text{O}_8$	pollutant removal in less than 2 h for magnetites having the highest Fe(II)/Fe(III) ratio (e.g., M2 and M3)	Fe leaching much below 1 mg L^{-1}	44, 553
H_2O_2	five magnetite (natural), (M1) $0.70 \text{ m}^2 \text{ g}^{-1}$, (M2) $3.30 \text{ m}^2 \text{ g}^{-1}$, (M3) $0.54 \text{ m}^2 \text{ g}^{-1}$, (M4) $2.46 \text{ m}^2 \text{ g}^{-1}$, (M5) $1.41 \text{ m}^2 \text{ g}^{-1}$	<i>p</i> -nitrophenol, 10 mg L^{-1}	aqueous medium/batch	pH 7, magnetite, 1 g L^{-1} , H_2O_2 , 10 mmol L^{-1}	MI showed highest degradation efficiency (95% after 24 h while < 30% by others) and $\bullet\text{OH}$ generation (reaction rate constant, $k = 0.24$, $300 \mu\text{g L}^{-1} \text{ min}^{-1}$)	ND	120
H_2O_2	magnetite (lab synthesized), 30 nm; $103 \text{ m}^2 \text{ g}^{-1}$	PAHs, 1100 mg kg^{-1}	real soil/batch	pH 7–8, magnetite 10% w/w, oxidant:Fe molar ratio equal to 20:1	PAH removal efficiency was 31, 36, and 47% in soil pretreated at 60, 100, and 150 $^\circ\text{C}$, respectively, after one week of chemical oxidation	ND	519
H_2O_2 / $\text{K}_2\text{S}_2\text{O}_8$	magnetite (lab synthesized), <20 nm; $59.8 \text{ m}^2 \text{ g}^{-1}$	PCBs, 5 $\mu\text{g g}^{-1}$	spiked sand/batch	pH 7.2, $T = 20 \text{ }^\circ\text{C}$, magnetite, 0.25 g g^{-1} , H_2O_2 , 2 M, $\text{K}_2\text{S}_2\text{O}_8$, 180 mM, L/S = 1:1	degradation extent of PCBs reached 69–77% (H_2O_2) and 90–99% ($\text{K}_2\text{S}_2\text{O}_8$) in spiked sand	ND	496
$\text{K}_2\text{S}_2\text{O}_8$	magnetite (natural), 500–1150 μm	acid orange 7, 15 mg L^{-1}	aqueous solution/recirculating pilot fluidized-bed reactor	pH 5, magnetite, 0.5 g L^{-1} , $\text{S}_2\text{O}_8^{2-}$, 0.2 mM	almost 75% removal of pollutant after 120 min of reaction	Fe leaching was 0.5 mg L^{-1} , degradation efficiency was approximately constant in six oxidation cycles	533
H_2O_2	magnetite (natural) 500–1150 μm , 5.15 $\text{m}^2 \text{ g}^{-1}$	basic blue 3, 5 mg L^{-1}	aqueous solution/recirculating pilot fluidized-bed reactor	pH 5, magnetite, 2.27 g L^{-1} , H_2O_2 , 4 mM	84% of pollutant degradation after 190 min of reaction	catalytic performance was maintained over five oxidation cycles (<20% loss in oxidation efficiency)	535
H_2O_2	magnetite (commercial), $6 \text{ m}^2 \text{ g}^{-1}$	gallic acid, 0.12 mM	aqueous medium/batch	pH 4.3, $T = 25 \text{ }^\circ\text{C}$, magnetite, 50 mg L^{-1} , H_2O_2 , 2.64 mM	rate constant (k) for pollutant degradation = 0.103 min^{-1} and for mineralization = 0.061 min^{-1} (95% mineralization)	Fe leaching = 0.06 mg L^{-1}	521
ultrasonics + H_2O_2 or + $\text{Na}_2\text{S}_2\text{O}_8$	magnetite (commercial), 200–300 nm	tetracycline, 100 mg L^{-1}	aqueous medium/batch	pH 3, magnetite, 1 g L^{-1} , H_2O_2 , 150 mM, ultrasound power 80 W at 22 $^\circ\text{C}$	93% of pollutant and 32% of TOC were removed after 60 min	79% of pollutant removal in third cycle	532, 554
H_2O_2	magnetite (natural), $8 \text{ m}^2 \text{ g}^{-1}$	phenol, 100 mg L^{-1}	aqueous medium/batch	pH 3, magnetite, 2 g L^{-1} , 500 mg L^{-1} H_2O_2 , 75 $^\circ\text{C}$	100% removal of phenol, 80% TOC reduction	3 runs and $X_{\text{TOC-brid}} = 77\%$	534
H_2O_2	magnetite (commercial), 0.3–0.5 μm , 7.9 $\text{m}^2 \text{ g}^{-1}$	trichloroethylene, 20 mg L^{-1}	aqueous solution fed in column of sand and magnetite	magnetite, 0.5 and 7 wt % feed solution: H_2O_2 , 50 mM, pH 8.2, nitrioltriacetic acid, 2 mM, up-flow mode, flow rate of 1.25 mL min^{-1}	74% and 94% of pollutant degradation with 0.5 and 7 wt % magnetite (chelates like EDTA and EDDS had an inhibitory effect)	magnetite remained stable during whole study (230 days) without any loss in catalytic ability (1 mM chelate)	530

^aStudies are arranged according to their order of appearance.

passivation of magnetite was also suggested as the limiting factor during the reduction of Cr(VI).^{41,492} A recent study compared the Cr(VI) reduction by various natural and synthetic magnetites having different particle sizes (and thus also different surface areas) and found that considerable reduction was obtained only by the finest magnetite.¹¹⁹

Bond and Fendorf⁴⁸⁰ compared the reduction rates of Cr(VI) by various GRs and reported the order $\text{GR}(\text{Cl}^-) > \text{GR}(\text{CO}_3^{2-}) > \text{GR}(\text{SO}_4^{2-})$ on a mass basis and proposed a second-order rate law $d[\text{Cr(VI)}]/dt = -k[\text{Cr(VI)}][\text{GR}]$ to describe the reaction kinetics at different Cr(IV) concentrations. Both Fe(II):Fe(III) ratio and accessible surface area may contribute to the observed reduction rate of GR minerals. While the Fe(II):Fe(III) ratio was highest in $\text{GR}(\text{Cl}^-)$ (3.1:1), followed by $\text{GR}(\text{CO}_3^{2-})$ (1.9:1) and $\text{GR}(\text{SO}_4^{2-})$ (2.0:1), the role of the external surface area was more important than the Fe(II):Fe(III) ratio within a structural group (GR1 or GR2). Reported values of surface area were 30.1, 19.0, and $3.6 \text{ m}^2 \text{ g}^{-1}$ for $\text{GR}(\text{CO}_3^{2-})$, $\text{GR}(\text{Cl}^-)$, and $\text{GR}(\text{SO}_4^{2-})$, respectively. However, Skovbjerg et al.⁴⁷⁵ argued that a single model may not be appropriate for three different types of GRs due to structural differences among them. Reduction of Cr(VI) by $\text{GR}(\text{CO}_3^{2-})$ involves reactions at the external surface only where a Cr-monolayer accumulated and progressively decreased the reactivity of $\text{GR}(\text{CO}_3^{2-})$.⁴⁹¹ In $\text{GR}(\text{SO}_4^{2-})$, however, Cr(VI) penetrates into the interlayer (due to higher d -spacing) by replacing SO_4^{2-} before reduction.⁴⁷⁵ This penetration offers quick access to large domains of the $\text{GR}(\text{SO}_4^{2-})$ structure that leads to fast reduction kinetics. Entry of Cr(VI) is then blocked by sparingly soluble precipitates of Cr, and further reduction of Cr(VI) occurs at the GR solid/solution interface.⁴⁷⁵ Recently, Latta et al.⁴⁷³ reported a complete reduction of U(VI) by $\text{GR}(\text{SO}_4^{2-})$ and $\text{GR}(\text{Cl}^-)$ while the amount of reduction ranged from 34 to 63% by $\text{GR}(\text{CO}_3^{2-})$. However, little impact of anions was observed for uptake of U(VI) at pH 8.0⁴⁷³ and that of Cr(VI) at pH 7.⁴⁸⁰

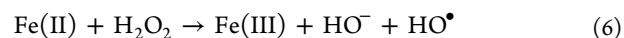
Mixed-valent Fe minerals have also been used to reduce chlorinated organic compounds such as CCl_4 and chlorinated ethylenes (vinyl chloride, cis-dichloroethylene, trichloroethylene, and tetrachloroethylene).^{457,481,493,494} The presence of transition metal cations such as Ag, Au, and Cu enhance the reductive dechlorination of CCl_4 by acting as catalysts. GR amended with such metals have been proposed for remediation of CCl_4 contamination in anoxic environments.⁴⁹⁵

While reduction alone has shown strong potential to remove pollutants from contaminated matrices, it also can be coupled with other remediation techniques to improve treatment efficiency.^{330,496} Such combined approaches as well as the impact of natural ligands on the reactivity of mixed-valent Fe minerals should be further evaluated in the future.

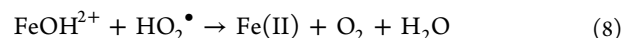
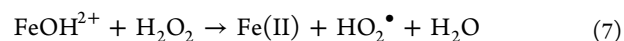
6.3. Use of Mixed-Valent Iron Minerals to Promote Advanced Oxidation Processes

Advanced oxidation processes (AOPs) are emerging as viable remediation technologies for soils and water contaminated with recalcitrant organic pollutants. These processes generally use a combination of oxidants and catalysts to generate highly reactive radicals having strong ability to degrade organic pollutants. The catalytic ability of mixed-valent Fe minerals is well-documented to promote two major oxidation reactions using hydrogen peroxide (Fenton-based oxidation) and persulfate (Table 12). Provided below is a brief discussion of the role of pure magnetite and GR in these processes.

Fenton oxidation is a complex catalytic reaction of hydrogen peroxide (H_2O_2) with iron [mostly Fe(II) ion] in acidic solution that predominantly generates highly reactive hydroxyl radicals (HO^\bullet). This process is based on Fenton's pioneering work (first report in 1876 followed by a deep study in 1894) which suggested the use of an aqueous mixture of H_2O_2 and Fe(II) salt (Fenton's reagent) to oxidize tartaric acid.^{497,498} Later in 1934, Haber and Weiss proposed a radical mechanism for this process and suggested that HO^\bullet radical is the actual oxidant.⁴⁹⁹ The simplest and most widely accepted form of this process is described as:^{498,500}

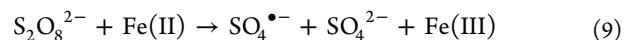


Reaction 6 is a stoichiometric process, but Fe is often used in a catalytic amount because of the subsequent pathways of H_2O_2 decomposition,⁵⁰¹ which regenerate Fe(II) through the classical Haber-Weiss cycle:



The HO^\bullet radical is among the most powerful oxidizing agents ($E^0 = 2.8 \text{ V}$) with strong potential to instantaneously react with organic pollutants and thus are widely used in remediation studies.⁵⁰⁰ Despite many advantages, conventional Fenton oxidation is mainly limited by the optimum pH (<4, required to keep metal ions in solution) and associated drawbacks such as the cost of initial acidification, negative impacts on native biota, and formation of Fe(III) sludge.⁵⁰² Similar process (modified Fenton) can take place at circumneutral pH if chelating agents (CAs) are used along with soluble Fe(II), but the use of CAs is linked to higher cost, elevated toxicity, and potentially negative effects on oxidation efficiency due to their nonproductive consumption by oxidants.^{503,504} These drawbacks can be avoided by using Fe minerals instead of soluble Fe(II) to generate HO^\bullet radicals at circumneutral pH in the Fenton-like oxidation reaction.⁵⁰⁵

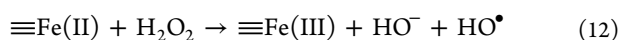
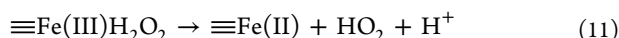
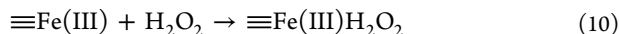
A more recent oxidant used for AOPs is the persulfate ($\text{S}_2\text{O}_8^{2-}$) that can be chemically or thermally activated to produce the sulfate free radical ($\text{SO}_4^{\bullet-}$), which is a stronger oxidant ($E^0 = 2.6 \text{ V}$) than the persulfate anion ($E^0 = 2.01 \text{ V}$).⁵⁰⁶ Generation of sulfate radical by Fe(II) activation is achieved through the following reaction:



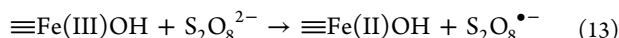
Fe minerals have shown strong capacity to activate both oxidants (H_2O_2 and $\text{S}_2\text{O}_8^{2-}$), leading to the production of highly reactive radicals (HO^\bullet and $\text{SO}_4^{\bullet-}$) at circumneutral pH. Moreover, mineral-catalyzed chemical oxidation shows better oxidant stability and pollutant degradation than by soluble Fe(II) activation as the latter is prone to precipitation at circumneutral pH.^{507–509} Mineral-catalyzed chemical oxidation is widely studied to remediate contaminated soils and water by using various Fe minerals including ferrihydrite,^{510–512} goethite,^{511–514} hematite,^{511,512,515} lepidocrocite,^{511,512} magnetite,^{507,511,512,515–521} and GR.^{42,330,522–524} Mixed-valent Fe minerals show higher catalytic efficiency than ferric minerals to promote chemical oxidation of organic pollutants which is correlated to the presence of structural Fe(II).^{511,512,515,525} For example, Matta et al.^{511,512} showed that magnetite (with 85% pollutant removal) was more effective than ferric oxyhydroxides (ferrihydrite, goethite, hematite, and lepidocrocite) (with <

10% of pollutant removal) for oxidative degradation of 2,4,6-trinitrotoluene.

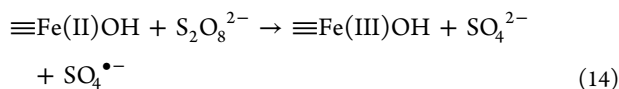
Even if the ability of magnetite or GR to promote Fenton oxidation is mainly dictated by its Fe(II) content, implications of Fe(III) in oxidation reaction cannot be ignored. Indeed, Kwan and Voelker⁵²⁶ have suggested the following chain of reactions in a mineral-catalyzed oxidation system:



The mineral-catalyzed reaction is a chain of reactions occurring on the surface where the regeneration of Fe(II) (eqs 10 and 11) is the rate-limiting step. If only Fe(III) is initially present, Fe(II) is slowly generated by reactions 10 and 11 initiating oxidation reactions. But in the case of iron (II) bearing minerals, the presence of iron (II) can enhance the production rate of HO^\bullet .^{511,515,527} By analogy to the Fenton-like system, Liu et al.⁵²⁸ have proposed a one-electron reduction of $\equiv\text{Fe(III)}$ surface site, which results in the formation of persulfate radical ($\text{S}_2\text{O}_8^{\bullet-}$):



This radical $\text{S}_2\text{O}_8^{\bullet-}$ can be involved in radical chain reactions with water, while freshly generated Fe(II) react with $\text{S}_2\text{O}_8^{2-}$ to generate radical sulfate $\text{SO}_4^{\bullet-}$ through



The catalytic ability of magnetite and GR to promote advanced oxidation strongly depends on their structural and surface properties, Fe(II)/Fe(III) ratio and solution chemistry.^{42–45} In this regard, Xue and colleagues⁴³ investigated the efficiency of two different kinds of magnetite (M1 and M2) to promote Fenton-like oxidation of Rhodamine B at neutral pH in aqueous solution. Both M1 and M2 exhibited different properties like Fe(II)/Fe(III) ratio (0.24 ± 0.2 and 0.43 ± 0.2 , respectively), while similar contents of total Fe: 70 ± 2 wt.%, mean particle diameter (<50 nm and <5 μm , respectively), and SSA (40 ± 3 and 2.4 ± 0.2 $\text{m}^2 \text{g}^{-1}$, respectively). The results indicated that M2 exhibited better oxidation efficiency than M1 at all tested ranges of $\text{H}_2\text{O}_2/\text{Fe}$ ratio (5–150) due to the higher Fe(II) content. For example, decolorization kinetic constant, k_{app} (min^{-1}) for M1 and M2 were 0.003 and 0.11, respectively, at $\text{H}_2\text{O}_2/\text{Fe}$ molar ratio = 100 (pH 7, magnetite = 2 g L^{-1}). The M2 also revealed higher decomposition rates of H_2O_2 than M1 when normalized to the surface area [$k = 3.10^{-4} \text{min}^{-1} (\text{m}^2/\text{L})^{-1}$ for M2 and $8.10^{-5} \text{min}^{-1} (\text{m}^2/\text{L})^{-1}$], while a reverse trend was found when based on mass basis. Hanna and co-workers⁴² evaluated the efficiency of three different kinds of GR including $\text{GR}(\text{Cl}^-)$, $\text{GR}(\text{CO}_3^{2-})$, and $\text{GR}(\text{SO}_4^{2-})$ and one type of magnetite to promote Fenton-like oxidation of phenol under similar experimental conditions (30 mM H_2O_2 , 1 g L^{-1} of GR or magnetite, pH 7.1, N_2 atmosphere). The Fe(II) contents were higher in $\text{GR}(\text{Cl}^-)$ with Fe(II):Fe(III) ratio of 3:1, while this ratio was 2:1 for $\text{GR}(\text{CO}_3^{2-})$ and $\text{GR}(\text{SO}_4^{2-})$ and 1:2 for magnetite. Obtained results indicated that mineralization rate of phenol as well as the decomposition rate of H_2O_2 was higher for $\text{GR}(\text{Cl}^-)$ followed by $\text{GR}(\text{SO}_4^{2-})$, $\text{GR}(\text{CO}_3^{2-})$, or magnetite, mainly due to the higher Fe(II) content of $\text{GR}(\text{Cl}^-)$. The

reaction kinetics were also dependent on the type of the interlayer anion. Pseudo-first order rate constants (k_{surf}) for phenol degradation were 13×10^{-4} , 3.3×10^{-4} , 3.5×10^{-4} , and $0.4 \times 10^{-4} \text{L m}^{-2} \text{s}^{-1}$ for $\text{GR}(\text{Cl}^-)$, $\text{GR}(\text{SO}_4^{2-})$, $\text{GR}(\text{CO}_3^{2-})$, and magnetite, respectively. Higher efficiency of GR than magnetite was also observed during Fenton-like oxidation of 2,4,6-trinitrotoluene in aqueous phase at circumneutral pH (Figure 22).⁵¹² The obtained values of degradation pseudo-

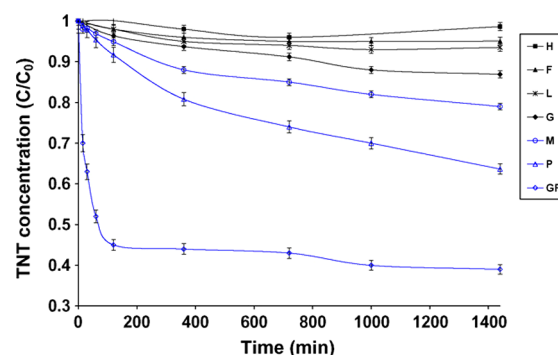


Figure 22. Fenton-like oxidation of TNT (0.11 mM) in the presence of six different iron minerals (2 g L^{-1}) at pH 7: (■) hematite, (▲) ferrihydrite, (*) lepidocrocite, (◆) goethite, (○) magnetite, (△) pyrite, (◇) green rust. H_2O_2 (3%, w/v). Reproduced with permission from ref 512. Copyright 2008 Elsevier.

first-order rate constant's (k_{surf}) for GR and magnetite were $2.55 \times 10^{-4} \text{L m}^{-2} \text{min}^{-1}$ and $1 \times 10^{-4} \text{L m}^{-2} \text{min}^{-1}$ respectively. These results were consistent with higher Fe(II) contents in GR (38%) than magnetite (24%).⁵¹² However, magnetite was found to be more stable than GR as degradation in the latter reached a plateau in 3 h of reaction after a quick start, while no such plateau was achieved for magnetite even after 24 h (Figure 22).⁵¹² Moreover, GR was transformed into a mixture of ferrihydrite and lepidocrocite at the end of the oxidation process while magnetite retained its structure and catalytic ability.⁵²² It should be noted that GRs are unstable under oxidizing conditions and their quick reaction with H_2O_2 or atmospheric oxygen transforms them into ferric GR, magnetite, or other ferric minerals depending on pH and composition of solution, rate of oxidation, oxidant type, and the dehydration rate.^{143,183} On the other hand, magnetite exhibits good structural and thermodynamic stability. Due to its ferromagnetic nature, it can be easily separated from aqueous solution by applying an external magnetic field.⁵²⁹ Therefore, it can be reused for several oxidation cycles with no loss in catalytic efficiency as reported by Xue et al.⁴⁶⁰ Recently, magnetite demonstrated strong stability without any significant loss in catalytic ability when it was used in nitrilotriacetic acid-assisted Fenton-like oxidation to degrade TCE for 230 days.⁵³⁰ Owing to the higher stability and ease of handling offered by magnetite, a major portion of literature is devoted to the use of magnetite to promote chemical oxidation, while studies using GR are scarce (Table 12). As a matter of fact, efficiency of GR has never been tested to activate persulfate oxidation.

Despite the strong stability of magnetite, several other researchers reported Fe leaching during subsequent oxidation cycles that could affect its reusability and efficiency to some extent (Table 12). Rusevova and co-workers⁴⁵ compared the efficiency of three different kinds of nanomagnetite (Fe(II)/Fe(III) ratio of 0.11, 0.52, and 1.44 in M_a , M_b , and M_c respectively) to catalyze Fenton-like oxidation of phenol at

neutral pH. It should be noted that, prior to use, M_c was subjected to reductive pretreatment (by reacting with NaBH_4) to improve Fe(II) content. Their results demonstrated similar catalytic ability for all magnetites (42–65% of phenol removal in 24 h) that was correlated to variation in Fe(II) leaching during reaction that led to different Fe(II)/Fe(III) ratios of 0.10, 0.15, and 1.07 in M_a , M_b , and M_c , respectively. It was also correlated to scavenging of radicals by nanoparticle agglomerates. Reusability tests of magnetite for three subsequent oxidation cycles of phenol also indicated a 20% decrease in oxidation efficiency in the third oxidation cycle (negligible effect in second cycle).⁴⁵ However, a dramatic decrease in oxidant decomposition rate was reported as evident from R_{25} values of 1200, 500, and 230 mol mol^{-1} obtained for the first, second, and third cycles. This was not observed in phenol-free reactions where crystalline structure also remained the same in recovered magnetite. Thus, observed instability of the magnetite nanoparticles was attributed to the passivation of the surface iron with intermediates of phenol oxidation.⁴⁵ Reusability tests of magnetite over 5–8 oxidation cycles showed a loss of 20–30% in oxidation efficiency which has been attributed to the loss of catalyst in the form of dissolved Fe(II) and/or loss of magnetite particles.^{529,531} Hou et al.⁵³² also deduced decline in degradation efficiency in sequential experiments to the conversion of $\equiv\text{Fe(II)}$ to $\equiv\text{Fe(III)}$ on the surface of magnetite.

Recently, natural magnetite has been shown to have strong stability (leached iron concentration of 0.5 mg L^{-1} against applied magnetite dosage of 0.5 g L^{-1}) after six subsequent oxidation cycles while oxidation efficiency remained almost constant.⁵³³ Recently, Munoz et al. reported that natural magnetite showed the best performance over three sequential runs as compared to the natural hematite and ilmenite.⁵³⁴ Magnetite maintained its catalytic ability as illustrated by 80% mineralization in the third oxidation cycle (similar to that in first cycle). Hematite yielded a slight decrease in mineralization (from 80% to 70%), while ilmenite suffered strong deactivation and showed negligible activity (from 78 to 1% mineralization) in the third cycle. Until now however, very few studies appeared in the literature which reported the use of natural magnetite^{120,533–535} that exhibited higher catalytic performance than that of the synthetic pure magnetite.¹²⁰ Indeed, up to 95% degradation of *p*-nitrophenol by H_2O_2 was achieved with a natural magnetite, while lab-synthesized magnetite did not cause any obvious pollutant degradation in one study dedicated to this aspect.¹²⁰ It should be noted that most chemical oxidation studies investigated synthetic magnetites rather than natural minerals (Table 12). Furthermore, there are several inconsistencies in the literature regarding the catalytic stability of magnetite. Such inconsistencies are not altogether surprising when considering the variety of experimental and analytical approaches adopted in different studies. Indeed, different magnetites are often characterized by contrasting structural properties, morphology, magnetization, and stoichiometry. Such differences can often be attributed to the different conditions under which they were synthesized or studied such as in oxic versus anoxic-controlled atmosphere, batch versus column study, solution chemistry, presence of dissolved Fe(II), target compounds, etc.

In this context, it is challenging to develop iron catalysts offering greater stability and lower iron leaching but without compromising the oxidation efficiency. Therefore, various supports or stabilizers have been used to anchor iron on the

surface of catalysts to improve the stability of magnetite even after several oxidation cycles including CeO_2 ,⁵³⁶ hydrogel,⁵³⁷ iron oxalate,⁵³⁸ MWCNTs,^{539–541} mesoporous SiO_2 ,⁵⁴² and rGO.⁵⁴³ Many researchers have tested metal doping for isomorphic substitution of Fe in magnetite structure to improve its stability.^{5,544–551} In addition, several other strategies have been developed to decrease iron leaching and to improve catalyst stability such as photo-Fenton,^{44,552,553} ultrasound assisted chemical oxidation,^{532,554} and UV-LED assisted oxidation.⁵⁵⁵ Separation of solid phase is an important issue in photo-Fenton oxidation that can be avoided by using magnetite which offers easy magnetic separation from aqueous solution.¹⁵¹

Although the use of magnetite could offer a promising alternative to homogeneous Fenton oxidation, its potential application is still limited due to the lack of studies at field-scale.⁵⁰⁵ While most chemical oxidation studies using magnetite as iron source were performed at lab-scale, no report has appeared concerning field applicability. Prior to industrial applications, injection mode, transport of particles in soil, or magnetite/soil mixing, eco-toxicity assessment, etc. should be addressed.

7. CONCLUSIONS AND OUTLOOK

Mixed-valent iron minerals such as magnetite and GR are among the most important iron compounds found on Earth due to their impact on biogeochemical cycling of trace elements, their role in controlling the fate and toxicity of environmental pollutants, and their use in various environmental remediation approaches. Magnetite and GR are present in many environmental settings; however, a firm understanding of the mechanisms of their formation and their reactivity remains a major challenge in environmental and applied sciences.

Magnetite and GR can be synthesized via a variety of abiotic and microbial pathways. Their chemical composition, crystallinity, morphology, and stoichiometry are controlled by various factors including the nature of the initial substrate, Fe(II)/Fe(III) ratio, reaction pH, and other geochemical conditions. These properties ultimately dictate the stability and reactivity of mixed-valent Fe minerals in aqueous environments. Nevertheless, through the use of diverse synthesis techniques, researchers have been able to create novel mineral structures (e.g., partially substituted, deprotonated, or organically modified GRs) with enhanced reactivity which could be used to develop new applications of mixed-valent Fe minerals. Further progress in developing new and improved synthesis methods with precise control over product composition (e.g., purity, stability, particle size, sorption capacity, and redox activity) or through the application of microbial strategies will further improve the ability to use mixed-valent Fe minerals in environmental applications due to their enhanced reactivity or stability.

Magnetite and GR play key roles for sorption and reductive transformation of metals and organic compounds. Magnetite may also contribute as an electron acceptor and electron donor for bacteria to the dynamics of environmental redox processes even though its significance needs to be further evaluated. Thus, development of in situ methods is needed to determine mixed-valent Fe-minerals in natural settings and to study the dynamics of their formation, transformation, and/or decay. Future challenges also include development of predictive models (both thermodynamic and kinetic) to describe and

predict formation and reactivity of mixed-valent Fe minerals in natural settings to assess their roles in the cycling of electrons under natural (and thus fluctuating) redox conditions.

The application of magnetite in bioremediation remains a challenge due to aggregation and changing reactivity over time. It would be desirable to maintain or even increase the reactivity of magnetite over time with the help of microorganisms.

Mixed-valent Fe minerals have also shown strong reactivity toward the chemical oxidation of a variety of organic contaminants. In environmental engineering applications (e.g., wastewater treatment, soil remediation, etc.), *in situ* or *ex situ*, the decontamination reactions generally take place under ambient environments containing O₂ and H₂O. In these conditions, the stability field of mixed-valent Fe minerals is relatively narrow. GR may quickly transform into other compounds generally less reactive than the parent GR, while magnetite may undergo surface oxidation. Indeed, formation of a passivating layer on the magnetite surface exposed to air alters the redox reactivity, a phenomenon that becomes particularly important for nanoscale particles with a higher surface-to-volume ratio. Consequently, fluctuations in redox and solution chemistry of contaminated systems with respect to the thermodynamic stability of mixed-valent oxides represent a significant level of challenges to engineers. As there is a growing interest in environmentally friendly catalytic processes based on magnetic solids, it would be highly rewarding to develop cheap and effective magnetite-based catalysts with greater stability and higher reactivity for full-scale applications. However, more knowledge is required to assess their implementation at large-scale, as further research is required regarding the mode of application, mobility, stability, and eco-toxicity of such minerals.

AUTHOR INFORMATION

Corresponding Author

*Environmental Mineralogy, Center for Applied Geosciences, University of Tübingen Hölderlinstraße 12, 72074 Tübingen, Germany. E-mail: muhammad.usman@uaf.edu.pk and musmanch@yahoo.com. Tel: +49 70 71 29 78 924. Fax: +49 70 71 29 50 59.

ORCID

M. Usman: 0000-0001-6900-1333

K. Hanna: 0000-0002-6072-1294

A. Kappler: 0000-0002-3558-9500

S. B. Haderlein: 0000-0002-9309-8523

Notes

The authors declare no competing financial interest.

Biographies

Muhammad Usman is an Alexander von Humboldt postdoctoral fellow with Stefan Haderlein at the University of Tübingen, Germany. He also holds the position of an Assistant Professor in the Institute of Soil and Environmental Sciences at the University of Agriculture, Faisalabad, Pakistan. He obtained his B.S. in Soil Science at the latter organization. He was, then, awarded a fellowship from Higher Education Commission of Pakistan to pursue further studies from France. He obtained his M.S. (2008) in environmental sciences from AgroParisTech and Ph.D. (2011) in iron geochemistry and environmental remediation from University of Lorraine under the supervision of Christian Ruby, Khalil Hanna, and Pierre Faure. His research concerns iron-mediated remediation of soil and water contaminants. Major focus of his research is the synthesis and use of mixed-valent

iron minerals for environmental remediation with an emphasis on advanced oxidation processes (Fenton and persulfate oxidation) and sorption.

James M. Byrne obtained a MPhys in Physics at the University of St. Andrews, UK, in 2008. He then went on to complete a Ph.D. in 2012 in the field of Geomicrobiology at the University of Manchester, UK, under the supervision of Jon Lloyd and Richard Patrick. He then moved to the University of Tübingen to start a Postdoc and now holds a permanent research position. His research has focused on combining mineralogy, magnetism, geochemistry, and microbiology to explore the interactions of iron-metabolizing bacteria with mixed-valent iron minerals. His analytical expertise includes magnetic characterization methods, Mössbauer spectroscopy, electron microscopy, and synchrotron-based techniques with a strong focus on the development of new bioinspired nanomaterials which could ultimately be used for environmental remediation and biomedical applications.

Aaifa Chaudhary obtained her M.S. in Environmental Sciences from the University of the Punjab, Pakistan, in 2011. She, then, joined as Lecturer in Department of Environmental Science and Engineering, Government College University, Faisalabad, Pakistan. Currently, she is pursuing her Ph.D. at the University of Tübingen under the supervision of Prof. Stefan Haderlein. Her research is focused on interactions of metals in iron-based redox systems in the presence of organic matter.

Silvia Orsetti obtained a Chemistry Diploma at the University of Buenos Aires in 2004. She completed her Ph.D. in 2010 at the same university in the area of Electrochemistry and Environmental Chemistry. Afterward, she started a Postdoc at the University of Tübingen in Environmental Mineralogy and Chemistry in Prof. Haderlein's group. She now holds a research position in the same group, where she focuses on electron transfer processes between natural organic matter and minerals. Her research combines electrochemistry, geochemistry, and analytical chemistry to study mechanisms of electron transfer reactions between humic substances and redox active minerals as well as changes of redox properties of humic substances upon sorption to different sorbents. Her analytical expertise includes photochemistry, electrochemistry, and HPLC applied to the optimization of characterizing humic substances' properties.

Khalil Hanna is a Professor of Chemistry at the Graduate School of Chemistry of Rennes and a junior member of the Institut Universitaire de France (IUF). He earned his Ph.D. (2004) in Environmental Science and Technology from INSA of Lyon. His research interests focus on iron-mediated reactions for soil and water treatments and an improved understanding of sorption and heterogeneous redox reactions taking place at the oxide/water interface. His research group in Rennes is engaged in elucidating molecular-scale reactions at mineral surfaces and in translating molecular-level information to observations made at the larger scales using thermodynamics and reactive transport modelling.

Christian Ruby is a full Professor of Materials Science at the University of Lorraine (France). He teaches at the engineering school Polytech Nancy. He obtained Ph.D. in 1997 at the University Henri Poincaré-Nancy I, concerning the synthesis of ultrathin iron oxides layers by molecular beam epitaxy. After postdoctoral training, performed in the MINT Centre at the University of Tuscaloosa in Alabama (USA), he joined the University of Lorraine in 2000 as an Assistant Professor and began his research activity concerning the formation and the chemical reactivity of iron species in aqueous medium at the "Laboratoire de Chimie Physique et Microbiologie pour les Matériaux et l'Environnement" (LCPME-UMR 7564 CNRS-UL). Professor Ruby's research

expertise is related to the synthesis and reactivity of iron-containing compounds, in particular Fe(II)-Fe(III) layered double hydroxides, more commonly called “green rust”. Recently, Christian Ruby managed different research projects devoted to the use of green rust and related iron-containing compounds for wastewater denitrification and dephosphatation.

Andreas Kappler is a professor for Geomicrobiology at the University of Tübingen. He received his M.Sc. in Chemistry and Ph.D. in Environmental Microbiology from University of Konstanz and had postdoc positions at the EAWAG/ETH Zürich in Environmental Chemistry and at Caltech in Geobiology. The major focus of his research is the biogeochemical cycling of iron and humic substances and the consequences for the environmental fate of toxic metals and nutrients. Other main research areas are the role of microbial iron oxidation in the deposition of Precambrian Banded Iron Formations, biochar as soil amendment, and the recovery of precious metals from waste from incineration plants.

Stefan B. Haderlein is a full Professor at the Center for Applied Geosciences (ZAG) of the Eberhard-Karls University Tübingen, Germany. He received his Ph.D. in Environmental Chemistry from the Swiss Federal Institute of Technology (ETH) Zurich, Switzerland, in 1992 (Major Professor: René P. Schwarzenbach) and earned his habilitation and *venia legendi* from the same institution in 1998; he served as research scientist at the Swiss Federal Institute for Water Resources and Water Pollution Control (EAWAG) and ETH Zurich from 1993 to 1999 and was a Postdoctoral Fellow at the Massachusetts Institute of Technology (1996 to 1997; with Philip Gschwend). His research concerns processes at the mineral–water interface such as sorption and oxidation–reduction reactions in the context of contaminant fate and biogeochemistry of subsurface environments.

ACKNOWLEDGMENTS

This work is supported by research grant from the Alexander von Humboldt Foundation of Germany and is gratefully acknowledged. K.H. thanks the ADEME (France) for their support. C.R. thanks the Institute of Advanced Study of the University of Durham (UK) for providing a Research Fellowship during the writing of this manuscript.

REFERENCES

- (1) Taylor, S. R. Abundance of Chemical Elements in the Continental Crust: A New Table. *Geochim. Cosmochim. Acta* **1964**, *28*, 1273–1285.
- (2) Cornell, R. M.; Schwertmann, U. *The Iron Oxides: Structure, Properties, Reactions, Occurrence and Uses*; 2nd ed.; Wiley-VCH, 2003.
- (3) Hansen, H. C. B. Environmental Chemistry of Iron(II)-Iron(III) LDHs (Green Rusts). In *Layered Double Hydroxides: Present and Future*; Nova Science Publishers: Huntington, NY, 2001; pp 469–493.
- (4) Su, C. Environmental Implications and Applications of Engineered Nanoscale Magnetite and Its Hybrid Nanocomposites: A Review of Recent Literature. *J. Hazard. Mater.* **2017**, *322*, 48–84.
- (5) Munoz, M.; de Pedro, Z. M.; Casas, J. A.; Rodriguez, J. J. Preparation of Magnetite-Based Catalysts and Their Application in Heterogeneous Fenton Oxidation – A Review. *Appl. Catal., B* **2015**, *176–177*, 249–265.
- (6) Tang, S. C. N.; Lo, I. M. C. Magnetic Nanoparticles: Essential Factors for Sustainable Environmental Applications. *Water Res.* **2013**, *47*, 2613–2632.
- (7) Pereira, M. C.; Oliveira, L. C. A.; Murad, E. Iron Oxide Catalysts: Fenton and Fenton Like Reactions- A Review. *Clay Miner.* **2012**, *47*, 285–302.
- (8) Trolard, F.; Bourrié, G. Chapter 5 Geochemistry of Green Rusts and Fougérite: A Reevaluation of Fe cycle in Soils. *Adv. Agron.* **2008**, *99*, 227–288.
- (9) He, Y. T.; Wilson, J. T.; Su, C.; Wilkin, R. T. Review of Abiotic Degradation of Chlorinated Solvents by Reactive Iron Minerals in Aquifers. *Ground Water Monitoring and Remediation* **2015**, *35*, 57–75.
- (10) Ray, P. Z.; Shipley, H. J. Inorganic Nano-Adsorbents for the Removal of Heavy Metals and Arsenic: A Review. *RSC Adv.* **2015**, *5*, 29885–29907.
- (11) Kaur, R.; Hasan, A.; Iqbal, N.; Alam, S.; Saini, M. K.; Raza, S. K. Synthesis and Surface Engineering of Magnetic Nanoparticles for Environmental Cleanup and Pesticide Residue Analysis: A Review. *J. Sep. Sci.* **2014**, *37*, 1805–1825.
- (12) Giakissikli, G.; Anthemidis, A. N. Magnetic Materials as Sorbents for Metal/Metalloid Preconcentration and/or Separation. A Review. *Anal. Chim. Acta* **2013**, *789*, 1–16.
- (13) Ngomsik, A.-F.; Bee, A.; Draye, M.; Cote, G.; Cabuil, V. Magnetic Nano- and Microparticles for Metal Removal and Environmental Applications: A Review. *C. R. Chim.* **2005**, *8*, 963–970.
- (14) Skomurski, F. N.; Kerisit, S.; Rosso, K. M. Structure, Charge Distribution, and Electron Hopping Dynamics in Magnetite (Fe₃O₄) (1 0 0) Surfaces from First Principles. *Geochim. Cosmochim. Acta* **2010**, *74*, 4234–4248.
- (15) Gorski, C. A.; Handler, R. M.; Beard, B. L.; Pasakarnis, T.; Johnson, C. M.; Scherer, M. M. Fe Atom Exchange between Aqueous Fe²⁺ and Magnetite. *Environ. Sci. Technol.* **2012**, *46*, 12399–12407.
- (16) Jolivet, J.-P.; Tronc, E. Interfacial Electron Transfer in Colloidal Spinel Iron Oxide. Conversion of Fe₃O₄-γ-Fe₂O₃ in Aqueous Medium. *J. Colloid Interface Sci.* **1988**, *125*, 688–701.
- (17) Jolivet, J. P.; Belleville, P.; Tronc, E.; Livage, J. Influence of Fe(II) on the Formation of the Spinel Iron Oxide in Alkaline Medium. *Clays Clay Miner.* **1992**, *40*, 531–539.
- (18) Tronc, E.; Jolivet, J.-P.; Lefebvre, J.; Massart, R. Ion Adsorption and Electron Transfer in Spinel-Like Iron Oxide Colloids. *J. Chem. Soc., Faraday Trans. 1* **1984**, *80*, 2619–2629.
- (19) Ruby, C.; Usman, M.; Naille, S.; Hanna, K.; Carteret, C.; Mullet, M.; François, M.; Abdelmoula, M. Synthesis and Transformation of Iron-Based Layered Double Hydroxides. *Appl. Clay Sci.* **2010**, *48*, 195–202.
- (20) Refait, P.; Simon, L.; Génin, J.-M. R. Reduction of SeO₄²⁻ Anions and Anoxic Formation of Iron(II)–Iron(III) Hydroxy-Selenate Green Rust. *Environ. Sci. Technol.* **2000**, *34*, 819–825.
- (21) Refait, P.; Abdelmoula, M.; Génin, J. M. R.; Jeannin, M. Synthesis and Characterisation of the Fe(II-III) Hydroxy-Formate Green Rust. *Hyperfine Interact.* **2006**, *167*, 717–722.
- (22) Ayala-Luis, K. B.; Koch, C. B.; Hansen, H. C. B. One-Pot Synthesis and Characterization of Fe^{II}–Fe^{III} Hydroxide (Green Rust) Intercalated with C9–C14 Linear Alkyl Carboxylates. *Appl. Clay Sci.* **2010**, *50*, 512–519.
- (23) Bourdoiseau, J. A.; Sabot, R.; Jeannin, M.; Termemil, F.; Refait, P. Determination of Standard Gibbs Free Energy of Formation of Green Rusts and Its Application to the Fe(II–III) Hydroxy-Oxalate. *Colloids Surf., A* **2012**, *410*, 72–80.
- (24) Simon, L.; François, M.; Refait, P.; Renaudin, G.; Lelaurain, M.; Génin, J.-M. R. Structure of the Fe(II-III) Layered Double Hydroxysulphate Green Rust Two from Rietveld Analysis. *Solid State Sci.* **2003**, *5*, 327–334.
- (25) Aissa, R.; François, M.; Ruby, C.; Fauth, F.; Medjahdi, G.; Abdelmoula, M.; Génin, J. M. Formation and Crystallographical Structure of Hydroxysulphate and Hydroxycarbonate Green Rusts Synthesised by Coprecipitation. *J. Phys. Chem. Solids* **2006**, *67*, 1016–1019.
- (26) Refait, P. H.; Abdelmoula, M.; Génin, J. M. R. Mechanisms of Formation and Structure of Green Rust One in Aqueous Corrosion of Iron in the Presence of Chloride Ions. *Corros. Sci.* **1998**, *40*, 1547–1560.
- (27) Bernal, J. D.; Dasgupta, D. R.; Mackay, A. L. The Oxides and Hydroxides of Iron and Their Structural Inter-Relationships. *Clay Miner.* **1959**, *4*, 15–30.
- (28) Génin, J. M. R.; Christy, A.; Kuzmann, E.; Mills, S.; Ruby, C. Structure and Occurrences of « Green Rust » Related New Minerals of the « Fougérite » Group, Trébeurdenite and Mössbauerite,

Belonging to the « Hydrotalcite » Supergroup; How Mössbauer Spectroscopy Helps XRD. *Hyperfine Interact.* **2014**, *226*, 459–482.

(29) Refait, P.; Bon, C.; Simon, L.; Bourrié, G.; Trolard, F.; Bessiere, J.; Génin, J.-M. Chemical Composition and Gibbs Standard Free Energy of Formation of Fe(II)-Fe(III) Hydroxysulphate Green Rust and Fe(II) Hydroxide. *Clay Miner.* **1999**, *34*, 499–510.

(30) Christiansen, B. C.; Balic-Zunic, T.; Petit, P. O.; Frandsen, C.; Mørup, S.; Geckeis, H.; Katerinopoulou, A.; Stipp, S. L. S. Composition and Structure of an Iron-Bearing, Layered Double Hydroxide (LDH) – Green Rust Sodium Sulphate. *Geochim. Cosmochim. Acta* **2009**, *73*, 3579–3592.

(31) Ruby, C.; Aïssa, R.; Géhin, A.; Cortot, J.; Abdelmoula, M.; Génin, J.-M. Green Rusts Synthesis by Coprecipitation of Fe^{II}-Fe^{III} ions and Mass-Balance Diagram. *C. R. Geosci.* **2006**, *338*, 420–432.

(32) Bocher, F.; Géhin, A.; Ruby, C.; Ghanbaja, J.; Abdelmoula, M.; Génin, J.-M. R. Coprecipitation of Fe(II–III) Hydroxycarbonate Green Rust Stabilised by Phosphate Adsorption. *Solid State Sci.* **2004**, *6*, 117–124.

(33) Génin, J.-M. R.; Refait, P.; Bourrié, G.; Abdelmoula, M.; Trolard, F. Structure and Stability of the Fe(II)–Fe(III) Green Rust “Fougerite” Mineral and Its Potential for Reducing Pollutants in Soil Solutions. *Appl. Geochem.* **2001**, *16*, 559–570.

(34) Génin, J.; Abdelmoula, M.; Refait, P.; Simon, L. Comparison of the Green Rust Two Lamellar Double Hydroxide Class with the Green Rust One Pyroaurite Class: Fe(II)-Fe(III) Sulphate and Selenate Hydroxides. *Hyperfine Interact. (C)* **1998**, *3*, 313–316.

(35) Gorski, C. A.; Scherer, M. M. Determination of Nanoparticulate Magnetite Stoichiometry by Mossbauer Spectroscopy, Acidic Dissolution, and Powder X-Ray Diffraction: A Critical Review. *Am. Mineral.* **2010**, *95*, 1017–1026.

(36) Zegeye, A.; Abdelmoula, M.; Usman, M.; Hanna, K.; Ruby, C. In Situ Monitoring of Lepidocrocite Bioreduction and Magnetite Formation by Reflection Mossbauer Spectroscopy. *Am. Mineral.* **2011**, *96*, 1410–1413.

(37) Usman, M.; Abdelmoula, M.; Hanna, K.; Grégoire, B.; Faure, P.; Ruby, C. Fe^{II} Induced Mineralogical Transformations of Ferric Oxyhydroxides into Magnetite of Variable Stoichiometry and Morphology. *J. Solid State Chem.* **2012**, *194*, 328–335.

(38) Annersten, H.; Hafner, S. S. Vacancy Distribution in Synthetic Spinel of the Series Fe₃O₄–γ-Fe₂O₃. *Z. Kristallogr. Cryst. Mater.* **1973**, *137*, 321–340.

(39) Gorski, C. A.; Nurmi, J. T.; Tratnyek, P. G.; Hofstetter, T. B.; Scherer, M. M. Redox Behavior of Magnetite: Implications for Contaminant Reduction. *Environ. Sci. Technol.* **2010**, *44*, 55–60.

(40) Gorski, C. A.; Scherer, M. M. Influence of Magnetite Stoichiometry on Fe^{II} Uptake and Nitrobenzene Reduction. *Environ. Sci. Technol.* **2009**, *43*, 3675–3680.

(41) Peterson, M. L.; White, A. F.; Brown, G. E.; Parks, G. A. Surface Passivation of Magnetite by Reaction with Aqueous Cr(VI): XAFS and TEM Results. *Environ. Sci. Technol.* **1997**, *31*, 1573–1576.

(42) Hanna, K.; Kone, T.; Ruby, C. Fenton-Like Oxidation and Mineralization of Phenol Using Synthetic Fe(II)-Fe(III) Green Rusts. *Environ. Sci. Pollut. Res.* **2010**, *17*, 124–134.

(43) Xue, X.; Hanna, K.; Deng, N. Fenton-Like Oxidation of Rhodamine B in the Presence of Two Types of Iron (II, III) Oxide. *J. Hazard. Mater.* **2009**, *166*, 407–414.

(44) Minella, M.; Marchetti, G.; De Laurentiis, E.; Malandrino, M.; Maurino, V.; Minero, C.; Vione, D.; Hanna, K. Photo-Fenton Oxidation of Phenol with Magnetite as Iron Source. *Appl. Catal., B* **2014**, *154–155*, 102–109.

(45) Rusevova, K.; Kopinke, F.-D.; Georgi, A. Nano-Sized Magnetic Iron Oxides as Catalysts for Heterogeneous Fenton-Like Reactions—Influence of Fe(II)/Fe(III) Ratio on Catalytic Performance. *J. Hazard. Mater.* **2012**, *241–242*, 433–440.

(46) Da Costa, G.; De Grave, E.; De Bakker, P.; Vandenberghe, R. Influence of Nonstoichiometry and the Presence of Maghemite on the Mössbauer Spectrum of Magnetite. *Clays Clay Miner.* **1995**, *43*, 656–668.

(47) Tronc, E.; Belleville, P.; Jolivet, J. P.; Livage, J. Transformation of Ferric Hydroxide into Spinel by Fe^{II} Adsorption. *Langmuir* **1992**, *8*, 313–319.

(48) Byrne, J. M.; van der Laan, G.; Figueroa, A. I.; Qafoku, O.; Wang, C.; Pearce, C. L.; Jackson, M.; Feinberg, J.; Rosso, K. M.; Kappler, A. Size Dependent Microbial Oxidation and Reduction of Magnetite Nano- and Micro-Particles. *Sci. Rep.* **2016**, *6*, 30969.

(49) Morrall, P.; Schedin, F.; Case, G. S.; Thomas, M. F.; Dudzik, E.; van der Laan, G.; Thornton, G. Stoichiometry of Fe_{3–δ}O₄(111) Ultrathin Films on Pt(111). *Phys. Rev. B: Condens. Matter Mater. Phys.* **2003**, *67*, 214408.

(50) Patrick, R. A. D.; van der Laan, G.; Henderson, C. M. B.; Kuiper, P.; Dudzik, E.; Vaughan, D. J. Cation Site Occupancy in Spinel Ferrites Studied by X-Ray Magnetic Circular Dichroism: Developing a Method for Mineralogists. *Eur. J. Mineral.* **2002**, *14*, 1095–1102.

(51) Usman, M.; Hanna, K.; Abdelmoula, M.; Zegeye, A.; Faure, P.; Ruby, C. Formation of Green Rust Via Mineralogical Transformation of Ferric Oxides (Ferrihydrite, Goethite and Hematite). *Appl. Clay Sci.* **2012**, *64*, 38–43.

(52) Thermodynamics and Microbial Metabolism. In *Advances in Marine Biology*; Canfield, D. E., Kristensen, E., Thamdrup, B., Eds.; Academic Press, 2005; Vol. 48, pp 65–94.

(53) White, A. F.; Peterson, M. L.; Hochella, M. F. Electrochemistry and Dissolution Kinetics of Magnetite and Ilmenite. *Geochim. Cosmochim. Acta* **1994**, *58*, 1859–1875.

(54) Gorski, C. A.; Scherer, M. M. Fe²⁺ Sorption at the Fe Oxide-Water Interface: A Revised Conceptual Framework. In *Aquatic Redox Chemistry*; American Chemical Society, 2011; Vol. 1071; pp 315–343.

(55) Thamdrup, B. Bacterial Manganese and Iron Reduction in Aquatic Sediments. In *Advances in Microbial Ecology*; Schink, B., Ed.; Springer: Boston, MA, 2000; pp 41–84.

(56) Linberg, R.; Runnels, D. Ground Water Redox Reactions: An Analysis of Equilibrium State Applied to Eh Measurements and Geochemical Modeling. *Science* **1984**, *225*, 925–927.

(57) Orsetti, S.; Laskov, C.; Haderlein, S. B. Electron Transfer between Iron Minerals and Quinones: Estimating the Reduction Potential of the Fe(II)-Goethite Surface from AQDS Speciation. *Environ. Sci. Technol.* **2013**, *47*, 14161–14168.

(58) Gorski, C. A.; Edwards, R.; Sander, M.; Hofstetter, T. B.; Stewart, S. M. Thermodynamic Characterization of Iron Oxide–Aqueous Fe²⁺ Redox Couples. *Environ. Sci. Technol.* **2016**, *50*, 8538–8547.

(59) Fischer, W. R. Standard Potentials (E_o) of Iron(III) Oxides under Reducing Conditions. *Z. Pflanzenernaehr. Bodenkd.* **1987**, *150*, 286–289.

(60) Sander, M.; Hofstetter, T. B.; Gorski, C. A. Electrochemical Analyses of Redox-Active Iron Minerals: A Review of Nonmediated and Mediated Approaches. *Environ. Sci. Technol.* **2015**, *49*, 5862–5878.

(61) Gorski, C. A.; Klüpfel, L.; Voegelin, A.; Sander, M.; Hofstetter, T. B. Redox Properties of Structural Fe in Clay Minerals. 2. Electrochemical and Spectroscopic Characterization of Electron Transfer Irreversibility in Ferruginous Smectite, SWa-1. *Environ. Sci. Technol.* **2012**, *46*, 9369–9377.

(62) Castro, P. A.; Vago, E. R.; Calvo, E. J. Surface Electrochemical Transformations on Spinel Iron Oxide Electrodes in Aqueous Solutions. *J. Chem. Soc., Faraday Trans.* **1996**, *92*, 3371–3379.

(63) Latta, D. E.; Gorski, C. A.; Boyanov, M. I.; O’Loughlin, E. J.; Kemner, K. M.; Scherer, M. M. Influence of Magnetite Stoichiometry on UVI Reduction. *Environ. Sci. Technol.* **2012**, *46*, 778–786.

(64) Maher, B. A. Rain and Dust: Magnetic Records of Climate and Pollution. *Elements* **2009**, *5*, 229–234.

(65) Evans, M.; Heller, F. *Environmental Magnetism: Principles and Applications of Enviromagnetics*; Academic Press, 2003.

(66) Dunlop, D. J.; Özdemir, Ö. *Rock Magnetism: Fundamentals and Frontiers*; Cambridge University Press, 2001.

(67) Coey, J. M. D. Noncollinear Spin Arrangement in Ultrafine Ferrimagnetic Crystallites. *Phys. Rev. Lett.* **1971**, *27*, 1140–1142.

(68) Byrne, J. M.; Coker, V. S.; Cespedes, E.; Wincott, P. L.; Vaughan, D. J.; Patrick, R. A. D.; van der Laan, G.; Arenholz, E.;

- Tuna, F.; Bencsik, M.; et al. Biosynthesis of Zinc Substituted Magnetite Nanoparticles with Enhanced Magnetic Properties. *Adv. Funct. Mater.* **2014**, *24*, 2518–2529.
- (69) Byrne, J. M.; Coker, V. S.; Moise, S.; Wincott, P. L.; Vaughan, D. J.; Tuna, F.; Arenholz, E.; van der Laan, G.; Patrick, R. A. D.; Lloyd, J. R.; et al. Controlled Cobalt Doping in Biogenic Magnetite Nanoparticles. *J. R. Soc., Interface* **2013**, *10*, 20130134.
- (70) Céspedes, E.; Byrne, J. M.; Farrow, N.; Moise, S.; Coker, V. S.; Bencsik, M.; Lloyd, J. R.; Telling, N. D. Bacterially Synthesized Ferrite Nanoparticles for Magnetic Hyperthermia Applications. *Nanoscale* **2014**, *6*, 12958–12970.
- (71) Verwey, E. Electronic Conduction of Magnetite (Fe_3O_4) and Its Transition Point at Low Temperatures. *Nature* **1939**, *144*, 327–328.
- (72) Kąkol, Z.; Sabol, J.; Stickler, J.; Honig, J. Effect of Low-Level Titanium (IV) Doping on the Resistivity of Magnetite near the Verwey Transition. *Phys. Rev. B: Condens. Matter Mater. Phys.* **1992**, *46*, 1975.
- (73) Kozłowski, A.; Metcalf, P.; Kąkol, Z.; Honig, J. M. Electrical Transport and Magnetization Measurements of $\text{Fe}_{3-z}\text{Al}_z\text{O}_4$, $z < 0.06$. *J. Magn. Magn. Mater.* **1996**, *157–158*, 415–416.
- (74) Özdemir, Ö.; Dunlop, D. J. Hallmarks of Maghemitization in Low-Temperature Remanence Cycling of Partially Oxidized Magnetite Nanoparticles. *J. Geophys. Res.* **2010**, *115*, 10.1029/2009JB006756.
- (75) Lee, J.; Kwon, S. G.; Park, J.-G.; Hyeon, T. Size Dependence of Metal–Insulator Transition in Stoichiometric Fe_3O_4 Nanocrystals. *Nano Lett.* **2015**, *15*, 4337–4342.
- (76) Goya, G.; Berquó, T. S.; Fonseca, F. C.; Morales, M. Static and Dynamic Magnetic Properties of Spherical Magnetite Nanoparticles. *J. Appl. Phys.* **2003**, *94*, 3520–3528.
- (77) Harrison, R. J.; Feinberg, J. M. Mineral Magnetism: Providing New Insights into Geoscience Processes. *Elements* **2009**, *5*, 209–215.
- (78) Beverskog, B.; Puigdomenech, I. Revised Pourbaix Diagrams for Iron at 25–300 °C. *Corros. Sci.* **1996**, *38*, 2121–2135.
- (79) Ayala-Luis, K. B.; Koch, C. B.; Hansen, H. C. B. The Standard Gibbs Energy of Formation of Fe(II)Fe(III) Hydroxide Sulfate Green Rust. *Clays Clay Miner.* **2008**, *56*, 633–644.
- (80) Refait, P.; Géhin, A.; Abdelmoula, M.; Génin, J. M. R. Coprecipitation Thermodynamics of iron(II-III) Hydroxysulphate Green Rust from Fe(II) and Fe(III) Salts. *Corros. Sci.* **2003**, *45*, 659–676.
- (81) Ruby, C.; Géhin, A.; Abdelmoula, M.; Génin, J.-M. R.; Jolivet, J.-P. Coprecipitation of Fe(II) and Fe(III) Cations in Sulphated Aqueous Medium and Formation of Hydroxysulphate Green Rust. *Solid State Sci.* **2003**, *5*, 1055–1062.
- (82) McGill, I. R.; McEnaney, B.; Smith, D. C. Crystal Structure of Green Rust Formed by Corrosion of Cast Iron. *Nature* **1976**, *259*, 200–201.
- (83) Bearcock, J.; Perkins, W.; Dinelli, E.; Wade, S. Fe (II)/Fe (III) ‘Green Rust’ Developed within Ochreous Coal Mine Drainage Sediment in South Wales, UK. *Mineral. Mag.* **2006**, *70*, 731–741.
- (84) Taylor, R. The Rapid Formation of Crystalline Double Hydroxy Salts and Other Compounds by Controlled Hydrolysis. *Clay Miner.* **1984**, *19*, 591–603.
- (85) Trolard, F.; Génin, J. M. R.; Abdelmoula, M.; Bourrié, G.; Humbert, B.; Herbillon, A. Identification of a Green Rust Mineral in a Reductomorphic Soil by Mossbauer and Raman Spectroscopies. *Geochim. Cosmochim. Acta* **1997**, *61*, 1107–1111.
- (86) Trolard, F.; Bourrié, G.; Abdelmoula, M.; Refait, P.; Feder, F. Fougerite, a New Mineral of the Pyroaurite-Iowaite Group: Description and Crystal Structure. *Clays Clay Miner.* **2007**, *55*, 323–334.
- (87) Feder, F.; Trolard, F.; Klingelhöfer, G.; Bourrié, G. In Situ Mössbauer Spectroscopy: Evidence for Green Rust (Fougerite) in a Gleysol and Its Mineralogical Transformations with Time and Depth. *Geochim. Cosmochim. Acta* **2005**, *69*, 4463–4483.
- (88) Christiansen, B. C.; Balic-Zunic, T.; Dideriksen, K.; Stipp, S. L. S. Identification of Green Rust in Groundwater. *Environ. Sci. Technol.* **2009**, *43*, 3436–3441.
- (89) Zegeye, A.; Bonneville, S.; Benning, L. G.; Sturm, A.; Fowle, D. A.; Jones, C.; Canfield, D. E.; Ruby, C.; MacLean, L. C.; Nomosatroy, S.; et al. Green Rust Formation Controls Nutrient Availability in a Ferruginous Water Column. *Geology* **2012**, *40*, 599–602.
- (90) Rennert, T.; Eusterhues, K.; De Andrade, V.; Totsche, K. U. Iron Species in Soils on a Mofette Site Studied by Fe K-Edge X-Ray Absorption near-Edge Spectroscopy. *Chem. Geol.* **2012**, *332–333*, 116–123.
- (91) Johnson, C. A.; Freyer, G.; Fabisch, M.; Caraballo, M. A.; Küsel, K.; Hochella, M. F. Observations and Assessment of Iron Oxide and Green Rust Nanoparticles in Metal-Polluted Mine Drainage within a Steep Redox Gradient. *Environ. Chem.* **2014**, *11*, 377–391.
- (92) Weatherington-Rice, J.; Bigham, J. M. Buried Pre-Illinoian-Age Lacustrine Deposits with “Green Rust” Colors in Clermont County, Ohio I. *Ohio J. Sci.* **2006**, *106*, 35–44.
- (93) Root, R. A.; Dixit, S.; Campbell, K. M.; Jew, A. D.; Hering, J. G.; O’Day, P. A. Arsenic Sequestration by Sorption Processes in High-Iron Sediments. *Geochim. Cosmochim. Acta* **2007**, *71*, 5782–5803.
- (94) Latta, D. E.; Boyanov, M. I.; Kemner, K. M.; O’Loughlin, E. J.; Scherer, M. M. Abiotic reduction of uranium by Fe(II) in soil. *Appl. Geochem.* **2012**, *27*, 1512–1524.
- (95) Miyata, S. Anion-Exchange Properties of Hydrocalcite-Like Compounds. *Clays Clay Miner.* **1983**, *31*, 305–311.
- (96) Génin, J.-M. R.; Olowe, A. A.; Benbouzid-Rollet, N.; Prieur, D.; Confente, M.; Resiak, B. The Simultaneous Presence of Green Rust 2 and Sulfate Reducing Bacteria in the Corrosion of Steel Sheet Piles in a Harbour Area. *Hyperfine Interact.* **1992**, *69*, 875–878.
- (97) Sphar, J. Occurrence of Magnetite in the Arkansas River Bed Between Ford and Arkansas City. *Trans. Kans. Acad. Sci.* **1962**, *65*, 257–262.
- (98) Maher, B. A. Characterisation of Soils by Mineral Magnetic Measurements. *Phys. Earth Planet. Inter.* **1986**, *42*, 76–92.
- (99) Maher, B. A.; Taylor, R. M. Formation of Ultrafine-Grained Magnetite in Soils. *Nature* **1988**, *336*, 368–370.
- (100) Auerswald, K.; Friedl, J.; Litaor, I.; H. S. Iron Oxide Mineralogy of a Semi-Arid Wetland. *Mitt. Deutsche Bodenkdl. Ges.* **2001**, *96*, 677–678.
- (101) Fassbinder, J. W. E.; Stanjekt, H.; Vali, H. Occurrence of Magnetic Bacteria in Soil. *Nature* **1990**, *343*, 161–163.
- (102) Maher, B. A.; Thompson, R. Mineral Magnetic Record of the Chinese Loess and Paleosols. *Geology* **1991**, *19*, 3–6.
- (103) de Jesus Filho, F. M.; Fabris, J. D.; Goulart, A. T.; Coey, J. M. D.; Ferreira, B. A.; Pinto, M. C. F. Ilmenite and Magnetite of a Tholeiitic Basalt. *Clays Clay Miner.* **1995**, *43*, 641–642.
- (104) Ramasamy, R.; Gwalani, L. G.; Subramanian, S. P. A Note on the Occurrence and Formation of Magnetite in the Carbonatites of Sevvattur, North Arcot District, Tamil Nadu, Southern India. *J. Asian Earth Sci.* **2001**, *19*, 297–304.
- (105) Viana, J. H. M.; Couceiro, P. R. C.; Pereira, M. C.; Fabris, J. D.; Fernandes Filho, E. I.; Schaefer, C. E. G. R.; Rechenberg, H. R.; Abrahão, W. A. P.; Mantovani, E. C. Occurrence of Magnetite in the Sand Fraction of an Oxisol in the Brazilian Savanna Ecosystem, Developed from a Magnetite-Free Lithology. *Aust. J. Soil Res.* **2006**, *44*, 71–83.
- (106) Jordanova, D.; Goddu, S. R.; Kotsev, T.; Jordanova, N. Industrial Contamination of Alluvial Soils near Fe–Pb Mining Site Revealed by Magnetic and Geochemical Studies. *Geoderma* **2013**, *192*, 237–248.
- (107) Ananthapadmanabha, A. L.; Shankar, R.; Sandeep, K. Rock Magnetic Properties of Lateritic Soil Profiles from Southern India: Evidence for Pedogenic Processes. *J. Appl. Geophys.* **2014**, *111*, 203–210.
- (108) Kissel, C.; Liu, Z.; Li, J.; Wandres, C. Magnetic Minerals in Three Asian Rivers Draining into the South China Sea: Pearl, Red, and Mekong Rivers. *Geochim., Geophys., Geosyst.* **2016**, *17*, 1678–1693.
- (109) Rijal, M. L.; Porsch, K.; Appel, E.; Kappler, A. Magnetic Signature of Hydrocarbon-Contaminated Soils and Sediments at the Former Oil Field Hänigsen, Germany. *Stud. Geophys. Geod.* **2012**, *56*, 889–908.
- (110) Ameen, N. N.; Klueglein, N.; Appel, E.; Petrovský, E.; Kappler, A.; Leven, C. Effect of Hydrocarbon-Contaminated Fluctuating

Groundwater on Magnetic Properties of Shallow Sediments. *Stud. Geophys. Geod.* **2014**, *58*, 442–460.

(111) Li, Y.-L.; Konhauser, K. O.; Zhai, M. The Formation of Magnetite in the Early Archean Oceans. *Earth Planet. Sci. Lett.* **2017**, *466*, 103–114.

(112) Churchman, G. J.; Lowe, D. J. *Alteration, Formation, and Occurrence of Minerals in Soils*; CRC Press, 2012.

(113) Oldfield, F.; Crowther, J. Establishing Fire Incidence in Temperate Soils Using Magnetic Measurements. *Palaeogeogr., Palaeoclimatol., Palaeoecol.* **2007**, *249*, 362–369.

(114) Geiss, C. E.; Egli, R.; Zanner, C. W. Direct Estimates of Pedogenic Magnetite as a Tool to Reconstruct Past Climates from Buried Soils. *J. Geophys. Res.* **2008**, *113*, 10.1029/2008JB005669.

(115) Salazar-Camacho, C.; Villalobos, M.; Rivas-Sánchez, M. d. I. L.; Arenas-Alatorre, J.; Alcaraz-Cienfuegos, J.; Gutiérrez-Ruiz, M. E. Characterization and Surface Reactivity of Natural and Synthetic Magnetites. *Chem. Geol.* **2013**, *347*, 233–245.

(116) Giménez, J.; Martínez, M.; de Pablo, J.; Rovira, M.; Duro, L. Arsenic Sorption onto Natural Hematite, Magnetite, and Goethite. *J. Hazard. Mater.* **2007**, *141*, 575–580.

(117) Marmier, N.; Delisée, A.; Fromage, F. Surface Complexation Modeling of Yb(III), Ni(II), and Cs(I) Sorption on Magnetite. *J. Colloid Interface Sci.* **1999**, *211*, 54–60.

(118) Marmier, N.; Fromage, F. Sorption of Cs(I) on Magnetite in the Presence of Silicates. *J. Colloid Interface Sci.* **2000**, *223*, 83–88.

(119) Villacís-García, M.; Villalobos, M.; Gutiérrez-Ruiz, M. Optimizing the Use of Natural and Synthetic Magnetites with Very Small Amounts of Coarse Fe(0) Particles for Reduction of Aqueous Cr(VI). *J. Hazard. Mater.* **2015**, *281*, 77–86.

(120) He, H.; Zhong, Y.; Liang, X.; Tan, W.; Zhu, J.; Yan Wang, C. Natural Magnetite: An Efficient Catalyst for the Degradation of Organic Contaminant. *Sci. Rep.* **2015**, *5*, 10139.

(121) Stampfl, P. P. Ein Basisches Eisen-II-III-Karbonat in Rost. *Corros. Sci.* **1969**, *9*, 185–187.

(122) Boucherit, N.; Hugot-Le Goff, A.; Joiret, S. Raman Studies of Corrosion Films Grown on Fe and Fe-6Mo in Pitting Conditions. *Corros. Sci.* **1991**, *32*, 497–507.

(123) Abdelmoula, M.; Refait, P.; Drissi, S. H.; Mihe, J. P.; Génin, J. M. R. Conversion Electron Mössbauer Spectroscopy and X-Ray Diffraction Studies of the Formation of Carbonate-Containing Green Rust One by Corrosion of Metallic Iron in NaHCO₃ and (NaHCO₃ + NaCl) Solutions. *Corros. Sci.* **1996**, *38*, 623–633.

(124) Simard, S.; Odziemkowski, M.; Irish, D. E.; Brossard, L.; Ménard, H. In Situ Micro-Raman Spectroscopy to Investigate Pitting Corrosion Product of 1024 Mild Steel in Phosphate and Bicarbonate Solutions Containing Chloride and Sulfate Ions. *J. Appl. Electrochem.* **2001**, *31*, 913–920.

(125) Refait, P.; Memet, J. B.; Bon, C.; Sabot, R.; Génin, J. M. R. Formation of the Fe(II)-Fe(III) Hydroxysulphate Green Rust During Marine Corrosion of Steel. *Corros. Sci.* **2003**, *45*, 833–845.

(126) Pineau, S.; Sabot, R.; Quillet, L.; Jeannin, M.; Caplat, C.; Dupont-Morrall, I.; Refait, P. Formation of the Fe(II–III) Hydroxysulphate Green Rust During Marine Corrosion of Steel Associated to Molecular Detection of Dissimilatory Sulphite-Reductase. *Corros. Sci.* **2008**, *50*, 1099–1111.

(127) Neff, D.; Dillmann, P.; Bellot-Gurlet, L.; Beranger, G. Corrosion of Iron Archaeological Artefacts in Soil: Characterisation of the Corrosion System. *Corros. Sci.* **2005**, *47*, 515–535.

(128) Colomban, P.; Cherifi, S.; Despert, G. Raman Identification of Corrosion Products on Automotive Galvanized Steel Sheets. *J. Raman Spectrosc.* **2008**, *39*, 881–886.

(129) Roh, Y.; Lee, S. Y.; Elles, M. P. Characterization of Corrosion Products in the Permeable Reactive Barriers. *Environ. Geol.* **2000**, *40*, 184–194.

(130) Huang, Y. H.; Zhang, T. C. Effects of Dissolved Oxygen on Formation of Corrosion Products and Concomitant Oxygen and Nitrate Reduction in Zero-Valent Iron Systems with or without Aqueous Fe²⁺. *Water Res.* **2005**, *39*, 1751–1760.

(131) Massart, R. Préparation de Ferrofluides Aqueux en l'Absence de Surfactant; Comportement en Fonction du pH et de la Nature des Ions Présents en Solution. *CR Acad. Sci. Paris C* **1980**, *1*, t291.

(132) Tamura, H.; Kawamura, S.; Hagayama, M. Acceleration of the Oxidation of Fe²⁺ Ions by Fe(III)-Oxyhydroxides. *Corros. Sci.* **1980**, *20*, 963–971.

(133) Hansen, H. C. B.; Guldborg, S.; Erbs, M.; Bender Koch, C. Kinetics of Nitrate Reduction by Green Rusts—Effects of Interlayer Anion and Fe(II):Fe(III) Ratio. *Appl. Clay Sci.* **2001**, *18*, 81–91.

(134) Vayssières, L.; Chanéac, C.; Tronc, E.; Jolivet, J. P. Size Tailoring of Magnetite Particles Formed by Aqueous Precipitation: An Example of Thermodynamic Stability of Nanometric Oxide Particles. *J. Colloid Interface Sci.* **1998**, *205*, 205–212.

(135) Stumm, W.; Lee, G. F. Oxygenation of Ferrous Iron. *Ind. Eng. Chem.* **1961**, *53*, 143–146.

(136) Davison, W.; Seed, G. The Kinetics of the Oxidation of Ferrous Iron in Synthetic and Natural Waters. *Geochim. Cosmochim. Acta* **1983**, *47*, 67–79.

(137) Millero, F. J.; Sotolongo, S.; Izaguirre, M. The Oxidation Kinetics of Fe(II) in Seawater. *Geochim. Cosmochim. Acta* **1987**, *51*, 793–801.

(138) Morgan, B.; Lahav, O. The effect of pH on the Kinetics of Spontaneous Fe(II) Oxidation by O₂ in Aqueous Solution – Basic Principles and a Simple Heuristic Description. *Chemosphere* **2007**, *68*, 2080–2084.

(139) Feitknecht, v. W.; Keller, G. Über die Dunkelgrünen Hydroxyverbindungen des Eisens. *Z. Anorg. Chem.* **1950**, *262*, 61–68.

(140) Refait, P.; Génin, J. M. R. The oxidation of Ferrous Hydroxide in Chloride-Containing Aqueous Media and Pourbaix Diagrams of Green Rust One. *Corros. Sci.* **1993**, *34*, 797–819.

(141) Detournay, J.; De Miranda, L.; Derie, R.; Ghodsi, M. The Region of Stability of Green Rust II in the Electrochemical Potential-pH Equilibrium Diagram of Iron in Sulphate Medium. *Corros. Sci.* **1975**, *15*, 295–306.

(142) Génin, J. M. R.; Olowe, A. A.; Refait, P.; Simon, L. On the Stoichiometry and Pourbaix Diagram of Fe(II)-Fe(III) Hydroxy-Sulphate or Sulphate-Containing Green Rust 2: An Electrochemical and Mössbauer Spectroscopy Study. *Corros. Sci.* **1996**, *38*, 1751–1762.

(143) Ruby, C.; Upadhyay, C.; Génin, A.; Ona-Nguema, G.; Génin, J.-M. R. In Situ Redox Flexibility of Fe^{II-III} Oxyhydroxycarbonate Green Rust and Fougerite. *Environ. Sci. Technol.* **2006**, *40*, 4696–4702.

(144) Sada, E.; Kumazawa, H.; Cho, H. M. Formation of Fine Magnetite Particles by Oxidation of Aqueous Suspensions of Ferrous Hydroxide. *Can. J. Chem. Eng.* **1990**, *68*, 622–626.

(145) Olowe, A.; Pauron, B.; Génin, J. The Influence of Temperature on the Oxidation of Ferrous Hydroxide in Sulphated Aqueous Medium: Activation Energies of Formation of the Products and Hyperfine Structure of Magnetite. *Corros. Sci.* **1991**, *32*, 985–1001.

(146) Domingo, C.; Rodriguez-Clemente, R.; Blesa, M. Kinetics of Oxidative Precipitation of Iron Oxide Particles. *Colloids Surf., A* **1993**, *79*, 177–189.

(147) Sugimoto, T.; Matijević, E. Formation of Uniform Spherical Magnetite Particles by Crystallization from Ferrous Hydroxide Gels. *J. Colloid Interface Sci.* **1980**, *74*, 227–243.

(148) Mürbe, J.; Rechtenbach, A.; Töpfer, J. Synthesis and Physical Characterization of Magnetite Nanoparticles for Biomedical Applications. *Mater. Chem. Phys.* **2008**, *110*, 426–433.

(149) Vereda, F.; De Vicente, J.; Hidalgo-Alvarez, R. Oxidation of Ferrous Hydroxides with Nitrate: A Versatile Method for the Preparation of Magnetic Colloidal Particles. *J. Colloid Interface Sci.* **2013**, *392*, 50–56.

(150) Legrand, L.; Savoye, S.; Chausse, A.; Messina, R. Study of Oxidation Products Formed on Iron in Solutions Containing Bicarbonate/Carbonate. *Electrochim. Acta* **2000**, *46*, 111–117.

(151) Refait, P.; Nguyen, D.; Jeannin, M.; Sable, S.; Langumier, M.; Sabot, R. Electrochemical Formation of Green Rusts in Deaerated Seawater-Like Solutions. *Electrochim. Acta* **2011**, *56*, 6481–6488.

(152) Antony, H.; Labrit, A.; Rouchaud, J.; Legrand, L.; Chaussé, A. Study of Fe^{II}/Fe^{III} Ratio in Thin Films of Carbonate or Sulphate

Green Rusts Obtained by Potentiostatic Electrosynthesis. *Electrochim. Acta* **2008**, *53*, 7173–7181.

(153) Legrand, L.; Abdelmoula, M.; Géhin, A.; Chaussé, A.; Génin, J. M. R. Electrochemical Formation of a New Fe(II)-Fe(III) Hydroxy-Carbonate Green Rust: Characterization and Morphology. *Electrochim. Acta* **2001**, *46*, 1815–1822.

(154) Génin, J. M. R.; Mills, S. J.; Christy, A. G.; Guérin; Herbillon, A. J.; Kuzmann, E.; Ona-Nguema, G.; Ruby, C.; Upadhyay, C. Mössbauerite, $\text{Fe}^{3+}_6\text{O}_4(\text{OH})_8[\text{CO}_3]_3\cdot 3\text{H}_2\text{O}$, the Fully Oxidized 'Green Rust' Mineral from Mont Saint-Michel Bay, France. *Mineral. Mag.* **2014**, *78*, 447–465.

(155) Franger, S.; Berthet, P.; Berthon, J. Electrochemical Synthesis of Fe_3O_4 Nanoparticles in Alkaline Aqueous Solutions Containing Complexing Agents. *J. Solid State Electrochem.* **2004**, *8*, 218–223.

(156) Cabrera, L.; Gutierrez, S.; Menendez, N.; Morales, M.; Herrasti, P. Magnetite Nanoparticles: Electrochemical Synthesis and Characterization. *Electrochim. Acta* **2008**, *53*, 3436–3441.

(157) Fajaroh, F.; Setyawan, H.; Widiyastuti, W.; Winardi, S. Synthesis of Magnetite Nanoparticles by Surfactant-Free Electrochemical Method in an Aqueous System. *Adv. Powder Technol.* **2012**, *23*, 328–333.

(158) Jeen, S.-W.; Jambor, J. L.; Blowes, D. W.; Gillham, R. W. Precipitates on Granular Iron in Solutions Containing Calcium Carbonate with Trichloroethene and Hexavalent Chromium. *Environ. Sci. Technol.* **2007**, *41*, 1989–1994.

(159) Liu, H.; Guo, H.; Li, P.; Wei, Y. The Transformation of Ferrihydrite in the Presence of Trace Fe(II): The Effect of the Anionic Media. *J. Solid State Chem.* **2008**, *181*, 2666–2671.

(160) Pedersen, H. D.; Postma, D.; Jakobsen, R.; Larsen, O. Fast transformation of iron oxyhydroxides by the catalytic action of aqueous Fe(II). *Geochim. Cosmochim. Acta* **2005**, *69*, 3967–3977.

(161) Jeon, B.-H.; Dempsey, B. A.; Burgos, W. D. Kinetics and Mechanisms for Reactions of Fe(II) with Iron(III) Oxides. *Environ. Sci. Technol.* **2003**, *37*, 3309–3315.

(162) Yee, N.; Shaw, S.; Benning, L. G.; Nguyen, T. H. The Rate of Ferrihydrite Transformation to Goethite via the Fe(II) Pathway. *Am. Mineral.* **2006**, *91*, 92–96.

(163) Liu, H.; Li, P.; Lu, B.; Wei, Y.; Sun, Y. Transformation of Ferrihydrite in the Presence or Absence of Trace Fe(II): The Effect of Preparation Procedures of Ferrihydrite. *J. Solid State Chem.* **2009**, *182*, 1767–1771.

(164) Tamaura, Y.; Ito, K.; Katsura, T. Transformation of γ - $\text{FeO}(\text{OH})$ to Fe_3O_4 by Adsorption of Iron(II) Ion on γ - $\text{FeO}(\text{OH})$. *J. Chem. Soc., Dalton Trans.* **1983**, 189–194.

(165) Ishikawa, T.; Kondo, Y.; Yasukawa, A.; Kandori, K. Formation of Magnetite in the Presence of Ferric Oxyhydroxides. *Corros. Sci.* **1998**, *40*, 1239–1251.

(166) Kahani, S. A.; Jafari, M. A New Method for Preparation of Magnetite from Iron Oxyhydroxide or Iron Oxide and Ferrous Salt in Aqueous Solution. *J. Magn. Magn. Mater.* **2009**, *321*, 1951–1954.

(167) Mann, S.; Sparks, N. H. C.; Couling, S. B.; Larcombe, M. C.; Frankel, R. B. Crystallochemical Characterization of Magnetic Spinel Prepared from Aqueous Solution. *J. Chem. Soc., Faraday Trans. 1* **1989**, *85*, 3033–3044.

(168) Usman, M.; Abdelmoula, M.; Faure, P.; Ruby, C.; Hanna, K. Transformation of Various Kinds of Goethite into Magnetite: Effect of Chemical and Surface Properties. *Geoderma* **2013**, *197–198*, 9–16.

(169) Yang, L.; Steefel, C. I.; Marcus, M. A.; Bargar, J. R. Kinetics of Fe(II)-Catalyzed Transformation of 6-line Ferrihydrite under Anaerobic Flow Conditions. *Environ. Sci. Technol.* **2010**, *44*, 5469–5475.

(170) Larese-Casanova, P.; Scherer, M. M. Abiotic Transformation of Hexahydro-1,3,5-Trinitro-1,3,5-Triazine (RDX) by Green Rusts. *Environ. Sci. Technol.* **2008**, *42*, 3975–3981.

(171) Tamaura, Y. Ferrite Formation from the Intermediate, Green Rust II, in the Transformation Reaction of Ferric Hydroxide Oxide, γ - $\text{FeO}(\text{OH})$, in Aqueous Suspension. *Inorg. Chem.* **1985**, *24*, 4363–4366.

(172) Hansel, C. M.; Benner, S. G.; Neiss, J.; Dohnalkova, A.; Kukkadapu, R. K.; Fendorf, S. Secondary Mineralization Pathways Induced by Dissimilatory Iron Reduction of Ferrihydrite under Advective Flow. *Geochim. Cosmochim. Acta* **2003**, *67*, 2977–2992.

(173) Hansel, C. M.; Benner, S. G.; Fendorf, S. Competing Fe(II)-Induced Mineralization Pathways of Ferrihydrite. *Environ. Sci. Technol.* **2005**, *39*, 7147–7153.

(174) Fredrickson, J. K.; Zachara, J. M.; Kennedy, D. W.; Dong, H.; Onstott, T. C.; Hinman, N. W.; Li, S.-m. Biogenic Iron Mineralization Accompanying the Dissimilatory Reduction of Hydrous Ferric Oxide by a Groundwater Bacterium. *Geochim. Cosmochim. Acta* **1998**, *62*, 3239–3257.

(175) Belleville, P.; Jolivet, J.-P.; Tronc, E.; Livage, J. Crystallization of Ferric Hydroxide into Spinel by Adsorption on Colloidal Magnetite. *J. Colloid Interface Sci.* **1992**, *150*, 453–460.

(176) Handler, R. M.; Beard, B. L.; Johnson, C. M.; Scherer, M. M. Atom Exchange between Aqueous Fe(II) and Goethite: An Fe Isotope Tracer Study. *Environ. Sci. Technol.* **2009**, *43*, 1102–1107.

(177) Williams, A. G. B.; Scherer, M. M. Spectroscopic Evidence for Fe(II)-Fe(III) Electron Transfer at the Iron Oxide-Water Interface. *Environ. Sci. Technol.* **2004**, *38*, 4782–4790.

(178) Frierdich, A. J.; Helgeson, M.; Liu, C.; Wang, C.; Rosso, K. M.; Scherer, M. M. Iron Atom Exchange between Hematite and Aqueous Fe(II). *Environ. Sci. Technol.* **2015**, *49*, 8479–8486.

(179) Handler, R. M.; Frierdich, A. J.; Johnson, C. M.; Rosso, K. M.; Beard, B. L.; Wang, C.; Latta, D. E.; Neumann, A.; Pasakarnis, T.; Premaratne, W. A. P. J.; et al. Fe(II)-Catalyzed Recrystallization of Goethite Revisited. *Environ. Sci. Technol.* **2014**, *48*, 11302–11311.

(180) Piepenbrock, A.; Dippon, U.; Porsch, K.; Appel, E.; Kappler, A. Dependence of Microbial Magnetite Formation on Humic Substance and Ferrihydrite Concentrations. *Geochim. Cosmochim. Acta* **2011**, *75*, 6844–6858.

(181) Barrón, V.; Galvez, N.; Hochella, M. F.; Torrent, J. Epitaxial Overgrowth of Goethite on Hematite Synthesized in Phosphate Media; A Scanning Force and Transmission Electron Microscopy Study. *Am. Mineral.* **1997**, *82*, 1091–1100.

(182) Borch, T.; Masue, Y.; Kukkadapu, R. K.; Fendorf, S. Phosphate Imposed Limitations on Biological Reduction and Alteration of Ferrihydrite. *Environ. Sci. Technol.* **2007**, *41*, 166–172.

(183) Benali, O.; Abdelmoula, M.; Refait, P.; Génin, J.-M. R. Effect of Orthophosphate on the Oxidation Products of Fe(II)-Fe(III) Hydroxycarbonate: The Transformation of Green Rust to Ferrihydrite. *Geochim. Cosmochim. Acta* **2001**, *65*, 1715–1726.

(184) Biber, M. V.; dos Santos Afonso, M.; Stumm, W. The Coordination Chemistry of Weathering: IV. Inhibition of the Dissolution of Oxide Minerals. *Geochim. Cosmochim. Acta* **1994**, *58*, 1999–2010.

(185) Dzombak, D. A.; Morel, F. M. *Surface Complexation Modeling: Hydrous Ferric Oxide*; John Wiley & Sons: New York, 1990.

(186) Rusch, B.; Hanna, K.; Humbert, B. Sorption and Transport of Salicylate in a Porous Heterogeneous Medium of Silica Quartz and Goethite. *Environ. Sci. Technol.* **2010**, *44*, 2447–2453.

(187) Larese-Casanova, P.; Scherer, M. M. Fe(II) sorption on hematite: New insights based on spectroscopic measurements. *Environ. Sci. Technol.* **2007**, *41*, 471–477.

(188) Hiemstra, T.; Van Riemsdijk, W. H. A Surface Structural Approach to Ion Adsorption: The Charge Distribution (CD) Model. *J. Colloid Interface Sci.* **1996**, *179*, 488–508.

(189) Manceau, A.; Nagy, K. L.; Spadini, L.; Ragnarsdottir, K. V. Influence of Anionic Layer Structure of Fe-Oxyhydroxides on the Structure of Cd Surface Complexes. *J. Colloid Interface Sci.* **2000**, *228*, 306–316.

(190) Spadini, L.; Schindler, P. W.; Charlet, L.; Manceau, A.; Vala Ragnarsdottir, K. Hydrous Ferric Oxide: Evaluation of Cd-HFO Surface Complexation Models Combining CdK EXAFS Data, Potentiometric Titration Results, and Surface Site Structures Identified from Mineralogical Knowledge. *J. Colloid Interface Sci.* **2003**, *266*, 1–18.

- (191) Weidler, P. G.; Hug, S. J.; Wetche, T. P.; Hiemstra, T. Determination of Growth Rates of (100) And (110) Faces of Synthetic Goethite by Scanning Force Microscopy. *Geochim. Cosmochim. Acta* **1998**, *62*, 3407–3412.
- (192) Dixit, S.; Hering, J. G. Sorption of Fe(II) and As(III) on Goethite in Single- and Dual-Sorbate Systems. *Chem. Geol.* **2006**, *228*, 6–15.
- (193) Chen, C.; Kukkadapu, R.; Sparks, D. L. Influence of Coprecipitated Organic Matter on Fe²⁺_(aq)-Catalyzed Transformation of Ferrihydrite: Implications for Carbon Dynamics. *Environ. Sci. Technol.* **2015**, *49*, 10927–10936.
- (194) Eusterhues, K.; Wagner, F. E.; Häusler, W.; Hanzlik, M.; Knicker, H.; Totsche, K. U.; Kögel-Knabner, L.; Schwertmann, U. Characterization of Ferrihydrite-Soil Organic Matter Coprecipitates by X-Ray Diffraction and Mössbauer Spectroscopy. *Environ. Sci. Technol.* **2008**, *42*, 7891–7897.
- (195) Chen, C.; Dynes, J. J.; Wang, J.; Sparks, D. L. Probing the Site Occupancies of Co-, Ni-, and Mn-Substituted Biogenic Magnetite Using. *Environ. Sci. Technol.* **2014**, *48*, 13751–13759.
- (196) Shimizu, M.; Zhou, J.; Schröder, C.; Obst, M.; Kappler, A.; Borch, T. Dissimilatory Reduction and Transformation of Ferrihydrite-Humic Acid Coprecipitates. *Environ. Sci. Technol.* **2013**, *47*, 13375–13384.
- (197) Posth, N. R.; Canfield, D. E.; Kappler, A. Biogenic Fe(III) Minerals: From Formation to Diagenesis and Preservation in the Rock Record. *Earth-Sci. Rev.* **2014**, *135*, 103–121.
- (198) Stumm, W.; Sulzberger, B. The Cycling of Iron in Natural Environments: Considerations Based on Laboratory Studies of Heterogeneous Redox Processes. *Geochim. Cosmochim. Acta* **1992**, *56*, 3233–3257.
- (199) Boumaiza, H.; Naille, S.; Renard, A.; Grégoire, B.; Mallet, M.; Ruby, C. Chemical Transformation of Ferrihydrite Coating into Green Rust Followed by Raman and X-Ray Photoelectron Spectroscopies. *Desalin. Water Treat.* **2015**, *53*, 1031–1036.
- (200) Usman, M.; Faure, P.; Hanna, K.; Abdelmoula, M.; Ruby, C. Application of Magnetite Catalyzed Chemical Oxidation (Fenton-Like and Persulfate) for the Remediation of Oil Hydrocarbon Contamination. *Fuel* **2012**, *96*, 270–276.
- (201) Jones, A. M.; Collins, R. N.; Rose, J.; Waite, T. D. The Effect of Silica and Natural Organic Matter on the Fe(II)-Catalyzed Transformation and Reactivity of Fe(III) Minerals. *Geochim. Cosmochim. Acta* **2009**, *73*, 4409–4422.
- (202) Poulton, S. W.; Canfield, D. E. Ferruginous Conditions: A Dominant Feature of the Ocean through Earth's History. *Elements* **2011**, *7*, 107–112.
- (203) Raiswell, R.; Canfield, D. E. The Iron Biogeochemical Cycle Past and Present. *Geochem. Perspect.* **2012**, *1*, 1–220.
- (204) Klein, C. Some Precambrian Banded Iron-Formations (BIFs) from around the World: Their Age, Geologic Setting, Mineralogy, Metamorphism, Geochemistry, and Origins. *Am. Mineral.* **2005**, *90*, 1473–1499.
- (205) Konhauser, K. O. Bacterial Iron Biomineralisation in Nature. *FEMS Microbiol. Rev.* **1997**, *20*, 315–326.
- (206) Caccavo, F.; Lonergan, D. J.; Lovley, D. R.; Davis, M.; Stolz, J. F.; McInerney, M. J. *Geobacter sulfurreducens* sp. nov., A Hydrogen- and Acetate-Oxidizing Dissimilatory Metal-Reducing Microorganism. *Appl. Environ. Microbiol.* **1994**, *60*, 3752–3759.
- (207) Lovley, D. R.; Phillips, E. J. P. Novel Mode of Microbial Energy-Metabolism - Organic-Carbon Oxidation Coupled to Dissimilatory Reduction of Iron or Manganese. *Appl. Environ. Microbiol.* **1988**, *54*, 1472–1480.
- (208) Lovley, D. R.; Phillips, E. J. P.; Lonergan, D. J. Hydrogen and Formate Oxidation Coupled to Dissimilatory Reduction of Iron or Manganese by *Alteromonas putrefaciens*. *Appl. Environ. Microbiol.* **1989**, *55*, 700–706.
- (209) MYERS, C. R.; NEALSON, K. H. Bacterial Manganese Reduction and Growth with Manganese Oxide as the Sole Electron Acceptor. *Science* **1988**, *240*, 1319–1321.
- (210) Obuekwe, C. O.; Westlake, D. W. S.; Cook, F. D. Effect of Nitrate on Reduction of Ferric Iron by a Bacterium Isolated from Crude Oil. *Can. J. Microbiol.* **1981**, *27*, 692–697.
- (211) Roden, E. E.; Lovley, D. R. Dissimilatory Fe(III) Reduction by the Marine Microorganism *Desulfuromonas acetoxidans*. *Appl. Environ. Microbiol.* **1993**, *59*, 734–742.
- (212) Coates, J. D.; Ellis, D. J.; Gaw, C. V.; Lovley, D. R. *Geothrix fermentans* gen. nov., sp. nov., A Novel Fe(III)-Reducing Bacterium from a Hydrocarbon-Contaminated Aquifer. *Int. J. Syst. Bacteriol.* **1999**, *49*, 1615–1622.
- (213) Lovley, D. R.; Baedeker, M. J.; Lonergan, D. J.; Cozzarelli, I. M.; Phillips, E. J. P.; Siegel, D. I. Oxidation of Aromatic Contaminants Coupled to Microbial Iron Reduction. *Nature* **1989**, *339*, 297–300.
- (214) Lovley, D. R.; Lonergan, D. J. Anaerobic Oxidation of Toluene, Phenol, and p-Cresol by the Dissimilatory Iron-Reducing Organism, GS-15. *Appl. Environ. Microbiol.* **1990**, *56*, 1858–1864.
- (215) Nixon, S. L.; Cockell, C. S.; Tranter, M. Limitations to a Microbial Iron Cycle on Mars. *Planet. Space Sci.* **2012**, *72*, 116–128.
- (216) Qu, B.; Fan, B.; Zhu, S.; Zheng, Y. Anaerobic Ammonium Oxidation with an Anode as the Electron Acceptor. *Environ. Microbiol. Rep.* **2014**, *6*, 100–105.
- (217) Shrestha, J.; Rich, J. J.; Ehrenfeld, J. G.; Jaffe, P. R. Oxidation of Ammonium to Nitrite Under Iron-Reducing Conditions in Wetland Soils: Laboratory, Field Demonstrations, and Push-Pull Rate Determination. *Soil Sci.* **2009**, *174*, 156–164.
- (218) Yang, W. H.; Weber, K. A.; Silver, W. L. Nitrogen Loss from Soil through Anaerobic Ammonium Oxidation Coupled to Iron Reduction. *Nat. Geosci.* **2012**, *5*, 538–541.
- (219) Beal, E. J.; House, C. H.; Orphan, V. J. Manganese- and Iron-Dependent Marine Methane Oxidation. *Science* **2009**, *325*, 184–187.
- (220) Riedinger, N.; Formolo, M. J.; Lyons, T. W.; Henkel, S.; Beck, A.; Kasten, S. An Inorganic Geochemical Argument for Coupled Anaerobic Oxidation of Methane and Iron Reduction in Marine Sediments. *Geobiology* **2014**, *12*, 172–181.
- (221) Segarra, K. E. A.; Comerford, C.; Slaughter, J.; Joye, S. B. Impact of Electron Acceptor Availability on the Anaerobic Oxidation of Methane in Coastal Freshwater and Brackish Wetland Sediments. *Geochim. Cosmochim. Acta* **2013**, *115*, 15–30.
- (222) Lovley, D. R.; Woodward, J. C. Mechanisms for Chelator Stimulation of Microbial Fe(III)-Oxide Reduction. *Chem. Geol.* **1996**, *132*, 19–24.
- (223) Roden, E. E. Fe(III) Oxide Reactivity Toward Biological versus Chemical Reduction. *Environ. Sci. Technol.* **2003**, *37*, 1319–1324.
- (224) Roden, E. E. Geochemical and Microbiological Controls on Dissimilatory Iron Reduction. *C. R. Geosci.* **2006**, *338*, 456–467.
- (225) Roden, E. E.; Zachara, J. M. Microbial Reduction of Crystalline Iron(III) Oxides: Influence of Oxide Surface Area and Potential for Cell Growth. *Environ. Sci. Technol.* **1996**, *30*, 1618–1628.
- (226) Cutting, R. S.; Coker, V. S.; Fellowes, J. W.; Lloyd, J. R.; Vaughan, D. J. Mineralogical and Morphological Constraints on the Reduction of Fe(III) Minerals by *Geobacter sulfurreducens*. *Geochim. Cosmochim. Acta* **2009**, *73*, 4004–4022.
- (227) Brown, D. A.; Sherriff, B. L.; Sawicki, J. A. Microbial Transformation of Magnetite to Hematite. *Geochim. Cosmochim. Acta* **1997**, *61*, 3341–3348.
- (228) Kostka, J. E.; Dalton, D. D.; Skelton, H.; Dollhopf, S.; Stucki, J. W. Growth of Iron(III)-Reducing Bacteria on Clay Minerals as the Sole Electron Acceptor and Comparison of Growth Yields on a Variety of Oxidized Iron Forms. *Appl. Environ. Microbiol.* **2002**, *68*, 6256–6262.
- (229) Kostka, J. E.; Nealson, K. H. Dissolution and Reduction of Magnetite by Bacteria. *Environ. Sci. Technol.* **1995**, *29*, 2535–2540.
- (230) Kostka, J. E.; Stucki, J. W.; Nealson, K. H.; Wu, J. Reduction of Structural Fe(III) in Smectite by a Pure Culture of *Shewanella putrefaciens* Strain MR-1. *Clays Clay Miner.* **1996**, *44*, 522–529.
- (231) Porsch, K.; Rijal, M. L.; Borch, T.; Troyer, L. D.; Behrens, S.; Wehland, F.; Appel, E.; Kappler, A. Impact of Organic Carbon and Iron Bioavailability on the Magnetic Susceptibility of Soils. *Geochim. Cosmochim. Acta* **2014**, *128*, 44–57.

- (232) Melton, E. D.; Swanner, E. D.; Behrens, S.; Schmidt, C.; Kappler, A. The Interplay of Microbially Mediated and Abiotic Reactions in the Biogeochemical Fe Cycle. *Nat. Rev. Microbiol.* **2014**, *12*, 797–808.
- (233) Shi, L.; Dong, H.; Reguera, G.; Beyenal, H.; Lu, A.; Liu, J.; Yu, H.-Q.; Fredrickson, J. K. Extracellular Electron Transfer Mechanisms between Microorganisms and Minerals. *Nat. Rev. Microbiol.* **2016**, *14*, 651–662.
- (234) Byrne, J. M.; Telling, N.D.; Coker, V. S.; Patrick, R. A. D.; van der Laan, G.; Arenholz, E.; Tuna, F.; Lloyd, J. R. Control of Nanoparticle Size, Reactivity and Magnetic Properties During the Bioproduction of Magnetite by *Geobacter sulfurreducens*. *Nanotechnology* **2011**, *22*, 455709.
- (235) Dippon, U.; Schmidt, C.; Behrens, S.; Kappler, A. Secondary Mineral Formation During Ferrihydrite Reduction by *Shewanella oneidensis* MR-1 Depends on Incubation Vessel Orientation and Resulting Gradients of Cells, Fe²⁺ and Fe Minerals. *Geomicrobiol. J.* **2015**, *32*, 878–889.
- (236) Sundman, A.; Byrne, J. M.; Bauer, I.; Menguy, N.; Kappler, A. Interactions Between Magnetite and Humic Substances: Redox Reactions and Dissolution Processes. *Geochem. Trans.* **2017**, *18*, 6.
- (237) Klueglein, N.; Lösekann-Behrens, T.; Obst, M.; Behrens, S.; Appel, E.; Kappler, A. Magnetite Formation by the Novel Fe (III)-Reducing *Geothrix fermentans* Strain HradG1 Isolated from a Hydrocarbon-Contaminated Sediment with Increased Magnetic Susceptibility. *Geomicrobiol. J.* **2013**, *30*, 863–873.
- (238) Wu, W.; Li, B.; Hu, J.; Li, J.; Wang, F.; Pan, Y. Iron Reduction and Magnetite Biomineralization Mediated by a Deep-Sea Iron-Reducing Bacterium *Shewanella piezotolerans* WP3. *J. Geophys. Res.* **2011**, *116*, 10.1029/2011JG001728.
- (239) Etique, M.; Jorand, F. P.; Ruby, C. Magnetite as a Precursor for Green Rust through the Hydrogenotrophic Activity of the Iron-Reducing Bacteria *Shewanella putrefaciens*. *Geobiology* **2016**, *14*, 237–254.
- (240) Ona-Nguema, G.; Abdelmoula, M.; Jorand, F.; Benali, O.; Géhin, A.; Block, J. C.; Génin, J. M. R. Microbial Reduction of Lepidocrocite γ -FeOOH by *Shewanella putrefaciens*; The Formation of Green Rust. *Hyperfine Interact.* **2002**, *139-140*, 231–237.
- (241) O'Loughlin, E. J.; Laresse-Casanova, P.; Scherer, M.; Cook, R. Green Rust Formation from the Bioreduction of γ -FeOOH (Lepidocrocite): Comparison of Several *Shewanella* Species. *Geomicrobiol. J.* **2007**, *24*, 211–230.
- (242) Zhang, C.; Vali, H.; Romaneck, C. S.; Phelps, T. J.; Liu, S. V. Formation of Single-Domain Magnetite by a Thermophilic Bacterium. *Am. Mineral.* **1998**, *83*, 1409–1418.
- (243) Konhauser, K. O.; Kappler, A.; Roden, E. E. Iron in Microbial Metabolisms. *Elements* **2011**, *7*, 89–93.
- (244) Emerson, D. Biogeochemistry and Microbiology of Microaerobic Fe(II) Oxidation. *Biochem. Soc. Trans.* **2012**, *40*, 1211–1216.
- (245) Bird, L. J.; Bonnefoy, V.; Newman, D. K. Bioenergetic Challenges of Microbial Iron Metabolisms. *Trends Microbiol.* **2011**, *19*, 330–340.
- (246) Barco, R. A.; Emerson, D.; Sylvan, J. B.; Orcutt, B. N.; Jacobson Meyers, M. E.; Ramirez, G. A.; Zhong, J. D.; Edwards, K. J. New Insight into Microbial Iron Oxidation as Revealed by the Proteomic Profile of an Obligate Iron-Oxidizing Chemolithoautotroph. *Appl. Environ. Microbiol.* **2015**, *81*, S927–S937.
- (247) Gault, A. G.; Langley, S.; Ibrahim, A.; Renaud, R.; Takahashi, Y.; Boothman, C.; Lloyd, J. R.; Clark, I. D.; Ferris, F. G.; Fortin, D. Seasonal Changes in Mineralogy, Geochemistry and Microbial Community of Bacteriogenic Iron Oxides (BIOS) Deposited in a Circumneutral Wetland. *Geomicrobiol. J.* **2012**, *29*, 161–172.
- (248) Chan, C. S.; Fakra, S. C.; Emerson, D.; Fleming, E. J.; Edwards, K. J. Lithotrophic Iron-Oxidizing Bacteria Produce Organic Stalks to Control Mineral Growth: Implications for Biosignature Formation. *ISME J.* **2011**, *5*, 717–727.
- (249) Chan, C. University of Delaware: Newark, DE, USA. Personal communication, 2017.
- (250) Emerson, D. Bigelow Laboratory for Ocean Sciences: East Booth Bay, ME, USA. Personal communication, 2017.
- (251) Amstaetter, K.; Borch, T.; Kappler, A. Influence of Humic Acid Imposed Changes of Ferrihydrite Aggregation on Microbial Fe(III) Reduction. *Geochim. Cosmochim. Acta* **2012**, *85*, 326–341.
- (252) Toner, B. M.; Berquó, T. S.; Michel, F. M.; Sorensen, J. V.; Templeton, A. S.; Edwards, K. J. Mineralogy of Iron Microbial Mats from Loihi Seamount. *Front. Microbiol.* **2012**, *3*, 10.3389/fmicb.2012.00118.
- (253) Benz, M.; Brune, A.; Schink, B. Anaerobic and Aerobic Oxidation of Ferrous Iron at Neutral pH by Chemoheterotrophic Nitrate-Reducing Bacteria. *Arch. Microbiol.* **1998**, *169*, 159–165.
- (254) Kappler, A.; Schink, B.; Newman, D. K. Fe(III) Mineral Formation and Cell Encrustation by the Nitrate-Dependent Fe(II)-Oxidizer strain BoFeN1. *Geobiology* **2005**, *3*, 235–245.
- (255) Lack, J.; Chaudhuri, S.; Chakraborty, R.; Achenbach, L.; Coates, J. Anaerobic Biooxidation of Fe (II) by *Dechlorosoma suillum*. *Microb. Ecol.* **2002**, *43*, 424–431.
- (256) Straub, K. L.; Benz, M.; Schink, B.; Widdel, F. Anaerobic, Nitrate-Dependent Microbial Oxidation of Ferrous Iron. *Appl. Environ. Microbiol.* **1996**, *62*, 1458–1460.
- (257) Weber, K. A.; Hedrick, D. B.; Peacock, A. D.; Thrash, J. C.; White, D. C.; Achenbach, L. A.; Coates, J. D. Physiological and Taxonomic Description of the Novel Autotrophic, Metal Oxidizing Bacterium, *Pseudogulbenkiania* sp. strain 2002. *Appl. Microbiol. Biotechnol.* **2009**, *83*, 555–565.
- (258) Chakraborty, A.; Picardal, F. Induction of Nitrate-Dependent Fe(II) Oxidation by Fe(II) in *Dechloromonas* sp. strain UWNR4 and *Acidovorax* sp. strain 2AN. *Appl. Environ. Microbiol.* **2013**, *79*, 748–752.
- (259) Muehe, E. M.; Gerhardt, S.; Schink, B.; Kappler, A. Ecophysiology and the Energetic Benefit of Mixotrophic Fe(II) Oxidation by Various Strains of Nitrate-reducing Bacteria. *FEMS Microbiol. Ecol.* **2009**, *70*, 335–343.
- (260) Byrne-Bailey, K. G.; Weber, K. A.; Bose, S.; Knox, T.; Spanbauer, T. L.; Chertkov, O.; Coates, J. D.; Chair, A. H. Completed Genome Sequence of the Anaerobic Iron-Oxidizing Bacterium *Acidovorax ebreus* strain TPSY. *J. Bacteriol.* **2010**, *192*, 1475–1476.
- (261) Coates, J. D.; Chakraborty, R.; Lack, J. G.; O'Connor, S. M.; Cole, K. A.; Bender, K. S.; Achenbach, L. A. Anaerobic Benzene Oxidation Coupled to Nitrate Reduction in Pure Culture by Two Strains of *Dechloromonas*. *Nature* **2001**, *411*, 1039–1043.
- (262) Klueglein, N.; Kappler, A. Abiotic Oxidation of Fe(II) by Reactive Nitrogen Species in Cultures of the Nitrate-Reducing Fe(II) Oxidizer *Acidovorax* sp. BoFeN1 – Questioning the Existence of Enzymatic Fe(II) Oxidation. *Geobiology* **2013**, *11*, 180.
- (263) Klueglein, N.; Zeitvogel, F.; Stierhof, Y.-D.; Floetenmeyer, M.; Konhauser, K. O.; Kappler, A.; Obst, M. Potential Role of Nitrite for Abiotic Fe (II) Oxidation and Cell Encrustation During Nitrate Reduction by Denitrifying Bacteria. *Appl. Environ. Microbiol.* **2014**, *80*, 1051–1061.
- (264) Hafenbradl, D.; Keller, M.; Dirmeier, R.; Rachel, R.; Roßnagel, P.; Burggraf, S.; Huber, H.; Stetter, K. O. *Ferroglobus placidus* gen. nov., sp. nov., A Novel Hyperthermophilic Archaeum that Oxidizes Fe²⁺ at Neutral pH under Anoxic Conditions. *Arch. Microbiol.* **1996**, *166*, 308–314.
- (265) Kumaraswamy, R.; Sjölema, K.; Kuenen, G.; Van Loosdrecht, M.; Muyzer, G. Nitrate-Dependent [Fe(II) EDTA]²⁻ Oxidation by *Paracoccus ferrooxidans* sp. nov., Isolated from a Denitrifying Bioreactor. *Syst. Appl. Microbiol.* **2006**, *29*, 276–286.
- (266) Li, B.; Tian, C.; Zhang, D.; Pan, X. Anaerobic Nitrate-Dependent Iron(II) Oxidation by a Novel Autotrophic Bacterium, *Citrobacter freundii* strain PXL1. *Geomicrobiol. J.* **2014**, *31*, 138–144.
- (267) Mattes, A.; Gould, D.; Taupp, M.; Glasauer, S. A Novel Autotrophic Bacterium Isolated from an Engineered Wetland System Links Nitrate-Coupled Iron Oxidation to the Removal of As, Zn and S. *Water, Air, Soil Pollut.* **2013**, *224*, 1–15.
- (268) Shelobolina, E.; Konishi, H.; Xu, H.; Benzine, J.; Xiong, M.; Wu, T.; Blöthe, M.; Roden, E. Isolation of Phyllosilicate–Iron Redox

Cycling Microorganisms from an Illite–Smectite Rich Hydromorphic Soil. *Front. Microbiol.* **2012**, *3*, 1.

(269) Weber, K. A.; Pollock, J.; Cole, K. A.; O'Connor, S. M.; Achenbach, L. A.; Coates, J. D. Anaerobic Nitrate-Dependent Iron(II) Bio-Oxidation by a Novel Lithoautotrophic Betaproteobacterium, Strain 2002. *Appl. Environ. Microbiol.* **2006**, *72*, 686–694.

(270) Zhou, J.; Wang, H.; Yang, K.; Ji, B.; Chen, D.; Zhang, H.; Sun, Y.; Tian, J. Autotrophic Denitrification by Nitrate-Dependent Fe(II) Oxidation in a Continuous up-Flow Biofilter. *Bioprocess Biosyst. Eng.* **2016**, *39*, 277–284.

(271) Su, J. F.; Shao, S. C.; Huang, T. L.; Ma, F.; Yang, S. F.; Zhou, Z. M.; Zheng, S. C. Anaerobic Nitrate-Dependent Iron(II) Oxidation by a Novel Autotrophic Bacterium, *Pseudomonas* sp. SZF15. *J. Environ. Chem. Eng.* **2015**, *3*, 2187–2193.

(272) Schädler, S.; Burkhardt, C.; Hegler, F.; Straub, K.; Miot, J.; Benzerara, K.; Kappler, A. Formation of Cell-Iron-Mineral Aggregates by Phototrophic and Nitrate-Reducing Anaerobic Fe(II)-Oxidizing Bacteria. *Geomicrobiol. J.* **2009**, *26*, 93–103.

(273) Schmid, G.; Zeitvogel, F.; Hao, L.; Ingino, P.; Flötenmeyer, M.; Stierhof, Y. D.; Schröppel, B.; Burkhardt, C.; Kappler, A.; Obst, M. 3-D Analysis of Bacterial Cell-(Iron) Mineral Aggregates Formed During Fe(II) Oxidation by the Nitrate-Reducing *Acidovorax* sp. Strain BoFeN1 Using Complementary Microscopy Tomography Approaches. *Geobiology* **2014**, *12*, 340–361.

(274) Nordhoff, M.; Tominski, C.; Halama, M.; Byrne, J. M.; Obst, M.; Kleindienst, S.; Behrens, S.; Kappler, A. Insights into Nitrate-Reducing Fe(II) Oxidation Mechanisms by Analyzing Cell-Mineral Associations, Cell Encrustation and Mineralogy in the Chemolithoautotrophic Nitrate-Reducing Fe(II)-Oxidizing Enrichment Culture KS. *Appl. Environ. Microbiol.* **2017**, *83*, No. e00752.

(275) Park, S.; Kim, D.-H.; Lee, J.-H.; Hur, H.-G. Sphaerotilus natans Encrusted with Nanoball-Shaped Fe(III) Oxide Minerals Formed by Nitrate-Reducing Mixotrophic Fe(II) Oxidation. *FEMS Microbiol. Ecol.* **2014**, *90*, 68–77.

(276) Pantke, C.; Obst, M.; Benzerara, K.; Morin, G.; Ona-Nguema, G.; Dippon, U.; Kappler, A. Green Rust Formation during Fe(II) Oxidation by the Nitrate-Reducing *Acidovorax* sp. Strain BoFeN1. *Environ. Sci. Technol.* **2012**, *46*, 1439–1446.

(277) Etique, M.; Jorand, F. d. r. P.; Zegeye, A.; Grégoire, B.; Despas, C.; Ruby, C. Abiotic Process for Fe (II) Oxidation and Green Rust Mineralization Driven by a Heterotrophic Nitrate Reducing Bacteria (*Klebsiella mobilis*). *Environ. Sci. Technol.* **2014**, *48*, 3742–3751.

(278) Miot, J.; Li, J.; Benzerara, K.; Sougrati, M. T.; Ona-Nguema, G.; Bernard, S.; Jumas, J.-C.; Guyot, F. Formation of Single Domain Magnetite by Green Rust Oxidation Promoted by Microbial Anaerobic Nitrate-Dependent Iron Oxidation. *Geochim. Cosmochim. Acta* **2014**, *139*, 327–343.

(279) Chaudhuri, S. K.; Lack, J. G.; Coates, J. D. Biogenic Magnetite Formation through Anaerobic Biooxidation of Fe(II). *Appl. Environ. Microbiol.* **2001**, *67*, 2844–2848.

(280) Dippon, U.; Pantke, C.; Porsch, K.; Larese-Casanova, P.; Kappler, A. Potential Function of Added Minerals as Nucleation Sites and Effect of Humic Substances on Mineral Formation by the Nitrate-Reducing Fe(II)-Oxidizing Strain *Acidovorax* sp. BoFeN1. *Environ. Sci. Technol.* **2012**, *46*, 6556–6565.

(281) O'Loughlin, E. J.; Gorski, C. A.; Scherer, M. M.; Boyanov, M. I.; Kemner, K. M. Effects of Oxyanions, Natural Organic Matter, and Bacterial Cell Numbers on the Bioreduction of Lepidocrocite (γ -FeOOH) and the Formation of Secondary Mineralization Products. *Environ. Sci. Technol.* **2010**, *44*, 4570–4576.

(282) Coker, V. S.; Pearce, C. I.; Lang, C.; van der Laan, G.; Patrick, R. A. D.; Telling, N. D.; Schüler, D.; Arenholz, E.; Lloyd, J. R. Cation Site Occupancy of Biogenic Magnetite Compared to Polygenic Ferrite Spinels Determined by X-Ray Magnetic Circular Dichroism. *Eur. J. Mineral.* **2007**, *19*, 707–716.

(283) Lam, K. P.; Hitchcock, A. P.; Obst, M.; Lawrence, J. R.; Swerhone, G. D. W.; Leppard, G. G.; Tyliszczak, T.; Karunakaran, C.; Wang, J.; Kaznatcheev, K.; et al. Characterizing Magnetism of Individual Magnetosomes by X-Ray Magnetic Circular Dichroism in

a Scanning Transmission X-Ray Microscope. *Chem. Geol.* **2010**, *270*, 110–116.

(284) Kappler, A.; Newman, D. K. Formation of Fe(III)-Minerals by Fe(II)-Oxidizing Photoautotrophic Bacteria. *Geochim. Cosmochim. Acta* **2004**, *68*, 1217–1226.

(285) Wu, W.; Swanner, E. D.; Hao, L.; Zeitvogel, F.; Obst, M.; Pan, Y.; Kappler, A. Characterization of the Physiology and Cell–Mineral Interactions of the Marine Anoxygenic Phototrophic Fe(II) Oxidizer *Rhodovulum iodolum* – Implications for Precambrian Fe(II) Oxidation. *FEMS Microbiol. Ecol.* **2014**, *88*, 503–515.

(286) Jiao, Y.; Kappler, A.; Croal, L. R.; Newman, D. K. Isolation and Characterization of a Genetically Tractable Photoautotrophic Fe(II)-Oxidizing Bacterium, *Rhodopseudomonas palustris* Strain TIE-1. *Appl. Environ. Microbiol.* **2005**, *71*, 4487–4496.

(287) Straub, K. L.; Rainey, F. A.; Widdel, F. *Rhodovulum iodolum* sp. nov. and *Rhodovulum robiginosum* sp. nov., Two New Marine Phototrophic Ferrous-Iron-Oxidizing Purple Bacteria. *Int. J. Syst. Bacteriol.* **1999**, *49*, 729–735.

(288) Crowe, S. A.; Jones, C.; Katsev, S.; Magen, C.; O'Neill, A. H.; Sturm, A.; Canfield, D. E.; Haffner, G. D.; Mucci, A.; Sundby, B.; et al. Photoferrotrophs Thrive in an Archean Ocean Analogue. *Proc. Natl. Acad. Sci. U. S. A.* **2008**, *105*, 15938–15943.

(289) Crowe, S. A.; O'Neill, A. H.; Katsev, S.; Hehanussa, P.; Haffner, G. D.; Sundby, B.; Mucci, A.; Fowle, D. A. The Biogeochemistry of Tropical Lakes: A Case Study from Lake Matano, Indonesia. *Limnol. Oceanogr.* **2008**, *53*, 319–331.

(290) Faivre, D.; Godec, T. U. From Bacteria to Mollusks: The Principles Underlying the Biomineralization of Iron Oxide Materials. *Angew. Chem., Int. Ed.* **2015**, *54*, 4728–4747.

(291) Lin, W.; Bazylinski, D. A.; Xiao, T.; Wu, L.-F.; Pan, Y. Life with Compass: Diversity and Biogeography of Magnetotactic Bacteria. *Environ. Microbiol.* **2014**, *16*, 2646–2658.

(292) Blakemore, R. Magnetotactic Bacteria. *Science* **1975**, *190*, 377–379.

(293) Bazylinski, D. A.; Moskowicz, B. M. Microbial Biomineralization of Magnetic Iron Minerals: Microbiology, Magnetism and Environmental Significance. *Rev. Mineral.* **1997**, *35*, 181–223.

(294) Bazylinski, D. A.; Frankel, R. B. Magnetosome Formation in Prokaryotes. *Nat. Rev. Microbiol.* **2004**, *2*, 217–230.

(295) Blakemore, R.; Short, K.; Bazylinski, D.; Rosenblatt, C.; Frankel, R. B. Microaerobic Conditions are Required for Magnetite Formation within *Aquaspirillum magnetotacticum*. *Geomicrobiol. J.* **1985**, *4*, 53–71.

(296) Uebe, R.; Schüler, D. Magnetosome Biogenesis in Magnetotactic Bacteria. *Nat. Rev. Microbiol.* **2016**, *14*, 621–637.

(297) Lohße, A.; Borg, S.; Raschdorf, O.; Kolinko, I.; Tompa, É.; Pósfai, M.; Faivre, D.; Baumgartner, J.; Schüler, D. Genetic Dissection of the mamAB and mms6 Operons Reveals a Gene Set Essential for Magnetosome Biogenesis in *Magnetospirillum gryphiswaldense*. *J. Bacteriol.* **2014**, *196*, 2658–2669.

(298) Komeili, A.; Li, Z.; Newman, D. K.; Jensen, G. J. Magnetosomes Are Cell Membrane Invaginations Organized by the Actin-Like Protein MamK. *Science* **2006**, *311*, 242–245.

(299) Komeili, A.; Vali, H.; Beveridge, T. J.; Newman, D. K. Magnetosome Vesicles Are Present before Magnetite Formation, and MamA is Required for Their Activation. *Proc. Natl. Acad. Sci. U. S. A.* **2004**, *101*, 3839–3844.

(300) Raschdorf, O.; Forstner, Y.; Kolinko, I.; Uebe, R.; Plitzko, J. M.; Schüler, D. Genetic and Ultrastructural Analysis Reveals the Key Players and Initial Steps of Bacterial Magnetosome Membrane Biogenesis. *PLoS Genet.* **2016**, *12*, e1006101.

(301) Faivre, D.; Schüler, D. Magnetotactic Bacteria and Magnetosomes. *Chem. Rev.* **2008**, *108*, 4875–4898.

(302) Grünberg, K.; Müller, E.-C.; Otto, A.; Reszka, R.; Linder, D.; Kube, M.; Reinhardt, R.; Schüler, D. Biochemical and Proteomic Analysis of the Magnetosome Membrane in *Magnetospirillum gryphiswaldense*. *Appl. Environ. Microbiol.* **2004**, *70*, 1040–1050.

- (303) Bazylinski, D. A.; Frankel, R. B. Biologically Controlled Mineralization in Prokaryotes. *Rev. Mineral. Geochem.* **2003**, *54*, 217–247.
- (304) Amor, M.; Busigny, V.; Durand-Dubief, M.; Tharaud, M.; Ona-Nguema, G.; Gélabert, A.; Alphanéry, E.; Menguy, N.; Benedetti, M. F.; Chebbi, I.; et al. Chemical Signature of Magnetotactic Bacteria. *Proc. Natl. Acad. Sci. U. S. A.* **2015**, *112*, 1699–1703.
- (305) Staniland, S.; Williams, W.; Telling, ND; van der Laan, G.; Harrison, A.; Ward, B. Controlled Cobalt Doping of Magnetosomes. *Nat. Nanotechnol.* **2008**, *3*, 158–162.
- (306) Tanaka, M.; Brown, R.; Hondow, N.; Arakaki, A.; Matsunaga, T.; Staniland, S. Highest Levels of Cu, Mn and Co Doped into Nanomagnetic Magnetosomes through Optimized Biomineralisation. *J. Mater. Chem.* **2012**, *22*, 11919–11921.
- (307) Bazylinski, D. A.; Frankel, R. B. Magnetic Iron Oxide and Iron Sulfide Minerals within Microorganisms. In *Biomineralization: From Biology to Biotechnology and Medical Application*; Wiley-VCH, 2000; pp 25–46.
- (308) Schüler, D. Formation of Magnetosomes in Magnetotactic Bacteria. *J. Mol. Microbiol. Biotechnol.* **1999**, *1*, 79–86.
- (309) Butler, R. F.; Banerjee, S. K. Theoretical Single-Domain Grain Size Range in Magnetite and Titanomagnetite. *J. Geophys. Res.* **1975**, *80*, 4049–4058.
- (310) Blakemore, R. P. Magnetotactic Bacteria. *Annu. Rev. Microbiol.* **1982**, *36*, 217–238.
- (311) Guo, F. F.; Yang, W.; Jiang, W.; Geng, S.; Peng, T.; Li, J. L. Magnetosomes Eliminate Intracellular Reactive Oxygen Species in *Magnetospirillum gryphiswaldense* MSR-1. *Environ. Microbiol.* **2012**, *14*, 1722–1729.
- (312) Bazylinski, D. A.; Frankel, R. B.; Konhauser, K. O. Modes of Biomineralization of Magnetite by Microbes. *Geomicrobiol. J.* **2007**, *24*, 465–475.
- (313) Simmons, S. L.; Edwards, K. J. Geobiology of Magnetotactic Bacteria. In *Magnetoreception and Magnetosomes in Bacteria*; Springer, 2006; pp 77–102.
- (314) Vali, H.; Kirschvink, J. L. Observations of Magnetosome Organization, Surface Structure, and Iron Biomineralization of Undescribed Magnetic Bacteria: Evolutionary Speculations. In *Iron Biominerals*; Springer, 1991; pp 97–115.
- (315) Byrne, J. M.; Klueglein, N.; Pearce, C.; Rosso, K. M.; Appel, E.; Kappler, A. Redox Cycling of Fe(II) and Fe(III) in Magnetite by Fe-Metabolizing Bacteria. *Science* **2015**, *347*, 1473–1476.
- (316) Gorby, Y. A.; Beveridge, T. J.; Blakemore, R. P. Characterization of the Bacterial Magnetosome Membrane. *J. Bacteriol.* **1988**, *170*, 834–841.
- (317) Chang, S.-B. R.; Kirschvink, J. L. Magnetofossils, the Magnetization of Sediments, and the Evolution of Magnetite Biomineralization. *Annu. Rev. Earth Planet. Sci.* **1989**, *17*, 169.
- (318) Kirschvink, J.; Lowenstam, H. Mineralization and Magnetization of Chiton Teeth: Paleomagnetic, Sedimentologic, and Biologic Implications of Organic Magnetite. *Earth Planet. Sci. Lett.* **1979**, *44*, 193–204.
- (319) Stolz, J. F.; Lovley, D. R.; Haggerty, S. E. Biogenic Magnetite and the Magnetization of Sediments. *J. Geophys. Res.* **1990**, *95*, 4355–4361.
- (320) McKay, D. S.; Gibson, E. K.; Thomas-Keppta, K. L.; Vali, H.; Romanek, C. S.; Clemett, S. J.; Chillier, X. D. F.; Maechling, C. R.; Zare, R. N. Search for Past Life on Mars: Possible Relic Biogenic Activity in Martian Meteorite ALH84001. *Science* **1996**, *273*, 924–930.
- (321) Treiman, A. Martian Life “Still Kicking” in Meteorite ALH84001. *Trans., Am. Geophys. Union* **1999**, *80*, 205–209.
- (322) Kopp, R. E.; Kirschvink, J. L. The Identification and Biogeochemical Interpretation of Fossil Magnetotactic Bacteria. *Earth-Sci. Rev.* **2008**, *86*, 42–61.
- (323) Lovley, D. R.; Stolz, J. F.; Nord, G. L.; Phillips, E. J. P. Anaerobic Production of Magnetite by a Dissimilatory Iron-Reducing Microorganism. *Nature* **1987**, *330*, 252–254.
- (324) Amor, M.; Busigny, V.; Louvat, P.; Gélabert, A.; Cartigny, P.; Durand-Dubief, M.; Ona-Nguema, G.; Alphanéry, E.; Chebbi, I.; Guyot, F. Mass-Dependent and-Independent Signature of Fe Isotopes in Magnetotactic Bacteria. *Science* **2016**, *352*, 705–708.
- (325) Kim, W.; Suh, C.-Y.; Cho, S.-W.; Roh, K.-M.; Kwon, H.; Song, K.; Shon, I.-J. A New Method for the Identification and Quantification of Magnetite–Maghemite Mixture Using Conventional X-Ray Diffraction Technique. *Talanta* **2012**, *94*, 348–352.
- (326) Itoh, H.; Sugimoto, T. Systematic Control of Size, Shape, Structure, and Magnetic Properties Of uniform Magnetite and Maghemite Particles. *J. Colloid Interface Sci.* **2003**, *265*, 283–295.
- (327) Mikhaylova, A. B.; Sirotinkin, V. P.; Fedotov, M. A.; Korneyev, V. P.; Shamray, B. F.; Kovalenko, L. V. Quantitative Determination of Content of Magnetite and Maghemite in Their Mixtures by X-Ray Diffraction Methods. *Inorg. Mater: Appl. Res.* **2016**, *7*, 130–136.
- (328) Faivre, D. *Iron Oxides: From Nature to Applications*; John Wiley & Sons, 2016.
- (329) Pearce, C. I.; Qafoku, O.; Liu, J.; Arenholz, E.; Heald, S. M.; Kukkadapu, R. K.; Gorski, C. A.; Henderson, C. M. B.; Rosso, K. M. Synthesis and Properties of Titanomagnetite (Fe_{3-x}Ti_xO₄) Nanoparticles: A Tunable Solid-State Fe(II/III) Redox System. *J. Colloid Interface Sci.* **2012**, *387*, 24–38.
- (330) Kone, T.; Hanna, K.; Usman, M. Interactions of Synthetic Fe(II)-Fe(III) Green Rusts with Pentachlorophenol under Various Experimental Conditions. *Colloids Surf., A* **2011**, *385*, 152–158.
- (331) Ruby, C.; Abdelmoula, M.; Naille, S.; Renard, A.; Khare, V.; Ona-Nguema, G.; Morin, G.; Génin, J.-M. R. Oxidation Modes and Thermodynamics of Fe^{II-III} Oxyhydroxycarbonate Green Rust: Dissolution–Precipitation Versus in Situ Deprotonation. *Geochim. Cosmochim. Acta* **2010**, *74*, 953–966.
- (332) Guilbaud, R.; White, M. L.; Poulton, S. W. Surface Charge and Growth of Sulphate and Carbonate Green Rust in Aqueous Media. *Geochim. Cosmochim. Acta* **2013**, *108*, 141–153.
- (333) U.S. Department of Commerce: National Bureau of Standards. Standard X-ray Diffraction Powder Patterns. *Natl. Bur. Stand., Monogr. (U.S.)* **25** **1967**, *5*, 31.
- (334) Jones, C. J.; Chattopadhyay, S.; Gonzalez-Pech, N. I.; Avendano, C.; Hwang, N.; Lee, S. S.; Cho, M.; Ozarowski, A.; Prakash, A.; Mayo, J. T.; et al. A Novel, Reactive Green Iron Sulfide (Sulfide Green Rust) Formed on Iron Oxide Nanocrystals. *Chem. Mater.* **2015**, *27*, 700–707.
- (335) Jones, C. *Iron: From Synthesis, Characterization, and Application of Sulfide Green Rust to Viability in Arsenic Water Treatment*; Rice University, 2013.
- (336) Mossbauer, R. L. Kernresonanzfluoreszenz von Gammatrahlung in Ir-191. *Eur. Phys. J. A* **1958**, *151*, 124–143.
- (337) Klingelhöfer, G.; Morris, R. V.; Bernhardt, B.; Rodionov, D.; de Souza, P. A.; Squyres, S. W.; Foh, J.; Kankeleit, E.; Bonnes, U.; Gellert, R.; et al. Athena MIMOS II Mössbauer Spectrometer Investigation. *J. Geophys. Res.: Planets* **2003**, *108*, 8067.
- (338) Markovski, C.; Byrne, J. M.; Lalla, E.; Lozano-Gorrín, A.; Klingelhoefer, G.; Rull, F.; Kappler, A.; Hoffmann, T.; Schröder, C. Abiotic Versus Biotic Iron Mineral Transformation Studied by a Miniaturized Backscattering Mössbauer Spectrometer (MIMOS II), X-Ray Diffraction and Raman Spectroscopy. *Icarus* **2017**, *296*, 49–58.
- (339) Dyar, M. D.; Agresti, D. G.; Schaefer, M. W.; Grant, C. A.; Sklute, E. C. Mössbauer Spectroscopy of Earth and Planetary Materials. *Annu. Rev. Earth Planet. Sci.* **2006**, *34*, 83–125.
- (340) Morice, J. A.; Rees, L. V. C.; Rickard, D. T. Mössbauer Studies of Iron Sulphides. *J. Inorg. Nucl. Chem.* **1969**, *31*, 3797–3802.
- (341) Kündig, W.; Steven Hargrove, R. Electron Hopping in Magnetite. *Solid State Commun.* **1969**, *7*, 223–227.
- (342) Srivastava, C. M.; Shringi, S. N.; Babu, M. V. Mössbauer Study of the Low-Temperature Phase of Magnetite. *Phys. Status Solidi A* **1981**, *65*, 731–735.
- (343) Génin, J.-M. R.; Bourrié, G.; Trolard, F.; Abdelmoula, M.; Jaffrezic, A.; Refait, P.; Maitre, V.; Humbert, B.; Herbillon, A. Thermodynamic Equilibria in Aqueous Suspensions of Synthetic and Natural Fe(II)–Fe(III) Green Rusts: Occurrences of the Mineral in Hydromorphic Soils. *Environ. Sci. Technol.* **1998**, *32*, 1058–1068.

- (344) De Faria, D.; Venâncio Silva, S.; De Oliveira, M. Raman Microspectroscopy of Some Iron Oxides and Oxyhydroxides. *J. Raman Spectrosc.* **1997**, *28*, 873–878.
- (345) Labbé, J.; Lédion, J.; Hui, F. Infrared Spectrometry for Solid Phase Analysis: Corrosion Rusts. *Corros. Sci.* **2008**, *50*, 1228–1234.
- (346) Gotić, M.; Musić, S. Mössbauer, FT-IR and FE SEM Investigation of Iron Oxides Precipitated from FeSO₄ Solutions. *J. Mol. Struct.* **2007**, *834–836*, 445–453.
- (347) Pérez, F.; Barrero, C.; Walker, A. H.; García, K.; Nomura, K. Effects of Chloride Concentration, Immersion Time and Steel Composition on the Spinel Phase Formation. *Mater. Chem. Phys.* **2009**, *117*, 214–223.
- (348) Pérez, F.; Barrero, C.; García, K. Factors Affecting the Amount of Corroded Iron Converted into Adherent Rust in Steels Submitted to Immersion Tests. *Corros. Sci.* **2010**, *52*, 2582–2591.
- (349) Jubb, A. M.; Allen, H. C. Vibrational Spectroscopic Characterization of Hematite, Maghemite, and Magnetite Thin Films Produced by Vapor Deposition. *ACS Appl. Mater. Interfaces* **2010**, *2*, 2804–2812.
- (350) Chamritski, I.; Burns, G. Infrared-and Raman-Active Phonons of Magnetite, Maghemite, and Hematite: A Computer Simulation and Spectroscopic Study. *J. Phys. Chem. B* **2005**, *109*, 4965–4968.
- (351) Serna, C. J.; Rendon, J. L.; Iglesias, J. E. Infrared Surface Modes in Corundum-Type Microcrystalline Oxides. *Spectrochim. Acta, Part A* **1982**, *38*, 797–802.
- (352) Shebanova, O. N.; Lazor, P. Raman Spectroscopic Study of Magnetite (FeFe₂O₄): A New Assignment for the Vibrational Spectrum. *J. Solid State Chem.* **2003**, *174*, 424–430.
- (353) Shebanova, O. N.; Lazor, P. Raman Study of Magnetite (Fe₃O₄): Laser-Induced Thermal Effects and Oxidation. *J. Raman Spectrosc.* **2003**, *34*, 845–852.
- (354) Dünnwald, J.; Otto, A. An Investigation of Phase Transitions in Rust Layers Using Raman Spectroscopy. *Corros. Sci.* **1989**, *29*, 1167–1176.
- (355) Ohtsuka, T.; Kubo, K.; Sato, N. Raman Spectroscopy of Thin Corrosion Films on Iron at 100 to 150 C in Air. *Corrosion* **1986**, *42*, 476–481.
- (356) Gasparov, L.; Tanner, D.; Romero, D.; Berger, H.; Margaritondo, G.; Forro, L. Infrared and Raman Studies of the Verwey Transition in Magnetite. *Phys. Rev. B: Condens. Matter Mater. Phys.* **2000**, *62*, 7939.
- (357) Graves, P. R.; Johnston, C.; Campaniello, J. J. Raman Scattering in Spinel Structure Ferrites. *Mater. Res. Bull.* **1988**, *23*, 1651–1660.
- (358) Li, J.-M.; Huan, A. C. H.; Wang, L.; Du, Y.-W.; Feng, D. Interface Effects on Magnetoresistance and Magnetic-Field-Reduced Raman Scattering in Magnetite. *Phys. Rev. B: Condens. Matter Mater. Phys.* **2000**, *61*, 6876–6878.
- (359) Gupta, R.; Sood, A.; Metcalf, P.; Honig, J. Raman Study of Stoichiometric and Zn-Doped Fe₃O₄. *Phys. Rev. B: Condens. Matter Mater. Phys.* **2002**, *65*, 104430.
- (360) Bersani, D.; Lottici, P.; Montenero, A. Micro-Raman Investigation of Iron Oxide Films and Powders Produced by Sol–Gel Syntheses. *J. Raman Spectrosc.* **1999**, *30*, 355–360.
- (361) Li, Y.-S.; Church, J. S.; Woodhead, A. L. Infrared and Raman Spectroscopic Studies on Iron Oxide Magnetic Nanoparticles and their Surface Modifications. *J. Magn. Magn. Mater.* **2012**, *324*, 1543–1550.
- (362) Zhang, J.; Srivastava, R. S.; Misra, R. D. K. Core–Shell Magnetite Nanoparticles Surface Encapsulated with Smart Stimuli-responsive Polymer: Synthesis, Characterization, and LCST of Viable Drug-targeting Delivery System. *Langmuir* **2007**, *23*, 6342–6351.
- (363) Ona-Nguema, G.; Carteret, C.; Benali, O.; Abdelmoula, M.; Génin, J.-M.; Jorand, F. Competitive Formation of Hydroxycarbonate Green Rust 1 Versus Hydroxysulphate Green Rust 2 in *Shewanella putrefaciens* Cultures. *Geomicrobiol. J.* **2004**, *21*, 79–90.
- (364) Bonin, P. M. L.; Odziemkowski, M. S.; Reardon, E. J.; Gillham, R. W. In Situ Identification of Carbonate-Containing Green Rust on Iron Electrodes in Solutions Simulating Groundwater. *J. Solution Chem.* **2000**, *29*, 1061–1074.
- (365) Namduri, H.; Nasrazadani, S. Quantitative Analysis of Iron Oxides Using Fourier Transform Infrared Spectrophotometry. *Corros. Sci.* **2008**, *50*, 2493–2497.
- (366) Oh, S. J.; Cook, D.; Townsend, H. Characterization of Iron Oxides Commonly Formed as Corrosion Products On Steel. *Hyperfine Interact.* **1998**, *112*, 59–66.
- (367) Legrand, L.; Sagon, G.; Lecomte, S.; Chausse, A.; Messina, R. Raman and Infrared Study of a New Carbonate Green Rust Obtained by Electrochemical Way. *Corros. Sci.* **2001**, *43*, 1739–1749.
- (368) Dubois, F.; Mendibide, C.; Pagnier, T.; Perrard, F.; Duret, C. Raman Mapping of Corrosion Products Formed onto Spring Steels During Salt Spray Experiments. A Correlation between the Scale Composition and the Corrosion Resistance. *Corros. Sci.* **2008**, *50*, 3401–3409.
- (369) Pérez, F.; Barreo Meneses, C.; García, K.; Hight Walker, A. Raman Microscopy as a Tool for the Rust Composition Distribution Analysis. *Rev. Colomb. Fis.* **2010**, *42*, 187–190.
- (370) Su, X.; Yu, C.; Qiang, C. Synthesis of α -Fe₂O₃ Nanobelts and Nanoflakes by Thermal Oxidation and Study to Their Magnetic Properties. *Appl. Surf. Sci.* **2011**, *257*, 9014–9018.
- (371) Zegeye, A.; Ona-Nguema, G.; Carteret, C.; Huguet, L.; Abdelmoula, M.; Jorand, F. Formation of Hydroxysulphate Green Rust 2 as a Single Iron(II-III) Mineral in Microbial Culture. *Geomicrobiol. J.* **2005**, *22*, 389–399.
- (372) Peulon, S.; Legrand, L.; Antony, H.; Chaussé, A. Electrochemical Deposition of Thin Films of Green Rusts 1 and 2 on Inert Gold Substrate. *Electrochem. Commun.* **2003**, *5*, 208–213.
- (373) Templeton, A.; Knowles, E. Microbial Transformations of Minerals and Metals: Recent Advances in Geomicrobiology Derived from Synchrotron-Based X-Ray Spectroscopy and X-Ray Microscopy. *Annu. Rev. Earth Planet. Sci.* **2009**, *37*, 367–391.
- (374) Wilke, M.; Farges, F.; Petit, P.-E.; Brown, G. E.; Martin, F. Oxidation State and Coordination of Fe in Minerals: An Fe K-XANES Spectroscopic Study. *Am. Mineral.* **2001**, *86*, 714.
- (375) Galois, L.; Calas, G.; Arrio, M. A. High-Resolution XANES Spectra of Iron in Minerals and Glasses: Structural Information from the Pre-Edge Region. *Chem. Geol.* **2001**, *174*, 307–319.
- (376) ThomasArrigo, L. K.; Mikutta, C.; Byrne, J.; Barmettler, K.; Kappler, A.; Kretzschmar, R. Iron and Arsenic Speciation and Distribution in Organic Flocs from Streambeds of an Arsenic-Enriched Peatland. *Environ. Sci. Technol.* **2014**, *48*, 13218–13228.
- (377) Laan, G. v. d. Applications of Soft X-Ray Magnetic Dichroism. *J. Phys.: Conf. Ser.* **2013**, *430*, 012127.
- (378) van der Laan, G.; Kirkman, I. W. The 2p Absorption-Spectra of 3d Transition-Metal Compounds in Tetrahedral and Octahedral Symmetry. *J. Phys.: Condens. Matter* **1992**, *4*, 4189–4204.
- (379) van der laan, G.; Thole, B. T. Strong Magnetic-X-Ray Dichroism in 2p Absorption-Spectra of 3d Transition-Metal Ions. *Phys. Rev. B: Condens. Matter Mater. Phys.* **1991**, *43*, 13401–13411.
- (380) Pearce, C. I.; Henderson, C. M. B.; Telling, ND; Patrick, R. A. D.; Charnock, J. M.; Coker, V. S.; Arenholz, E.; Tuna, F.; van der Laan, G. Fe Site Occupancy in Magnetite-Ulvöspinel Solid Solutions: A New Approach Using X-Ray Magnetic Circular Dichroism. *Am. Mineral.* **2010**, *95*, 425–439.
- (381) Coker, V. S.; Gault, A. G.; Pearce, C. I.; van der Laan, G.; Telling, ND; Charnock, J. M.; Polya, D. A.; Lloyd, J. R. XAS and XMCD Evidence for Species-Dependent Partitioning of Arsenic During Microbial Reduction of Ferrihydrite to Magnetite. *Environ. Sci. Technol.* **2006**, *40*, 7745–7750.
- (382) Crean, D. E.; Coker, V. S.; van der Laan, G.; Lloyd, J. R. Engineering Biogenic Magnetite for Sustained Cr(VI) Remediation in Flow-through Systems. *Environ. Sci. Technol.* **2012**, *46*, 3352–3359.
- (383) Cutting, R. S.; Coker, V. S.; Telling, ND; Kimber, R. L.; Pearce, C. I.; Ellis, B. L.; Lawson, R. S.; van der Laan, G.; Patrick, R. A. D.; Vaughan, D. J.; et al. Optimizing Cr(VI) and Tc(VII) Remediation through Nanoscale Biomineral Engineering. *Environ. Sci. Technol.* **2010**, *44*, 2577–2584.
- (384) Telling, ND; Coker, V. S.; Cutting, R. S.; van der Laan, G.; Pearce, C. I.; Patrick, R. A. D.; Arenholz, E.; Lloyd, J. R. Remediation

of Cr(VI) by Biogenic Magnetic Nanoparticles: An X-Ray Magnetic Circular Dichroism Study. *Appl. Phys. Lett.* **2009**, *95*, 163701.

(385) Watts, M. P.; Coker, V. S.; Parry, S. A.; Patrick, R. A. D.; Thomas, R. A. P.; Kalin, R.; Lloyd, J. R. Biogenic Nano-Magnetite and Nano-Zero Valent Iron Treatment of Alkaline Cr(VI) Leachate and Chromite Ore Processing Residue. *Appl. Geochem.* **2015**, *54*, 27–42.

(386) Coker, V. S.; Pearce, C. I.; Patrick, R. A. D.; van der Laan, G.; Telling, ND; Charnock, J. M.; Arenholz, E.; Lloyd, J. R. Probing the Site Occupancies of Co-, Ni-, and Mn-Substituted Biogenic Magnetite Using XAS and XMCD. *Am. Mineral.* **2008**, *93*, 1119–1132.

(387) Coker, V. S.; Telling, ND; van der Laan, G.; Patrick, R. A. D.; Pearce, C. I.; Arenholz, E.; Tuna, F.; Winpenny, R. E. P.; Lloyd, J. R. Harnessing the Extracellular Bacterial Production of Nanoscale Cobalt Ferrite with Exploitable Magnetic Properties. *ACS Nano* **2009**, *3*, 1922–1928.

(388) Coker, V. S.; Bennett, J. A.; Telling, ND; Henkel, T.; Charnock, J. M.; van der Laan, G.; Patrick, R. A. D.; Pearce, C. I.; Cutting, R. S.; Shannon, I. J.; et al. Microbial Engineering of Nanoheterostructures: Biological Synthesis of a Magnetically Recoverable Palladium Nanocatalyst. *ACS Nano* **2010**, *4*, 2577–2584.

(389) Chang, L.; Patrick, R. A. D.; van der Laan, G.; Coker, V. S.; Roberts, A. P. Enigmatic X-Ray Magnetic Circular Dichroism in Greigite (Fe₃S₄). *Can. Mineral.* **2012**, *50*, 667–674.

(390) Letard, I.; Sainctavit, P.; Deudon, C. XMCD at Fe L_{2,3} Edges, Fe and S K Edges on Fe₇S₈. *Phys. Chem. Miner.* **2007**, *34*, 113–120.

(391) Patrick, R. A. D.; Coker, V. S.; Akhtar, M.; Malik, M. A.; Lewis, E.; Haigh, E.; O'Brien, P.; Shafer, P. C.; van der Laan, G. Magnetic Spectroscopy of Nanoparticulate Greigite, Fe₃S₄. *Mineral. Mag.* **2016**, *81*, 857.

(392) von der Heyden, B. P.; Roychoudhury, A. N.; Mtshali, T. N.; Tyliczszak, T.; Myneni, S. C. B. Chemically and Geographically Distinct Solid-Phase Iron Pools in the Southern Ocean. *Science* **2012**, *338*, 1199.

(393) Coker, V. S.; Byrne, J. M.; Telling, ND; Van Der Laan, G.; Lloyd, J. R.; Hitchcock, A. P.; Wang, J.; Patrick, R. A. D. Characterisation of the Dissimilatory Reduction of Fe(III)-Oxyhydroxide at the Microbe – Mineral Interface: The Application of STXM–XMCD. *Geobiology* **2012**, *10*, 347–354.

(394) Ona-Nguema, G.; Abdelmoula, M.; Jorand, F.; Benali, O.; Block, J. C.; Génin, J. M. R. Iron(II,III) hydroxycarbonate green rust formation and stabilization from lepidocrocite bioreduction. *Environ. Sci. Technol.* **2002**, *36*, 16–20.

(395) Barthélémy, K.; Naille, S.; Despas, C.; Ruby, C.; Mallet, M. Carbonated Ferric Green Rust as a New Material for Efficient Phosphate Removal. *J. Colloid Interface Sci.* **2012**, *384*, 121–127.

(396) Schwertmann, U.; Murad, E. The Influence of Aluminum on Iron Oxides: XIV. Al-Substituted Magnetite Synthesized at Ambient Temperatures. *Clays Clay Miner.* **1990**, *38*, 196–202.

(397) Schwertmann, U.; Cornell, R. M. *Iron Oxides in the Laboratory: Preparation and Characterization*; Wiley-VCH: New York, 2000.

(398) Heller, F.; Evans, M. E. Loess Magnetism. *Rev. Geophys.* **1995**, *33*, 211–240.

(399) Maher, B. A.; Ahmed, I. A.; Karloukovski, V.; MacLaren, D. A.; Foulds, P. G.; Allsop, D.; Mann, D. M.; Torres-Jardón, R.; Calderon-Garciduenas, L. Magnetite Pollution Nanoparticles in the Human Brain. *Proc. Natl. Acad. Sci. U. S. A.* **2016**, *113*, 10797–10801.

(400) Day, R.; Fuller, M.; Schmidt, V. A. Hysteresis Properties of Titanomagnetites: Grain-Size and Compositional Dependence. *Phys. Earth Planet. Inter.* **1977**, *13*, 260–267.

(401) Dunlop, D. J. Theory and Application of the Day Plot (Mrs/Ms versus Hcr/Hc) 2. Application to Data for Rocks, Sediments, and Soils. *J. Geophys. Res.* **2002**, *107*, 4-1–4-22.

(402) Mullins, C. Magnetic Susceptibility of the Soil and its Significance in Soil Science—A Review. *J. Soil Sci.* **1977**, *28*, 223–246.

(403) Porsch, K.; Dippon, U.; Rijal, M. L.; Appel, E.; Kappler, A. In-situ magnetic susceptibility measurements as a tool to follow geomicrobiological transformation of Fe minerals. *Environ. Sci. Technol.* **2010**, *44*, 3846–3852.

(404) Boyd, T. E.; Cusick, M.; Navratil, J. *Ferrite Use in Separation Science and Technology*; Rockwell International Corp.: Golden, CO, 1983.

(405) Yavuz, C. T.; Mayo, J.; William, W. Y.; Prakash, A.; Falkner, J. C.; Yean, S.; Cong, L.; Shipley, H. J.; Kan, A.; Tomson, M.; et al. Low-Field Magnetic Separation of Monodisperse Fe₃O₄ Nanocrystals. *Science* **2006**, *314*, 964–967.

(406) Barriga, C.; Gaitan, M.; Pavlovic, I.; Ulibarri, M. A.; Hermosin, M. C.; Cornejo, J. Hydrotalcites as Sorbent for 2,4,6-Trinitrophenol: Influence of the Layer Composition and Interlayer Anion. *J. Mater. Chem.* **2002**, *12*, 1027–1034.

(407) Pavlovic, I.; Barriga, C.; Hermosin, M. C.; Cornejo, J.; Ulibarri, M. A. Adsorption of Acidic Pesticides 2,4-D, Clopyralid and Picloram on Calcined Hydrotalcite. *Appl. Clay Sci.* **2005**, *30*, 125–133.

(408) Sergent, A. S.; Jorand, F.; Hanna, K. Effects of Si-Bearing Minerals on the Nature of Secondary Iron Mineral Products from Lepidocrocite Bioreduction. *Chem. Geol.* **2011**, *289*, 86–97.

(409) Chowdhury, S. R.; Yanful, E. K. Arsenic and Chromium Removal by Mixed Magnetite-Maghemite Nanoparticles and the Effect of Phosphate on Removal. *J. Environ. Manage.* **2010**, *91*, 2238–2247.

(410) Martínez, M.; Giménez, J.; de Pablo, J.; Rovira, M.; Duro, L. Sorption of Selenium(IV) and Selenium(VI) onto Magnetite. *Appl. Surf. Sci.* **2006**, *252*, 3767–3773.

(411) Dixit, S.; Hering, J. G. Comparison of Arsenic(V) and Arsenic(III) Sorption onto Iron Oxide Minerals: Implications for Arsenic Mobility. *Environ. Sci. Technol.* **2003**, *37*, 4182–4189.

(412) Missana, T.; García-Gutiérrez, M.; Fernández, V. Uranium (VI) Sorption on Colloidal Magnetite under Anoxic Environment: Experimental Study and Surface Complexation Modelling. *Geochim. Cosmochim. Acta* **2003**, *67*, 2543–2550.

(413) Missana, T.; Alonso, U.; Scheinost, A. C.; Granizo, N.; García-Gutiérrez, M. Selenite Retention by Nanocrystalline Magnetite: Role of Adsorption, Reduction and Dissolution/Co-Precipitation Processes. *Geochim. Cosmochim. Acta* **2009**, *73*, 6205–6217.

(414) Mayo, J. T.; Yavuz, C.; Yean, S.; Cong, L.; Shipley, H.; Yu, W.; Falkner, J.; Kan, A.; Tomson, M.; Colvin, V. L. The Effect of Nanocrystalline Magnetite Size on Arsenic Removal. *Sci. Technol. Adv. Mater.* **2007**, *8*, 71–75.

(415) Yean, S.; Cong, L.; Yavuz, C. T.; Mayo, J. T.; Yu, W. W.; Kan, A. T.; Colvin, V. L.; Tomson, M. B. Effect of Magnetite Particle Size on Adsorption and Desorption of Arsenite and Arsenate. *J. Mater. Res.* **2005**, *20*, 3255–3264.

(416) Liu, C.-H.; Chuang, Y.-H.; Chen, T.-Y.; Tian, Y.; Li, H.; Wang, M.-K.; Zhang, W. Mechanism of Arsenic Adsorption on Magnetite Nanoparticles from Water: Thermodynamic and Spectroscopic Studies. *Environ. Sci. Technol.* **2015**, *49*, 7726–7734.

(417) Mohan, D.; Pittman, C. U., Jr Arsenic Removal from Water/Wastewater Using Adsorbents—A Critical Review. *J. Hazard. Mater.* **2007**, *142*, 1–53.

(418) Shipley, H. J.; Yean, S.; Kan, A. T.; Tomson, M. B. Adsorption of Arsenic to Magnetite Nanoparticles: Effect of Particle Concentration, pH, Ionic Strength, and Temperature. *Environ. Toxicol. Chem.* **2009**, *28*, 509–515.

(419) Jönsson, J.; Sherman, D. M. Sorption of As(III) and As(V) to Siderite, Green Rust (Fougerite) and Magnetite: Implications for Arsenic Release in Anoxic Groundwaters. *Chem. Geol.* **2008**, *255*, 173–181.

(420) Wang, Y.; Morin, G.; Ona-Nguema, G.; Menguy, N.; Juillot, F.; Aubry, E.; Guyot, F.; Calas, G.; Brown, G. E., Jr Arsenite Sorption at the Magnetite–Water Interface During Aqueous Precipitation of Magnetite: EXAFS Evidence for a New Arsenite Surface Complex. *Geochim. Cosmochim. Acta* **2008**, *72*, 2573–2586.

(421) Wang, Y.; Morin, G.; Ona-Nguema, G.; Juillot, F.; Guyot, F.; Calas, G.; Brown, G. E. Evidence for Different Surface Speciation of Arsenite and Arsenate on Green Rust: An EXAFS and XANES Study. *Environ. Sci. Technol.* **2010**, *44*, 109–115.

(422) Hansen, B. H. C.; Poulsen, I. F. Interaction of Synthetic Sulphate “Green Rust” with Phosphate and the Crystallization of Vivianite. *Clays Clay Miner.* **1999**, *47*, 312–318.

- (423) Giraldo, L.; Erto, A.; Moreno-Piraján, J. C. Magnetite Nanoparticles for Removal of Heavy Metals from Aqueous Solutions: Synthesis and Characterization. *Adsorption* **2013**, *19*, 465–474.
- (424) Lasheen, M. R.; El-Sherif, I. Y.; Sabry, D. Y.; El-Wakeel, S. T.; El-Shahat, M. F. Removal and Recovery of Cr(VI) by Magnetite Nanoparticles. *Desalin. Water Treat.* **2014**, *52*, 6464–6473.
- (425) Lasheen, M. R.; El-Sherif, I. Y.; Tawfik, M. E.; El-Wakeel, S. T.; El-Shahat, M. F. Preparation and Adsorption Properties of Nano Magnetite Chitosan Films for Heavy Metal Ions from Aqueous Solution. *Mater. Res. Bull.* **2016**, *80*, 344–350.
- (426) Liu, J.-f.; Zhao, Z.-s.; Jiang, G.-b. Coating Fe₃O₄ Magnetic Nanoparticles with Humic Acid for High Efficient Removal of Heavy Metals in Water. *Environ. Sci. Technol.* **2008**, *42*, 6949–6954.
- (427) Singh, B. K.; Jain, A.; Kumar, S.; Tomar, B. S.; Tomar, R.; Manchanda, V. K.; Ramanathan, S. Role of Magnetite and Humic Acid in Radionuclide Migration in the Environment. *J. Contam. Hydrol.* **2009**, *106*, 144–149.
- (428) Catalette, H.; Dumonceau, J.; Ollar, P. Sorption of Cesium, Barium and Europium on Magnetite. *J. Contam. Hydrol.* **1998**, *35*, 151–159.
- (429) Ebner, A. D.; Ritter, J. A.; Navratil, J. D. Adsorption of Cesium, Strontium, and Cobalt Ions on Magnetite and a Magnetite–Silica Composite. *Ind. Eng. Chem. Res.* **2001**, *40*, 1615–1623.
- (430) Aamrani, S. E.; Giménez, J.; Rovira, M.; Seco, F.; Grivé, M.; Bruno, J.; Duro, L.; de Pablo, J. A Spectroscopic Study of Uranium(VI) Interaction with Magnetite. *Appl. Surf. Sci.* **2007**, *253*, 8794–8797.
- (431) Rojo, L.; Seco, F.; Rovira, M.; Giménez, J.; Cervantes, G.; Martí, V.; de Pablo, J. Thorium Sorption onto Magnetite and Ferrihydrite in Acidic Conditions. *J. Nucl. Mater.* **2009**, *385*, 474–478.
- (432) Ahmed, I. M.; Gamal, R.; Helal, A. A.; Abo-El-Enein, S. A.; Helal, A. A. Kinetic Sorption Study of Cerium (IV) on Magnetite Nanoparticles. *Part. Sci. Technol.* **2017**, *35*, 643–652.
- (433) Sagert, N. H.; Ho, C. H.; Miller, N. H. The Adsorption of Uranium(VI) onto a Magnetite Sol. *J. Colloid Interface Sci.* **1989**, *130*, 283–287.
- (434) Crane, R. A.; Dickinson, M.; Popescu, I. C.; Scott, T. B. Magnetite and Zero-Valent Iron Nanoparticles for the Remediation of Uranium Contaminated Environmental Water. *Water Res.* **2011**, *45*, 2931–2942.
- (435) Das, D.; Sureshkumar, M. K.; Koley, S.; Mithal, N.; Pillai, C. G. S. Sorption of Uranium on Magnetite Nanoparticles. *J. Radioanal. Nucl. Chem.* **2010**, *285*, 447–454.
- (436) Singer, D. M.; Chatman, S. M.; Ilton, E. S.; Rosso, K. M.; Banfield, J. F.; Waychunas, G. A. Sorption and Reduction Kinetics on the Magnetite (111) Surface. *Environ. Sci. Technol.* **2012**, *46*, 3821–3830.
- (437) Singer, D. M.; Chatman, S. M.; Ilton, E. S.; Rosso, K. M.; Banfield, J. F.; Waychunas, G. A. Identification of Simultaneous U(VI) Sorption Complexes and U(IV) Nanoprecipitates on the Magnetite (111) Surface. *Environ. Sci. Technol.* **2012**, *46*, 3811–3820.
- (438) Jordan, N.; Marmier, N.; Lomenech, C.; Giffaut, E.; Ehrhardt, J.-J. Sorption of Silicates on Goethite, Hematite, and Magnetite: Experiments and Modelling. *J. Colloid Interface Sci.* **2007**, *312*, 224–229.
- (439) Daou, T. J.; Begin-Colin, S.; Grenèche, J. M.; Thomas, F.; Derory, A.; Bernhardt, P.; Legaré, P.; Pourroy, G. Phosphate Adsorption Properties of Magnetite-Based Nanoparticles. *Chem. Mater.* **2007**, *19*, 4494–4505.
- (440) Yang, X.; Roonasi, P.; Jolsterá, R.; Holmgren, A. Kinetics of Silicate Sorption on Magnetite and Maghemite: An In Situ ATR-FTIR Study. *Colloids Surf., A* **2009**, *343*, 24–29.
- (441) Mansour, C.; Lefèvre, G.; Pavageau, E. M.; Catalette, H.; Fédoroff, M.; Zanna, S. Sorption of Sulfate Ions onto Magnetite. *J. Colloid Interface Sci.* **2009**, *331*, 77–82.
- (442) Roonasi, P.; Holmgren, A. An ATR-FTIR Study of Sulphate Sorption on Magnetite; Rate of Adsorption, Surface Speciation, and Effect of Calcium Ions. *J. Colloid Interface Sci.* **2009**, *333*, 27–32.
- (443) Roonasi, P.; Holmgren, A. An ATR-FTIR Study of Carbonate Sorption onto Magnetite. *Surf. Interface Anal.* **2010**, *42*, 1118–1121.
- (444) Rakshit, S.; Sarkar, D.; Punamiya, P.; Datta, R. Kinetics of Oxytetracycline Sorption on Magnetite Nanoparticles. *Int. J. Environ. Sci. Technol.* **2014**, *11*, 1207–1214.
- (445) Zhang, D.; Niu, H.; Zhang, X.; Meng, Z.; Cai, Y. Strong Adsorption of Chlorotetracycline on Magnetite Nanoparticles. *J. Hazard. Mater.* **2011**, *192*, 1088–1093.
- (446) Usman, M.; Martin, S.; Cimetière, N.; Giraudet, S.; Chatain, V.; Hanna, K. Sorption of Nalidixic Acid onto Micrometric and Nanometric Magnetites: Experimental Study and Modeling. *Appl. Surf. Sci.* **2014**, *299*, 136–145.
- (447) Liang, X.; Butler, E. C. Effects of Natural Organic Matter Model Compounds on the Transformation of Carbon Tetrachloride by Chloride Green Rust. *Water Res.* **2010**, *44*, 2125–2132.
- (448) Zhao, X.; Shi, Y.; Cai, Y.; Mou, S. Cetyltrimethylammonium Bromide-Coated Magnetic Nanoparticles for the Preconcentration of Phenolic Compounds from Environmental Water Samples. *Environ. Sci. Technol.* **2008**, *42*, 1201–1206.
- (449) Ghosh, S.; Badruddoza, A. Z. M.; Hidajat, K.; Uddin, M. S. Adsorptive Removal of Emerging Contaminants from Water Using Superparamagnetic Fe₃O₄ Nanoparticles Bearing Aminated β -Cyclodextrin. *J. Environ. Chem. Eng.* **2013**, *1*, 122–130.
- (450) Ayala-Luis, K. B.; Cooper, N. G. A.; Koch, C. B.; Hansen, H. C. B. Efficient Dechlorination of Carbon Tetrachloride by Hydrophobic Green Rust Intercalated with Dodecanoate Anions. *Environ. Sci. Technol.* **2012**, *46*, 3390–3397.
- (451) Huang, L.-Z.; Hansen, H. C. B. Synthesis and Reactivity of Surfactant-intercalated Layered Iron(II)Iron(III) Hydroxides. *Curr. Inorg. Chem.* **2016**, *6*, 68–82.
- (452) Tombácz, E.; Tóth, I. Y.; Nesztor, D.; Illés, E.; Hajdú, A.; Szekeres, M.; Vékás, L. Adsorption of Organic Acids on Magnetite Nanoparticles, pH-Dependent Colloidal Stability and Salt Tolerance. *Colloids Surf., A* **2013**, *435*, 91–96.
- (453) Illés, E.; Tombácz, E. The Effect of Humic Acid Adsorption on pH-Dependent Surface Charging and Aggregation of Magnetite Nanoparticles. *J. Colloid Interface Sci.* **2006**, *295*, 115–123.
- (454) MacRae, I. C.; Evans, S. K. Removal of Bacteria from Water by Adsorption to Magnetite. *Water Res.* **1984**, *18*, 1377–1380.
- (455) Mac Rae, I. C. Removal of Pesticides in Water by Microbial Cells Adsorbed to Magnetite. *Water Res.* **1985**, *19*, 825–830.
- (456) Cheng, W.; Marsac, R.; Hanna, K. Influence of Magnetite Stoichiometry on the Binding of Emerging Organic Contaminants. *Environ. Sci. Technol.* **2018**, *52*, 467–473.
- (457) Erbs, M.; Hansen, H. C. B.; Olsen, C. E. Reductive Dechlorination of Carbon Tetrachloride using Iron(II) Iron(III) Hydroxide Sulfate (Green Rust). *Environ. Sci. Technol.* **1999**, *33*, 307–311.
- (458) Oliveira, L. C. A.; Rios, R. V. R. A.; Fabris, J. D.; Garg, V.; Sapag, K.; Lago, R. M. Activated Carbon/Iron Oxide Magnetic Composites for the Adsorption of Contaminants in Water. *Carbon* **2002**, *40*, 2177–2183.
- (459) Pang, K. M.; Ng, S.; Chung, W. K.; Wong, P. K. Removal of Pentachlorophenol by Adsorption on Magnetite-immobilized Chitin. *Water, Air, Soil Pollut.* **2007**, *183*, 355–365.
- (460) Xue, X.; Hanna, K.; Abdelmoula, M.; Deng, N. Adsorption and Oxidation of Pcp on the Surface of Magnetite: Kinetic Experiments and Spectroscopic Investigations. *Appl. Catal., B* **2009**, *89*, 432–440.
- (461) Shen, Y. F.; Tang, J.; Nie, Z. H.; Wang, Y. D.; Ren, Y.; Zuo, L. Preparation and Application of Magnetic Fe₃O₄ Nanoparticles for Wastewater Purification. *Sep. Purif. Technol.* **2009**, *68*, 312–319.
- (462) Bujňáková, Z.; Baláž, P.; Zorkovská, A.; Sayagués, M. J.; Kováč, J.; Timko, M. Arsenic Sorption by Nanocrystalline Magnetite: An Example of Environmentally Promising Interface with Geosphere. *J. Hazard. Mater.* **2013**, *262*, 1204–1212.
- (463) Parsons, J. G.; Hernandez, J.; Gonzalez, C. M.; Gardea-Torresdey, J. L. Sorption of Cr(III) and Cr(VI) to High and Low Pressure Synthetic Nano-Magnetite (Fe₃O₄) Particles. *Chem. Eng. J.* **2014**, *254*, 171–180.

- (464) Stumm, W.; Morgan, J. J. *Aquatic Chemistry: Chemical Equilibria and Rates in Natural Waters*; 3rd ed.; John Wiley and Sons: New York, 1996.
- (465) Haderlein Stefan, B.; Pecher, K. Pollutant Reduction in Heterogeneous Fe(II)-Fe(III) Systems. In *Mineral-Water Interfacial Reactions*; American Chemical Society, 1999; Vol. 715, pp 342–357.
- (466) Williams, A. G. B.; Scherer, M. M. Kinetics of Cr(VI) Reduction by Carbonate Green Rust. *Environ. Sci. Technol.* **2001**, *35*, 3488–3494.
- (467) Choi, J.; Batchelor, B. Nitrate Reduction by Fluoride Green Rust Modified with Copper. *Chemosphere* **2008**, *70*, 1108–1116.
- (468) Hansen, H. C. B.; Koch, C. B. Reduction of Nitrate to Ammonium by Sulphate Green Rust: Activation Energy and Reaction Mechanism. *Clay Miner.* **1998**, *33*, 87–101.
- (469) O'Loughlin, E. J.; Kelly, S. D.; Cook, R. E.; Csencsits, R.; Kemner, K. M. Reduction of Uranium(VI) by Mixed Iron(II)/Iron(III) Hydroxide (Green Rust): Formation of UO₂ Nanoparticles. *Environ. Sci. Technol.* **2003**, *37*, 721–727.
- (470) O'Loughlin, E. J.; Kelly, S. D.; Kemner, K. M.; Csencsits, R.; Cook, R. E. Reduction of Ag^I, Au^{III}, Cu^{II}, and Hg^{II} by Fe^{II}/Fe^{III} Hydroxysulfate Green Rust. *Chemosphere* **2003**, *53*, 437–446.
- (471) Pepper, S. E.; Bunker, D. J.; Bryan, ND; Livens, F. R.; Charnock, J. M.; Patrick, R. A. D.; Collison, D. Treatment of Radioactive Wastes: An X-Ray Absorption Spectroscopy Study of the Reaction of Technetium with Green Rust. *J. Colloid Interface Sci.* **2003**, *268*, 408–412.
- (472) Gregory, K. B.; Larese-Casanova, P.; Parkin, G. F.; Scherer, M. M. Abiotic Transformation of Hexahydro-1,3,5-Trinitro-1,3,5-Triazine by Fe^{II} Bound to Magnetite. *Environ. Sci. Technol.* **2004**, *38*, 1408–1414.
- (473) Latta, D.; Boyanov, M.; Kemner, K.; O'Loughlin, E.; Scherer, M. Reaction of Uranium(VI) with Green Rusts: Effect of Interlayer Anion. *Curr. Inorg. Chem.* **2015**, *5*, 156–168.
- (474) Klein, C.; Hurlbut, C., Jr. *Manual of Mineralogy*; John Wiley & Sons, Inc: Hoboken, NJ, 1993.
- (475) Skovbjerg, L. L.; Stipp, S. L. S.; Utsunomiya, S.; Ewing, R. C. The Mechanisms of Reduction of Hexavalent Chromium by Green Rust Sodium Sulphate: Formation of Cr-Goethite. *Geochim. Cosmochim. Acta* **2006**, *70*, 3582–3592.
- (476) Dhakal, P.; Matocha, C. J.; Huggins, F. E.; Vandiviere, M. M. Nitrite Reactivity with Magnetite. *Environ. Sci. Technol.* **2013**, *47*, 6206–6213.
- (477) Loyaux-Lawniczak, S.; Refait, P.; Ehrhardt, J. J.; Lecomte, P.; Génin, J. M. R. Trapping of Cr by Formation of Ferrihydrite During the Reduction of Chromate Ions by Fe(II)-Fe(III) Hydroxysalt Green Rusts. *Environ. Sci. Technol.* **2000**, *34*, 438–443.
- (478) Hansen, H. C. B.; Koch, C. B.; Nancke-Krogh, H.; Borggaard, O. K.; Sørensen, J. Abiotic Nitrate Reduction to Ammonium: Key Role of Green Rust. *Environ. Sci. Technol.* **1996**, *30*, 2053–2056.
- (479) Myneni, S. C. B.; Tokunaga, T. K.; Brown, G. E. Abiotic Selenium Redox Transformations in the Presence of Fe(II,III) Oxides. *Science* **1997**, *278*, 1106–1109.
- (480) Bond, D. L.; Fendorf, S. Kinetics and Structural Constraints of Chromate Reduction by Green Rusts. *Environ. Sci. Technol.* **2003**, *37*, 2750–2757.
- (481) Lee, W.; Batchelor, B. Reductive Capacity of Natural Reductants. *Environ. Sci. Technol.* **2003**, *37*, 535–541.
- (482) Lee, W.; Batchelor, B. Abiotic Reductive Dechlorination of Chlorinated Ethylenes by Iron-Bearing Soil Minerals. 2. Green Rust. *Environ. Sci. Technol.* **2002**, *36*, 5348–5354.
- (483) Jung, Y.; Choi, J.; Lee, W. Spectroscopic Investigation of Magnetite Surface for the Reduction of Hexavalent Chromium. *Chemosphere* **2007**, *68*, 1968–1975.
- (484) Klausen, J.; Troeber, S. P.; Haderlein, S. B.; Schwarzenbach, R. P. Reduction of Substituted Nitrobenzenes by Fe (II) in Aqueous Mineral Suspensions. *Environ. Sci. Technol.* **1995**, *29*, 2396–2404.
- (485) Amonette, J. E.; Workman, D. J.; Kennedy, D. W.; Fruchter, J. S.; Gorby, Y. A. Dechlorination of Carbon Tetrachloride by Fe(II) Associated with Goethite. *Environ. Sci. Technol.* **2000**, *34*, 4606–4613.
- (486) Klupinski, T. P.; Chin, Y.-P.; Traina, S. J. Abiotic Degradation of Pentachloronitrobenzene by Fe(II): Reactions on Goethite and Iron Oxide Nanoparticles. *Environ. Sci. Technol.* **2004**, *38*, 4353–4360.
- (487) Hansen, H. C. B.; Borggaard, O. K.; Sørensen, J. Evaluation of the Free Energy of Formation of Fe(II)-Fe(III) Hydroxide-Sulphate (Green Rust) and Its Reduction of Nitrite. *Geochim. Cosmochim. Acta* **1994**, *58*, 2599–2608.
- (488) Etique, M.; Zegeye, A.; Grégoire, B.; Carteret, C.; Ruby, C. Nitrate Reduction by Mixed Iron (II-III) Hydroxycarbonate Green Rust in the Presence of Phosphate Anions: The Key Parameters Influencing the Ammonium Selectivity. *Water Res.* **2014**, *62*, 29–39.
- (489) Jorand, F. P. A.; Sergent, A. S.; Remy, P. P.; Bihannic, I.; Ghanbaja, J.; Lartiges, B.; Hanna, K.; Zegeye, A. Contribution of Anionic vs. Neutral Polymers to the Formation of Green Rust 1 from γ -FeOOH Bioreduction. *Geomicrobiol. J.* **2013**, *30*, 600–615.
- (490) Remy, P. P.; Etique, M.; Hazotte, A. A.; Sergent, A. S.; Estrade, N.; Cloquet, C.; Hanna, K.; Jorand, F. P. A. Pseudo-First-Order Reaction of Chemically and Biologically Formed Green Rusts with Hg^{II} and C₁₅H₁₅N₃O₂: Effects of pH and Stabilizing Agents (Phosphate, Silicate, Polyacrylic Acid, and Bacterial Cells). *Water Res.* **2015**, *70*, 266–278.
- (491) Legrand, L.; El Figuigui, A.; Mercier, F.; Chausse, A. Reduction of Aqueous Chromate by Fe(II)/Fe(III) Carbonate Green Rust: Kinetic and Mechanistic Studies. *Environ. Sci. Technol.* **2004**, *38*, 4587–4595.
- (492) He, Y. T.; Traina, S. J. Cr(VI) Reduction and Immobilization by Magnetite under Alkaline pH Conditions: The Role of Passivation. *Environ. Sci. Technol.* **2005**, *39*, 4499–4504.
- (493) Vikesland, P. J.; Heathcock, A. M.; Rebodos, R. L.; Makus, K. E. Particle Size and Aggregation Effects on Magnetite Reactivity toward Carbon Tetrachloride. *Environ. Sci. Technol.* **2007**, *41*, 5277–5283.
- (494) Danielsen, K. M.; Hayes, K. F. pH Dependence of Carbon Tetrachloride Reductive Dechlorination by Magnetite. *Environ. Sci. Technol.* **2004**, *38*, 4745–4752.
- (495) O'Loughlin, E. J.; Kemner, K. M.; Burris, D. R. Effects of Ag^I, Au^{III}, and Cu^{II} on the Reductive Dechlorination of Carbon Tetrachloride by Green Rust. *Environ. Sci. Technol.* **2003**, *37*, 2905–2912.
- (496) Rybnikova, V.; Usman, M.; Hanna, K. Removal of PCBs in Contaminated Soils by Means of Chemical Reduction and Advanced Oxidation Processes. *Environ. Sci. Pollut. Res.* **2016**, *23*, 17035–17048.
- (497) Fenton, H. J. H. On a New Reaction of Tartaric Acid. *Chemical News* **1876**, *33*, 190.
- (498) Fenton, H. J. H. Oxidation of Tartaric Acid in Presence of Iron. *J. Chem. Soc., Trans.* **1894**, *65*, 899–910.
- (499) Haber, F.; Weiss, J. The catalytic decomposition of hydrogen peroxide by iron salts. *Proc. R. Soc. London, Ser. A* **1934**, *147*, 332–351.
- (500) Gligorovski, S.; Streckowski, R.; Barbat, S.; Vione, D. Environmental Implications of Hydroxyl Radicals (\bullet OH). *Chem. Rev.* **2015**, *115*, 13051–13092.
- (501) De Laat, J.; Gallard, H. Catalytic Decomposition of Hydrogen Peroxide by Fe(III) in Homogeneous Aqueous Solution: Mechanism and Kinetic Modeling. *Environ. Sci. Technol.* **1999**, *33*, 2726–2732.
- (502) Sirguey, C.; Tereza de Souza e Silva, P.; Schwartz, C.; Simonnot, M.-O. Impact of Chemical Oxidation on Soil Quality. *Chemosphere* **2008**, *72*, 282–289.
- (503) Xue, X.; Hanna, K.; Despas, C.; Wu, F.; Deng, N. Effect of Chelating Agent on the Oxidation Rate of PCP in the Magnetite/H₂O₂ System at Neutral pH. *J. Mol. Catal. A: Chem.* **2009**, *311*, 29–35.
- (504) Pardo, F.; Rosas, J.; Santos, A.; Romero, A. Remediation of a Biodiesel Blend-Contaminated Soil by Using a Modified Fenton Process. *Environ. Sci. Pollut. Res.* **2014**, *21*, 12198–12207.
- (505) Usman, M.; Hanna, K.; Haderlein, S. Fenton Oxidation to Remediate PAHs in Contaminated Soils: A Critical Review of Major Limitations and Counter-Strategies. *Sci. Total Environ.* **2016**, *569*–570, 179–190.
- (506) Tsitonaki, A.; Petri, B.; Crimi, M.; Mosbaek, H.; Siegrist, R. L.; Bjerg, P. L. In Situ Chemical Oxidation of Contaminated Soil and

Groundwater Using Persulfate: A Review. *Crit. Rev. Environ. Sci. Technol.* **2010**, *40*, 55–91.

(507) Usman, M.; Faure, P.; Ruby, C.; Hanna, K. Remediation of PAH-Contaminated Soils by Magnetite Catalyzed Fenton-Like Oxidation. *Appl. Catal., B* **2012**, *117–118*, 10–17.

(508) Usman, M.; Faure, P.; Ruby, C.; Hanna, K. Application of Magnetite-Activated Persulfate Oxidation for the Degradation of PAHs in Contaminated Soils. *Chemosphere* **2012**, *87*, 234–240.

(509) Jung, Y. S.; Lim, W. T.; Park, J. Y.; Kim, Y. H. Effect of pH on Fenton and Fenton-like oxidation. *Environ. Technol.* **2009**, *30*, 183–190.

(510) Barreiro, J. C.; Capelato, M. D.; Martin-Neto, L.; Bruun Hansen, H. C. Oxidative Decomposition of Atrazine by a Fenton-Like Reaction in a H₂O₂/Ferrihydrite System. *Water Res.* **2007**, *41*, 55–62.

(511) Matta, R.; Hanna, K.; Chiron, S. Fenton-Like Oxidation of 2,4,6-Trinitrotoluene Using Different Iron Minerals. *Sci. Total Environ.* **2007**, *385*, 242–251.

(512) Matta, R.; Hanna, K.; Kone, T.; Chiron, S. Oxidation of 2, 4, 6-Trinitrotoluene in the Presence of Different Iron-Bearing Minerals at Neutral pH. *Chem. Eng. J.* **2008**, *144*, 453–458.

(513) Kanel, S. R.; Neppolian, B.; Choi, H.; Yang, J. W. Heterogeneous Catalytic Oxidation of Phenanthrene by Hydrogen Peroxide in Soil Slurry: Kinetics, Mechanism, and Implication. *Soil Sediment Contam.* **2003**, *12*, 101–117.

(514) Kanel, S. R.; Neppolian, B.; Jung, H.; Choi, H. Comparative Removal of Polycyclic Aromatic Hydrocarbons Using Iron Oxide and Hydrogen Peroxide in Soil Slurries. *Environ. Eng. Sci.* **2004**, *21*, 741–751.

(515) Watts, R. J.; Udell, M. D.; Kong, S.; Leung, S. W. Fenton-Like Soil Remediation Catalysed by Naturally Occurring Iron Minerals. *Environ. Eng. Sci.* **1999**, *16*, 93–103.

(516) Sabri, N.; Hanna, K.; Yargeau, V. Chemical Oxidation of Ibuprofen in the Presence of Iron Species at near Neutral pH. *Sci. Total Environ.* **2012**, *427–428*, 382–389.

(517) Usman, M.; Faure, P.; Lorgeoux, C.; Ruby, C.; Hanna, K. Treatment of Hydrocarbon Contamination under Flow through Conditions by Using Magnetite Catalyzed Chemical Oxidation. *Environ. Sci. Pollut. Res.* **2013**, *20*, 22–30.

(518) Tyre, B. W.; Watts, R. J.; Miller, G. C. Treatment of Four Biorefractory Contaminants in Soils Using Catalyzed Hydrogen Peroxide. *J. Environ. Qual.* **1991**, *20*, 832–838.

(519) Usman, M.; Chaudhary, A.; Biache, C.; Faure, P.; Hanna, K. Effect of Thermal Pre-Treatment on the Availability of PAHs for Successive Chemical Oxidation in Contaminated Soils. *Environ. Sci. Pollut. Res.* **2016**, *23*, 1371–1380.

(520) Sun, S.-P.; Lemley, A. T. p-Nitrophenol Degradation by a Heterogeneous Fenton-Like Reaction on Nano-Magnetite: Process Optimization, Kinetics, and Degradation Pathways. *J. Mol. Catal. A: Chem.* **2011**, *349*, 71–79.

(521) Fontecha-Cámara, M. A.; Moreno-Castilla, C.; López-Ramón, M. V.; Álvarez, M. A. Mixed Iron Oxides as Fenton Catalysts for Gallic Acid Removal from Aqueous Solutions. *Appl. Catal., B* **2016**, *196*, 207–215.

(522) Matta, R.; Hanna, K.; Chiron, S. Oxidation of Phenol by Green Rust and Hydrogen Peroxide at Neutral pH. *Sep. Purif. Technol.* **2008**, *61*, 442–446.

(523) Kone, T.; Hanna, K.; Abdelmoula, M.; Ruby, C.; Carteret, C. Reductive Transformation and Mineralization of an Azo Dye by Hydroxysulphate Green Rust Preceding Oxidation Using H₂O₂ at Neutral pH. *Chemosphere* **2009**, *75*, 212–219.

(524) Lin, Y.; Yang, C.; Xiu, R.; Wang, J.; Wei, Y.; Sun, Y. Decolorization of Methyl Orange by Green Rusts with Hydrogen Peroxide at Neutral pH. *Water Sci. Technol.* **2014**, *69*, 371–377.

(525) Hanna, K.; Kone, T.; Medjahdi, G. Synthesis of the Mixed Oxides of Iron and Quartz and Their Catalytic Activities for the Fenton-Like Oxidation. *Catal. Commun.* **2008**, *9*, 955–959.

(526) Kwan, W. P.; Voelker, B. M. Rates of Hydroxyl Radical Generation and Organic Compound Oxidation in Mineral-Catalyzed Fenton-like Systems. *Environ. Sci. Technol.* **2003**, *37*, 1150–1158.

(527) Valentine, R. L.; Wang, H. C. A. Iron Oxide Surface Catalyzed Oxidation of Quinoline by Hydrogen Peroxide. *J. Environ. Eng.* **1998**, *124*, 31–38.

(528) Liu, H.; Bruton, T. A.; Doyle, F. M.; Sedlak, D. L. In Situ Chemical Oxidation of Contaminated Groundwater by Persulfate: Decomposition by Fe(III)- and Mn(IV)-Containing Oxides and Aquifer Materials. *Environ. Sci. Technol.* **2014**, *48*, 10330–10336.

(529) Zhang, S.; Zhao, X.; Niu, H.; Shi, Y.; Cai, Y.; Jiang, G. Superparamagnetic Fe₃O₄ Nanoparticles as Catalysts for the Catalytic Oxidation of Phenolic and Aniline Compounds. *J. Hazard. Mater.* **2009**, *167*, 560–566.

(530) Jia, D.; Sun, S.-P.; Wu, Z.; Wang, N.; Jin, Y.; Dong, W.; Chen, X. D.; Ke, Q. TCE Degradation in Groundwater by Chelators-Assisted Fenton-like Reaction of Magnetite: Sand Columns Demonstration. *J. Hazard. Mater.* **2018**, *346*, 124–132.

(531) Huang, R.; Fang, Z.; Yan, X.; Cheng, W. Heterogeneous Sono-Fenton Catalytic Degradation of Bisphenol A by Fe₃O₄ Magnetic Nanoparticles under Neutral Condition. *Chem. Eng. J.* **2012**, *197*, 242–249.

(532) Hou, L.; Zhang, H.; Xue, X. Ultrasound Enhanced Heterogeneous Activation of Peroxydisulfate by Magnetite Catalyst for the Degradation of Tetracycline in Water. *Sep. Purif. Technol.* **2012**, *84*, 147–152.

(533) Aghdasinia, H.; Arehjani, P.; Vahid, B.; Khataee, A. Fluidized-Bed Fenton-Like Oxidation of a Textile Dye Using Natural Magnetite. *Res. Chem. Intermed.* **2016**, *42*, 8083–8095.

(534) Munoz, M.; Domínguez, P.; de Pedro, Z. M.; Casas, J. A.; Rodriguez, J. J. Naturally-Occurring Iron Minerals as Inexpensive Catalysts for CWPO. *Appl. Catal., B* **2017**, *203*, 166–173.

(535) Aghdasinia, H.; Khataee, A.; Sheikhi, M.; Takhtfiroozeh, P. Pilot Plant Fluidized-Bed Reactor for Degradation of Basic Blue 3 in Heterogeneous Fenton Process in the Presence of Natural Magnetite. *Environ. Prog. Sustainable Energy* **2017**, *36*, 1039–1048.

(536) Xu, L.; Wang, J. Magnetic Nanoscaled Fe₃O₄/CeO₂ Composite as an Efficient Fenton-Like Heterogeneous Catalyst for Degradation of 4-Chlorophenol. *Environ. Sci. Technol.* **2012**, *46*, 10145–10153.

(537) Wang, W.; Liu, Y.; Li, T.; Zhou, M. Heterogeneous Fenton Catalytic Degradation of Phenol Based on Controlled Release of Magnetic Nanoparticles. *Chem. Eng. J.* **2014**, *242*, 1–9.

(538) Nadejde, C.; Neamtu, M.; Hodoroaba, V. D.; Schneider, R. J.; Paul, A.; Ababei, G.; Panne, U. Green Fenton-Like Magnetic Nanocatalysts: Synthesis, Characterization and Catalytic Application. *Appl. Catal., B* **2015**, *176–177*, 667–677.

(539) Deng, J.; Wen, X.; Wang, Q. Solvothermal in situ synthesis of Fe₃O₄-Multi-Walled Carbon Nanotubes with Enhanced Heterogeneous Fenton-Like Activity. *Mater. Res. Bull.* **2012**, *47*, 3369–3376.

(540) Xu, H.-Y.; Shi, T.-N.; Zhao, H.; Jin, L.-G.; Wang, F.-C.; Wang, C.-Y.; Qi, S.-Y. Heterogeneous Fenton-Like Discoloration of Methyl Orange Using Fe₃O₄/MWCNTs as Catalyst: Process Optimization by Response Surface Methodology. *Front. Mater. Sci.* **2016**, *10*, 45–55.

(541) Hu, X.; Liu, B.; Deng, Y.; Chen, H.; Luo, S.; Sun, C.; Yang, P.; Yang, S. Adsorption and Heterogeneous Fenton Degradation of 17 α -Methyltestosterone on Nano Fe₃O₄/MWCNTs in aqueous solution. *Appl. Catal., B* **2011**, *107*, 274–283.

(542) Ferroudj, N.; Nzimoto, J.; Davidson, A.; Talbot, D.; Briot, E.; Dupuis, V.; Bée, A.; Medjram, M. S.; Abramson, S. Maghemite Nanoparticles and Maghemite/Silica Nanocomposite Microspheres as Magnetic Fenton Catalysts for the Removal of Water Pollutants. *Appl. Catal., B* **2013**, *136–137*, 9–18.

(543) Liu, W.; Qian, J.; Wang, K.; Xu, H.; Jiang, D.; Liu, Q.; Yang, X.; Li, H. Magnetically Separable Fe₃O₄ Nanoparticles-Decorated Reduced Graphene Oxide Nanocomposite for Catalytic Wet Hydrogen Peroxide Oxidation. *J. Inorg. Organomet. Polym. Mater.* **2013**, *23*, 907–916.

(544) Magalhães, F.; Pereira, M. C.; Botrel, S. E. C.; Fabris, J. D.; Macedo, W. A.; Mendonça, R.; Lago, R. M.; Oliveira, L. C. A. Cr-containing Magnetites Fe_{3-x}Cr_xO₄: The Role of Cr³⁺ and Fe²⁺ on the

Stability and Reactivity Towards H_2O_2 Reactions. *Appl. Catal., A* **2007**, *332*, 115–123.

(545) Liang, X.; He, Z.; Wei, G.; Liu, P.; Zhong, Y.; Tan, W.; Du, P.; Zhu, J.; He, H.; Zhang, J. The Distinct Effects of Mn Substitution on the Reactivity of Magnetite in Heterogeneous Fenton Reaction and Pb(II) Adsorption. *J. Colloid Interface Sci.* **2014**, *426*, 181–189.

(546) Baldrian, P.; Merhautová, V.; Gabriel, J.; Nerud, F.; Stopka, P.; Hrubý, M.; Beneš, M. J. Decolorization of Synthetic Dyes by Hydrogen Peroxide with Heterogeneous Catalysis by Mixed Iron Oxides. *Appl. Catal., B* **2006**, *66*, 258–264.

(547) Costa, R. C. C.; Lelis, M. F. F.; Oliveira, L. C. A.; Fabris, J. D.; Ardisson, J. D.; Rios, R. R. V. A.; Silva, C. N.; Lago, R. M. Novel Active Heterogeneous Fenton System Based on $Fe_{3-x}M_xO_4$ (Fe, Co, Mn, Ni): The Role of M^{2+} Species on the Reactivity Towards H_2O_2 Reactions. *J. Hazard. Mater.* **2006**, *129*, 171–178.

(548) Zhong, Y.; Liang, X.; He, Z.; Tan, W.; Zhu, J.; Yuan, P.; Zhu, R.; He, H. The Constraints of Transition Metal Substitutions (Ti, Cr, Mn, Co and Ni) in Magnetite on Its Catalytic Activity in Heterogeneous Fenton and UV/Fenton Reaction: From the Perspective of Hydroxyl Radical Generation. *Appl. Catal., B* **2014**, *150–151*, 612–618.

(549) Liang, X.; He, Z.; Zhong, Y.; Tan, W.; He, H.; Yuan, P.; Zhu, J.; Zhang, J. The Effect of Transition Metal Substitution on the Catalytic Activity of Magnetite in Heterogeneous Fenton Reaction: In Interfacial View. *Colloids Surf., A* **2013**, *435*, 28–35.

(550) Liang, X.; Zhong, Y.; He, H.; Yuan, P.; Zhu, J.; Zhu, S.; Jiang, Z. The Application of Chromium Substituted Magnetite as Heterogeneous Fenton Catalyst for the Degradation of Aqueous Cationic and Anionic Dyes. *Chem. Eng. J.* **2012**, *191*, 177–184.

(551) Liu, J.; Zhao, Z.; Ding, Z.; Fang, Z.; Cui, F. Degradation of 4-Chlorophenol in a Fenton-Like System Using $Au-Fe_3O_4$ Magnetic Nanocomposites as the Heterogeneous Catalyst at near Neutral Conditions. *RSC Adv.* **2016**, *6*, 53080–53088.

(552) Lima, M. J.; Leblebici, M. E.; Dias, M. M.; Lopes, J. C. B.; Silva, C. G.; Silva, A. M. T.; Faria, J. L. Continuous Flow Photo-Fenton Treatment of Ciprofloxacin in Aqueous Solutions Using Homogeneous and Magnetically Recoverable Catalysts. *Environ. Sci. Pollut. Res.* **2014**, *21*, 11116–11125.

(553) Avetta, P.; Pensato, A.; Minella, M.; Malandrino, M.; Maurino, V.; Minero, C.; Hanna, K.; Vione, D. Activation of Persulfate by Irradiated Magnetite: Implications for the Degradation of Phenol under Heterogeneous Photo-Fenton-Like Conditions. *Environ. Sci. Technol.* **2015**, *49*, 1043–1050.

(554) Hou, L.; Wang, L.; Royer, S.; Zhang, H. Ultrasound-Assisted Heterogeneous Fenton-Like Degradation of Tetracycline over a Magnetite Catalyst. *J. Hazard. Mater.* **2016**, *302*, 458–467.

(555) Zazo, J. A.; Pliego, G.; García-Muñoz, P.; Casas, J. A.; Rodríguez, J. J. UV-LED Assisted Catalytic Wet Peroxide Oxidation with a Fe(II)-Fe(III)/Activated Carbon Catalyst. *Appl. Catal., B* **2016**, *192*, 350–356.

(556) Kong, S. H.; Watts, R. J.; Choi, J. H. Treatment of Petroleum-Contaminated Soils Using Iron Mineral Catalyzed Hydrogen Peroxide. *Chemosphere* **1998**, *37*, 1473–1482.

(557) Zeng, X.; Hanna, K.; Lemley, A. T. Cathodic Fenton Degradation of 4,6-Dinitro-o-cresol with Nano-Magnetite. *J. Mol. Catal. A* **2011**, *339*, 1–7.